Synchrotron radiation linear dichroism (SRLD) investigations of the electronic transitions of samples aligned in stretched low-density polyethylene

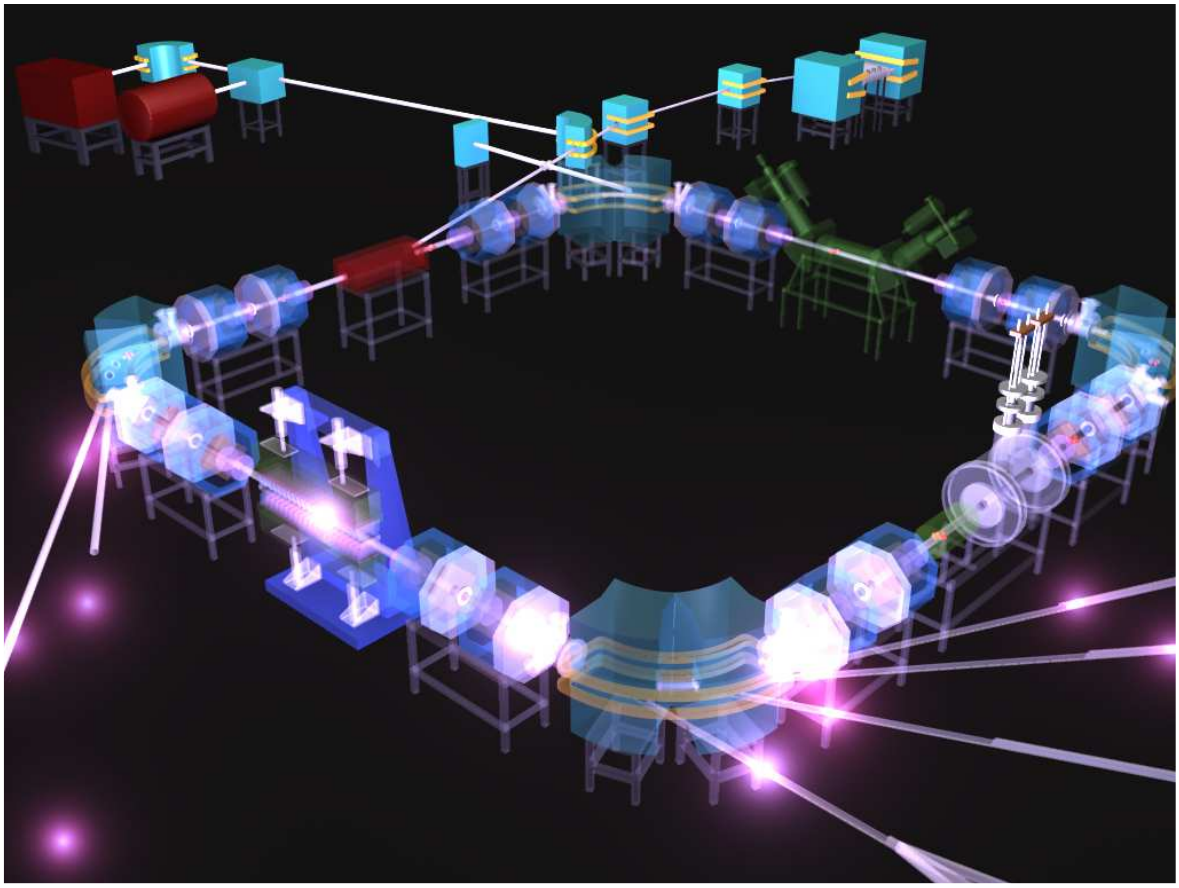

PhD Thesis by

Duy Duc Nguyen

Department of Science, Systems and Models
Roskilde University, Denmark – 2010

Abstract

The ultraviolet-visible (UV-VIS) optical properties of organic compounds which are energy, intensity and moment of electronic transitions are studied in this thesis by using synchrotron radiation linear dichroism (SRLD) spectroscopic method and computational chemistry. The spectroscopic measurements are performed on compounds of interest which are oriented partially in stretched low-density polyethylene (LDPE) matrix. This method can extend spectral region to higher energy with reliability and precision, providing more spectroscopic information than those obtained from traditional spectroscopic method. The observed SRLD spectra are compared with the predicted data, and good agreement between them results in the assignment of the electronic transitions and symmetry of the absorption bands.

LDPE is used as an anisotropic solvent for preparing samples. And the stretched LDPE is a main technique that is used to align compounds for the SRLD measurements in this thesis. Although this method is considered as a relatively simple, inexpensive one and solvent-molecule interactions is neglectful in this polymer matrix, the introduction of molecules of compounds into the polymer matrix is quite difficult, depending strongly on the effect of factors such as temperature, concentration of compounds, nature of polymer matrix and compounds of interest. Therefore, each compound in a group should be treated in its own conditions to introduce enough amount of molecule of compound into the polymer matrix. The sample preparation procedure will be described in detail in this thesis.

Density functional theory (DFT) and time-dependent density functional theory (TD-DFT) are used to optimize molecular geometry for ground states and calculate electronic transition energies for excited states, respectively. These methods are applied successfully to heterocycles and dihydroxy derivatives of anthraquinone, in most cases leading to good agreement with the experimental data. In case of hydrocarbons group, since these methods can not always predict well the observed spectra, a semi-empirical method, linear combination of orthogonalized atomic orbitals (LCOAO), is used to calculate the electronic transitions. And this method shows a good agreement with the observed spectra.

The application of synchrotron radiation in linear dichroism (LD) measurements extends the spectral region to higher energy, approximately 11000 cm^{-1} (from 47000 – 58000 cm^{-1} in relation to traditional technology) in measurements using LDPE as a solvent, leading to resolution of overlapping, differently polarized transitions and providing more optical information in this region.

Preface

Linear dichroism (LD) spectroscopy was introduced and researched many decades ago in the world. This spectroscopic method was used to investigate optical properties of compounds, for instance, direction of transition dipole moments in molecular framework which is of particularly important feature in many applications. And the research was published as books and articles during that period. The new and useful information obtained from LD investigations of compounds of interest provides valuable insights into nature of electronic transitions and molecular structure.

And in recent decades, synchrotron radiation as a photon source has been widely applied to many research fields due to its striking properties which are high signal to noise ratio, high degree of polarization and wide spectral region. Hence, this type of light source can provide reliable and precise measurements in its spectral region.

In recent years, quantum mechanics have been developed and applied to many research fields as a supporting tool. In particular, quantum chemical calculations become useful tools for the predictions and assignments of the electronic transitions of compounds in spectroscopic investigations.

The combination of these methods is used to investigate the electronic transitions of compounds in this thesis. This means that LD measurements using synchrotron radiation are performed and the observed spectra are compared with the calculated results, leading to the assignment of the electronic transitions and symmetry of the observed spectra.

In Vietnam, scientific research has increasingly developed in recent years. Therefore, it is necessary to study new theories and methods and apply to many research fields as possible, increasing the development of scientific research and country. LD spectroscopy and synchrotron radiation are of new and important methods needing to be introduced.

The aim of this thesis is to introduce synchrotron radiation linear dichroism (SRLD) spectroscopy and computational chemistry which are used to investigate the optical properties of compounds. This method can be applied and developed at laboratories which interest in spectroscopic behaviours of compounds which are used in biology and chemistry.

With my knowledge about this method obtained during three year study and practice at the optical laboratory at Roskilde University, Denmark, the thesis tries to present the applications of mentioned method for the investigations of the electronic transitions of some groups of compounds.

In chapter 1, we introduce briefly the applications of SRLD spectroscopy and computational chemistry in recent years. And we also describe shortly the theory of LD spectroscopy and synchrotron radiation and how to choose the computational method for the compounds.

Sample preparation procedure using the stretched low-density polyethylene (LDPE) technique is described in detail in chapter 2, providing general view of experimental procedures which are used for different compounds in this thesis.

The next chapters, chapter 3, 4 and 5, describe more detail about each group of the compounds, hydrocarbons, heterocycles, and dihydroxy derivatives of anthraquinone. Their molecular structure, the observed spectra and the predicted electronic transitions are presented and discussed to give precise assignments of the electronic transitions of the compounds.

Chapter 6 is a concluding remark, summarizing the achievement of this thesis.

Finally, there are a glossary, references and appendices, collecting and containing detailed information concerning the contents which are mentioned in previous chapters in this thesis.

Financial support for three year study at Roskilde University, Denmark is mainly provided by Project 322, Vietnamese Ministry of Training and Education, Vietnam. And an additional support is given by ENRECA grant, Denmark.

Fisrt of all, I would like to thank my PhD supervisor, Prof. Jens Spanget-Larsen, who encouraged and introduced me to the interesting field of SRLD spectroscopy and computational chemistry.

In addition, I would like to thank Prof. Erik W. Thulstrup, Prof. Fritz Duus and Ms. Nguyen Thi Ngoc Lien and all officers of Project 322 for administrative assistance. And I would also like to thank Søren Vrønning Hoffmann, Nykola C. Jones and Eva M. Karlsen for technical assistance during my experiment at Aarhus and Roskilde University.

I also wish to thank all lecturers at Chemistry Faculty, University of Science, HoChiMinh City, Vietnam for teaching and providing the fundamentals of chemistry to me.

Finally, I am especially grateful to my family, my parents and parents-in-law and above all special thanks to my wife, Le Kim Ngan, who encouraged and supported me during three year study in Denmark.

List of publications

(Attached in Appendix 11)

1. **Synchrotron radiation linear dichroism (SRLD) investigation of the electronic transitions of quinizarin, chrysazin and anthrarufin**
Duy Duc Nguyen, Nykola C. Jones, Søren Vrønning Hoffmann, Jens Spanget-Larsen
Spectrochimica Acta Part A: Molecular and Biomolecular Spectroscopy, **77** (2010) 279-286

2. **Electronic transitions of fluorene, dibenzofuran, carbazole, and dibenzothiophene. From the onset of absorption to the ionization threshold**
Duy Duc Nguyen, John Trunk, Lina Nakhimovsky, Jens Spanget-Larsen
Journal of Molecular Spectroscopy, Accepted.

Table of contents

Figure acknowledgement

Figure in cover is taken from http://www.isa.au.dk/animations/pictures/astrid_sr_012c.htm (April 24th, 2010)
Figure 1.1 is taken from www.bbemg.ulg.ac.be/UK/2Basis/emwave.html (April 24th, 2010)
Figures 1.2, 1.3, 1.4 are taken from hyperphysics.phy-astr.gsu.edu/.../polclas.html (April 24th, 2010)
Figure 1.5 is taken from astro-canada.ca/_en/a2312.html (April 24th, 2010)
Figure 1.6 is taken from http://en.wikipedia.org/wiki/File:Glan-taylor.png (April 24th, 2010)
Figure 1.7 is taken from http://en.wikipedia.org/wiki/File:Rochon_Prism.svg (April 24th, 2010)
Figures 1.13, 1.14 are taken from References 29, 30
Figures 1.15 is taken from http://en.wikipedia.org/wiki/File:ASTRID-schematic.png (June 24th, 2010)
Figure 1.16 is taken from web-page of the Institute for Storage Ring Facilities (ISA): (June 24th, 2010) http://www.isa.au.dk/facilities/astrid/beamlines/cd1/CD1OpticalSpecs.asp
Figure 2.2 is taken from www.bbc.co.uk/schools/gcsebitesize/science/21... (April 24th, 2010)
Figure 2.3 is taken from Reference 63

Chapter 1

Introduction

1.1 Introduction

The nature of the electronic transitions of molecules has been studied since early decades of twentieth century [1-3]. However, most studies have only obtained information on energy and intensity of vibrational and electronic transitions. The limit of information obtained is subjected to development of theories, techniques as well as interest of researchers and applicabilities of researches. Hence, the information on direction of transition moments has not been fascinated and studied yet during that period.

Even though directional property of the transition moments in molecular framework is a crucially important factor leading to interaction between molecules and electromagnetic radiation and providing varieties of spectroscopic behaviours of compounds, biological and chemical researchers have just interested in this important information in recent decades [4]. It is significant to obtain the information on the transition moment directions because it has been used in many applications such as dyes, pharmaceuticals. And this information can only be obtained by using polarization spectroscopy, especially linear dichroism spectroscopy as described and used in this thesis [5-15].

During that period, most LD studies were mainly studied in spectral region from infrared, visible to ultraviolet. Traditional lamps were used as light source for the LD measurements throughout the spectral region. And the observed spectra have not been analyzed in detail yet. Theoretical calculations based on fundamental of quantum mechanics were applied to predict and explain experimental data. However, calculated results were not in good agreement with the observed spectra until recent decades. Many quantum chemical calculation methods were used to predict and analyze the electronic transitions in detail with better precision, providing more insights on spectroscopic properties of compounds [16,17].

Because of limited intensity of light source and high baseline absorption as well as strong light scattering of materials in high energy region, most LD measurements can not be performed in this region. But with synchrotron radiation as a photon source, the LD measurements can perform and extend up to 58000 cm^{-1} (7.2eV) in case of using LDPE as a solvent, providing additional information on optical properties of compounds [18,23].

In this thesis, all SRLD measurements are performed on groups of compounds such as hydrocarbons, heterocycles and dihydroxy anthraquinones. The compounds of interest are aligned in the stretched LDPE matrix and then measured in a high photon flux beamlight coming from synchrotron system. The groups of compounds chosen in this thesis have different molecular symmetries and geometries which expected to reveal variety of spectral features due to differences in the direction of the transition moments in the molecular framework. And the aim of this work is also to provide additional information on the electronic transition moment directions in the high energy region for these groups of compounds.

1.2 Spectroscopy with polarized light

1.2.1 Polarized light

Light is a term that is used to define one form of electromagnetic radiations which human's eyes can recognize in nature. The electromagnetic radiations cover a wide spectral region which is divided into variety of radiations from radio waves to Gamma rays (which is arrange in increasing order of energy: radio waves, microwaves, infrared, visible, ultraviolet, X rays, Gamma rays). The properties of the electromagnetic radiations are described by wave-particle theory which means that the electromagnetic radiation has both waved and particle properties.

The electromagnetic radiation is composed of electric and magnetic fields which are mutually perpendicular. The electric and magnetic fields are distributed in all directions and perpendicular to the propagation of radiation in space and in time. Both the electric and magnetic fields are characterized by four main properties: frequency (or wavelength or wavenumber), intensity, polarization and phase [24].

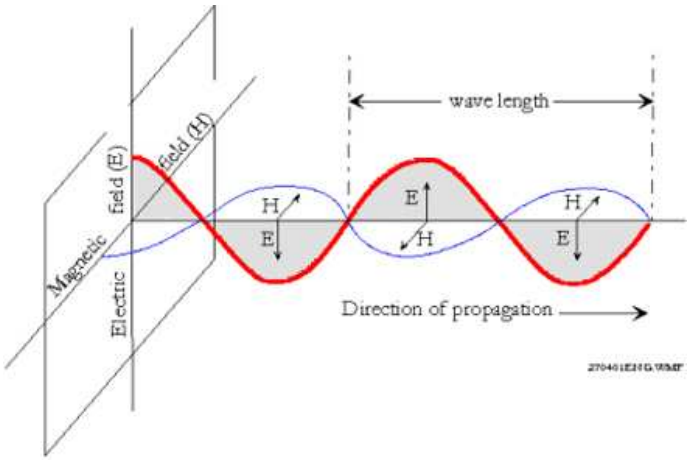

Figure 1.1: Illustration of electric and magnetic components in an arbitrary direction

Variations in and combination of numeric values of the four characteristics of the electric fields or magnetic fields produce varieties of polarized light which are classified into three main different types such as linear, elliptical and circular polarizations [25].

When the electric fields oscillate only in a plane, light is defined as linear polarization (as shown in figure 1.2). In other words, linearly polarized light is considered to be composed of two electric fields which are in the same phase and perpendicular to each other. The difference in their intensity produces difference in polarized directions.

And when the two electric fields are perpendicular and in the same intensity but in ninety degree out of phase, light is considered as circular polarization. The direction which the electric fields rotate in depends on the phase relationship between components. These cases are called right and left circular polarizations. Figure 1.3 will show illustration of right circular polarization.

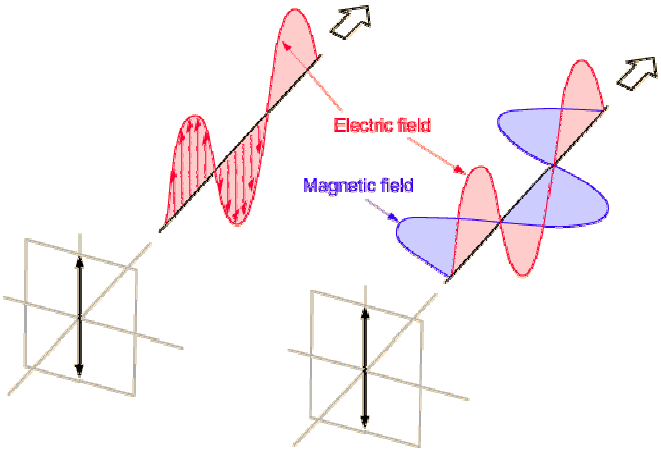

Figure 1.2: Linearly polarized light

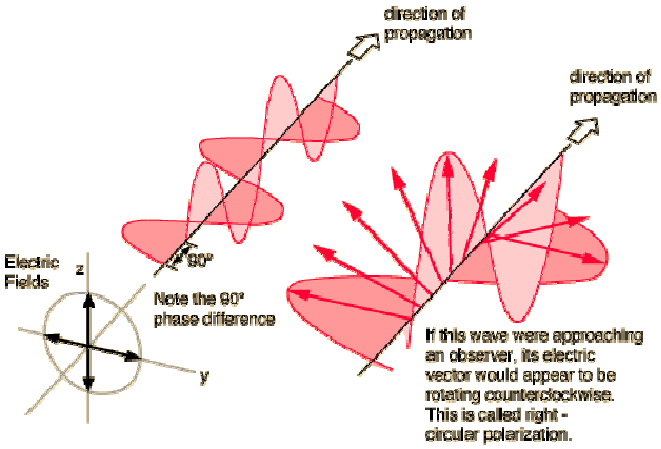

Figure 1.3: Right-Circular polarized light

And when the two electric fields are in the conditions described in circular polarization, but with difference in the intensity, light is polarized elliptically. In this case, light also has right and left elliptical polarization depending on the phase relationship. Figure 1.4 shows the illustration of right elliptical polarization.

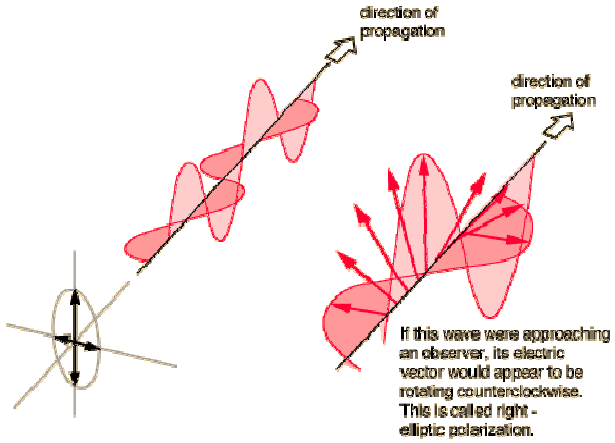

Figure 1.4: Right-Elliptical polarized light

1.2.2 Transition energy

When molecules absorb light, electron density distribution in molecules changes and reach to a new equilibrium. This means that the absorbed energy must be equivalent to difference in energy between two vibrational or electronic states in molecule. The relationship between the absorbed energy and the difference in energy of two states is shown in expression below [26-28]:

$$\Delta E = E_2 - E_1 = h \cdot \nu \tag{1}$$

Where, E_2 and E_1 are energy of excited and ground states in molecule, h is Planck's constant ($6{,}626 \cdot 10^{-34}$Js), and ν is frequency of light (Hz). In spectroscopic literature, two different quantities are usually used to describe the relationship of energy. They are wavelength (λ, nm) and wavenumber ($\tilde{\nu}$, cm^{-1}):

$$\lambda = \frac{c}{\nu} \tag{2}$$

And

$$\tilde{\nu} = \frac{1}{\lambda} \tag{3}$$

Where, c is velocity of light in vacuum ($3 \cdot 10^8$m/s).

All spectral data and results are shown in wavenumber in this thesis because of proportion of this quantity to energy. It should be convenient to analyze the spectral data in wavenumber as shown in following expression:

$$\Delta E = h \cdot c \cdot \tilde{\nu} \tag{4}$$

The quantities ν, λ, $\tilde{\nu}$ are characteristics of individual absorption band of molecule and depend on the molecular symmetry and geometry [26].

The difference in energy of electronic states in molecules is usually equivalent to the energy of light in the visible and ultraviolet region. Hence, ultraviolet – visible (UV-VIS) spectroscopy is a commonly used method to study the properties of the electronic transitions. In particular, all spectroscopic measurements in this thesis are performed in this region (15000 – 58000 cm^{-1}).

1.2.3 Transition intensity

Light absorption ability of molecules at a particular wavelength is subjected to nature of compound and characterized by a specific quantity, molar extinction coefficient $\varepsilon(\tilde{\nu})$ ($L \cdot mol^{-1} \cdot cm^{-1}$), and the intensity of the absorption band is described by Lambert-Beer's law [26-28]:

$$A(\tilde{\nu}) = \varepsilon(\tilde{\nu}) \cdot C \cdot d \tag{5}$$

Where, $A(\tilde{\nu})$ is absorbance of molecule at a particular wavenumber (dimensionless) and defined in expression (6), C is molar concentration of compound which is in the propagation of light ($mol \cdot L^{-1}$), d is pathlength of sample which light goes through (cm).

$$A(\tilde{\nu}) = \log \frac{I_0(\tilde{\nu})}{I(\tilde{\nu})} \tag{6}$$

And probability of electronic transitions between ground and excited states of the absorption band is characterized by oscillator strength (f, dimensionless). The value of this quantity could be obtained from integral of the observed absorption band [26,27,29,30]:

$$f = 4.319 \cdot 10^{-9} \int_{band} \varepsilon(\tilde{\nu}) d\tilde{\nu} \tag{7}$$

Or

$$f = 4.702 \cdot 10^{-7} \cdot \tilde{\nu} \cdot \left|\vec{M}\right|^2 \tag{8}$$

Where, $\int_{band}$ = integral over entire electronic band profile including vibronic components, $\left|\vec{M}\right|$ is length of moment vector of transition in question (Debye) for an isotropic sample. The intensities of strong transitions in UV-VIS region are usually 10 times higher than those in IR region.

From both expressions (7) and (8), the strength of the molar extinction coefficient and the transition moment is a crucial factor in determining the intensity of the electronic transitions in molecules. Both the molar extinction coefficient and the transition moment depend on molecular symmetry and geometry, leading to that the oscillator strength changes according to the variation of molecular structure.

1.2.4 Transition moment

Transition moment, also called as transition dipole moment, is a vector which is composed of three components along to Cartesian coordinate system (*x*, *y*, *z*) of molecule. In nature, transition moment concerns with transient variations in electron density distribution of a certain state in molecule as the molecule interacts with the electric field of light. This distribution induces polarity and orientation of the electron density in molecule which determine the energy and intensity of the absorption bands. Therefore, the electronic transition moment is considered as a quantity used to describe dependence of absorbance on direction of transitions.

According to quantum mechanics, the transition moment of two vibrational or electronic states is defined as following expression [29-32]:

$$\vec{M}_{nm} = \int_{-\infty}^{\infty} \psi_n \hat{\vec{\mu}} \psi_m d\tau \tag{9}$$

Where, ψ_n and ψ_m are wavefunctions of states n and m, and $\hat{\vec{\mu}}$ is dipole moment operator or transition moment operator. This integral is of significant importance because it is a fundamental of selection rules in spectroscopic method. If value of M_{nm} of a transition of interest is zero, this transition will be forbidden and vice versa.

In practice, it is frequently not necessary to calculate the value of this integral in order to predict possible transitions between vibrational and electronic states in molecule because it is convenient to get information on possible transitions by considering symmetrical properties of expression (9). This method bases on point group theory and character tables. The symmetrical properties of wavefunctions of the vibrational and electronic states and of the transition moment operator can be extracted from character table as irreducible representations. The integrand must be totally symmetry in the point group, if $M_{nm} \neq 0$. This means that the corresponding transitions are optically allowed.

Transition probability (*P*), also called as absorption probability of certain transition, is directly proportional to square of length of transition moment vector which is projected onto direction of electric vector of light, and is defined as below [27,29,30,32]:

$$P \propto (\vec{M}_i \cdot \vec{e})^2 = \left|\vec{M}_i\right|^2 \cos^2(\vec{M}_i, \vec{e}) \tag{10}$$

Where, $(\vec{M}_i, \vec{e})$ is angle which is composed of the transition moment vector $\vec{M}_i$ and unity vector $\vec{e}$ of the electric field of light. And absorbance $E_i(\tilde{\nu})$ of this transition is calculated by following equation [27,29,30]:

$$E_i(\tilde{\nu}) = A_i(\tilde{\nu}) \cdot \cos^2(\vec{M}_i, \vec{e}) \tag{11}$$

Where, $A_i(\tilde{\nu})$ is absorbance of i^{th} transition obtained with $(\vec{M}_i, \vec{e}) = 0$.

According to two above expressions, the transition probability and absorbance reach maximum value when the transition moment vector is parallel to the electric vector $\vec{e}$ of light. And vice versa, they get minimum value, zero, when the moment vector is perpendicular to the electric vector $\vec{e}$. In summary, the direction and length of the moment vector determines the orientation and intensity of transitions between vibrational and electronic states, respectively. Hence, the direction of the transition moment vector is usually considered as polarization of transitions in molecules. And this information can only be obtained by polarization spectroscopy.

1.2.5 Linear dichroism (LD) spectroscopy

Linear dichroism is a term that is used to describe difference in intensity of a specific absorption band of aligned sample when this sample interacts with light which is linearly polarized in two different directions. The definition is described in following expression [29,30,33]:

$$\Delta A_i = A_Z - A_Y \tag{12}$$

Where, A_Z and A_Y are the absorption spectra that are measured with the electric vector of linearly polarized light along and perpendicular to the sample axis, respectively.

LD spectroscopy is a main experimental method which is studied and discussed in this thesis. Here, a short description of basic theory is presented, providing fundamentals to understand and analyze the observed LD spectra of compounds. The LD measurements are performed by using linearly polarized light as a photon source which interacts with

oriented samples. Linear polarization can be produced by using a polarizer transforming unpolarized into light which is polarized in desired directions. Polarizer is classified into absorptive polarizer and beam splitting polarizer.

When the unpolarized light passes through the absorptive polarizer, only the electric vector parallel to the desired direction can be emerged from and the others are absorbed by polarizer [34]. This would produce light which is linearly polarized in a certain direction suited for the LD measurements. Figure 1.5 shows illustration of this type of polarizer.

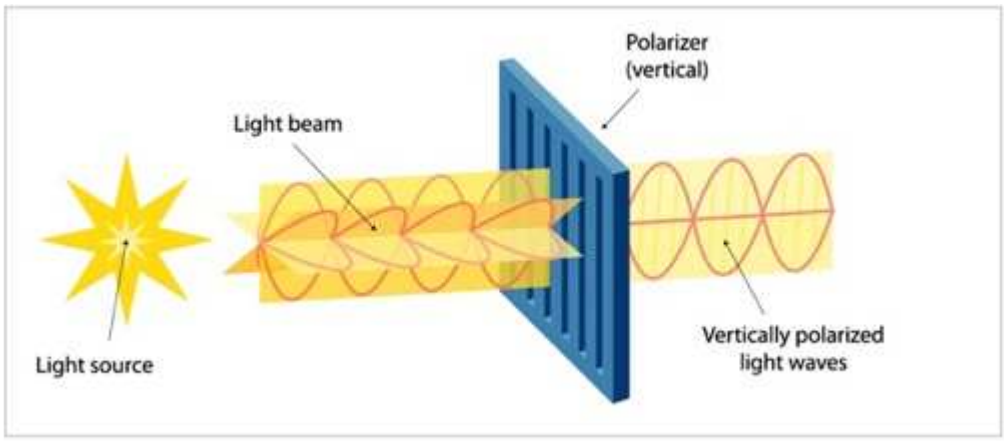

Figure 1.5: The absorptive linear polarizer

The beam splitting polarizer produces two emerged electric vectors which are perpendicular and linearly polarized when the unpolarized light passes through. The two electric components are splitted into two different beams and emerged from the polarizer in different directions. Depending on direction of the polarized light, there would be many types of the beam splitting polarizer [34]. Figure 1.6 shows illustration of one of them.

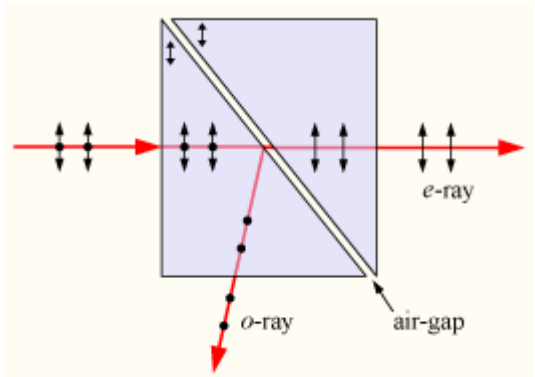

Figure 1.6: The beam splitting polarizer (Glan - Taylor). The ordinary ray (o-ray) is reflected at the air-gap while the extraordinary ray (e-ray) is transmitted through.

All LD measurements in this thesis are performed by using linearly polarized light which is produced by the beam splitting polarizer (Glan – Taylor polarizer is used for the LD measurements on a traditional UV-VIS spectrophotometer in the spectral region 15000 – 47000 cm^{-1}, and Rochon polarizer is used for the SRLD measurements in the spectral region 47000 – 58000 cm^{-1}). Structure of these polarizers is shown in figures 1.6 and 1.7.

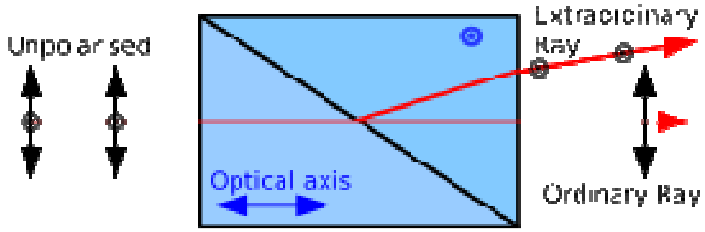

Figure 1.7: Rochon polarizer. Both ordinary ray (o-ray) and extraordinary ray (e-ray) are transmitted through, but the e-ray is deviated while the o-ray is not.

The linearly polarized light produced by either the absorptive or beam splitting polarizers always has much lower intensity than unpolarized light source. This limits the LD measurements performed on low concentration samples or samples that absorb and scatter light strongly.

1.2.5.1 Uniaxial samples

Anisotropic materials have been frequently used as a solvent to orient molecule in the LD measurements. Unfortunately, the molecules have just been partially aligned in these solvents, resulting in smaller number of molecules well oriented to stretching direction. When this sample interacts with the linearly polarized light, the LD will be low. This means that the difference in intensity of a particular band will be small in two linearly polarized directions. Among these materials, thin LDPE films are considered as a suitable solvent for aligning molecules, which shows better ability than other solvents. And molecules are also assumed to be aligned uniaxially in the stretched LDPE. With the assumption of uniaxial samples, the absorptive properties of aligned molecules in directions which are perpendicular to the stretching direction of LDPE are considered to be equivalent at microscopic level [29,30,32]. This leads to the fact that it is quite simple to measure the LD spectra and to understand and analyze the LD results with reliability.

When the linearly polarized light interacts with molecules aligned uniaxially, the two independent LD spectra can be obtained corresponding to the direction between the electric vector of light and the stretching axis. When the electric vector is parallel to the stretching axis, the observed LD spectra is denoted as E_U. And when the electric vector is perpendicular to the stretching axis, the E_V spectrum is obtained. In this experiment, the difference in intensity of absorption bands between E_U and E_V curves is linear dichroism. The illustration of this is shown in figures 1.8 and 1.9, and following expressions [27,29,30,32]:

$$E_U(\tilde{\nu}) = \sum_i A_i(\tilde{\nu}) \cdot \left\langle \cos^2(\vec{M}_i, U) \right\rangle \tag{13}$$

$$E_V(\tilde{\nu}) = \sum_i A_i(\tilde{\nu}) \cdot \left\langle \cos^2(\vec{M}_i, V) \right\rangle \tag{14}$$

$$LD = E_U - E_V \tag{15}$$

Where, $\vec{M}_i$ is moment vector of i^{th} transition, $\left\langle \cos^2(\vec{M}_i, U) \right\rangle$ and $\left\langle \cos^2(\vec{M}_i, V) \right\rangle$ are average values of cosine squared of angles which are composed of the electric vector and the moment vector of i^{th} transition of all molecules interacting with the polarized light.

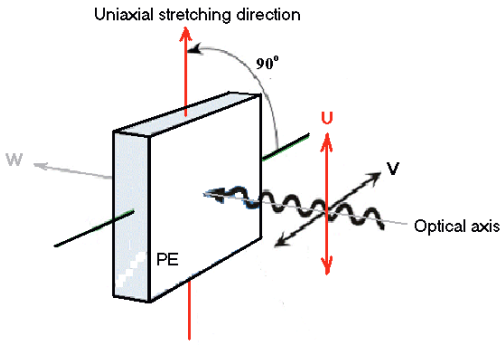

Figure 1.8: Interaction between uniaxial sample and linearly polarized light. Two linearly independent LD curves are obtained: one corresponds to the electric vector parallel to the stretching direction (E_U) and other corresponds to the electric vector perpendicular to the stretching direction (E_V)

Because electromagnetic radiation is a transversal wave which the electric and magnetic fields are perpendicular to each other and to the propagation of light, there is no electric vector in direction along the propagation of light. This is a reason to explain for the fact that the LD spectrum can not be measured in this direction. However, as the assumption above, the LD curve in this direction can be deduced from the other observed LD spectra in uniaxial samples as described in following expressions:

$$\left\langle \cos^2(\vec{M}_i, V) \right\rangle = \left\langle \cos^2(\vec{M}_i, W) \right\rangle \tag{16}$$

And with assumption of same number of molecules in light path:

$$E_V(\tilde{\nu}) = E_W(\tilde{\nu}) \tag{17}$$

In isotropic solvent, molecules are distributed randomly with equivalent probability; resulting in the interaction with the linearly polarized light would give equivalent absorbance in all directions. If the absorbance obtained from the interacton between unpolarized light and unoriented samples was considered as sum of the absorbance obtained from the interaction between linearly polarized light and oriented samples, this relationship would be described as below [27,29,30,32]:

$$3 \cdot E_{ISO} = E_U + E_V + E_W = E_U + 2 \cdot E_V \tag{18}$$

Where, E_{ISO} is absorbance of compound in isotropic solvent when interacted with unpolarized light. This expression shows that optical features of absorption bands are relatively similar but their intensities are changed in two different spectroscopic measurements: traditional and LD spectroscopy. And this leads to the fact that this relationship can be used to check the observed spectra in both methods, providing reliable data. This is shown in figure 1.9.

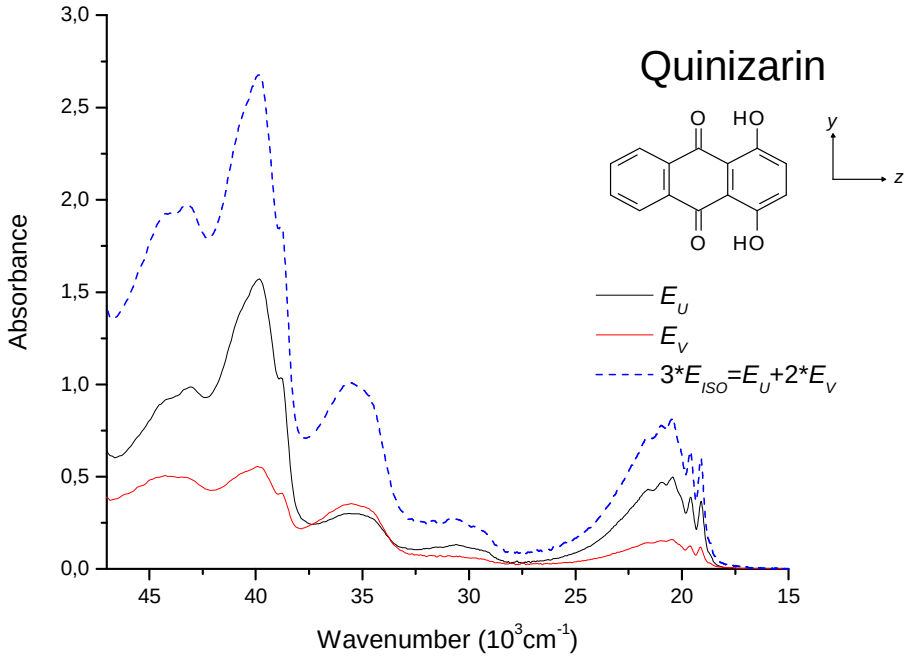

Figure 1.9: Isotropic and UV-VIS LD spectra of Quinizarin. The sample is partially aligned in stretched LDPE. The two LD curves (E_U - black and E_V - red solid curves) are measured at room temperature on a traditional UV-VIS spectrophotometer equipped with a rotatable Glan – Taylor polarizer. And the isotropic curve (E_{ISO} – dashed blue curve) is plotted by using equation (18).

1.2.5.2 Orientation factor

According to properties of cosine function, sum of square cosine function of a vector in directions of Cartesian coordinate system would be unity and shown as below:

$$\left\langle \cos^2(\vec{M}_i,U)\right\rangle + \left\langle \cos^2(\vec{M}_i,V)\right\rangle + \left\langle \cos^2(\vec{M}_i,W)\right\rangle = 1 \qquad (19)$$

From expressions (16) and (19), all square of cosine functions can be described and determined by a common quantity:

$$\left\langle \cos^2(\vec{M}_i,V)\right\rangle = \left\langle \cos^2(\vec{M}_i,W)\right\rangle = \frac{1}{2}\left(1-\left\langle \cos^2(\vec{M}_i,U)\right\rangle\right) \qquad (20)$$

This means that the average orientation of the transition moment vectors can be simply determined by value of angle composed of the transition moment vector and the main axis of the uniaxial sample or the stretching direction of the LDPE film. To simplify the determination and description of the direction of the transition moment vector $\vec{M}_i$ in following chapters, orientation factor, K_i, is used and defined as below [27,29,30,32]:

$$K_i = \left\langle \cos^2(\vec{M}_i,U)\right\rangle \qquad (21)$$

And substitutes the definition in expressions (19) and (20) to expressions (13) and (14), we can derive following expressions:

$$E_U(\tilde{\nu}) = \sum_i A_i(\tilde{\nu}) \cdot K_i \tag{22}$$

$$E_V(\tilde{\nu}) = \sum_i A_i(\tilde{\nu}) \cdot \frac{1}{2}(1 - K_i) \tag{23}$$

The orientation factor can be experimentally determined by the LD measurements. This factor can only provide information on the direction of vector $\vec{M}_i$ with respect to the stretching direction. This will not provide information on the direction of vector $\vec{M}_i$ in molecular coordinate system and of molecules with respect to the stretching axis. With the exception of molecular structure which is in rod shape and high symmetry, the molecules is assumed to be well aligned with the stretching direction, and the transition moment vector $\vec{M}_i$ is also oriented along to axes of molecular coordinate system. In this case, the information on the direction of the electronic transition moments can be obtained.

The difference in intensity of the absorption bands in the two LD spectra E_U and E_V shows that the moment vector $\vec{M}_i$ of transitions in molecular framework interacts differently with the electric vector $\vec{e}$ of the linearly polarized light, resulting in dichroic property of these optical features. And the dichroic property is defined in following equation [29,30,32]:

$$d(\tilde{\nu}) = \frac{E_U(\tilde{\nu})}{E_V(\tilde{\nu})} \tag{24}$$

Where, $d(\tilde{\nu})$ is dichroic ratio of a certain transtition. If $d(\tilde{\nu})>1$ ($E_U>E_V$), linear polarization is positive and vice versa, if $d(\tilde{\nu})<1$ ($E_U<E_V$), it is negatively linear polarization. In case of absorption bands that do not overlap with other differently polarized transitions, value of $d(\tilde{\nu})$ is calculated by following equation which is related to value of K_i:

$$d_i = \frac{2 \cdot K_i}{1 - K_i} \Rightarrow K_i = \frac{d_i}{2 + d_i} \tag{25}$$

But in case of overlapping absorption bands, the relationship between $d(\tilde{\nu})$ and K_i becomes more complicated, leading to difficulty of determination of orientation factor and dichroic ratio.

1.2.5.3 Trial-and-Error Method (TEM)

In practice, the determination of optical properties of the electronic transitions is relatively troublesome because of overlapping transitions. But fortunately, absorbance of optical features is additive property, that is, we assume the validity or applicability of Lambert-Beer's law, allowing determining the orientation factor of individual transition simply regardless of strongly overlapping bands [27,29,30,32].

The Trial-and-Error Method (TEM) bases on linear combination of the two LD spectra, E_U and E_V, and the orientation factor (or dichroic ratio). This linear combination is described in following equation [27,32]:

$$r_{K_i}(\tilde{\nu}) = (1 - K_i) \cdot E_U(\tilde{\nu}) - 2 \cdot K_i \cdot E_V(\tilde{\nu}) \qquad (26)$$

This equation will produce a family of spectral curves corresponding to variation of K_i value from 0 to 1. In this linear combination, the optical features will vanish when K_i value reaches to a value $K_i = K$ which K value varies from 0 to 1. The family of spectral curves provides a graphic method used to determine the orientation factor K_i simply. This is shown in figure 1.10.

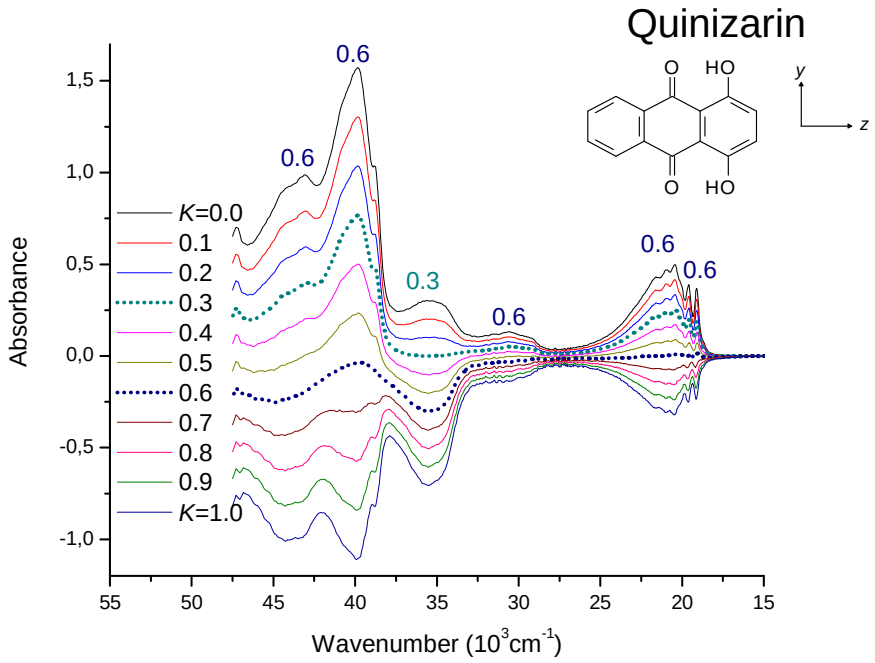

Figure 1.10: Trial-and-Error Method (TEM). The linear combination of the two independent LD curves (E_U and E_V) produces a family of reduced spectra. And value of orientation factor of an absorption band is visually determined as described in the text.

Depending on the molecular symmetrical properties, the information on the direction of the electronic transition moments can be extracted from the orientation factors which are determined by either expression (25) or TEM model, expression (26).

1.2.5.4 Molecular symmetry and partial absorption spectra

The electronic transition will result in redistribution of the electron density which is subjected to the molecular geometry and symmetry when the molecule interacts with light. Therefore, the electronic transitions are influenced and limited by the geometrical and symmetrical properties of molecules. In other words, the molecular geometry and symmetry are crucial factors in number of possible electronic transitions. And this also provides a convenient and simple method in order to analyze the LD spectra.

In case of "high" molecular symmetry, e.g., C_{2v}, D_{2h} and D_2, all possible transition moments are in directions along the axes *x*, *y* and *z* of molecular coordinate system [27,29,30,32]. And the orientation factors will be in three distinct groups of value corresponding to the orientation of transition moment vectors along *x*, *y*, *z* axes of molecular framework, $K_S = \left\langle \cos^2(\vec{s},U) \right\rangle$, with *s*=*x*, *y*, *z*. These values of the orientation factor are dependent and related to each other by expression (19), which means that:

$$K_x + K_y + K_z = 1 \tag{27}$$

Thereby, it is remarked that if molecular structure possesses high symmetrical property, the orientation factor will receive values belong to three distinct groups and vice versa, if the orientation factors obtained experimentally from the LD measurements are belong to three distinct groups, the molecular symmetry will probably be high. As a consequence, if the orientation factor has more than three distinct values, the molecular symmetry will be low and vice versa [29,30].

In principle, absorption bands of molecule can be described as three partial absorption curves which belong to three axes of molecular coordinate system, $A_S(\tilde{\nu})$ with *s*=*x*, *y*, *z* as in the expressions (11, 13, 14). This is done by using the obtained value of the orientation factor. Each partial absorption curve is considered as a sum of absorbance of all possible transitions in corresponding molecular axis. And it is described as below expression [27]:

$$A_S(\tilde{\nu}) = \sum_{i:s} A_i(\tilde{\nu}) \tag{28}$$

Where, the sum is calculated for all i^{th} transitions which are polarized in the *s* direction.

However, only two independent LD spectra are measured in practice, and therefore, the absorption bands of molecule can only be described as two partial absorption curves corresponding to E_U and E_V spectra. There are three situations of special molecular shapes that are considered to be able to obtain all partial absorption curves from the two observed LD spectra. These molecular shapes are: (1) disc-like, (2) rod-like and (3) aromatic planar molecules in which out-of-plane polarized intensities are assumed to be negligible in the visible and near ultraviolet regions. Among these cases, truly disc-shaped and rod-shaped molecules are relatively rare in practice [29,30].

There are π planar orbitals in aromatic molecules, and transitions between electronic states corresponding to energy in UV-VIS spectral region are assumed to be mainly from π - π^* transitions which are in-plane polarized, called *yz* plane. Intensity of out-of-plane polarized transitions is relatively small or negligible, resulting in the partial absorption curve in this direction is almost zero, $A_x(\tilde{\nu}) = 0$. And the partial absorption curves in *y* and *z* directions are described in following expressions [29,30]:

$$A_y(\tilde{\nu}) = \frac{(1-K_y)\cdot E_U(\tilde{\nu}) - 2\cdot K_y \cdot E_V(\tilde{\nu})}{K_y - K_z} \tag{29}$$

And

$$A_z(\tilde{\nu}) = \frac{(1-K_z)\cdot E_U(\tilde{\nu}) - 2\cdot K_z \cdot E_V(\tilde{\nu})}{K_z - K_y} \tag{30}$$

According to expressions (29) and (30), the partial absorption curves can be plotted in following graph with clear remark on molecular axes.

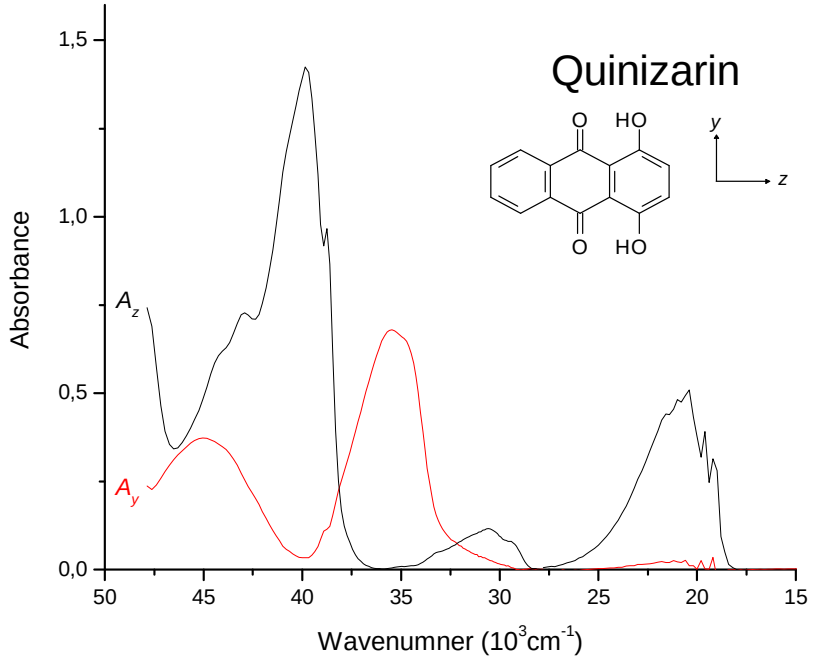

Figure 1.11: The partial absorption curves of Quinizarin. This compound belongs to "high" molecular symmetry with C_{2v} point group. The black curve (A_z) and the red curve (A_y) describe absorption bands whose electronic transition moment are in direction along the long in-plane axis (z) and the short in-plane axis (y) of molecular framework, respectively.

In case of "low" molecular symmetry, e.g., C_{2h}, C_2 and C_s, it is not easy and simple to analyze and extract information from the observed LD spectra because the direction of the transition moment vector is not limited by the molecular symmetry, for example, transitions of molecule which belongs to C_s symmetry are polarized in the molecular plane or in directions which are perpendicular to it. And the transitions of molecule which is in C_{2h} and C_2 groups are polarized along the molecular axis of symmetry or in any directions perpendicular to it [27,29,30,32]. The values of orientation factor will belong to many distinct groups.

The molecules belonging to "low" symmetrical group (C_{2h}, C_2, C_s) will be placed into a molecular coordinate system which molecular plane (if possible) is in the same position as *xy* plane, or molecular axis of symmetry (if possible) coincides with *z* axis (see figure 1.12). For instance, in a particular molecule, that is, Anthrarufin with C_{2h} point group, long in-plane axis of molecule will be along direction which distance between atoms is longest (*x* axis in figure 1.12). And it is assumed that this axis is close to the effective orientation axis. The axis perpendicular to the long in-plane axis is called short in-plane axis of molecule (*y* axis in figure 1.12). And out-of-plane axis of molecule is perpendicular to the molecular plane (*z* axis in figure 1.12).

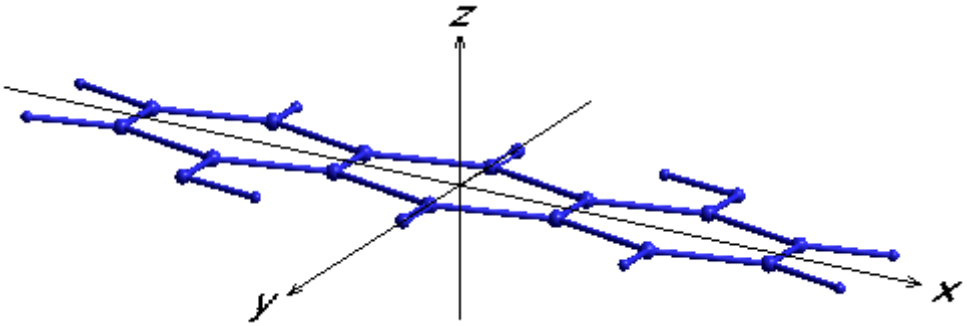

Figure 1.12: Illustration of molecular coordinate system (case of Anthrarufin): xy plane is also a molecular plane, x and y axes are considered as long and short in-plane axes, respectively, and z axis is out-of-plane axis.

Depending on author's conventions, the label of molecular axes will be different but the values of orientation factor which are extracted from the observed LD spectra of corresponding molecular coordinate system are unchanged.

In case of planar molecules, the molecular plane is also symmetrical plane. And the out-of-plane transitions are polarized along *z* axis according to above conventions. The orientation factor in this direction will be denoted as K_z. And the in-plane transitions are polarized along directions in the molecular plane, leading to the fact that the determination of directions of transition moments is complicated in the molecular framework [27,29,30,32].

However, in stretching LDPE method, the molecular orientation axis is the one that on the average is most efficiently aligned with the stretching direction. The in-plane transitions will form different angles with this axis, resulting in different values of the orientation factor. Transitions in direction of molecular axis (*x* axis) correspond to largest average values of the orientation factor, $K_x=\langle\cos^2(x, U)\rangle$. If the value of these orientation factors, K_x, K_y can be determined, the angle composed of the transition moments and the molecular axis is calculated as described in following equation [29,30].

$$\tan^2\phi_i = \frac{K_x - K_i}{K_i - K_y} \tag{31}$$

Where, K_i is experimental values of the orientation factor (as mentioned in 1.2.5.3 section), ϕ_i is angle composed of the moment vector $\vec{M}_i$ and the molecular orientation axis. The value of ϕ_i obtained from equation (31) only provides numeric value, but do not show sign of the angle which describes direction of vector $\vec{M}_i$ in molecular framework because ϕ_i values can be positive or negative. Polarized fluorescence spectroscopy can provide necessary information so as to determine the relative signs of the ϕ_i [15].

According to the conventions in figure 1.12, the value of the orientation factors is arranged in increasing order as below:

$$K_z \le K_y \le K_x \tag{32}$$

In case of transitions which are in-plane polarized, the value of the orientation factors is in following range:

$$K_y \leq K_i \leq K_x \tag{33}$$

And from expression (27), following expression can be derived:

$$K_x + K_y = 1 - K_z \tag{34}$$

The value of K_z, out-of-plane polarized transition, can be obtained from TEM model based on infrared linear dichroism (IR LD) measurements [14]. And combining with expressions (32-34), value of K_x and K_y can be estimated by using experimental value of K_i and K_z. In this case, K_y can accept maximum value which is less than or equal to the minimum of experimental value of K_i:

$$K_{y,\,\max} \leq K_{i,\,\min} \tag{35}$$

And K_x can accept values which are in range from the maximum of experimental value of K_i to $(1 - 2 \cdot K_z)$:

$$K_{i,\,\max} \leq K_x \leq 1 - 2 \cdot K_z \tag{36}$$

Combining with information on the molecular shape, the proper value of K_y and K_x can be determined. If molecules are disc-shaped structure, the relationship between the orientation factors will be [29,30]:

$$K_y = K_x = \frac{1 - K_z}{2} \tag{37}$$

If molecules are rod-shaped structure, the relationship will be as following expressions [29,30]:

$$K_x = \frac{1 - K_z}{2} \tag{38}$$

And

$$K_y = K_z \tag{39}$$

The relationship between the molecular shape and the experimental value of the orientation factors has been described and proved in hundreds of aromatic compounds possessing differenlyt molecular geometry and symmetry. This is a useful reference which is used to estimate values of the orientation factor of organic compounds (see figures 1.13 and 1.14).

And according to equations (29) and (30), the partial absorption curves of transitions can be calculated and plotted by using the value of the orientation factors which have just been determined.

In summary, the LD spectroscopic method provides useful information on the electronic transition moment directions, resulting in resolution of overlapping, differently polarized transitions and assignments of the molecular symmetry. This information is of significant importance in research of molecular theory.

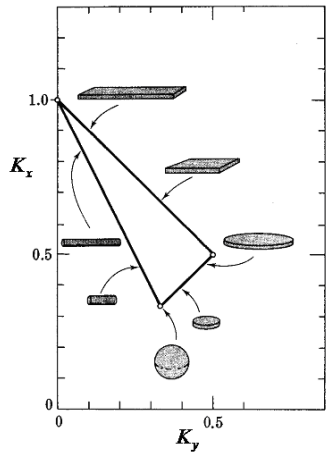

Figure 1.13: The relationship between molecular shape and orientation factor (This figure is taken from: J. Michl, E.W. Thulstrup, Spectroscopy with polarized light. Solute alignment by photoselection, in liquid crystals, polymers and membranes, VCH publishers, Inc., New York 1986, 1995) with slight modification on axis labels according to the convention in figure 1.12.

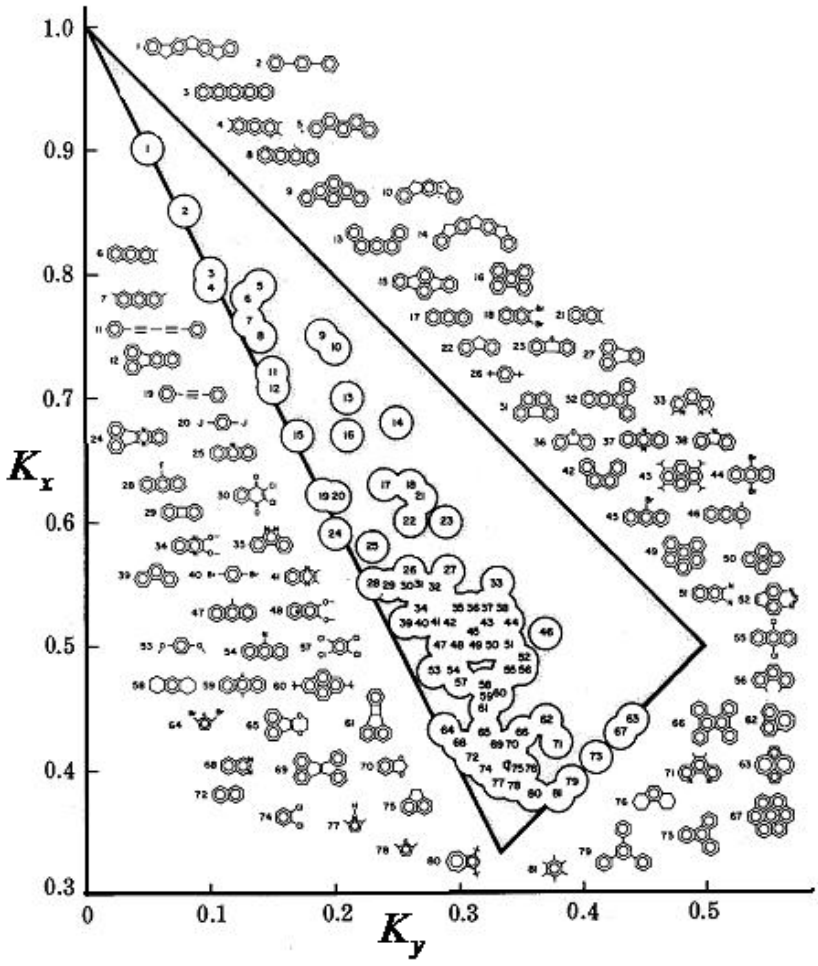

Figure 1.14: The relationship between molecular shape and experimental value of orientation factor (This figure is also taken from: J. Michl, E.W. Thulstrup, Spectroscopy with polarized light. Solute alignment by photoselection, in liquid crystals, polymers and membranes, VCH publishers, Inc., New York 1986, 1995) with slight modification on axis labels according to the convention in figure 1.12.

1.3 Synchrotron radiation

In these studies, synchrotron radiation (SR) is used as a photon source for LD measurements, because of its high photon flux in a wide spectral region that gives highly intense and collimated radiation and a continuous spectrum compared to a xenon arc lamp. The basic principles and general structure of a SR system as well as its striking properties will only be briefly described here, the theoretical and experimental aspects of producing SR can be found in more detail in the literature.

Synchrotron radiation is a term that is used to describe electromagnetic radiation which is emitted from charged particles when they move with velocities close to the speed of light in a circular trajectory. These charged particles are accelerated by electric and magnetic fields in a circular system which is called a Synchrotron [35]. In its early history, SR was considered to be a useless and harmful by-product radiation which is generated in circular accelerators [35], but it has since become of great interest and is utilized in many application fields, especially in materials science, as an intense and versatile photon source [35-38]. SR covers a wide spectral region from the infra-red to X-rays, and is a powerful photon source for spectroscopy in the energy region ranging from the visible to X-rays [35-38].

1.3.1 Production of synchrotron radiation

The SRLD spectra of compounds investigated in this thesis were measured using the CD1 beamline on the storage ring in Aarhus called ASTRID – Aarhus Storage Ring in Denmark.

The ASTRID storage ring is actually a square with a circumference of 40 m consisting of four 90^{o} bends and four straight sections [39]. A schematic diagram of the ring is shown in figure 1.15.

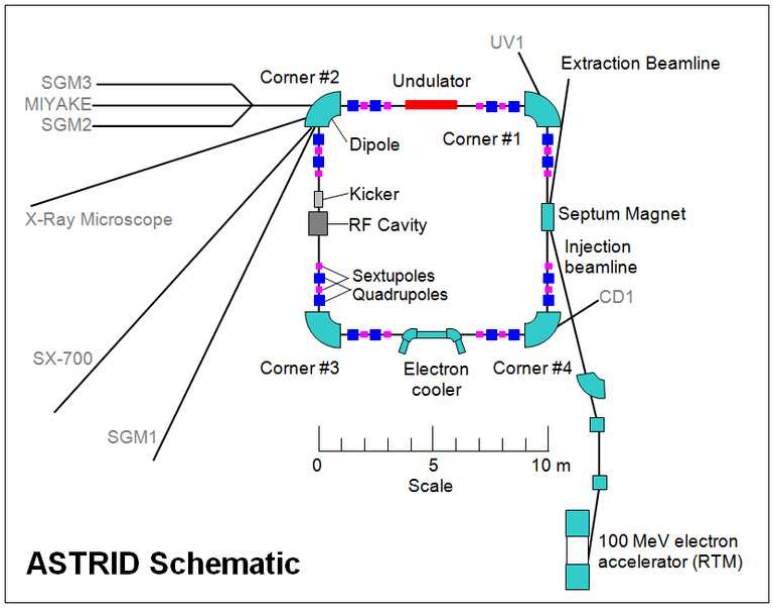

Figure 1.15: Schematic of the ASTRID storage ring at Aarhus University, Denmark. The SRLD measurements are performed at CD1 beamline located at Corner #4 in the figure.

The magnetic system consists of four sets of two 45^{o} dipole bending magnets and four groups of four quadrupoles focusing magnets which bend and focus the electron beams in the ring, respectively, and two groups of eight sextupoles for chromaticity correction. The ring is kept under ultra-high vacuum (UHV) conditions with 24 ion pumps. The electrons are generated from a 100MeV race-track microtron and injected into the ring via an electrostatic septum in 4-5 mA pulses. The electrons are captured by a 105 MHz RF system which bunches and accelerates the electrons to 580MeV with negligible loss of beam when the electrons pass through the RF cavities. The loss energy is compensated by acceleration the electrons in the electric and magnetic fields. The electrons are stored in the ring circulating at relativistic velocities for many hours, with a lifetime of the beam of 100 – 120 hours for a 160 mA stored beam [39].

1.3.2 Advantages of synchrotron radiation

Because SR is emitted by deflection of the high density electron stream which travels in circular path at relativistic velocities, it has many outstanding properties such as high collimation, high intensity and stability, high degree of polarization and a wide continuous spectrum compared to other photon sources [35,38].

High collimation and intensity provide a high brilliance of SR [35,38] which propagates longer distance without losing intensity, and improves the signal to noise ratio in data collection. Therefore, spectroscopic measurements could be performed for low concentration samples or samples which absorb and scatter light strongly.

A high degree of polarization is an important property of SR compared to those from other photon sources which normally generate unpolarized light. However, SR can only obtain highly linear polarization in a plane of the electron orbit. Radiation which is not along the orbital plane changes its polarity, from elliptical to circular polarization corresponding to divergence of SR from the electron orbit [35,38]. Therefore, a linear polarizer is used to ensure the highly linear polarization of SR in all LD measurements which is discussed further in the next section.

1.3.3 The CD1 beamline and experimental setup

Along the circular path in the bending magnets, the electrons lose energy and emit SR in a tangential direction of the electron orbit. There are eight beamlines on ASTRID, utilising radiation from both the bending magnets and from an undulator. In each beamline, SR passes through an appropriate monochromator system to generate a specific radiation of interest which is used for spectroscopic experiments.

In the CD1 beamline (Figure 1.16 shows a schematic of the beamline), SR is reflected by a plane mirror into a toroidal grating. The grating is optimized for high 1st order flux and low 2nd and 3rd order flux in the wavelength range of 115 – 500 nm. The typical flux from the beamline is $1 \cdot 10^{12}$ photons/sec and it has a resolving power of 500 (approximately 0.5 nm). The monochromator is kept under ultra-high vacuum conditions and separated from the sample compartment by a CaF_2 window [39].

The SR then passes through an exit slit, the rochon polarizer, through the sample and into the detector.

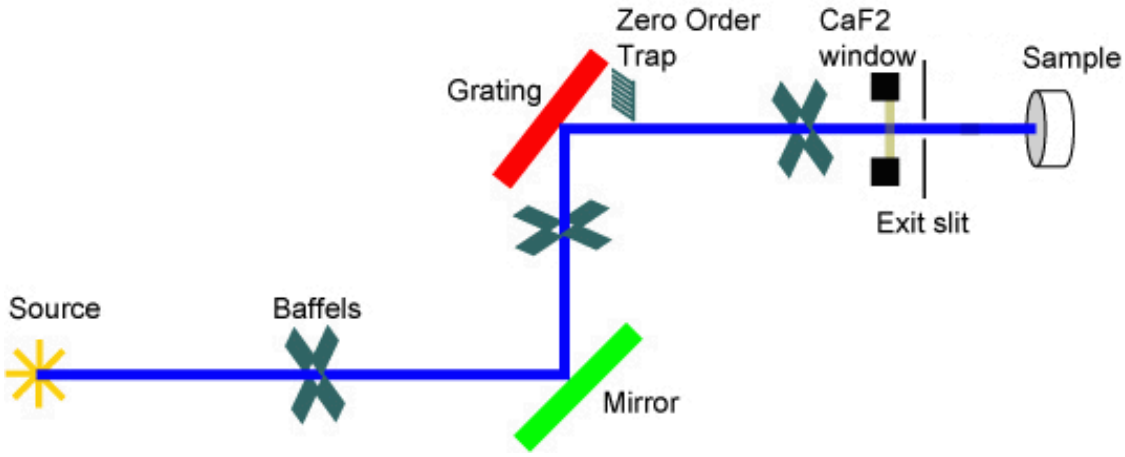

Figure 1.16: Schematic of the CD1 beamline on the ASTRID storage ring. The monochromator is operated at beamline vacuum and separated from sample compartment by a CaF_2 window. This figure is taken from http://www.isa.au.dk/facilities/astrid/beamlines/cd1/CD1OpticalSpecs.asp (June 24th, 2010) with a slight modification. The PEM (Photo Elastic Modulator) component which is placed before sample holder and used to convert linearly polarized light to circularly polarized light in synchrotron radiation circular dichroism (SRCD) spectroscopy is removed.

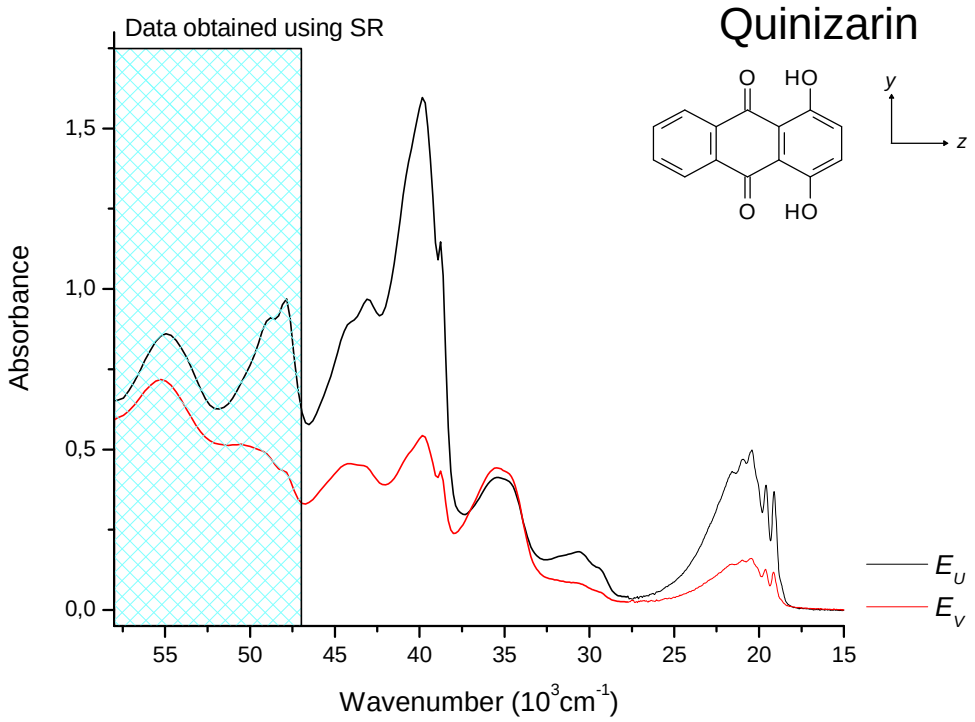

Figure 1.17: The SRLD spectra of Quinizarin with extended spectral region ca. 11000 cm^{-1} (from 47000 cm^{-1} to 58000 cm^{-1}). The sample is partially aligned in stretched LDPE. The two LD curves (E_U - black and E_V - red solid curves) are measured at room temperature in spectral region from ca. 27000 cm^{-1} (360 nm) to ca. 58000 cm^{-1} (170 nm) at the CD1 beamline on the ASTRID storage ring at the Institute for Storage Ring Facilities (ISA), Aarhus University. The low energy absorption band is measured at room temperature on a traditional spectrophotometer (UV-VIS scanning spectrophotometer – UV-2101PC Shimadzu) at our laboratory, Roskilde University.

As a result, the SRLD measurements improve significantly signal to noise ratio due to high flux of photon of SR, and provide more optical information in high energy region compared to traditional spectroscopic measurements using Deuterium lamp as photon source (as shown in figure 1.17). This is a great advantage for the measurements using LDPE as an anisotropic solvent because LDPE absorbs and scatters light strongly which leads to severe baseline problems in the high energy spectral region (above 47000 cm^{-1}). Unfortunately, the baseline problem can not be removed completely, we have to prepare and measure several samples until reliable SRLD spectra are obtained. The good SRLD measurements produce reliable polarization data of compounds aligned in stretched LDPE matrix, resulting in better and more precise information on orientation factors [22].

1.4 Quantum chemical calculations

Quantum chemical calculations have been applied to predict spectroscopic characteristics of absorption bands of compounds in UV-VIS spectral region for many decades. These methods are Configuration Interaction (CI) [40], Semi-empirical (INDO/S, ZINDO/S, PM3, LCOAO …) [41,58], and Density functional theory (DFT, TD-DFT …) [42-44] which have been applied for prediction of energy and electronic states of several hundred organic compounds. Among these methods, density functional theory method shows better precision and is less expensive than other so-called ab initio methods, becoming useful method which is commonly used in many studies in recent years [45-47]. In particular, it has been applied successfully for prediction of the electronic transitions of anthraquinone and its derivatives [22,48,49].

Therefore, this method is chosen and applied for the prediction and assignment of the electronic transitions of organic compounds of interest in this thesis.

Density functional theory (DFT) with B3LYP model and 6-31G(d,p) basis set is used to optimize geometry of compounds. And time-dependent density functional theory (TD-DFT) with B3LYP and basis set 6-31G+(d,p) is applied for prediction of the electronic transitions of compounds, basing on optimized geometry which is obtained from DFT calculation [50,51]. These calculations predict well for the electronic transitions of compounds in UV-VIS region in previous studies [22]. They are, therefore, used to predict and assign for transitions in the high energy region which can be observed by the SRLD measurements.

As will be shown in following chapters, this computational method predicts well for transitions in the near UV-VIS region. Because transitions are dense and overlapped strongly in the high energy region, resulting in complication of determination of precise information on these transitions, we can only predict and assign for predominant transitions in this region for all compounds investigated here.

In some cases, this computational method can not provide results which are in good agreement with the observed spectra due to errors in functions of density functional theory [52-57]. And this is the case of hydrocarbon compounds which have conjugated π system studied here, TD-DFT calculations become lengthy and expensive. Sometimes, the calculations exhibit convergence problems. Therefore, another calculation method, a semi-empirical method (LCOAO) is developed and applied for this group [58]. The results show that LCOAO is an inexpensive method which can be used to predict and assign for transitions of the hydrocarbons in the present study.

In general, quantum chemical calculations are a useful tool which is commonly used to predict and assign for the electronic transitions of organic compounds.

Chapter 2

Experimental

All LD measurements are performed in required conditions as described in above section of chapter 1 (linear dichroism spectroscopy, 1.2.5). This chapter will describe in more detail about experimental procedures such as sample preparation, LD measurements with traditional spectrophotometer and synchrotron radiation.

2.1 Aligned samples

Molecules can be oriented in a certain direction by different methods such as (1) single crystals, (2) electric or magnetic field, (3) flow field, (4) photoselection, and (5) anisotropic solvents [29,30].

As mentioned above, stretched LDPE is used as an anisotrpic solvent for aligning molecules throughout experiments in this thesis. It is considered as a simple and inexpensive technique which can be used to align molecules with highest orientation compared to other methods and be applied for both small and medium sized molecules.

The polymers which are commonly used to align samples in the LD measurements are polyethylene (PE) and poly(vinyl alcohol) (PVA). PE is usually compatible with non-polar compounds and PVA is used for polar compounds [29,30,32].

PE is still a material which is mainly used as an anisotropic solvent in the LD spectroscopic studies at optical laboratory at Roskilde University because many organic molecules can be introduced into PE matrix and be partially or well aligned in this solvent, providing much LD polarization data of absorption bands in UV-VIS region (below 47000 cm^{-1} for traditional spectrophotometer, and below 58000 cm^{-1} for synchrotron system) and IR region. However, in IR measurements, PE absorbs strongly in some wavenumber ranges such as 720-750 cm^{-1}, 1440-1480 cm^{-1}, and 2800-3000 cm^{-1}, we can not observe absorption bands of compounds in these ranges. This disadvantage can be solved by using deuterated PE for the IR measurements [27,29,30]. The IR LD spectra of PE are shown in figure 2.1.

PE is composed of crystalline and non-crystalline structures whose ratio is a crucial factor in forming properties of PE. If crystalline structure is predominant, PE is considered as high-density polymer. And vice versa, if non-crystalline structure is predominant, PE is classified into low-density polymer group. Structure of low-density PE (LDPE) usually contains chains with about thousand of carbon atoms which form about 20-30 branches, and about 40-55% of crystalline structure [61,62]. This leads to the fact that LDPE is soft, easy to stretch, and high transparency. And especially, there is more space in polymer lattice to contain molecules of organic compounds, increasing concentration of compound which is introduced into polymer matrix. Figure 2.2 shows the structure of low-density PE (LDPE) and high density PE (HDPE).

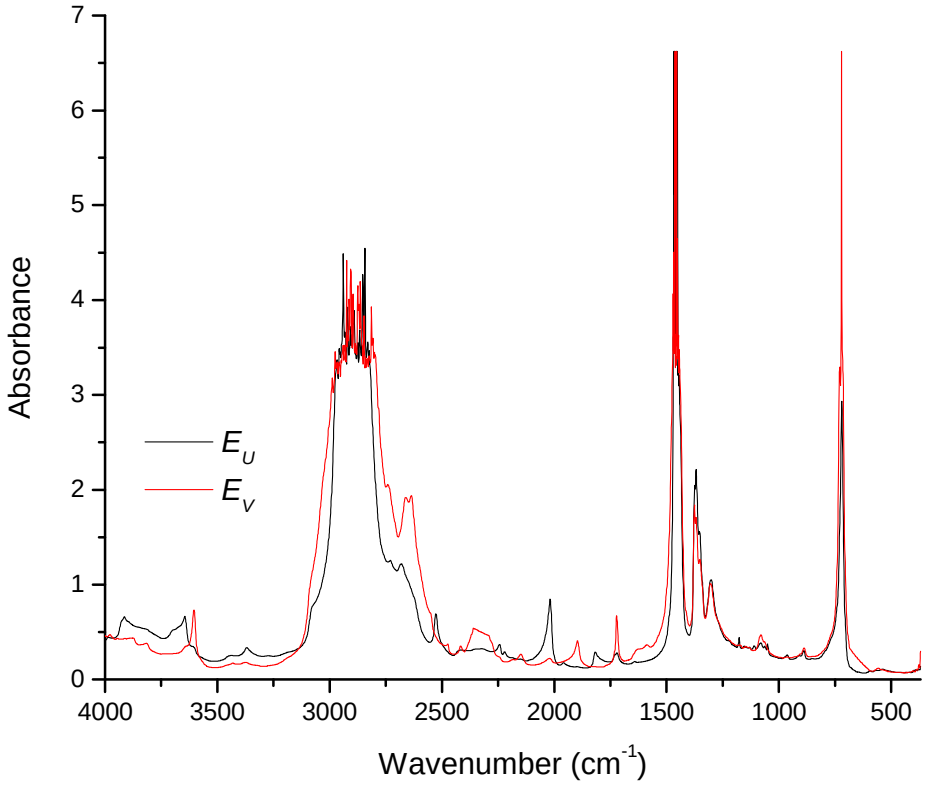

Figue 2.1: Baseline absorption of thick LDPE in IR spectral region. The two LD curves are measured at room temperature on a FT-IR spectrophotometer equipped with a rotatable aluminium grid polarizer.

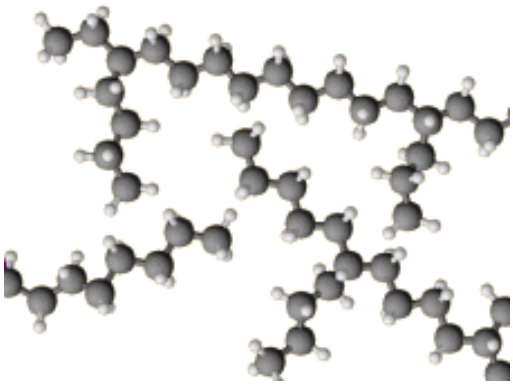

Structure of low-density polyethylene (LDPE)

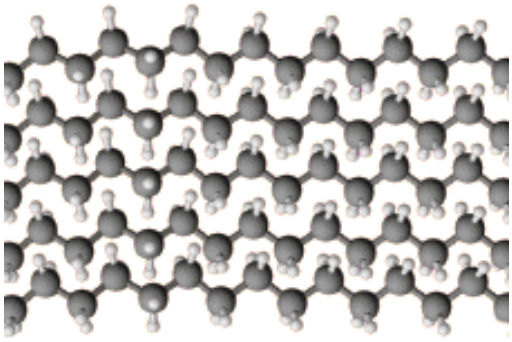

Structure of high density polyethylene (HDPE)

Figure 2.2: Structure of polyethylene

In principle, branches of LDPE can be used to partially align molecules with stretching direction at different temperature as LDPE is stretched in a certain direction [29]. And the orientation of molecules depends on the nature of polymer matrices and compounds. Therefore, different molecules will be aligned differently in the polymer matrix. Figure 2.3 illustrates the alignment of branches in LDPE structure which is used to orient molecules.

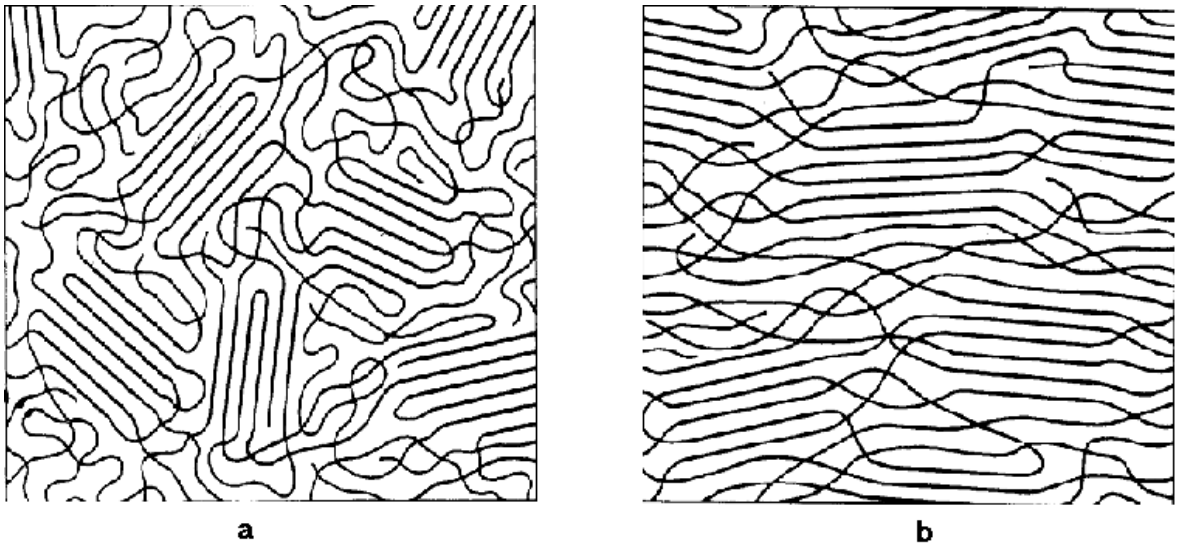

Figure 2.3: Illustration of LDPE structure including amorphous and crystalline structures (the branching structure is not shown). (a) In unstretched LDPE, the polymer chains in amorphous region are distributed randomly generating more space that solute can penetrate into; (b) In stretched LDPE, the polymer chains in amorphous region are aligned with the stretching direction leading to the alignment of solutes.

The most advantage feature of using LDPE as a solvent is a negligible interaction between LDPE and molecules which can be considered as an inert stretching medium. Molecules which are oriented in this solvent behave similarly to ones in gas phase. This simplifies the computational procedure, and improves consistency between calculated and experimental results.

2.2 Sample preparation

PE is obtained from commercial sources (Hinnum Plast, DK-4760 Vordingborg, Denmark) which is a LDPE and 100µm of thickness.

The LDPE is cut into small sheets in dimensions 2.5cm×6cm. These PE sheets are washed by chloroform at 50^{o}C for a day to extract and eliminate impurities and additives which are used to improve properties of polymer during manufacture of the LDPE. Depending on desired properties of PE, the additives are different in component. The additives which are commonly used in manufacture of PE are BHT, BHEB, Isonox 129, Irganox 1010, and Irganox 1076 [64].

In addition to eliminating additives, washing procedure also extracts short chains of polymer in the polymer matrix, generating low baseline absorption PE sheets [65].

After washing, PE sheets are ready for sample preparation. If we are lucky, the compound can sublimate directly into the LDPE matrix, otherwise chloroform is used as a solvent to introduce solute into the LDPE. The LDPE sheets will be submerged in saturated chloroform solution of compound in a sealed container at 50^{o}C. Sealed container and temperature are used to improve penetration of molecules into the LDPE matrix, achieving enough concentration of compound for the LD spectroscopic measurements.

Besides, ultrasound can also be used as an improving tool to increase the concentration of compound in the polymer matrix [29,30]. In case of compounds which are easy to penetrate into the LDPE matrix, it is not necessary to use ultrasound and temperature, and sample preparation procedure can be performed in shorter time than the procedure of compounds which are difficult to introduce into the polymer matrix. In latter case, the ultrasound and elevated temperature should be used, and the procedure frequently takes longer time to get enough concentration in the LDPE matrix.

However, when temperature is applied to sample preparation procedure, boiling point of chloroform becomes significant importance because high pressure will cause an expansion of the sealed container at elevated temperature which is higher than the boiling point of chloroform.

After submerging in the chloroform solution of compound for a certain time, the LDPE sheets are taken out for solvent (chloroform) evaporation. Because chloroform absorbs strongly in UV region, it is essential to completely evaporate chloroform from the LDPE matrix. Figure 2.4 shows absorption curve of several solvents which are commonly used in laboratories.

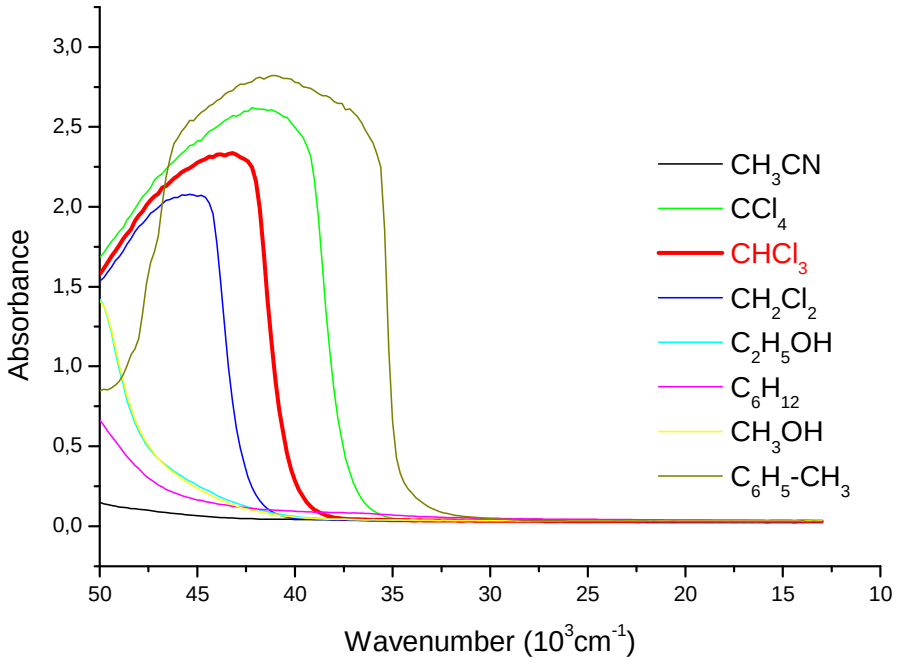

Figure 2.4: The UV-VIS absorption curve of pure solvents is measured at room temperature on a traditional spectrophotometer. The distortion of the absorption curves is due to high absorbance.

The evaporation rate of solvent (chloroform) is subjected to thickness of the polymer sheet. This means that the thicker the polymer sheet, the slower the evaporation rate. It takes longer time for chloroform to evaporate from the thicker LDPE sheet. Unfortunately, the concentration of compound in polymer matrix decreases as a function of time. Therefore, it is necessary to choose a compromised condition between the evaporation of chloroform and the loss of the concentration of compound which ensures enough concentration and less chloroform for measurements. In case of thin LDPE sheets which are used in this thesis, the evaporation of chloroform is less than one hour.

Any crystal of compound on surface of the LDPE sheet is cleaned by methanol or ethanol because the crystal will not be aligned as molecules in stretched polymer matrix, but it still absorbs light, causing errors in the LD measurements.

Afterward, the cleaned LDPE sheet is stretched approximately 500% by mechanical stretcher at room temperature. Because the orientation of molecules in the stretched polymer matrix varies significantly as the polymer is stretched less than 400% (100 – 400%) while it almost unchanges when the polymer is stretched more than 400% [29,30]. Although, this leads to advantage that it is not necessary to stretch polymer too much, the LDPE sheets should be stretched in the same conditions to eliminate difference in thickness causing baseline problem in the LD measurements, especially in UV region.

The stretched LDPE sheet is held on plastic frame to keep its surface always flat and perpendicular to the propagation of linearly polarized light during the LD measurements. And the plastic frame is marked with clear arrow symbol which indicates the stretching direction of polymer sheet in order to ensure that the sample is placed identically in the sample compartment for both E_U and E_V measurements.

The LDPE blank is prepared in exactly the same conditions as samples, but the polymer sheet is submerged into pure chloroform solvent instead of chloroform solution of compound.

Apart from LDPE, PVA is occasionally used as an anisotropic solvent for LD measurements. The casting procedure and sample preparation of PVA sheets are described in Appendix 1.

2.3 Chemical information

All chemicals are obtained from commercial sources or synthesized according to standard procedure [66]. Their purity is checked by comparing their solution spectra with those in standard literature.

Hydrocarbons:
1,4-Bis(phenylethynyl)benzene (BPEB): Fluorochem, 97%
Diphenylacetylene (DPA): Aldrich, 98%
Diphenylbutadiene (DPB): Aldrich, 98%
Diphenylhexatriene (DPHT): Aldrich, 98%
Distyrylbenzene (DSB): ChemDiv, >95%
p-Terphenyl: Aldrich, 99%
Trans-Stilbene: BDH chemicals Ltd. Poole England, 97%

***Heterocycles*:**
2,2´-Bithiophene: Aldrich, 97%
Carbazole: Ega-chemie, 98-99%
Dibenzofuran (DBF): Aldrich, 99%
Dibenzothiophene (DBT): Aldrich, 99%
Dibenzo-p-dioxin (DpD): TCI Europe nv, >99%
Dibromo diphenyl ether: Aldrich, 99%
Diphenyl ether: Lancaster synthesis, 99%

2,5-Diphenylfuran: Alfa-Aesar, 98%
2,5-Diphenylthiophene: TCI Europe nv, >98%
Fluorene: Aldrich, 98%
Terthiophene: Aldrich, 99%

***Hydroxy anthraquinones*:**
Alizarin: Sigma-Aldrich, 97%
Anthralin: Sigma, 97%
Anthrarufin: Lancaster synthesis, 90%
Chrysazin: BDH chemicals Ltd. Poole England, 98%
Cynodontin: APIN chemicals Ltd.,
Naphthazarin: Aldrich-Chemie, 95%
Naphthoquinone: Aldrich-Chemie, 96%
Purpurin: Acros organics, 98%
Quinizarin: reference 66

In following section, the sample preparation procedure is described in detail for compounds that are investigated in this thesis.

As mentioned above, the compounds of interest can be introduced into the LDPE matrix by two methods such as submersion of the LDPE sheets into their chloroform solution, and sublimation of compounds into the LDPE sheets. The former can be applied for chemicals which are high boiling point and low vapour pressure while the latter can be used to introduce compounds which are low boiling point and high vapour pressure into the LDPE matrix.

In the submersion method, chemicals are dissolved in chloroform solvent until saturated concentration in the sealed container. Depending on solubility of chemical in chloroform solvent and their penetration into the LDPE matrix, other factors such as temperature, ultrasound and longer submersion time can be used to improve the concentration of compound in the LDPE matrix.

Chemicals which can be introduced into the LDPE matrix by the submersion method are anthralin, chrysazin, naphthoquinone, naphthazarin, quinizarin, stilbene, diphenylbutadiene, p-terphenyl, diphenylacetylene, diphenylthiophene, bithiophene, terthiophene, diphenylfuran, diphenyl ether, dibromo diphenyl ether, dibenzo-p-dioxin, fluorene, dibenzofuran, dibenzothiophene. The LDPE sheets are submerged into the saturated chloroform solution of these chemicals in the sealed container at room temperature for a week. In this condition, molecules penetrate slowly into the polymer matrix, and the concentration is not high but it is enough for the LD measurements. The elevated temperature can be used to increase the concentration and obtain better intensity of absorption bands. The highest temperature which can be used for this method in the present study is 50^{o}C because of the use of chloroform solvent. At elevated temperature, the penetration of molecules into the LDPE matrix takes place quickly, obtaining higher concentration of compound in the LDPE. Hence, submersion time will shorten in about three days. When the LDPE sheet is submerged in solution at elevated temperature, it is important to take it out of the solution at the same condition after a certain desired period of time because there are different equilibriums of concentration of compound in the solution and in the LDPE matrix at different temperature. This means that if the LDPE sheet is submerged into the solution at the elevated temperature but is taken out at room

temperature, the concentration of compound which penetrated into the polymer is equivalent to those obtained in case of submersion at room temperature. In this case, although it is impossible to increase the concentration, the submersion time can be shortened, leading to high sample throughput.

Chemicals such as alizarin, anthrarufin, cynodontin, purpurin, distyrylbenzene, bis(phenylethynyl)benzene, diphenylhexetriene can also be introduced into the LDPE matrix by the submersion method. But these experiments are performed at different conditions including elevated temperature and ultrasound because it is quite difficult to introduce enough concentration of these chemicals into the LDPE at the above conditions. These solutions are placed in an oven at 50^{o}C for a week, and are sonicated thirty minutes every day during experiment. After finishing submersion, the LDPE sheets are taken out at the elevated temperature as discussed above.

In case of chemicals which are difficult to introduce enough concentration into the polymer even at the elevated temperature and ultrasound conditions, thicker LDPE sheets are used and longer submersion time is needed. Although the thicker LDPE sheet can improve the concentration of compound in lightpath, it can cause several disadvantages such as high baseline absorption, strongly scattering and depolarizing light, affecting the LD measurements, especially in UV region [29,30]. And it is more important fact that the SRLD measurements can not be performed by using the thicker LDPE sheets in the UV region.

In the sublimation method, crystals of chemicals are contained in a sealed bottle. The LDPE sheets are put into bottle and above crystals. Vapour pressure of chemical increases gradually in the sealed bottle and gas molecules penetrate into the LDPE matrix. Depending on properties of chemical, the penetration can take place quickly or slowly. Elevated temperature can be used to accelerate the penetration of molecules and shorten experimental time. It takes long time for molecules to penetrate into the LDPE matrix in this method in order to obtain enough concentration for measurements, but it is convenient and useful method for the LD measurements in the IR region because of no solvent absorption bands.

Carbazole compound is introduced into the LDPE sheet by using the sublimation method. The LDPE sheets are put into the sealed bottle containing crystals of Carbazole at 50^{o}C for a day. After finishing the sublimation procedure, the LDPE sheets are taken out at the elevated temperature. Residue crystals on LDPE surface can be cleaned with ethanol or methanol. The blank is prepared in the same conditions but without crystals of carbazole.

Solvents

Chloroform, Methanol and Ethanol used in all experiments are high grade solvents (spectroscopic quality).

Chloroform is chosen as a solvent for washing the LDPE sheets and dissolving chemicals because it can swell the LDPE matrix which generates more space in polymer structure, and can extract impurities and additives from the polymer, as well as introduce molecules of interest into the polymer as mentioned above. And it also evaporates easily from the LDPE sheets compared to other solvents, for example, Toluene [29,30].

Therefore, it is necessary to evaporate completely chloroform after submerging. This does not only eliminate absorption bands of solvent which can interfere in the LD measurements, but also improve orientation of molecules in the polymer matrix. But the latter can only be observed for experiments which use thick LDPE sheets because both the evaporation of chloroform and the loss of concentration of compound processes take place slowly in thick sheets compared to in thin sheets. Figure 2.5 shows the illustration of this effect.

Ethanol and Methanol are used as solvents for cleaning the surface of the LDPE sheets because they are polar solvents which can not swell the LDPE matrix and, hence, they can only dissolve the crystals of compound on the surface. This leads to the fact that the concentration of compound which is introduced into the polymer matrix is not influenced significantly by these cleaning solvents.

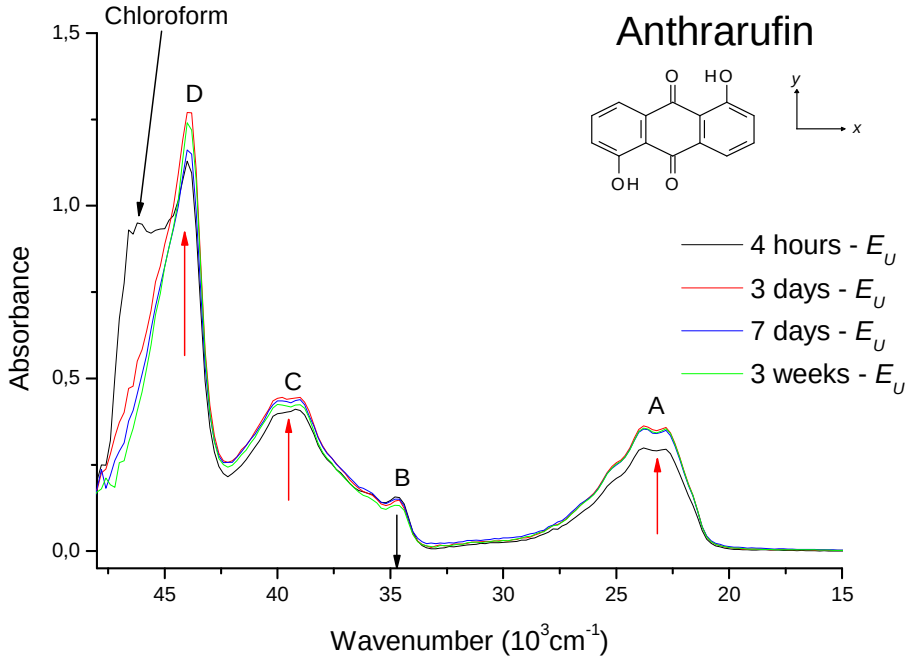

Figure 2.5: Illustration of evaporation of chloroform solvent from thick LDPE (case of Anthrarufin). As can be seen in the figure which only shows the E_U curve, chloroform solvent still remains in thick LDPE matrix after 4 hour evaporation. After 3 week evaporation, the intensity of the absorption bands slightly changes: A, C and D increase while B decreases as indicated by arrows. This indicates that the alignment of molecules with the stretching direction becomes better, leading to the increase in intensity of long polarized transitions and the decrease in intensity of short polarized transitions. The E_V curve can be seen in Appendix 2.

2.4 Linear dichroism measurements

The two independent LD curves are obtained in each LD measurement corresponding to relationship between direction of electric vector of linearly polarized light and stretching direction of the LDPE sheet: one corresponds to the electric vector parallel to and another corresponds to the electric vector perpendicular to the stretching direction. In both measurements, the propagation of light is always perpendicular to the surface of the LDPE sheet. After baseline correction, the LD curves are denoted as E_U and E_V.

Sample and blank sheets are measured separately in the same conditions.

2.4.1 Traditional UV-VIS spectrophotometer

All UV-VIS LD measurements in spectral region from 15000 to 47000 cm^{-1} are performed at room temperature with Shimadzu UV-2101PC traditional spectrophotometer. This is equipped with Glan – Taylor prism for both sample and reference positions. The prism acts as a linear polarizer and can rotate up to 90^{o} which can generates linearly polarized lights perpendicular to each other. The polarized light beam interacts with samples in closed and dark compartment. Spectral data are acquired and recorded by computer.

2.4.2 Synchrotron radiation

All SRLD measurements in high energy spectral region above 47000 cm^{-1} are also performed at room temperature with UV1 [59] or CD1 [60] beamlines of synchrotron system at The Institute for Storage Ring Facilities in Aarhus University, Denmark. Synchrotron radiation emitted from the storage ring passes through CaF_2 optical window and then MgF_2 Rochon linear polarizer, and interacts with samples in closed and dark compartment which is equipped dried nitrogen purging gas. The nitrogen gas removes other gases in sample compartment including oxygen, water and chemical vapour which can absorb light strongly in the high energy region. The optical signal is detected, transformed and recorded by Photo Multiplier Tube which is compatible and sensitive with ultraviolet (PMT Model 9402B, Electron Tubes, UK). Data acquisition is controlled by computer.

However, the SRLD measurements can only be performed in region up to 58000 cm^{-1} by using the LDPE as an anisotropic solvent because the LDPE matrix scatters and absorbs light strongly in the UV region. Therefore, the SRLD spectroscopic measurements can provide optical information in approximately 11000 cm^{-1} extended region compared to the traditional LD measurements. The strong absorption of baseline also limits the use of thick LDPE sheets to improve the intensity of the LD spectra of compounds which are hardly introduced into the polymer. Figure 2.6 shows baseline absorption of the LDPE sheet in the UV-VIS region.

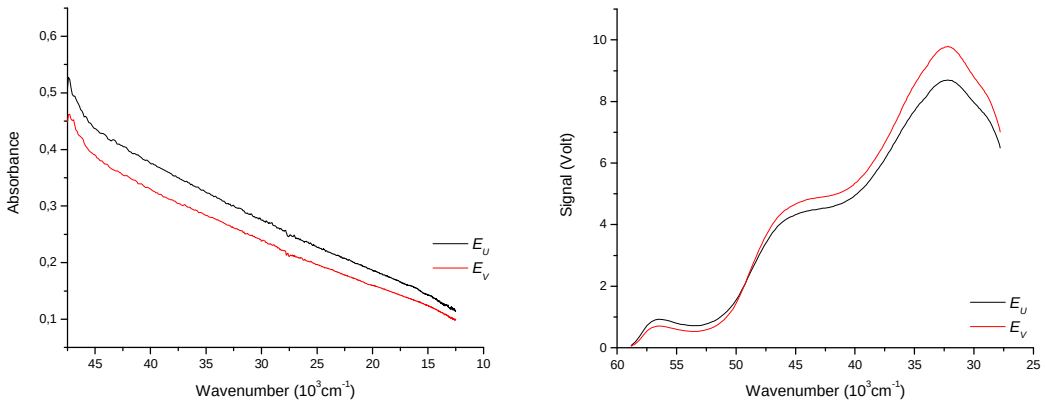

a *b*

Figure 2.6: The LD measurements of stretched LDPE in the UV-VIS region at room temperature. (a) On a traditional spectrophotometer, the optical signal is recorded as an absorbance in wavenumber region below 47000 cm^{-1}; (b) At CD1 beamline on storage ring, the optical signal is recorded as a transmitted light in wavenumber region from 28000 cm^{-1} to 58000cm^{-1}.

The observed LD spectra of all compounds investigated in this thesis are listed in Appendix 3.

2.5 Stretcher

The LDPE sheets are stretched mechanically by simple designed stretcher. This apparatus consists of two pairs of metal bar which are used to hold the LDPE sheets in place. One of them is fixed and another can move back and forth. The LDPE sheet is stretched as one metal pair moves away from another. Because the sheet is held by the two metal pairs, sharp edges of the metal bars can cause a breakage of the LDPE sheet during the stretching process. This problem can be overcome by using pieces of Teflon, LDPE, and denim to isolate the sample sheets from the sharp edges of the metal bars [29,30].

The sample sheets are stretched slowly up to about 500% at room temperature. This procedure is performed in the same conditions for both sample and reference sheets to ensure that the orientation of molecules and baseline absorption are equivalent for all stretched sheets. The mechanic stretcher is shown in following figure.

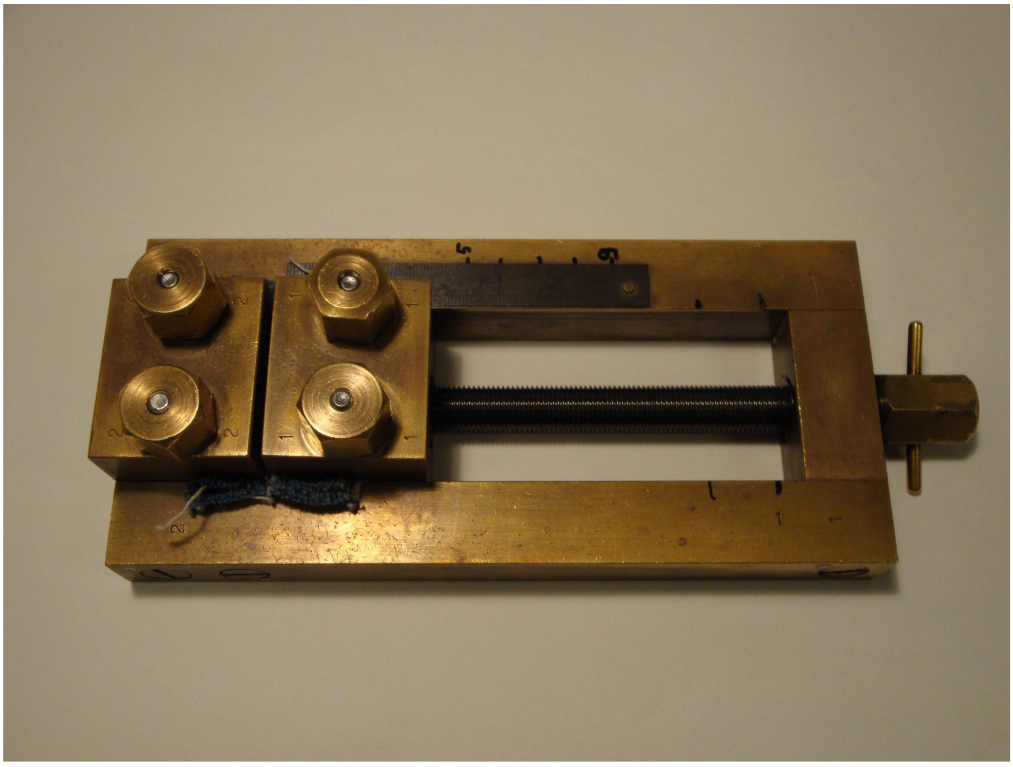

Figure 2.7: The mechanic stretcher in dimensions: length (20cm)×wide (10cm)×thick (2.5cm)

Chapter 3

1,4-Bis(phenylethynyl)benzene (BPEB)

3.1 Introduction

1,4-Bis(phenylethynyl)benzene (BPEB) is classified into hydrocarbon group. Its structure is composed of aromatic rings that are linearly conjugated through acetylene linkages. The cylindrical symmetry of the triple bond of the acetylene linkages leads to the efficient electronic conjugation between adjacent phenyl groups. In addition, the relatively free rotation of the phenyl groups about the alkyne-aryl single bond leads to coexistence of rotamers which are an equilibration of coplanar and twisted structures [68,69] (The structure of the rotamers is shown in Figure 3.1). The equilibration between the rotamers of BPEB generates fascinating characteristics such as changing resistivity, spectral shifts in absorption and emission spectroscopy. These effects are of particular interest, leading to interesting properties of BPEB and its derivatives as emitting layers in fluorescent and electroluminescent devices, "molecular wires" in organic semiconductors, and other applications [68,69].

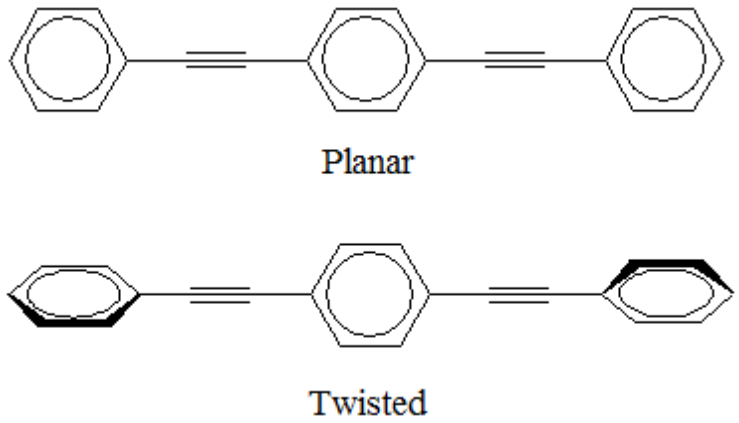

Figure 3.1: The coplanar and twisted structures of BPEB. The relatively free rotation of the phenyl groups about the acetylene linkages generates different rotamers.

The photophysical and physicochemical properties of BPEB are investigated by using different spectroscopic methods such as fluorescence [68] used to study the spectral shifts of BPEB in different solvents, cavity ring-down [69] applied to investigate the rotation of the phenyl groups about the alkyne-aryl single bond, and so on. This chapter will present the investigation of the polarization and assignment of the electronic transitions of BPEB by using the SRLD measurements on uniaxially stretched LDPE matrix and LCOAO calculations, respectively.

3.2 Results and discussions

The procedure of sample preparation, LD measurements and theoretical calculations is described in the previous sections.

From the observed LD data of BPEB sample in stretched LDPE matrix, E_U and E_V, we can calculate an isotropic absorption curve by using expression (18) (The observed LD spectra and isotropic absorption curve are shown in Figure 3.2). The isotropic curve is used to compare with the absorption curve of BPEB measured in different solvents [70] in order to ensure reliability of the observed LD data.

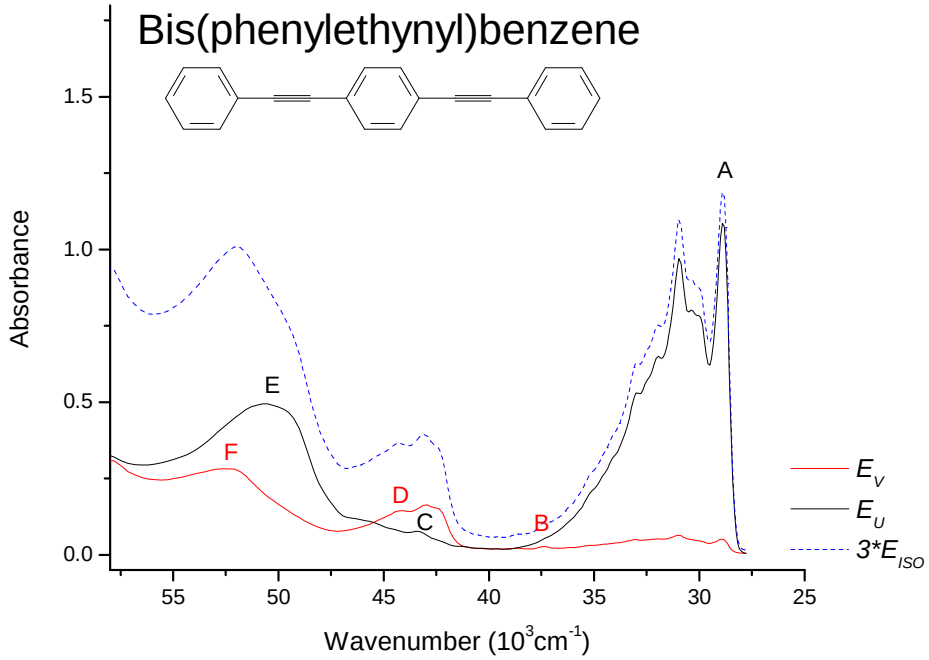

Figure 3.2: The isotropic and UV-VIS LD spectra of BPEB. The sample is partially aligned in stretched LDPE. The two LD curves (E_U - black and E_V - red solid curves) are measured at room temperature by using synchrotron radiation at CD1 beamline on ASTRID ring. And the isotropic curve (E_{ISO} - dashed blue curve) is plotted by using equation (18).

The similarity in spectral shapes of the absorption bands measured in liquid solvent (n-Hexane) and in unstretched LDPE matrix [70] indicates that the molecular structure and symmetry of BPEB molecule in both media are similar. This means that the proportion of the relatively free rotation of the phenyl groups about the acetylene linkages are equivalent in both the LDPE matrix and liquid solution.

The differences in shapes and intensities of the absorption bands between spectra measured in the unstretched and stretched LDPE matrix indicate that there are differences in molecular structure and symmetry of BPEB in both media. In particular, the shapes and intensities of the absorption peaks in the first band are slightly changed (see Figure 3.3). These differences can be due to the increase of coplanar arrangement of the phenyl groups in the stretched LDPE matrix and efficient alignment of rod-like molecular shape of BPEB with the stretching direction. And the negligible chemical interaction between BPEB molecules and the LDPE matrix leads to clear spectral features in the absorption bands.

The significant increase in the intensity of the spectral feature at 28000 cm^{-1} can be considered as an indication of the increase in coplanar distribution of BPEB molecule in the stretched LDPE. There is a significant contribution from twisted conformations in the

unstretched LDPE matrix, whereas the coplanar conformations are favoured in the stretched LDPE matrix. The increase of the coplanar conformations leads to the increase in proportion of the extension of delocalized π-electron system which causes red-shift of the electronic transitions. This explanation is supported by studies in the changing of the spectral features as a function of temperature. The investigation shows that the structure of BPEB molecule is the coplanar arrangement at low temperature (77 K) compared to the twisted structure at high temperature (298 K) [68]. In our analysis, we assume that BPEB in the stretched LDPE is practically planar.

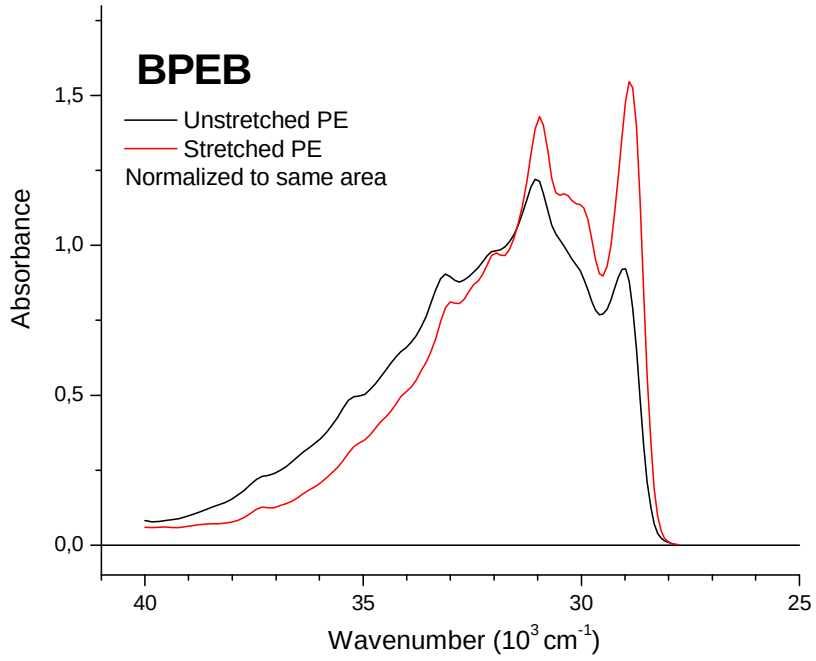

Figure 3.3: The isotropic spectra of BPEB in the stretched and unstretched LDPE.

And basing on the observed LD data, value of orientation factor can be determined by using TEM procedure – expression (26). As described above, TEM procedure is a linear combination of the two independent LD curves, E_U and E_V, producing a family of reduced spectral curves corresponding to the changing of K value from 0 to 1. And K value of an absorption band is visually derived from the vanishing point of the spectral feature in the series of reduced curves. Figure 3.4 shows the family of reduced spectral curves with indication of derived orientation factors.

As shown in Figure 3.4, the derived orientation factors of the spectral features are 0.95 and 0.9. As already discussed, BPEB molecule has coplanar structure in the stretched LDPE matrix which belongs to "high" molecular symmetry with D_{2h} point group. The properties of this point group determine possible directions of the electronic transition moments in the molecular framework. As a result, the orientation of transition moment is restricted in three directions corresponding to x, y, z axes of the molecular coordinate, and therefore, the orientation factor will belong to three distinct values whose sum are unity. The value of 0.9 is approximate because of broad and overlapping bands. Hence, it is considered as an approximation and can obtain final value of 0.95 which is used in LD analysis.

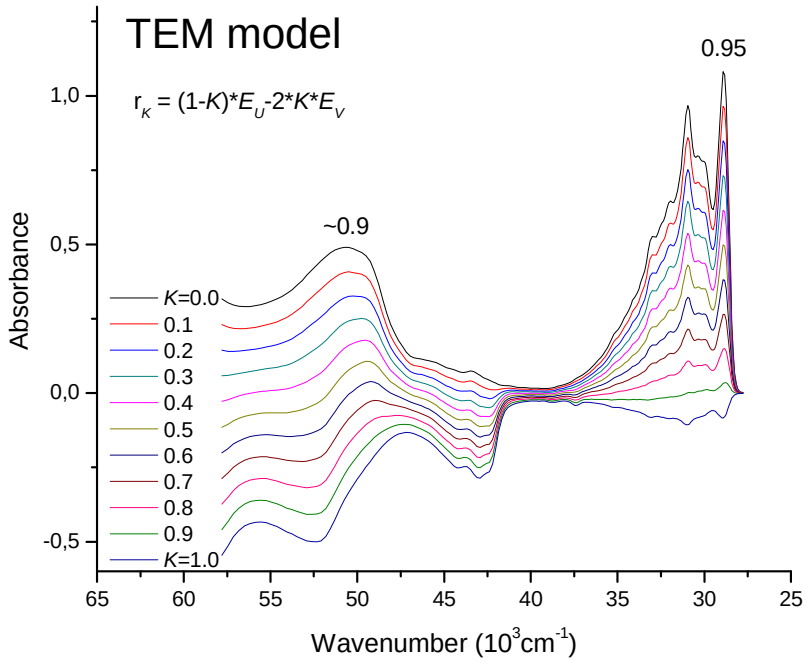

Figure 3.4: The TEM procedure of BPEB. The family of reduced spectral curves with indication of the derived orientation factors (see text for more detail).

According to the convention in Figure 3.5, the orientation factor of transition moments along *z* axis will receive highest value corresponding to efficient alignment of BPEB molecule with the stretching direction, K_z=0.95. Because the sum of three distinct *K* values is unity, the sum of two other *K* values (K_y + K_x) can only be equal to 0.05. And BPEB has a rod-like molecular shape, giving following relationship: $K_y \approx K_x$. Therefore, the value of the orientation factors is in order $K_z > K_y \approx K_x$ with K_z and K_y are the values of the transition moments oriented along the long and short in-plane axes, and K_x is the value of the transition moments perpendicular to the molecular plane. K_y is taken as 0.03 in our analysis.

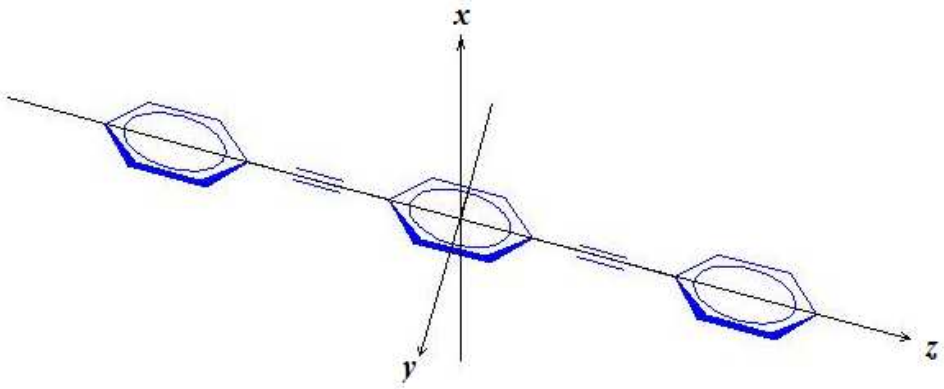

Figure 3.5: The molecular coordinate system of BPEB, with z axis is a long in-plane axis, also called molecular orientation axis, and y axis is a short in-plane axis, and x axis is a out-of-plane axis which is perpendicular to the molecular plane (yz plane).

Basing on the determined orientation factors, K_z=0.95 and K_y=0.03, and "high" molecular symmetry and coplanar properties of BPEB structure, the expressions (29) and (30) can be applied to construct partial absorption curves of the electronic transitions polarized along the long and short in-plane axes, A_z and A_y, with an assumption $A_x \approx 0$. These partial absorption curves are shown in the top of Figure 3.6.

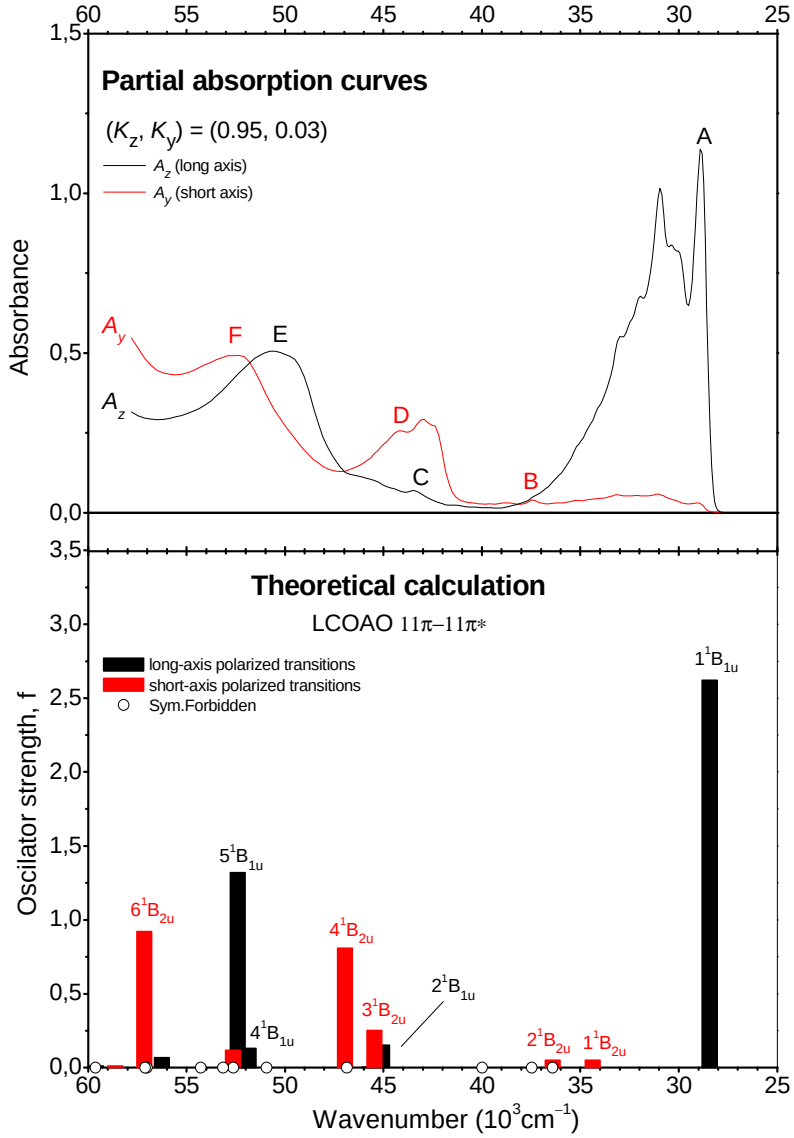

Figure 3.6: Top: The partial absorption curves of BPEB. This compound belongs to "high" molecular symmetry with D_{2h} point group. The black curve (A_z) and the red curve (A_y) describe absorption bands whose electronic transition moment are in direction along the long in-plane axis (z) and the short in-plane axis (y) of molecular framework, respectively. Bottom: Theoretically predicted transitions (Table 3.1).

Andersen et al. have performed standard TD-DFT calculations on this compound, but the agreement of the results with the observed transitions was problematic [70]. Therefore, the LCOAO method is used to predict electronic transitions for BPEB in this chapter. The LCOAO all-valence electrons method was developed particularly for the prediction of the transitions in conjugated, planar hydrocarbons [58]. The present LCOAO calculation considers configuration interaction (CI) between all configurations generated by promotion

of an electron from the eleven π to the eleven π* orbitals. The two in-plane π components of two acetylene linkages are not taken into account in the CI procedure. This means that only π-π* transitions are predicted in this method.

The experimental partial absorption curves and theoretical calculations of the electronic transitions are described and listed in Figure 3.6 and Table 3.1. The partial absorption curves show that differently polarized overlapping transitions are resolved into independent absorption curves of the electronic transitions polarized along the long and short in-plane axes, *z* and *y*. The spectral bands A, C, and E at 28900, 43500 and 50500 cm^{-1} are polarized along the long in-plane *z* axis, whereas the spectral bands B, D and F at 37400, 44200 and 52900 cm^{-1} are polarized along the short in-plane *y* axis. The theoretical calculations provide predicted electronic transitions which are in good agreement with relative ratio of oscillator strength of the electronic transitions compared with those of the partial absorption curves. The electronic transitions that are predicted at 28400, 45100 and 52400 cm^{-1} are $^1B_{1u}$ state, and other predicted transitions at 36400, 47000 and 57200 cm^{-1} are $^1B_{2u}$ state.

Table 3.1: Observed and predicted electronic transitions for BPEB

	Stretched PE [a]				LCOAO 11π-11π* [b]			
	$\tilde{\nu}$ [c]	A [d]	K [e]	Pol. [f]	Term	$\tilde{\nu}$ [c]	f [g]	Leading Configurations
A	28.9	1.14	*0.95*	*z*	$1\,^1B_{1u}$	28.4	2.62	93%($4b_{2g}$-$5b_{3u}$)
B	37.4	0.04	-	*y*	$1\,^1B_{2u}$	34.4	$9\cdot10^{-4}$	47%($1b_{1g}$-$5b_{3u}$), 39%($4b_{2g}$-$2a_u$)
					$2\,^1B_{2u}$	36.4	$2\cdot10^{-3}$	26%($2b_{1g}$-$5b_{3u}$), 21%($1a_u$-$5b_{2g}$), 20%($4b_{2g}$-$3a_u$), 18%($4b_{3u}$-$3b_{1g}$)
C	43.5	0.07	-	*z*	$2\,^1B_{1u}$	45.1	0.15	43%($4b_{2g}$-$6b_{3u}$), 29%($4b_{3u}$-$5b_{2g}$), 12%($3b_{2g}$-$5b_{3u}$)
D	44.2	0.26	*0.03*	*y*	$3\,^1B_{2u}$	45.4	0.25	48%($4b_{2g}$-$2a_u$), 45%($1b_{1g}$-$5b_{3u}$)
					$4\,^1B_{2u}$	47.0	0.81	48%($2b_{1g}$-$5b_{3u}$), 33%($4b_{2g}$-$3a_u$)
E	50.5	0.51	*0.90*	*z*	$4\,^1B_{1u}$	51.9	0.13	39%($4b_{3u}$-$5b_{2g}$), 13%($4b_{2g}$-$6b_{3u}$), 12%($3b_{2g}$-$5b_{3u}$), 11%($1b_{1g}$-$2a_u$)
					$5\,^1B_{1u}$	52.4	1.32	27%($1b_{1g}$-$2a_u$), 19%($1a_u$-$3b_{1g}$), 19%($2b_{1g}$-$3a_u$), 16%($4b_{3u}$-$5b_{2g}$)
F	52.9	0.49	-	*y*	$5\,^1B_{2u}$	52.6	0.12	29%($1a_u$-$3b_{1g}$), 19%($2b_{1g}$-$6b_{3u}$), 18%($2b_{1g}$-$5b_{3u}$), 17%($2b_{1g}$-$6b_{3u}$)
					$6\,^1B_{1u}$	56.3	0.07	47%($1b_{1g}$-$2a_u$), 19%($2b_{1g}$-$3a_u$), 19%($1a_u$-$3b_{1g}$)
					$6\,^1B_{2u}$	57.2	0.92	38%($4b_{3u}$-$3b_{1g}$), 27%($1a_u$-$5b_{2g}$), 16%($3b_{2g}$-$3a_u$)
					$7\,^1B_{2u}$	58.6	0.01	50%($1b_{1g}$-$6b_{3u}$), 25%($3b_{2g}$-$2a_u$)
					$7\,^1B_{1u}$	59.6	0.01	43%($2b_{2g}$-$5b_{3u}$), 32%($4b_{2g}$-$7b_{3u}$), 11%($3b_{3u}$-$5b_{2g}$)

[a] Absorption peaks measured in stretched polyethylene.
[b] In the region above 45000 cm^{-1}, only predicted transitions with $f \geq 0.01$ are listed (see Appendix 4 for full listing of all transitions).
[c] Wavenumber in 10^3 cm^{-1}.
[d] Absorbance from the partial absorption curves in Fig. 3.6.
[e] Orientation factor, see text.
[f] Polarization of electronic transitions.
[g] Oscillator strength.

The comparison shows that the predicted data are in agreement with the observed spectra. Spectral band A at 28900 cm^{-1} is easily assigned to 1^1B_{1u} state which is predicted at 28400 cm^{-1}. This transitions is mainly due to the promotion of an electron from HOMO (4 b_{2g}) to LUMO (5 b_{3u}). The shape of molecular orbitals shown in Figure 3.7 indicates that the electronic transition concerns the extended delocalized π-electron system and small charge-transfer between the phenyl groups and the acetylene linkages in BPEB molecule.

Spectral band B at 37400 cm^{-1} is also easily assigned to 1^1B_{2u} and 2^1B_{2u} states that are predicted at 34400 and 36400 cm^{-1}. They are weak electronic transitions (oscillator strength, $f = 9 \cdot 10^{-4}$ and $2 \cdot 10^{-3}$) and complicated. They consist of contribution of several promotions between different orbitals (as listed in Table 3.1). The shape of orbitals corresponding to these states can be seen in Appendix 5.

And band C at 43500 cm^{-1} is polarized along the long in-plane *z* axis. It will be assigned to 2^1B_{1u} state calculated at 45100 cm^{-1} because the other long-axis polarized transition (3^1B_{1u} state predicted at 45700 cm^{-1}) is very weak (oscillator strength, $f = 2 \cdot 10^{-3}$). This electronic transition also contains the contribution of two different electronic promotions from two different pair of orbitals.

Because band D at 44200 cm^{-1} is polarized along the short in-plane *y* axis, it can be assigned to 3^1B_{2u} and 4^1B_{2u} states predicted at 45400 and 47000 cm^{-1}. These transitions are comprised of the contribution of several electronic promotions between two different pair of orbitals.

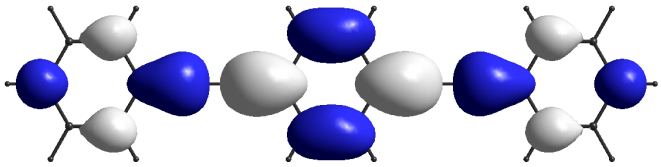

5 $b_{3u}(\pi^*)$

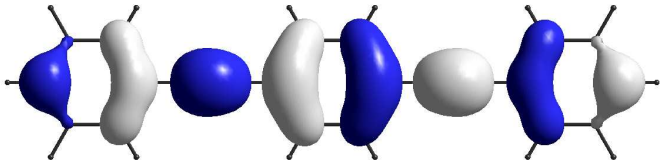

4 $b_{2g}(\pi)$

Figure 3.7: Diagrams of the highest occupied and lowest unoccupied molecular orbitals for BPEB. More orbital diagrams can be seen in Appendix 5.

Band E at 50500 cm^{-1} is a long-axis polarized transition and will be assigned to 4^1B_{1u} and 5^1B_{1u} states that are calculated at 51900 and 52400 cm^{-1}. Because the other long-axis polarized transitions (6^1B_{1u} and 7^1B_{1u} states predicted at 56300 and 59600 cm^{-1}) are relative weak (oscillator strength, f = 0.07 and 0.01) and quite far from band E. These transitions are complicated due to several contributions.

And finally, band F at 52900 cm^{-1} is a short-axis polarized transition and can be assigned to 5^1B_{2u} and 6^1B_{2u} states which are predicted at 52600 and 57200 cm^{-1}. The 6^1B_{2u} state is quite far from 52900 cm^{-1} of band F, but its oscillator strength (f = 0.92) is associated with the observed data. The other short-axis polarized transition (7^1B_{2u} predicted at 58600 cm^{-1}) is weak (oscillator strength, f = 0.01) and quite far from band F. These electronic transitions are also composed of several contributions of different electronic promotions.

3.3 Conclusion

The present study provides the polarization data of the absorption bands for BPEB in spectral region from ca. 25000 cm^{-1} to ca. 58000 cm^{-1}, especially in the high energy region from ca. 47000 cm^{-1} to ca. 58000 cm^{-1}. This means that we can obtain more spectroscopic

information in extended 11000 cm^{-1} than those by a traditional spectrophotometer. The analysis of the LD spectra shows that the differently polarized overlapping transitions can be resolved and identified clearly, particularly bands C and D, bands E and F in the spectrum of BPEB.

The agreement between the observed and predicted electronic transitions provides a useful tool for the reliable and precise assignment of the electronic transitions. In this case, the information on the molecular symmetry and polarization of the electronic transitions is obtained for six spectral features throughout the spectrum. And finally, this investigated method can confirm the coplanar structure of BPEB molecule in the stretched LDPE matrix.

Chapter 4

Dibenzofuran

4.1 Introduction

Dibenzofuran (DBF) belongs to heterocyclic organic group. This compound is composed of two benzene rings fused to one furan ring in the middle (as shown in Figure 4.1). DBF is created from the production of coal tar, and also found in coke dust, grate ash, fly ash and flame soot, and especially in tobacco smoke. It is used as an insecticide and model compound for synthesizing other chemicals. DBF can cause skin, eye, nose and throat irritation in short-term exposure, and long-term exposure can cause rashes and growths on your skin [71]. But polychlorinated derivatives of DBF are known as highly toxic compounds. These derivatives are formed in the incineration of chlorine containing materials, and emitted into the atmosphere, becoming pollutants in environment. It can also be accumulated in human tissues and food [72].

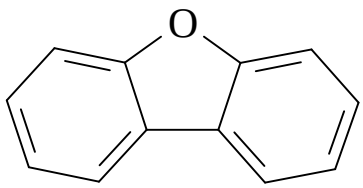

Figure 4.1: Molecular structure of dibenzofuran (DBF)

The physicochemical properties of DBF have been investigated by different spectroscopic methods such as phosphorescence [73], fluorescence [74], and polarization [75,76]. However, information on the polarization and molecular symmetry as well as the assignments of the electronic transitions can only be obtained in spectral region below 50000 cm^{-1} in previous studies [76]. In present study, spectroscopic information of DBF can be obtained in the extended region of 11000 cm^{-1} by using the SRLD spectroscopy on samples aligned in the stretched LDPE matrix and theoretical calculations.

4.2 Results and discussions

The procedure of sample preparation, LD measurements and quantum chemical calculations is mentioned in the previous sections.

As known that an isotropic absorption curve of DBF can be constructed from the two independently observed LD spectra, E_U and E_V, and expression (18). This absorption curve is shown in Figure 4.2, and can be used to compare with the absorption curve of DBF measured in liquid solution (n-Hexane) [75] and in stretched LDPE matrix [76]. The similarity in spectral shapes indicates that the observed LD spectra are reliable.

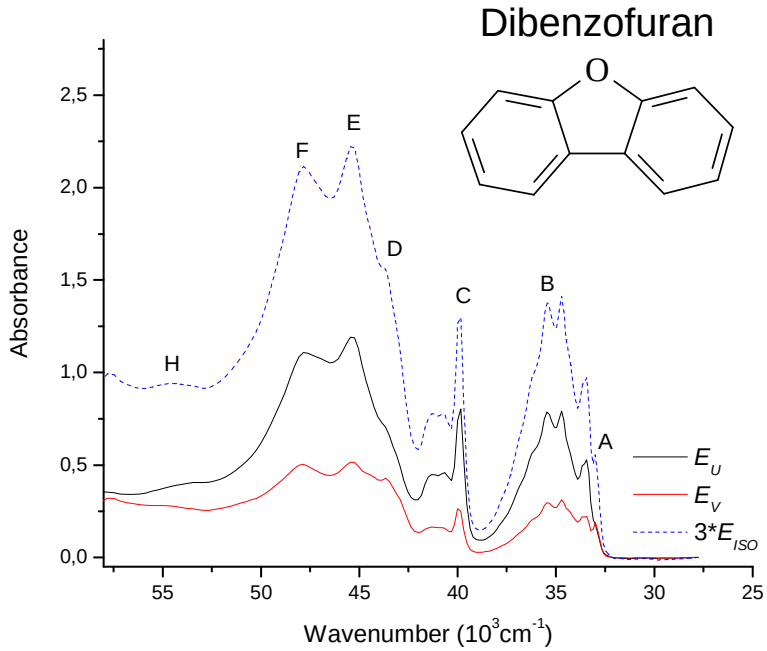

Figure 4.2: The isotropic and UV-VIS LD spectra of DBF. The sample is partially aligned in stretched LDPE. The two LD curves (E_U – black and E_V – red solid curves) are measured at room temperature by using synchrotron radiation at CD1 beamline on ASTRID ring. And the isotropic curve (E_{ISO} – dashed blue curve) is plotted by using equation (18).

And the linear combination of the two LD curves produces a family of reduced spectra which is used to determine orientation factors of the absorption bands in spectrum of DBF (as shown in Figure 4.3). According to the TEM procedure, value of the orientation factors can be visually determined by the vanishing of the spectral features corresponding to the *K* value in expression (26) changes from 0 to 1.

As can be seen in Figure 4.3, the obtained values of the orientation factor of the absorption bands are in two distinct groups 0.60 and 0.30. These *K* values are slightly different from those in previous studies [76], namely *K* values of long-axis polarized transitions in present studies are higher, and those of short-axis polarized transitions are lower than in previous. This can be due to better alignment of DBF molecules in the stretched LDPE matrix.

Molecular geometry of DBF belongs to "high" symmetry with C_{2v} point group. As mentioned in chapter 1, allowed electronic transitions in this kind of the molecular symmetry are restricted and polarized in directions along *x*, *y*, and *z* axes of the molecular coordinate system. This means that the orientation factors will accept values which are in three distinct groups. The sum of these values is unity. Therefore, we can obtain *K* values of the absorption bands in spectrum of DBF as follow: 0.60, 0.30 and 0.10. These values are used in LD analysis.

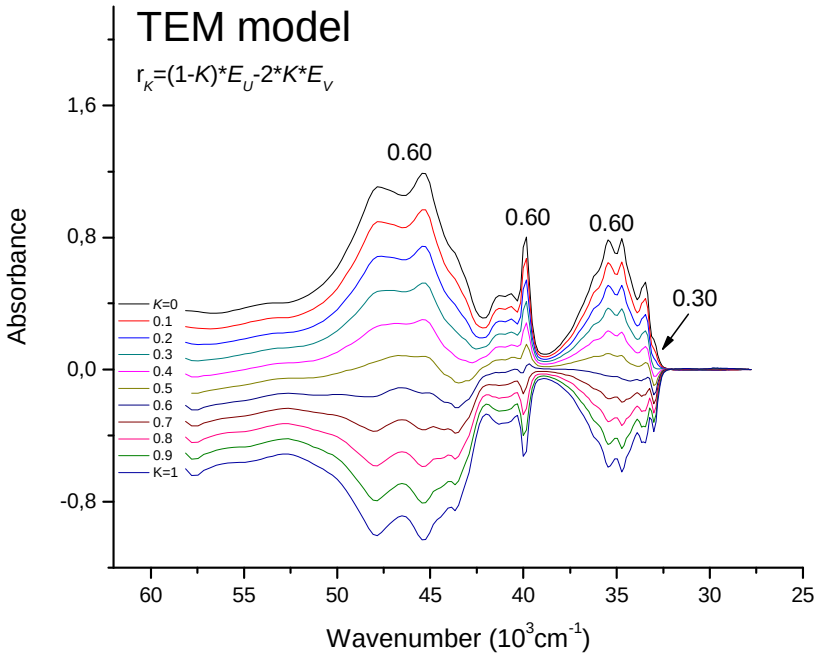

Figure 4.3: The family of reduced spectral curves with indication of the derived orientation factors (see text for more detail).

According to the convention of the molecular coordinate system of DBF (as shown in Figure 4.4), the electronic transitions polarized along symmetrical axis, *z*, are considered as short in-plane polarized transitions, and along *y* axis are long in-plane polarized transitions, and along *x* axis are out-of-plane polarized transitions. In the stretched LDPE matrix, *y* axis is efficiently aligned with stretching direction, leading to the fact that the orientation factor of the transitions along this axis accepts largest value, K_y = 0.60. We assume that the electronic transitions in the near UV-VIS region is mainly contributed by π-π* transitions, and thus the out-of-plane polarized transitions are negligible, the orientation factor of these transitions will accept lowest value, K_x = 0.10. Therefore, we can derive easily the value of the orientation factor of the short in-plane polarized transitions, K_z = 0.30. And the obtained *K* values can be arranged in following order: $K_y > K_z > K_x$.

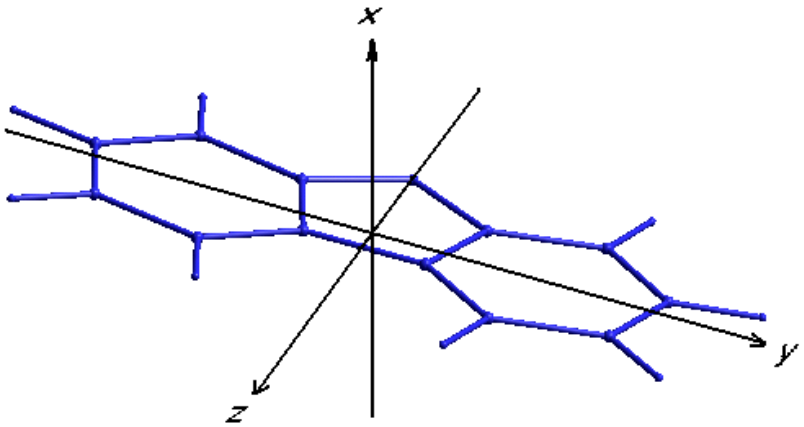

Figure 4.4: The molecular coordinate system of DBF, with y axis is a long in-plane axis, also called molecular orientation axis, and z axis is a short in-plane axis, also called symmetrical axis, and x axis is a out-of-plane axis which is perpendicular to the molecular plane (yz plane).

Using the obtained K values, we can construct the partial absorption curves corresponding to the long- and short-axis polarized transitions by using expressions (29) and (30), A_y and A_z. As our assumption, absorbance of the out-of-plane polarized transitions is negligible, $A_x \approx 0$. These partial absorption curves are shown in Figure 4.5.

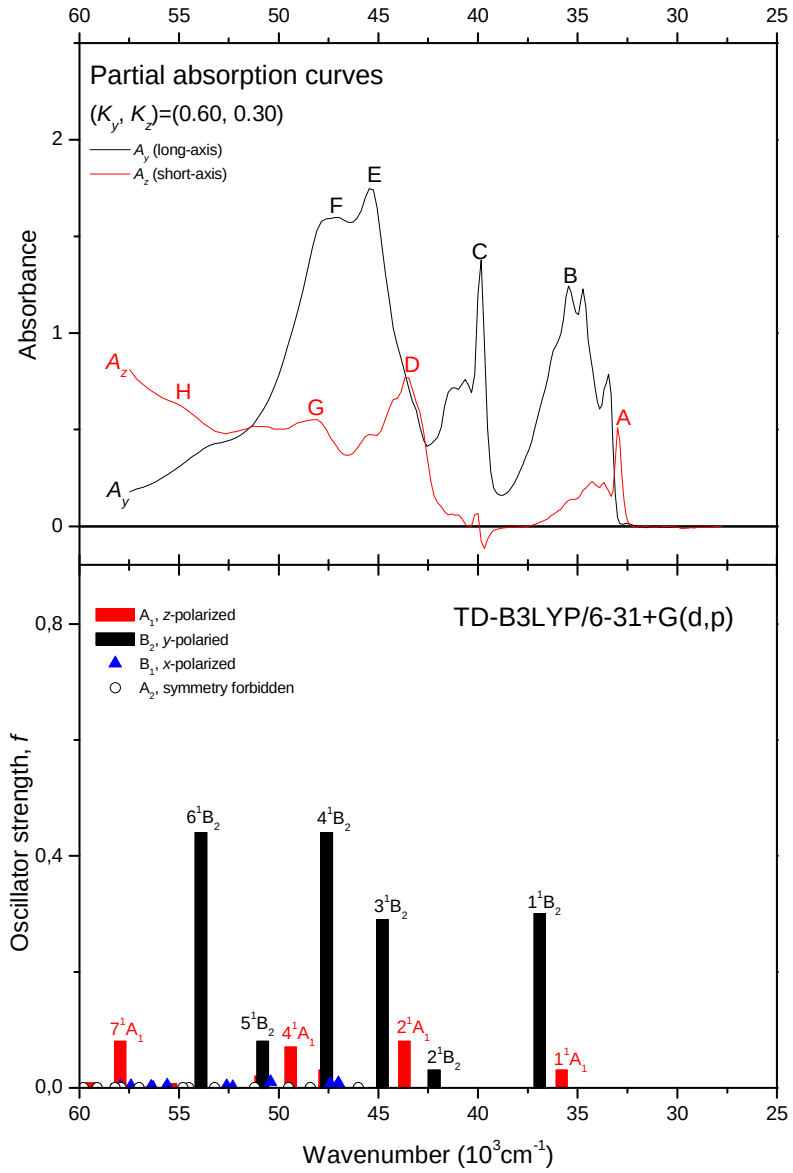

Figure 4.5: Top: The partial absorption curves of DBF. This compound belongs to "high" molecular symmetry with C_{2v} point group. The black curve (A_y) and the red curve (A_z) describe absorption bands whose electronic transition moment are in direction along the long in-plane axis (y) and the short in-plane axis (z) of the molecular framework, respectively. Bottom: Theoretically predicted transitions (Table 4.1).

The partial absorption curves, A_y and A_z, describe the absorbance of the long- and short-axis polarized transitions which are resolved from differently polarized and overlapping transitions. The absorption bands A, D, G and H at 33000, 43500, 48100 and 54900 cm^{-1} are the short-axis polarized transitions, and the absorption bands B, C, E and F at 35500, 39800, 45400 and 46900 cm^{-1} are the long-axis polarized transitions. The theoretical calculation of the electronic transitions that is listed in Table 4.1 and also shown in Figure

4.5 indicates that the transitions predicted at 35800, 43700, 49400 and 58000 cm^{-1} are $^1A_1$ state, and those predicted at 36900, 42200, 44800 and 47600 cm^{-1} are $^1B_2$ state. The "wiggle" observed at 40000 cm^{-1} in the A_z curve is due to the slight difference in energy of the transitions in efficiently aligned and poorly aligned molecules [29,30,76]. The predicted transitions are not all in good agreement with the observed data. It can be due to rearrangement of excited state geometry and vibronic coupling phenomena, resulting in significant differences between vertical and adiabatic transition energies [77,78].

Band A at 33000 cm^{-1} can be assigned to 1^1A_1 state predicted at 35800 cm^{-1}. This transition consists of contribution of several promotions between different orbitals. The shape of these orbitals is shown in Appendix 7.

Table 4.1: Observed and predicted electronic transitions for DBF

	Stretched PE [a]				TD-B3LYP/6-31+G(d,p) [b]			
	$\tilde{\nu}$ [c]	A [d]	K [e]	Pol. [f]	Term	$\tilde{\nu}$ [c]	f [g]	Leading Configurations [h]
A	33.0	0.51	*0.30*	*z*	1^1A_1	35.8	0.03	80%(2,-1), 16%(1,-2)
B	35.5	1.24	*0.60*	*y*	1^1B_2	36.9	0.30	76%(1,-1)
C	39.8	1.38	*0.60*	*y*	2^1B_2	42.2	0.03	50%(3,-1), 39%(1,-3)
D	43.5	0.77	*0.30*	*z*	2^1A_1	43.7	0.08	22%(2,-3), 57%(1,-2)
E	45.4	1.75	*0.60*	*y*	3^1B_2	44.8	0.29	14%(3,-1), 63%(2,-2)
F	46.9	1.60	*0.60*	*y*	4^1B_2	47.6	0.44	21%(3,-1), 16%(2,-2), 37%(1,-3)
					3^1A_1	47.7	0.03	27%(4,-1), 50%(2,-3)
G	48.1	0.55	-	*z*	4^1A_1	49.4	0.07	21%(4,-1), 51%(1,-6)
					5^1B_2	50.8	0.08	15%(4,-2), 72%(2,-6)
					5^1A_1	50.9	0.02	25%(4,-1), 50%(3,-2), 14%(1,-6)
					6^1B_2	53.9	0.44	83%(3,-3)
H	54.9	0.62	-	*z*	7^1A_1	58.0	0.08	89%(2,-13)

[a] Absorption peaks measured in stretched polyethylene.
[b] In the region above 45000 cm^{-1}, only predicted transitions with $f \geq 0.01$ are listed (see Appendix 6 for full listing of all calculated transitions).
[c] Wavenumber in 10^3 cm^{-1}.
[d] Absorbance from the partial absorption curves in Fig. 4.5.
[e] Orientation factor, see text.
[f] Polarization of electronic transitions.
[g] Oscillator strength.
[h] The notation (*i*,-*j*) indicates an excited singlet configuration derived from the ground configuration by promotion of an electron from the i^{th} highest occupied to the j^{th} lowest unoccupied molecular orbital.

Band B at 35500 cm^{-1} is assigned to 1^1B_2 which is predicted at 36900 cm^{-1}. This transition is mainly contributed by promotion of an electron from HOMO (3 a_2) to LUMO (5 b_1). The orbital shapes are shown in Figure 4.6.

Absorption band C at 39800 cm^{-1} can be assigned to 2^1B_2 that is calculated at 42200 cm^{-1} although its oscillator strength is not in good agreement with the observed absorbance. This transition is also consists of several promotions between different orbitals.

Band D at 43500 cm^{-1} is assigned to 2^1A_1 state calculated at 43700 cm^{-1}. The orbital shapes corresponding to this transition can be found in Appendix 7.

Bands E and F at 45400 and 46900 cm^{-1} are assigned to 3^1B_2 and 4^1B_2 states predicted at 44800 and 47600 cm^{-1}. These transitions are also composed of contribution of several electronic promotions.

Band G at 48100 cm^{-1} is assigned to 4^1A_1 state predicted at 49400 cm^{-1} with oscillator strength f = 0.07 because other short-axis polarized transitions are 3^1A_1 and 5^1A_1 states that are calculated at 47700 and 50900 cm^{-1} with relatively weak oscillator strength f = 0.03 and 0.02, respectively.

Small band H at 54900 cm^{-1} can be assigned to 7^1A_1 state that is predicted at 58000 cm^{-1} with oscillator strength f = 0.08 because other 6^1A_1 state which is predicted at 55400 cm^{-1} has weak oscillator strength f = 0.007 (This transition can be seen in Appendix 6).

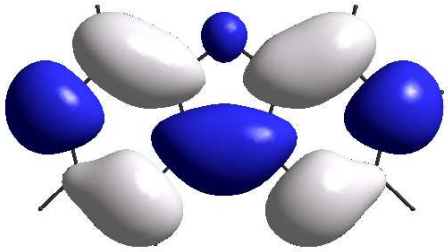

5 b_1 (π^*)

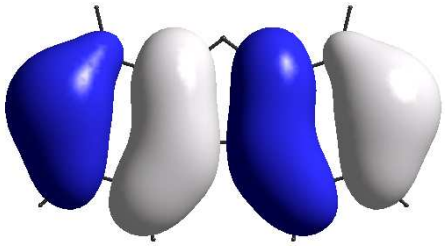

3 a_2 (π)

Figure 4.6: Diagrams of the highest occupied and lowest unoccupied molecular orbitals for DBF. More orbital diagrams can be seen in Appendix 7.

4.3 Conclusion

The polarization data and assignment of the electronic transitions obtained in energy region below 47000 cm^{-1} in this study are consistent with those in the previous [76]. This means that this investigation provides additional spectroscopic information in high energy region from ca. 47000 cm^{-1} to ca. 58000 cm^{-1}. And the SRLD spectroscopic measurements on samples aligned in stretched LDPE matrix can resolve differently polarized and overlapping transitions, particularly bands F and G, which are difficult to identify with traditional spectroscopic methods.

Even though the theoretical calculations are not all in good agreement with the experimental data, but TD-B3LYP/6-31+G(d,p) is an economical and useful tool which is used to predict and assign information on the molecular symmetry and polarization of the electronic transitions for eight spectral features in spectrum of DBF. This means that it can provide information for three absorption bands in the high energy region compared to those in the previous [76].

Chapter 5

Anthrarufin

5.1 Introduction

1,5-dihydroxyanthraquinone (Anthrarufin) is one of dihydroxy derivatives of anthraquinone with hydroxyl groups substituted at α, α' positions (as shown in Figure 5.1). The proximity of these hydroxyl groups and carbonyl groups enables formation of intramolecular hydrogen bonds in Anthrarufin molecule. This kind of hydrogen bonding does not only stabilize molecular geometry of Anthrarufin compared to those of other dihydroxy derivatives [79], but also generates several physicochemical properties which are applied for several application fields such as drugs, dyestuffs. In addition, Anthrarufin can be used as an intermediate in synthesis of other compounds [80].

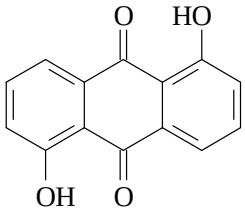

Figure 5.1: Molecular structure of Anthrarufin

Spectroscopic methods [81] and theoretical calculations [79] have been done to provide useful information on optical characteristics of this compound. However, none of the previous studies investigated and obtained spectral features and information of this compound in high energy region (far UV region) which is expected to contain more useful spectroscopic information. The difficulties in technical requirements (low signal to noise ratio) and strong overlap of absorption bands in this region are most challenged. In present work, additional spectroscopic features of Anthrarufin in the high energy region are obtained by using the SRLD measurements on samples aligned in stretched LDPE matrix. The results are compared to those of quantum chemical calculations to provide reliable information on the electronic transitions and molecular transition moment directions of the observed absorption bands.

5.2 Results and discussions

The procedure of sample preparation, LD measurements and theoretical calculations is described in the previous sections.

The two independent LD curves obtained from the SRLD measurements on samples aligned in the stretched LDPE matrix, E_U and E_V, can be used to construct an isotropic absorption curve (as shown in Figure 5.2). This curve is used to compare with the absorption curve of Anthrarufin which is measured in liquid solution (Methanol) [82] in order to ensure reliability and precision of the LD measurements. The similarity in the spectra shape indicates good observed LD data and the same molecular geometry in both media: liquid solution and stretched LDPE matrix.

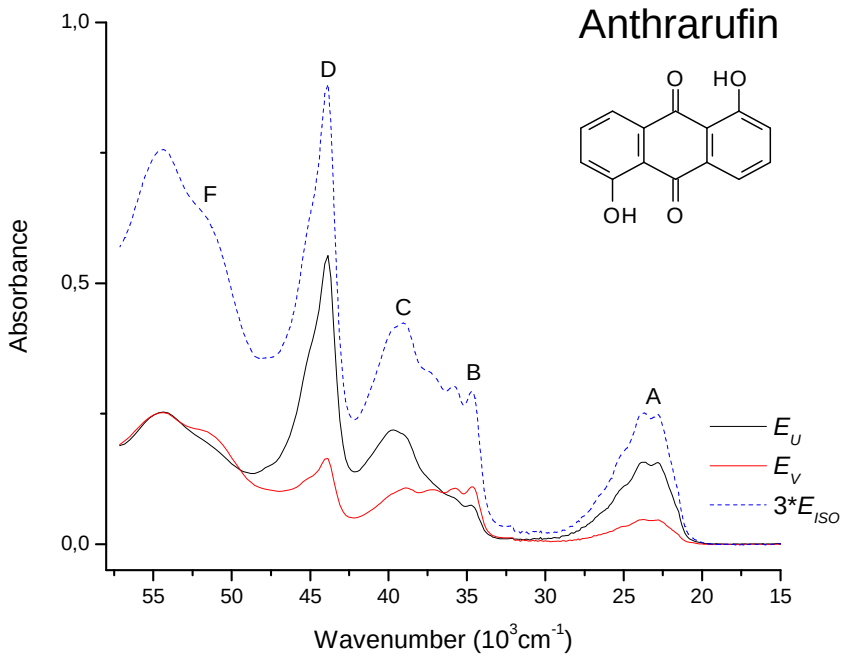

Figure 5.2: The isotropic and UV-VIS LD spectra of Anthrarufin. The sample is partially aligned in stretched LDPE. The two LD curves (E_U – black and E_V – red curves) are measured at room temperature by using a traditional spectrophotometer for energy region below 47000 cm^{-1}, and synchrotron radiation at CD1 beamline on ASTRID ring for energy region above 47000 cm^{-1}. And the isotropic curve (E_{ISO} – dashed blue curve) is plotted by using expression (18).

The linear combination of the two observed LD curves, E_U and E_V, produces a family of reduced spectra (see Figure 5.3) which is used to determine value of orientation factors of absorption bands in spectrum of Anthrarufin. As can be seen in Figure 5.3, the low energy absorption band at 23800 cm^{-1} will vanish for a value of 0.65 when K value in expression (26) varies from 0 to 1. This means that the orientation factor of this absorption band will be equal to 0.65. And the value of orientation factor of other bands can be visually determined in a similar way. The K values that are derived precisely from the vanishing of the sharp spectral features are considered as reliable values and they can be used in LD analysis. Therefore, the K values of the absorption bands in the spectrum are in two distinct values 0.65 and 0.20. Values of 0.4 and 0.6 are only approximately determined because of broad and overlapping bands.

Molecular geometry of Anthrarufin belongs to “low” symmetry group with C_{2h} point group. The LD analysis is not straightforward as in “high” molecular symmetry. Because the electronic transitions are not restricted and polarized along x, y, z axes of the molecular coordinate. We assume that the electronic transitions in the near UV-VIS region are mainly π-π^* transitions, and thus are polarized in the molecular plane. Intensity of out-of-plane polarized transitions is assumed to be negligible. The in-plane transitions can be polarized in any direction generating several values of the orientation factor. But fortunately, the values of the orientation factor in this case are only the two distinct values 0.65 and 0.20. This facilitates the LD analysis procedure.

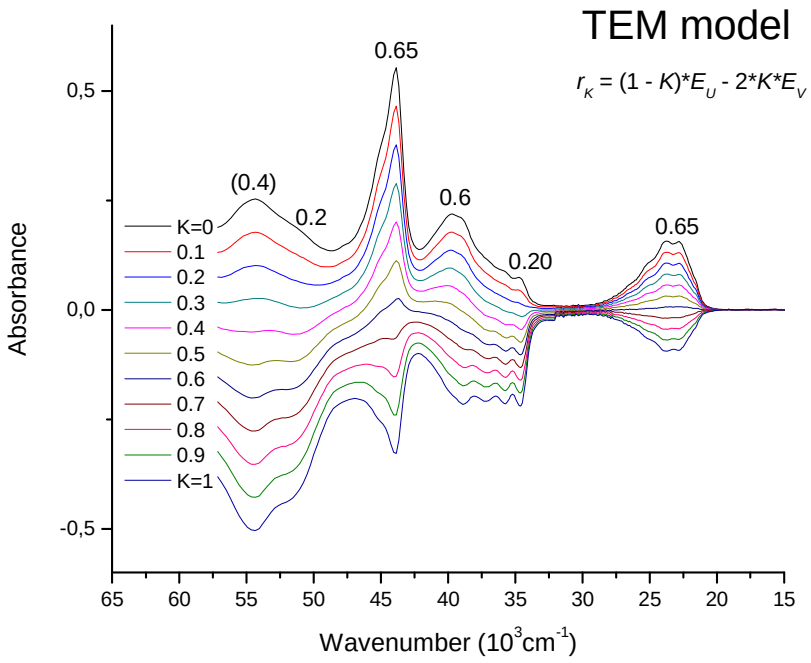

Figure 5.3: The TEM procedure for determining the orientation factors of the spectral features for Anthrarufin. The family of reduced spectral curves with indication of the derived orientation factors (see text for more detail).

Due to unrestricted polarization of the in-plane transitions, it is essential to determine angle ϕ_i that is formed by moment vector of i^{th} transition with a well-defined axis in the molecular plane (as shown in Figure 5.4). This axis is tentatively defined as *x* axis which is parallel to the long-axis of the parent anthraquinone framework. We shall assume that this axis (*x*) corresponds to the molecular orientation axis, i.e., the axis with the largest value of the average cosine squared, $\langle \cos^2(x,U) \rangle = K_x$. And *y* is the in-plane axis that is perpendicular to *x* which corresponds to the lowest value of the average cosine squared, $\langle \cos^2(y,U) \rangle = K_y$, among directions in the plane. Moreover, we shall assume that the orientation factors K_x and K_y are equal to 0.65 and 0.20, respectively.

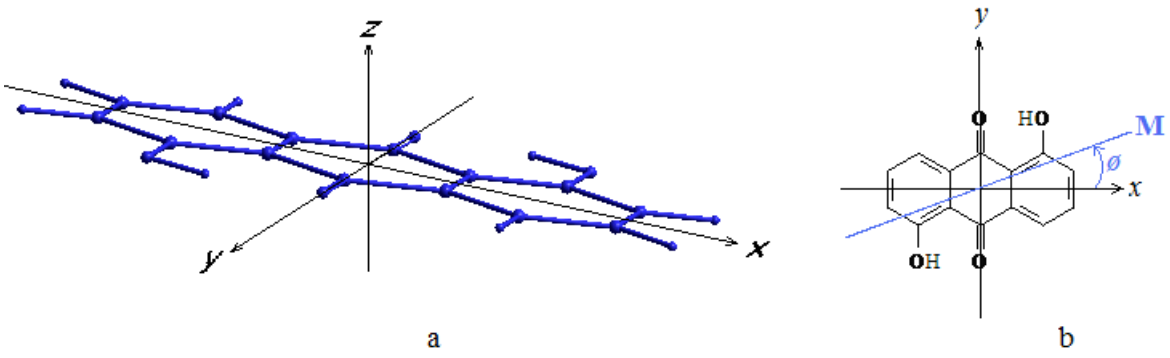

Figure 5.4: (a) The molecular coordinate system of Anthrarufin, with x axis is a specific, well-defined axis in the molecular plane, and chosen as the molecular orientation axis; y is the in-plane axis perpendicular to x; and z axis is the out-of-plane axis which is perpendicular to xy plane. (b) Illustration of the angle ϕ_i which is formed by the moment vectors of i^{th} transitions with x axis.

The value of the moment angles ϕ can be determined for the absorption bands by substituting the obtained K values into expression (31), and listed in Table 5.1. The results show that these moment angles are close to values of 0^o and 90^o. This indicates that the electronic transitions are predominantly polarized along the long- and short-axis in the molecular plane as chosen and defined above. This result is supported by the calculated transition moment directions (see below).

Because the orientation factor of the absorption bands are in two distinct values 0.65 and 0.20 as discussed above, we can construct the two partial absorption curves, A_1 and A_2, which indicate absorbance of the electronic transitions whose moment angles are close to 0^o and 90^o corresponding to the long- and short-axis polarized transitions. These curves are shown in Figure 5.5.

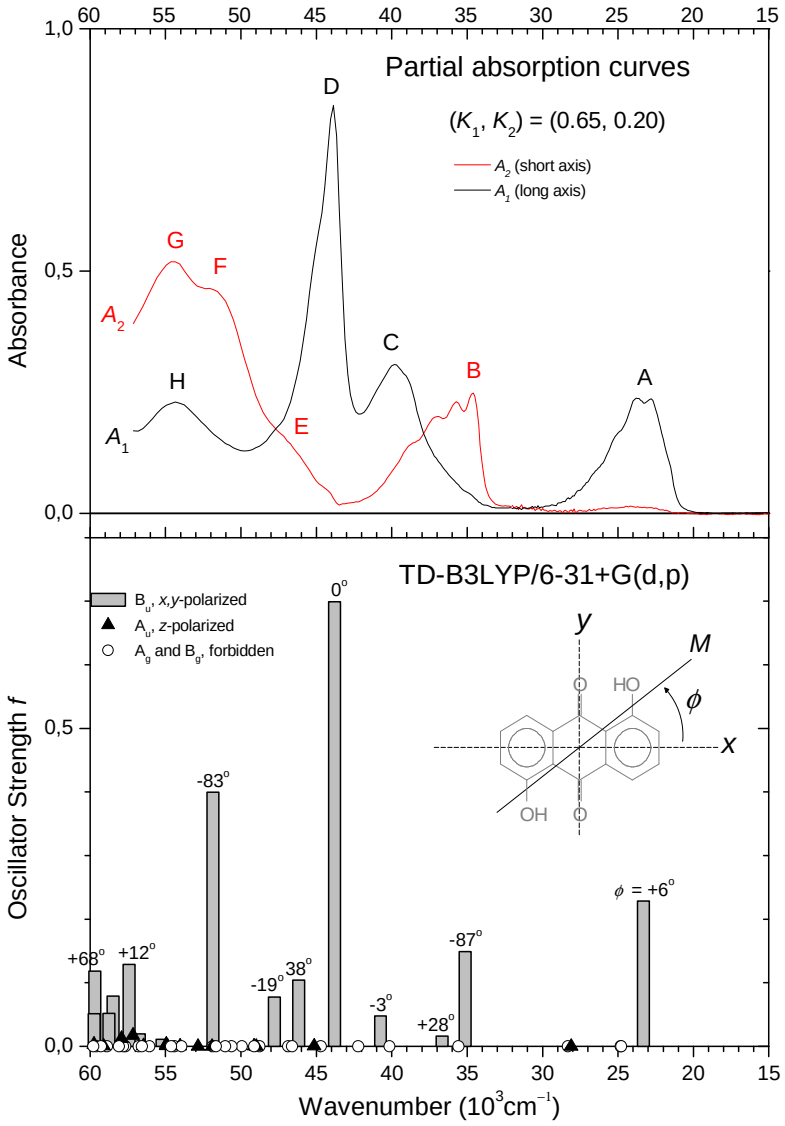

Figure 5.5: Top: The partial absorption curves of Anthrarufin. This compound belongs to "low" molecular symmetry with C_{2h} point group. The red curve (A_2) and the black curve (A_1) describe absorption bands whose electronic transition moment are predominant in direction along the short in-plane axis (y) and the long in-plane axis (x) of the molecular framework, respectively. Bottom: Theoretically predicted transitions (Table 5.1).

The observed and predicted electronic transitions are described and listed in Figure 5.5 and Table 5.1. Due to the properties of C_{2h} point group, the in-plane polarized transitions are assigned to ^1B_u state (The character tables are shown in Appendix 10).

The comparison of the experimental and calculated transitions shows that the absorption bands A, C and D at 23800, 39800 and 43900 cm^{-1} can be assigned to essentially long-axis polarized transitions predicted at 23300, 40700 and 43800 cm^{-1}, and band B at 34600 cm^{-1} is assigned to essentially short-axis polarized transition predicted at 35100 cm^{-1}. Shoulder F at 49300 cm^{-1} can also be assigned to the short-axis polarized transition predicted at 51900 cm^{-1} if the orientation factor of this absorption band accepts the value of 0.20 which in turns is used to determine the value of the moment angle ϕ.

Table 5.1: Observed and predicted electronic transitions for Anthrarufin

	Stretched PE [a]				TD-B3LYP/6-31+G(d,p) [b]				
	$\tilde{\nu}$ [c]	A [d]	K [e]	$\lvert\phi\rvert$ [f]	Term	$\tilde{\nu}$ [c]	f [g]	ϕ [f]	Leading configurations [h]
A	23.8	0.24	0.60	~0°	$1\,^1B_u$	23.3	0.23	+6°	85%(1,-1)
					$1\,^1B_g$	24.8	0	-	94%(3,-1)
					$2\,^1A_g$	24.8	0	-	83%(2,-1)
					$1\,^1A_u$	28.1	$1\cdot10^{-4}$	*z*	91%(6,-1)
					$3\,^1A_g$	28.3	0	-	90%(4,-1)
B	34.6	0.25	0.20	~90°	$2\,^1B_u$	35.1	0.15	+93°	81%(5,-1)
					$4\,^1A_g$	35.6	0	-	88%(1,-2)
					$3\,^1B_u$	36.7	0.02	+28°	90%(2,-2)
					$2\,^1A_u$	38.9	$<10^{-4}$	*z*	93%(3,-2)
					$5\,^1A_g$	40.2	0	-	81%(1,-3), 11%(5,-2)
C	39.8	0.31	0.60	~0°	$4\,^1B_u$	40.7	0.05	–3°	63%(2,-3), 31%(4,-2)
					$2\,^1B_g$	42.2	0	-	92%(6,-2)
D	43.9	0.84	0.60	~0°	$5\,^1B_u$	43.8	0.70	0°	54%(4,-2), 28%(2,-3)
					$6\,^1A_g$	44.7	0	-	67%(7,-1), 18%(5,-2)
					$3\,^1A_u$	45.1	$3\cdot10^{-4}$	*z*	96%(3,-3)
E [i]	46.3	0.10	-	-	$6\,^1B_u$	46.2	0.10	+38°	61%(8,-1), 25%(1,-4)
					$7\,^1B_u$	47.8	0.08	–19°	41%(1,-4), 25%(4,-3), 24%(8,-1)
F [i]	49.3	0.07	0.20	~90°	$8\,^1B_u$	51.9	0.40	–83°	51%(4,-3), 20%(1,-4)
G	54.3	0.29	-	-	$9\,^1B_u$	55.2	0.01	+3°	56%(1,-9), 40%(5,-4)
					$10\,^1B_u$	56.7	0.02	–6°	56%(13,-1), 19%(5,-4), 14%(1,-9)
					$12\,^1A_u$	57.2	0.02	*z*	66%(1,-10), 16%(2,-8)
H	54.3	0.08	-	-	$11\,^1B_u$	57.4	0.13	+12°	40%(7,-2), 21%(13,-1), 20%(5,-4), 13%(1,-9)
					$13\,^1A_u$	57.9	0.01	*z*	69%(4,-6), 20%(5,-5)
					$12\,^1B_u$	58.5	0.08	–1°	23%(2,-12), 20%(7,-2), 18%(3,-6)
					$13\,^1B_u$	58.8	0.05	–49°	49%(3,-6), 14%(2,-12), 14%(2,-11)
					$14\,^1B_u$	59.7	0.12	+68°	34%(6,-5), 22%(3,-8), 10%(2,-11)
					$15\,^1B_u$	59.7	0.05	–38°	22%(7,-2), 20%(2,-12), 19%(3,-6)

[a] Absorption peaks measured in stretched polyethylene.
[b] In the region above 45000 cm^{-1}, only predicted transitions with $f \geq 0.01$ are listed (see Appendix 8 for full listing of all calculated transitions).
[c] Wavenumber in 10^3 cm^{-1}.
[d] Absorbance from the partial absorption curves in Fig. 5.5.
[e] Orientation factor, see text.
[f] In-plane transition moment angle ϕ (*z* designates out-of-plane polarization).
[g] Oscillator strength.
[h] The notation (*i*,-*j*) indicates an excited singlet configuration derived from the ground configuration by promotion of an electron from the i^{th} highest occupied to the j^{th} lowest unoccupied molecular orbital.
[i] Shoulder

The determination of *K* values for the absorption bands in the high energy region is not straightforward due to the complicated overlapping of differently polarized transitions. This leads to the fact that it is difficult to assign information to bands E, G and H at 46300 and 54300 cm^{-1}. However, these bands can probably be assigned to transitions predicted at 46200, 55200 and 57400 cm^{-1} with the values of the moment angle 38^o, 3^o and 12^o, respectively; if we assume that the comparison is only done for the energy and intensity of the electronic transitions.

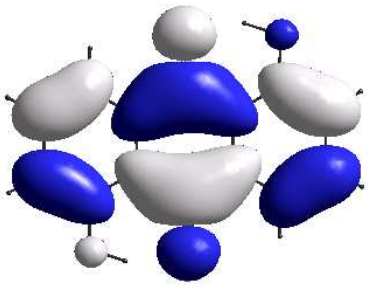

6 b_g (π^*)

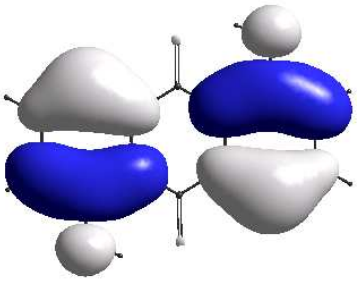

5 a_u (π)

Figure 5.6: Diagrams of the highest occupied and lowest unoccupied molecular orbitals for Anthrarufin. More orbital diagrams can be seen in Appendix 9.

The shape of molecular orbitals which correspond to the electronic promotions of the absorption bands is shown in Appendix 9. Figure 5.6 shows the orbital shapes of the HOMO 5 a_u (π) and LUMO 6 b_g (π^*) corresponding to the electronic promotion of the low energy band A in the spectrum of Anthrarufin.

5.3 Conclusion

This study provides information on the polarization and molecular symmetry of the electronic transitions in the region from ca. 15000 cm^{-1} to ca. 58000 cm^{-1}, especially in the high energy region from ca. 47000 cm^{-1} to ca. 58000 cm^{-1} for Anthrarufin. In addition, this method can resolve the overlapping, differently polarized transitions, particularly bands D and E, bands G and H. This results in that the assignment of the electronic transitions is reliable and precise.

The good agreement between the observed and predicted transitions indicates that quantum chemical calculation is actually a useful tool for prediction and assignment of the electronic transitions. In particular, the spectroscopic information of eight absorption bands is obtained in the present work.

Chapter 6
Concluding remarks

The SRLD investigations in the present study provide more information on the polarization data of the electronic transitions in 15000 – 58000 cm^{-1} spectral region, especially the transitions in the high energy region (above 50000 cm^{-1}) of compounds in question. This means that optical information can be extended up to 11000 cm^{-1} compared to the LD traditional measurements.

The experimental results also show that all compounds of interest are introduced successfully into the LDPE matrix with enough concentration for the LD measurements, especially in the high energy region. Although the stretched LDPE is a simple and inexpensive method which can produce highest orientation of molecules, the procedure of sample preparation is not always straightforward. During this work, the sample procedures have been developed and refined carefully and meticulously for each compound of interest, producing good samples for the SRLD measurements. Therefore, this method can be applied in any laboratory in the world which interest in spectroscopic properties of compounds.

The analysis of the LD spectra indicates that this investigation method provides more reliable and precise polarization data than those from other methods. All optical features of studied compounds including shape, intensity and energy of absorption bands are revealed clearly in the investigated spectral region, especially overlapping bands. It is an advantage of this technique.

The good agreement between theoretical and experimental results leads to precise prediction and assignment of the electronic transitions and molecular symmetry as well as the direction of the transition moment vectors in the molecular framework. This provides new and useful information on the electronic transitions and their moment vectors for groups of compounds. And this also shows that quantum chemical calculation is a useful tool which can be applied for many studies, particularly in spectroscopic method. Because there is no versatile computational method which can be used for all studies, it is important to find out and apply an appropriate method for each investigation.

In summary, the results obtained in this thesis indicate that the stretched LDPE technique and computational method can be applied to other compounds, providing more additional and useful information on the optical properties of compounds. This will generate a basic data source which can be use as a reference in further studies.

As mentioned above, the molecular symmetry facilitates the analysis procedure of the UV-VIS LD data, resulting in precise assignments of the electronic transitions, especially the compounds which belong to “high” symmetry group. In case of “low” symmetrical compounds, the LD measurements should be performed by combining several spectroscopic methods including IR, UV-VIS and fluorescence LD spectroscopies. The IR LD measurements will provide information on the orientation of the moment vector of the out-of-plane transitions. And the fluorescence LD measurements will provide information on the relative sign of the angle which is composed of the molecular orientation axis and the moment vector of the in-plane transitions.

Glossary

6-31G(d,p): is a split valence basis set with polarization functions (d functions are added to heavy atoms and p functions are added to hydrogen atoms).
6-31G+(d,p): is a split valence basis set with diffusion and polarization functions (d functions are added to heavy atoms and p functions are added to hydrogen atoms).
Aligned sample: is a sample which is oriented to a certain direction.
Anisotropy: is differently directional dependence of a material's physical properties (absorbance, refractive index,…).
B3LYP: is a hydrid functional (exchange and correlation) which is used in DFT.
C_2: is a rotation of molecule by $2\pi/2 = \pi$ radian about an axis which produces an indistinguishable configuration from the initial one.
C_{2v}: is a point group which contains one C_2 axis and two vertical planes of symmetry containing the C_2 axis.
C_s also called C_{1v}: is a point group which contains one C_1 axis and one vertical plane of symmetry containing the C_1 axis.
C_{2h}: is a point group containing one C_2 axis and one horizontal plane of symmetry perpendicular to the C_2 axis.
Character table: is a representation of all operations of symmetry in a point group.
D_2: is a point group which contains three mutually perpendicular C_2 axes.
D_{2h}: is a point group which contains three mutually perpendicular C_2 axes and three mutually perpendicular planes of symmetry containing the C_2 axes.
Density functional theory (DFT): is a quantum mechanical theory used to optimize molecular geometry, and investigate the ground state electronic structure of many-body systems.
Dichroism: is dependence of absorption on the type of polarization of the measuring beam which can be linear or circular polarization.
Dissociation constant (pK_a): is the equilibrium constant of a protolytic reaction as defined below:

$$AH + H_2O \leftrightarrows A^- + H_3O^+$$

$$K_a = \frac{C_{A^-} \cdot f_{A^-}}{C_{AH} \cdot f_{AH}} \cdot \frac{a_{H_3O^+}}{a_{H_2O}}$$

Where: C_{AH}, C_{A^-} are molar concentration of AH and A^-; $f_{AH}=1$, f_{A^-} are activity coefficients; $a_{H_2O} = 1$, $a_{H_3O^+}$ are activity of H_2O and H_3O^+.

Isotropy: is homogeneity of a material's physical properties in all directions.
Linear combination of orthogonalized atomic orbitals (LCOAO): is a semi-empirical method which is used to investigate the electronic absorption and magnetic circular dichroism data for organic π systems.
Linear dichroism (LD): is difference in absorption for two perpendicularly linearly polarized beams: $\Delta A_L = A_Z - A_Y$
Low density polyethylene (LDPE): is polyethylene whose structure has about 2% branching and its density range is of 0.910 – 0.940 g/cm^3
Polarization: refers to the orientation of the electric field of the optical radiation.
Polarization spectroscopy: is a method in which polarized light passes through an anisotropic sample.

Point group: is a group of elements of symmetry. When all operations of the group are carried, at least one point is unaffected.
Synchrotron radiation (SR): is light emitted from circular motion of charged particles in a storage ring.
Synchrotron radiation linear dichroism (SRLD): is the difference in absorption for two perpendicularly linearly polarized beams which are emitted from synchrotron system.
Time-dependent density functional theory (TD-DFT): is extended theorem of DFT with the presence of time-dependent potentials. This method can be used to describe the properties of the excited states (excitation energies, frequency-dependent response properties, photoabsorption spectra).
Uniaxial sample: is a sample which is characterized by a unique sample axis *z* with all directions perpendicular to *z* being equivalent.

References

1. (a) R.S. Mulliken, The interpretation of band spectra. Parts I, IIa, IIb, *Rev. Mod. Phys.*, **2** (1930) 60-115; (b) Additions and corrections for Parts I, IIa, IIb, *Rev. Mod. Phys.*, **2** (1930) 506-508; (c) Part IIc. Empirical band types, *Rev. Mod. Phys.*, **3** (1931) 89-155; (d) Part III. Electron quantum numbers and states of molecules and their atoms, *Rev. Mod. Phys.*, **4** (1932) 1-86
2. H. Sponer, E. Teller, Electronic spectra of polyatomic molecules, *Rev. Mod. Phys.*, **13** (1941) 75-170
3. R.S. Mulliken, Carol A. Rieke, Molecular electronic spectra, dispersion and polarization: the theoretical interpretation and computation of oscillator strengths and intennsities, *Rep. Prog. Phys.*, **8** (1941) 231-273
4. W. Bernreuther, M. Suzuki, The electric dipole moment of the electron, *Rev. Mod. Phys.*, **63** (1991) 313-340
5. (a) R.G. Burns, Apparatus for measuring polarized absorption spectra of small crystals, *J. Sci. Instrum.*, **43** (1966) 58-60; (b) J.H. Jaffe, H. Jaffe, K. Rosenheck, New method of measuring linear dichroism in the ultraviolet: Application to helical polymers, *Rev. Sci. Instrum.*, **38** (1967) 935-938; (c) J. Brahms, J. Pilet, H. Damany, V. Chandrasekharan, Application of a new modulation method for linear dichroism studies of oriented biopolymers in the vacuum ultraviolet, *Proc. Natl. Acad. Sci. U.S.*, **60** (1968) 1130-1137; (d) R. Mandel, G. Holzwarth, High sensitivity linear dichroism measurement with a modified commercial spectropolarimeter, *Rev. Sci. Instrum.*, **41** (1970) 755-758; (e) T. Terada, M. Koyanagi, Y. Kanda, A development in polarization experiments: Emission spectra of anthracene, Dibenzothiophene, and xanthone in stretched polyethylene films, *Bull. Chem. Soc. Jpn.*, **53** (1980) 352-358
6. A. Rich, M. Kasha, The n $\rightarrow \pi^*$ transition in nucleic acids and polynucleotides, *J. Am. Chem. Soc.*, **82** (1960) 6197-6199
7. W.B. Gratzer, G.M. Holzwarth, P. Doty, Polarization of the ultraviolet absorption bands in α-Helical polypeptides, *Proc. Natl. Acad. Sci. U.S.*, **47** (1961) 1785-1791
8. (a) A. Yogev, L. Margulies, D. Amar, Y. Mazur, Studies in linear dichroism. Part I: Quantitative evaluation of linear dichroic properties of molecules in stretched polyethylene films, *J. Am. Chem. Soc.*, **91** (1969) 4558-4559; (b) A. Yogev, J. Riboid, J. Marero, Y. Mazur, Studies in linear dichroism. Part II: Measurement of the transition moment vector of α,β-Unsaturated ketones, and of some geometrical properties of steroids, *J. Am. Chem. Soc.*, **91** (1969) 4559-4561; (c) A. Yogev, L. Margulies, Y. Mazur, Studies in linear dichroism. Part III: Application to molecular associations, *J. Am. Chem. Soc.*, **92** (1970) 6059-6061; (d) Part V: Spectroscopic and conformational properties of the benzyloxy group, *J. Am. Chem. Soc.*, **93** (1971) 249-251
9. E.W. Thulstrup, J.H. Eggers, Moment directions of the electronic transitions of fluoranthene, *Chem. Phys. Lett.*, **1** (1968) 690-692
10. (a) J. Michl, E.W. Thulstrup, J.H. Eggers, Polarization spectra in stretched polymer sheets. Part I: Physical significance of the orientation factors and determination of pi-pi* transition moment directions in molecules of low symmetry, *J. Phys. Chem.*, **74** (1970) 3878-3884; (b) E.W. Thulstrup, J. Michl, J.H. Eggers, Part II: Separation of pi-pi* absorption of symmetrical molecules into components, *J. Phys. Chem.*, **74** (1970) 3868-3878; (c) E.W. Thulstrup, J. Michl, A critical comparison of methods for analysis of linear dichroism of solutes in stretched polymers, *J. Phys. Chem.*, **84** (1980) 82-93; (d) E.W. Thulstrup, J. Michl, Orientation and linear dichroism of

symmetrical aromatic molecules imbedded in stretched polyethylene, *J. Am. Chem. Soc.*, **104** (1982) 5594-5604; (e) J. Michl, E.W. Thulstrup, Ultraviolet and infrared linear dichroism: polarized light as a probe of molecular and electronic structure, *Acc. Chem. Res.*, **20** (1987) 192-199; (f) E.W. Thulstrup, J. Michl, Polarized absorption spectroscopy of molecules aligned in stretched polymers bl, *Spectrochim. Acta A*, **44** (1988) 767-782

11. (a) B.O. Myrvold, J. Spanget-Larsen, E.W. Thulstrup, Transition moment directions in 9,10-anthraquinones. Symmetrical cases, *Chem. Phys.*, **104** (1986) 305-313; (b) J. Spanget-Larsen, D.H. Christensen, E.W. Thulstrup, Symmetry assignments of vibrations in 9,10-anthraquinone aligned in stretched polyethylene, *Spectrochim. Acta A*, **43** (1987) 331-335
12. F. Madsen, I. Terpager, K. Olskær, J. Spanget-Larsen, Ultraviolet-visible and infrared linear dichroism spectroscopy of 1,8-dihydroxy-9,10-anthraquinone aligned in stretched polyethylene, *Chem. Phys.*, **165** (1992) 351-360
13. (a) K.B. Andersen, J. Spanget-Larsen, Electronic transitions and intramolecular hydrogen bonding in anthralin. UV-VIS linear dichroism spectroscopy and quantum chemical calculations, *Spectrochim. Acta A*, **53** (1997) 2615-2625; (b) K.B. Andersen, E. Vogel, J. Waluk, Electronic transition moment directions and tautomerization of 9,10,19 20-tetra-n-propylporphycene, *Chem. Phys. Lett.*, **271** (1997) 341-348
14. (a) K.B. Andersen, M. Langgård, J. Spanget-Larsen, Molecular and vibrational structure of anthralin. Infrared linear dichroism spectroscopy and quantum chemical calculations, *J. Mol. Struct.*, **475** (1999) 131-140; (b) B.K.V. Hansen, S. Møller, J. Spanget-Larsen, The vibrational structure of (E,E´)-1,4-diphenyl-1,3-butadiene. Linear dichroism FT-IR spectroscopy and quantum chemical calculations, *Spectrochim. Acta A*, **65** (2006) 770-778; (c) T.K. Eriksen, B.K.V. Hansen, J. Spanget-Larsen, The vibrational structure of Dibenzo-p-dioxin. IR linear dichroism, Raman spectroscopy, and quantum chemical calculations, *Polish J. Chem.*, **82** (2008) 921-934
15. (a) S. Møller, K.B. Andersen, J. Spanget-Larsen, J. Waluk, Excited-state intramolecular proton transfer in anthralin. Quantum chemical calculations and fluorescence spectra, *Chem. Phys. Lett.*, **291** (1998) 51-56; (b) K.B. Andersen, J. Waluk, E.W. Thulstrup, The electronic structure of carcinogenic of dibenzopyrenes: Linear dichroism, fluorescence polarization spectroscopy and quantum mechanical calculations, *Photochem. Photobiol.*, **69** (1999) 158-166; (c) C. Johannessen, A. Gorski, J. Waluk, J. Spanget-Larsen, Electronic states of anthanthrene. Linear and magnetic circular dichroism, fluorescence anisotropy, and quantum chemical calculations, *Polycyclic Aromat. Compd.*, **25** (2005) 23-45
16. J.R. Chelikowsky, L. Kronik, I. Vasiliev, Time-dependent density-functional calculations for the optical spectra of molecules, clusters and nanocrystals, *J. Phys.: Condens. Matter*, **15** (2003) R1517-R1547
17. M. Dierksen, S. Grimme, Density functional calculations of the vibronic structure of electronic absorption spectra, *J. Chem. Phys.*, **120** (2004) 3544-3554
18. M. Sacchi, F. Sirotti, G. Rossi, R.J.H. Kappert, J. Vogel, J.C. Fuggle, Linear and circular dichroism with soft X-rays, *J. Electron Spectrosc. Relat. Phenom.*, **58** (1992) 393-398
19. K. Yagi-Watanabe, T. Yamada, M. Tanaka, F. Kaneko, T. Kitada, Y. Ohta, K. Nakagawa, Design and implementation of VUV-CD and LD measurements using an ac modulated polarizing undulator, *J. Electron Spectrosc. Relat. Phenom.*, **144-147** (2005) 1015-1018

20. M. Schmidt, U. Schade, M. Grunze, Microspectroscopic observation of vibrational linear dichroism using polarization-modulated infrared synchrotron radiation, *Infrared Phys. Technol.*, **49** (2006) 69-73
21. C. Dicko, M.R. Hicks, T.R. Dafforn, F. Vollrath, A. Rodger, S.V. Hoffmann, Breaking the 200 nm limit for routine flow linear dichroism measurements using UV synchrotron radiation, *Biophys. J.*, **95** (2008) 5974-5977
22. S.C. Nguyen, B.K.V. Hansen, S.V. Hoffmann, J. Spanget-Larsen, Electronic states of emodin and its conjugate base. Synchrotron linear dichroism spectroscopy and quantum chemical calculations, *Chem. Phys.*, **352** (2008) 167-174
23. M.R. Hicks, T.R. Dafforn, A. Damianoglou, P. Wormell, A. Rodger, S.V. Hoffmann, Synchrotron radiation linear dichroism spectroscopy of the antibiotic peptide gramicidin in lipid membranes, *Analyst*, **134** (2009) 1623-1628
24. http://en.wikipedia.org/wiki/Light (April 24th, 2010)
25. http://en.wikipedia.org/wiki/Polarization_(waves) (April 24th, 2010)
26. Heinz-Helmut Perkampus, UV-VIS spectroscopy and its applications, Translated by H. Charlotte Grinter and T.L. Threlfall, Springer-Verlag Berlin Heidelberg, Germany (1992)
27. K.B. Andersen, Polarization spectroscopic studies of β-Hydroxy carbonyl compound with intramolecular H-bonding, PhD thesis, Roskilde University, Denmark 1999
28. D.C. Harris, Quantitative chemical analysis, 7th edition, W.H. Freeman and Company, New York (2007)
29. J. Michl, E.W. Thulstrup, Spectroscopy with polarized light. Solute alignment by photoselection, in liquid crystals, polymers and membranes, VCH publishers, Inc., New York 1986, 1995
30. (a) E.W. Thulstrup, J. Michl, Elementary polarization spectroscopy, VCH publishers, Inc., New York 1989; (b) E.W. Thulstrup, P.W. Thulstrup, Polarization spectroscopic studies of ordered samples, *Acta Chim. Slov.*, **52** (2005) 371-383; (c) P.W. Thulstrup, E.W. Thulstrup, Information content in Linear dichroism spectra, *Polish J. Chem.*, **82** (2008) 901-920
31. D.C. Harris, M.D. Bertolucci, Symmetry and spectroscopy. An introduction to vibrational and electronic spectroscopy, Dover publications, Inc., New York (1989)
32. S.C. Nguyen, Linear dichroism spectroscopic and theoretical investigations of the compound Emodin, Master thesis, Roskilde University, Denmark, 2004
33. S.E. Braslavsky, Glossary of terms used in photochemistry, 3rd edition, International union of pure and applied chemistry – Organic and biomolecular chemistry division sub-committee on photochemistry (2005)
34. http://en.wikipedia.org/wiki/Polarizer (April 24th, 2010)
35. H. Saisho, Y. Gohshi, Applications of synchrotron radiation to materials analysis, Elsevier science BV, Netherlands 1996
36. S. Khan, Collective phenomena in synchrotron radiation sources, Springer-Verlag Berlin Heidelberg 2006
37. B.A. Wallace, R.W. Janes, Modern techniques for circular dichroism and synchrotron radiation circular dichroism spectroscopy, IOS press BV, Netherlands 2009
38. R. Rohlsberger, Nuclear condensed matter physics with synchrotron radiation, Springer-Verlag Berlin Heidelberg 2004
39. R. Stensgaard, ASTRID – The Aarhus Storage Ring, *Phys. Scr.*, **T22** (1988) 315-317; http://en.wikipedia.org/wiki/ASTRID and suitable links therein (June 24th, 2010).

40. J. Fabian, L.A. Diaz, G. Seifert, T. Niehaus, Calculation of excitation-energies of organic chromophores: a critical evaluation, *J. Mol. Struct. Theochem*, **594** (2002) 41-53

41. (a) M.C. Zerner, G.H. Loew, R.F. Kirchner, U.T. Mueller-Westerhoff, An intermediate neglect of differential overlap technique for spectroscopy of transition-metal complexes: Ferrocene, *J. Am. Chem. Soc.*, **102** (1980) 589-599; (b) W.P. Anderson, W.D. Edwards, M.C. Zerner, Calculated spectra of hydrated ions of the first transition-metal series, *Inorg. Chem.*, **25** (1986) 2728-2732; (c) J.J.P. Stewart, Optimization of parameters for semiempirical method II. Applications, *J. Comput. Chem.*, **10** (1989) 221-264; (d) M.A. Thompson, M.C. Zerner, A theoretical examination of the electronic structure and spectroscopy of the photosynthetic reaction center from Rhodopseudomonas viridis, *J. Am. Chem. Soc.*, **113** (1991) 8210-8215

42. (a) B. Hohenberg, W. Kohn, Inhomogeneous electron gas, *Phys. Rev.*, **136** (1964) B864-B871; (b) J.P. Perdew, W. Yue, Accurate and simple density functional for the electron exchange energy: Generalized gradient approximation, *Phys. Rev. B*, **33** (1986) 8800-8802; (c) J.P. Perdew, Density-functional approximation for the correlation energy of the inhomogeneous electron gas, *Phys. Rev. B*, **33** (1986) 8822-8824; (d) C. Lee, W. Yang, R.G. Parr, Development of the Colle-Salvetti correlation-energy formula into a functional of the electron density, *Phys. Rev. B*, **37** (1988) 785-789; (e) A.D. Becke, Density-functional exchange-energy approximation with correct asymptotic behavior, *Phys. Rev. A*, **38** (1988) 3098-3100; (f) M.E. Casida, C. Jamorski, K.C. Casida, D.R. Salahub, Molecular excitation energies to high-lying bound states from time-dependent density-functional response theory: Characterization and correction of the time-dependent local density approximation ionization threshold, *J. Chem. Phys.*, **108** (1998) 4439-4449; (g) R.E. Stratmann, G.E. Scuseria, M.J. Frisch, An efficient implementation of time-dependent density-functional theory for the calculation of excitation energies of large molecules, *J. Chem. Phys.*, **109** (1998) 8218-8224

43. (a) W.J. Hehre, R. Ditchfield, J.A. Pople, Self-consistent molecular orbital methods. XII. Further extensions of Gaussian-type basis sets for use in molecular orbital studies of organic molecules, *J. Chem. Phys.*, **56** (1972) 2257-2261; (b) M.M. Francl, W.J. Pietro, W.J. Hehre, J.S. Binkley, D.J. DeFrees, J.A. Pople, M.S. Gordon, Self-consistent molecular orbital methods. XXIII. A polarization-type basis set for second-row elements, *J. Chem. Phys.*, **77** (1982) 3654-3665

44. (a) A.D. Becke, Density-functional thermochemistry. I. The effect of the exchange-only gradient correction, *J. Chem. Phys.*, **96** (1992) 2155-2160; (b) II. The effect of the Perdew-Wang generalized-gradient correlation correction, *J. Chem. Phys.*, **97** (1992) 9173-9177; (c) III. The role of exact exchange, *J. Chem. Phys.*, **98** (1993) 5648-5652

45. R. Bauernschmitt, R. Ahlrichs, Treatment of electronic excitations within the adiabatic approximation of time dependent density functional theory, *Chem. Phys. Lett.*, **256** (1996) 454-464

46. M. Stener, G. Fronzoni, D. Toffoli, P. Decleva, Time dependent density functional photoionization of CH_4, NH_3, H_2O and HF, *Chem. Phys.*, **282** (2002) 337-351

47. J.E. Monat, J.H. Rodriguez, J.K. McCusker, Ground- and excited-state electronic structures of the solar cell sensitizer Bis(4,4'-dicarboxylato-2,2'-bipyridine) bis(isothiocyanato)ruthenium(II), *J. Phys. Chem. A*, **106** (2002) 7399-7406

48. M. Savko, S. Kascáková, P. Gbur, P. Miskovský, J. Ulicný, Performance of time dependent density functional theory on excitations of medium sized molecules – Test

on ionic forms of anthraquinone dihydroxy derivatives, *J. Mol. Struct. Theochem*, **823** (2007) 78-86

49. J. Fabian, TDDFT-calculations of Vis/NIR absorbing compounds, *Dyes Pigm.*, **84** (2010) 36-53
50. J.B. Foresman, Æ. Frish, Exploring chemistry with electronic structure methods, Gaussian, Pittsburgh, USA 1996
51. M.J. Frisch, G.W. Trucks, H.B. Schlegel, G.E. Scuseria, M.A. Robb, J.R. Cheeseman, J.A. Montgomery, Jr., T. Vreven, K.N. Kudin, J.C. Burant, J.M. Millam, S.S. Iyengar, J. Tomasi, V. Barone, B. Mennucci, M. Cossi, G. Scalmani, N. Rega, G.A. Petersson, H. Nakatsuji, M. Hada, M. Ehara, K. Toyota, R. Fukuda, J. Hasegawa, M. Ishida, T. Nakajima, Y. Honda, O. Kitao, H. Nakai, M. Klene, X. Li, J.E. Knox, H.P. Hratchian, J.B. Cross, V. Bakken, C. Adamo, J. Jaramillo, R. Gomperts, R.E. Stratmann, O. Yazyev, A.J. Austin, R. Cammi, C. Pomelli, J.W. Ochterski, P.Y. Ayala, K. Morokuma, G.A. Voth, P. Salvador, J.J. Dannenberg, V.G. Zakrzewski, S. Dapprich, A.D. Daniels, M.C. Strain, O. Farkas, D.K. Malick, A.D. Rabuck, K. Raghavachari, J.B. Foresman, J.V. Ortiz, Q. Cui, A.G. Baboul, S. Clifford, J. Cioslowski, B.B. Stefanov, G. Liu, A. Liashenko, P. Piskorz, I. Komaromi, R.L. Martin, D.J. Fox, T. Keith, M.A. Al-Laham, C.Y. Peng, A. Nanayakkara, M. Challacombe, P.M.W. Gill, B. Johnson, W. Chen, M.W. Wong, C. Gonzalez, J.A. Pople, GAUSSIAN 03, Revision C.02, Gaussian, Inc., Wallingford CT, 2004.
52. Zheng-Li Cai, K. Sendt, J. R. Reimers, Failure of density-functional theory and time-dependent density-functional theory for large extended π systems, *J. Chem. Phys.*, **117** (2002) 5543-5549
53. A. Dreuw, M. Head-Gordon, Failure of time-dependent density functional theory for long-range charge-transfer excited states: The zincbacteriochlorin-bacteriochlorin and bacteriochlorophyll-spheroidene complexes, *J. Am. Chem. Soc.*, **126** (2004) 4007-4016
54. (a) W. Heiringer, A. Gorling, Failure of time-dependent density functional methods for excitations in spatially separated systems, *Chem. Phys. Lett.*, **419** (2006) 557-562; (b) A. Dreuw, M. Head-Gordon, Comment on: 'Failure of time-dependent density functional methods for excitations in spatially separated systems' by Wolfgang Heiringer and Andreas Gorling, *Chem. Phys. Lett.*, **426** (2006) 231-233; (c) W. Heiringer, A. Gorling, Reply to comment on 'Failure of time-dependent density functional methods for excitations in spatially separated systems' by Andreas Dreuw and Martin Head-Gordon, *Chem. Phys. Lett.*, **426** (2006) 234-236
55. M.V. Faassen, K. Burke, A new challenge for time-dependent density functional theory, *Chem. Phys. Lett.*, **431** (2006) 410-414
56. M. Gruning, X. Gonze, Macroscopic limit of time-dependent density-functional theory for adiabatic local approximations of the exchange-correlation kernel, *Phys. Rev. B*, **76** (2007) 035126-(1-6)
57. K.J.H. Giesbertz, E. J. Baerends, Failure of time-dependent density functional theory for excited state surfaces in case of homolytic bond dissociation, *Chem. Phys. Lett.*, **461** (2008) 338-342
58. (a) J. Spanget-Larsen, On bridging the gap between extended Huckel and NDO type LCAO-MO theories, *Theoret. Chim. Acta*, **55** (1980) 165-172; (b) The alternant hydrocarbon pairing theorem and all-valence electrons theory. An approximate LCOAO theory for the electronic absorption and MCD spectra of conjugated organic compounds. Part 1, *Croat. Chem. Acta*, **59** (1986) 711-717; (c) Part 2, *Theor. Chem. Acc.*, **98** (1997) 137-153

59. (a) S. Eden, P. Limao-Vieira, S.V. Hoffmann, N.J. Mason, VUV photoabsorption in CF_3X (X=Cl, Br, I) fluoro-alkanes, *Chem. Phys.*, **323** (2006) 313-333; (b) M. Nobre, A. Fernandes, F. Ferreira da Silva, R. Antunes, D. Almeida, V. Kokhan, S.V. Hoffmann, N.J. Mason, S. Eden and P. Limao-Vieira, The VUV electronic spectroscopy of acetone studied by synchrotron radiation, *Phys. Chem. Chem. Phys.*, **10** (2008) 550-560

60. (a) A.J. Miles, S.V. Hoffmann, Y. Tao, R.W. Janes, B.A. Wallace, Synchrotron radiation circular dichroism (SRCD) spectroscopy: New beamlines and new applications in biology, *Spectroscopy*, **21** (2007) 245-255; (b) A.J. Miles, R.W. Janes, A. Brown, D.T. Clarke, J.C. Sutherland, Y. Tao, B.A. Wallace and S.V. Hoffmann, Light flux density threshold at which protein denaturation is induced by synchrotron radiation circular dichroism beamlines, *J. Synchrotron Rad.*, **15** (2008) 420-422

61. C. Vasile, M. Pascu, Practical guide to Polyethylene, Rapra Technology Limited, Shawbury, Shrewsbury, Shropshine, UK 2005

62. A.J. Peacock, Handbook of polyethylene: Structures, properties and applications plastics engineering, Marcel Dekker Inc., New York 2000

63. L.R.G. Treloar, Introduction to polymer science, Wykeham publications (London) Ltd., London & Winchester 1970

64. L. Y. Zhou, Quantitative analysis of additives in low-density polyethylene using on-line supercritical fluid extraction/supercritical fluid chromatography, Master thesis, Faculty of the Virginia Polytechnic Institute and State University, Blacksburg, Virginia (1998)

65. I.E. Helmroth, M. Dekker, Th. Hankemeier, Additive diffusion from LDPE slabs into contacting solvents as a function of solvent absorption, *J. Appl. Polym. Sci.*, **90** (2003) 1609-1617

66. L.A. Pigelow, H.H. Reynolds, Quinizarin, *Org. Synth.*, **6** (1926) 78-80; *Org. Synth.*, Coll. **1** (1941) 476-478

67. (a) V. Kuban, J. Havel, Some 2-(2-thiazolylazo)-4-methoxyphenol (TAMP) complex equilibria. I. Acid-base properties of TAMP in water and in various mixed solvents, *Acta Chem. Scand.*, **27** (1973) 528-540; (b) D. Wang, G. Yang, X. Song, Determination of pK_a values of anthraquinone compounds by capillary electrophoresis, *Electrophoresis*, **22** (2001) 464-469

68. (a) M. Levitus, K. Schmieder, H. Ricks, K.D. Shimizu, U.H.F. Bunz, M.A. Garcia-Garibay, Steps to demarcate the effects of chromophore aggregation and planarization in poly(phenyleneethynylene)s. 1. Rotationally interrupted conjugation in the excited states of 1,4-Bis(phenylethynyl)benzene, *J. Am. Chem. Soc.*, **123** (2001) 4259-4265; (b) A. Beeby, K. Findlay, P.J. Low, T.B. Marder, A re-evaluation of the photophysical properties of 1,4-Bis(phenylethynyl)benzene: A model for poly(phenyleneethynylene), *J. Am. Chem. Soc.*, **124** (2002) 8280-8284; (c) J.M. Seminario, A.G. Zacarias, J.M. Tour, Theoretical study of a molecular resonant tunneling diode, *J. Am. Chem. Soc.*, **122** (2000) 3015-3020.

69. (a) S.J. Greaves, E.L. Flynn, E.L. Futcher, E. Wrede, D.P. Lydon, P.J. Low, S.R. Rutter, A. Beeby, Cavity ring-down spectroscopy of the torsional motions of 1,4-Bis(phenylethynyl)benzene, *J. Phys. Chem. A*, **110** (2006) 2114-2121; (b) T. Fujiwara, M.Z. Zgierski, E.C. Lim, Spectroscopy and photophysics of 1,4-Bis(phenylethynyl) benzene: Effects of ring torsion and dark $\pi\sigma^*$ state, *J. Phys. Chem. A*, **112** (2008) 4736-4741; (c) K. Kilså, J. Kajanus, J. Mårtensson, B. Albinsson, Mediated electronic coupling: singlet energy transfer in porphyrin dimers enhanced by the bridging chromophore, *J. Phys. Chem. B*, **103** (1999) 7329-7339

70. (a) S.H. Andersen, Konformation og molekylsymmetri af modelforbindelser for elektrisk ledende polymerer, Master thesis (Danish), Roskilde University, Denmark (2008); (b) J. Spanget-Larsen, Prediction of electronic transitions for organic chromophores, Oral presentation at KOMPKEM meeting, Bogense (2009) (is taken from http://akira.ruc.dk/~spanget/duy/, August 10th, 2010)
71. www.epa.gov/osw/hazard/wastemin/minimize/factshts/dibenzof.pdf (August 10th, 2010)
72. (a) L.G. Pedersen, T.A. Darden, S.J. Oatley, J.D. McKinney, A theoretical study of the binding of polychlorinated biphenyls (PCBs), dibenzodioxins, and dibenzofuran to human plasma prealbumin, *J. Med. Chem.*, **29** (1986) 2451-2457; (b) R. Atkinson, Atmospheric lifetime of dibenzo-p-dioxins and dibenzofurans, *Sci. Total Environ.*, **104** (1991) 17-33; (c) S. Kobayashi, A. Shigihara, H. Ichikawa, A. Tanaka, S. Tobinaga, Relationships between biological potency and electronic states of polychlorinated dibenzofurans and polychlorinated biphenyls, *Chem. Pharm. Bull.*, **40** (1992) 3062-3066; (d) O.V. Dorofeeva, V.S. Iorish, N.F. Moiseeva, Thermodynamic properties of dibenzo-p-dioxin, dibenzofuran, and their polychlorinated derivatives in the gaseous and condensed phases. 1. Thermodynamic properties of gaseous compounds, *J. Chem. Eng. Data*, **44** (1999) 516-523; (e) R. Wenning, D. Dodge, B. Peck, K. Shearer, W. Luksemburg, S.D. Sala, R. Scazzola, Screening-level ecological risk assessment of polychlorinated dibenzo-p-dioxins and dibenzofurans in sediments and aquatic biota from the Venice lagoon, Italy, *Chemosphere*, **40** (2000) 1179-1187
73. Y. Kanda, R. Shimada, K. Hanada, S. Kajigaeshi, Phosphorescence spectra of polycyclic compounds. 1. Fluorene and dibenzofuran, *Spectrochimica Acta*, **17** (1961) 1268-1274
74. M. Baba, K. Mori, M. Yamawaki, K. Akita, M. Ito, S. Kasahara, T. Yamanaka, Vibronic structure in the S_1-S_0 transition of jet-cooled dibenzofuran, *J. Phys. Chem.*, **110** (2006) 10000-10005
75. (a) A. Bree, V.V.B. Vilkos, R. Zwarich, Some electronic spectra of dibenzofuran, *J. Mol. Spectrosc.*, **48** (1973) 135-147; (b) H. Yamaguchi, M. Higashi, Electronic spectra of carbazole, dibenzofuran and dibenzothiophene, *Spectrochimica Acta Part A*, **43** (1987) 1431-1433; (c) N. Igarashi, A. Tajiri, M. Hatano, The magnetic circular dichroism of the conjugated O- and S-Heterocycles, *Bull. Chem. Soc. Jpn.*, 54 (1981) 1511-1516
76. (a) J. Spanget-Larsen, D. Liang, E. Chen, E.W. Thulstrup, Assignments of the IR and UV spectra of dibenzofuran: linear dichroism spectroscopy and quantum chemical calculations, *Asian Chemistry Letters*, **4** (2000) 121-134; (b) D.D. Nguyen, J. Trunk, L. Nakhimovsky, J. Spanget-Larsen, Electronic transitions of fluorene, dibenzofuran, carbazole, and dibenzothiophene. From the onset of absorption to the ionization threshold, *J. Mol. Spectrosc.*, **Accepted**.
77. I. Ljubic, A. Sabljic, Theoretical study of structure, vibrational frequencies, and electronic spectra of dibenzofuran and its polychlorinated derivatives, *J. Phys. Chem. A*, **111** (2007) 1339-1350
78. A. Bree, A.R. Lacey, I.G. Ross, R. Zwarich, Vibronic coupling in the lowest singlet state of dibenzofuran, *Chem. Phys. Lett.*, **26** (1974) 329-333
79. (a) M. Kuzuya, A. Noguchi, K. Kawai, H. Mori, Quantum chemical study for genotoxic and antitumor activities of hydroxyanthraquinones, *Regul. Toxicol. Pharmacol.*, **13** (1991) 185-194; (b) V.Ya. Fain, B.E. Zaitsev, M.A. Ryabov, Tautomerism in anthraquinones: II. *α-hydroxy-substituted anthraquinones, *Russ. J. Org. Chem.*, **41** (2005) 707-714; (c) V.Ya. Fain, B.E. Zaitsev, M.A. Ryabov,

Tautomeric and conformational isomerism of natural hydroxyanthraquinones, *Chem. Nat. Compd.*, **42** (2006) 269-276

80. M.D. Bercich, R.C. Cambie, T.A. Howe, P.S. Rutledge, S.D. Thomson, P.D. Woodgate, Experiments directed towards the synthesis of anthracyclinones. XXV* Synthesis of a vineomycinone B_2 methyl ester intermediate from anthrarufin, *Aust. J. Chem.*, **48** (1995) 531-549

81. N. Namsrai, T. Yoshinari, H. Itoh, S.-I. Nagasaka, Y. Kuriyama, M. Sakamoto, Y. Takahashi, Polarization dependence of absorption and luminescence spectra of a 1,5-dihydroxyanthraquinone single crystal, *J. Phys. Soc. Jpn.*, **75** (2006) 044703-044711

82. D.D Nguyen, N.C. Jones, S.V. Hoffmann, J. Spanget-Larsen, Synchrotron radiation linear dichroism (SRLD) investigation of the electronic transitions of quinizarin, chrysazin, and anthrarufin, *Spectrochimica Acta Part A*, **77** (2010) 279-286

Appendix 1

Sample preparation for PVA sheets

A1.1 Casting procedure of PVA:

Put a magnetic stirring bar and 9.1g of polyvinyl alcohol (PVA) powder whose molecular weight is about 70,000-100,000 into a 100mL Erlenmeyer flask. And also add about 100mL distilled water to the Erlenmeyer flask. The top of the flask is covered by laboratory film (parafilm) to prevent evaporation of water from solution during heating. And then, the flask is placed into a simple water bath which is composed of a big beaker of distilled water and a stirring hotplate. Stirring speed is increased gradually to mix solution well at elevated temperature (150-175^{o}C). Heating is performed until the solution of PVA powder changes from opaque to clear and no bubble. It takes normally about 2-3 hours. After that, the heating is turned off and the stirring speed is decreased to slowest. The PVA solution is allowed to cool until room temperature while stirring as slowly as possible. The cooled PVA solution is poured slowly into a simple mould that is already prepared in dimensions 20cm×20cm to avoid forming bubbles in the PVA layer. The simple mould is a piece of glass which is kept balance, and its dimension is defined by using sticky tape. If there are few bubbles forming during the casting procedure, it can be removed carefully by a little rod.

The PVA layer is covered carefully to avoid contaminating from dust and allowed to dry at room temperature in 5-7 days. This procedure can produce a PVA layer whose thickness is about 0.15mm. If a thicker PVA layer is required, this procedure can be modified in two ways: (1) increasing amount of the PVA powder and distilled water, and (2) decreasing the dimensions of the mould. And of course, it will take longer time for the PVA layer to dry.

After drying, the PVA layer is taken out of the mould and cut into small sheets in dimensions 2.5cm×6.0cm.

A1.2 Solution preparation of compounds:

It is necessary to determine dissociation constants of protic compounds that are investigated by using PVA as an anisotropic solvent. Because PVA is a medium that can exchange protons with compounds, interaction between PVA and compounds is substantial, affecting acidic or basic properties of compounds which are introduced into the PVA matrix.

A1.2.1 Determination of dissociation constant (pK_a):

The experimental procedure is carried out as follow: a known amount of compound of interest is dissolved in methanol to form a stock solution. 17.5mL of this solution is taken and put into a 25mL volumetric flask together with an appropriate volume of acid (used for low pH range) and base (used for high pH range). And add distilled water until the volumetric mark. The flask is closed by a lid, and shaken well. The pH value of the solution is measured by a pH meter. The UV-VIS absorption measurements are performed in studied wavelength ranges. Blank solution is prepared in the same procedure in which

pure methanol is used instead of the solution of compound. And this procedure is applied to solutions at different pH values to get enough data for determining the dissociation constants of compound [26,67].

A1.2.2 Solution of compound:

After the pK_a values are determined, the solutions of compound are prepared for submerging the PVA sheets. If compound has one pK_a value, two solutions are prepared corresponding to two molecular forms, neutral and mono-deprotonated, of the compound. And if compound has two pK_a values, three solutions are prepared corresponding to three molecular forms, neutral, mono-deprotonated and di-deprotonated, of the compound. Acid or base is used to adjust the pH value of the solution to desired value of each form.

The compound is dissolved in a mixture of 35mL of pure methanol and 10mL of distilled water in a sealed container. Acid or base is added to adjust the pH value of the solution and water is added again to reach volume of 50mL. This means that the compound is prepared in a mixed solvent of methanol and water with ratio of 7:3, respectively. The PVA sheets are submerged into these solutions at room temperature in 7 days. The sealed container is sometimes shaken well. Depending on penetration of the compound into the PVA matrix, it can take longer time to introduce enough concentration into the PVA. Normally, the deprotonated forms are introduced more easily into the PVA than neutral one.

After submerging, the PVA sheets are taken out and let solvent evaporate. Pure ethanol is used to cleaned surface of the PVA sheets to remove any crystal of the compound.

A1.3 Stretching of the PVA sample

These PVA sheets are stretched 500-600% by using a mechanical stretcher. Heat from hair-dryer is used to facilitate the stretching procedure. But, heating can also degrade the PVA surface, causing errors in the LD measurements. The stretching procedure is applied for other PVA sheets including samples and blank.

The stretched PVA sheets are held by plastic frame to ensure that the surface of the PVA sheets are always flat and perpendicular to propagation of linearly polarized light during all LD measurements.

A1.4 Results

A1.4.1 Graphical method for determination of the dissociation constant

The experimental procedure is performed to determine the dissociation constant of four protic compounds of interest: alizarin, catenarin, purpurin and quinalizarin as well as some compounds (MB39, MB96 and FZ123) which are from Prof. Lyazidi in Morocco. He asked us for performing the LD measurements of these compounds. The changing of their spectra as a function of pH provides information on determining the dissociation constants. It can be visually estimated on series of spectra or accurately calculated by following equation [26,67]:

$$\log\frac{A-\varepsilon_1\cdot C_R}{\varepsilon_2\cdot C_R-A}=\log K_x+q\cdot pH$$

Where, A is an absorbance (dimensionless), C_R is the total molar concentration of compound ($mol\cdot L^{-1}$), ε_1 and ε_2 are molar absorption coefficients ($L\cdot mol^{-1}\cdot cm^{-1}$) of two

different molecular forms of compound in the dissociation reaction, K_x is the equiblirium constant of the dissociation reaction, q is the number of protons liberated in the dissociation reaction.

All spectra are measured at room temperature on a traditional spectrophotometer (UV-VIS scanning spectrophotometer – UV-2101PC Shimadzu) and 1 cm fused quartz cuvette in the ultraviolet region.

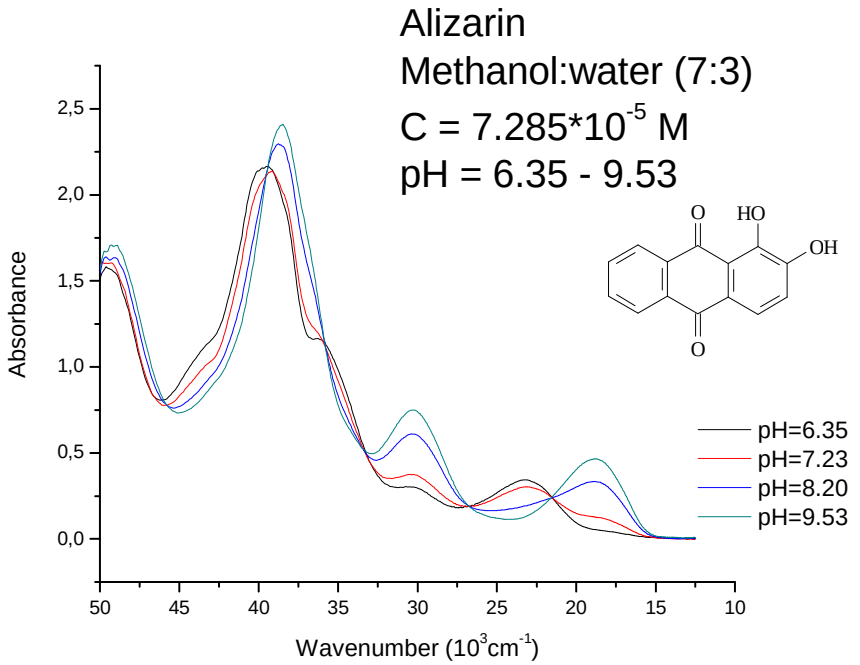

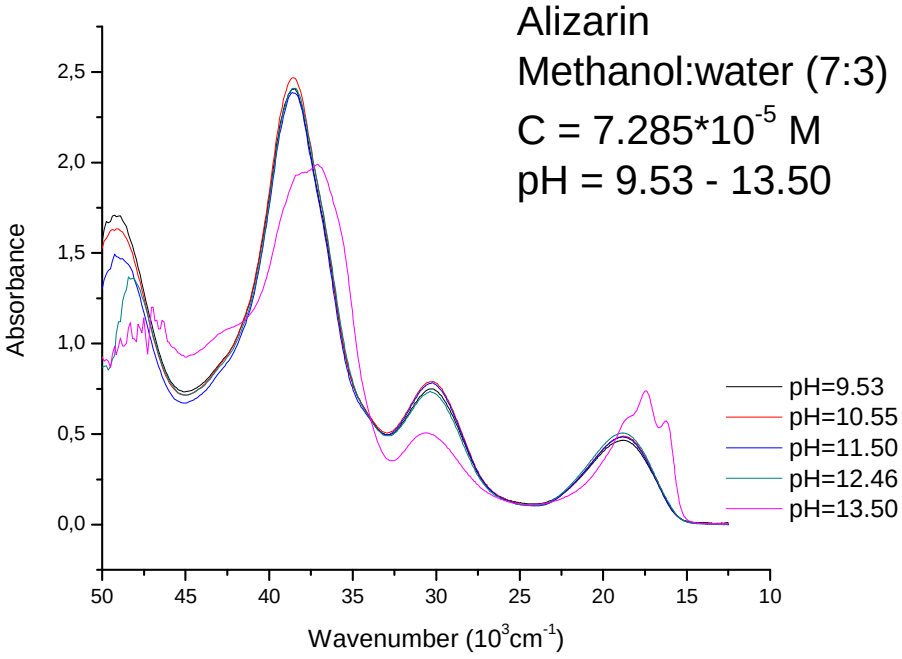

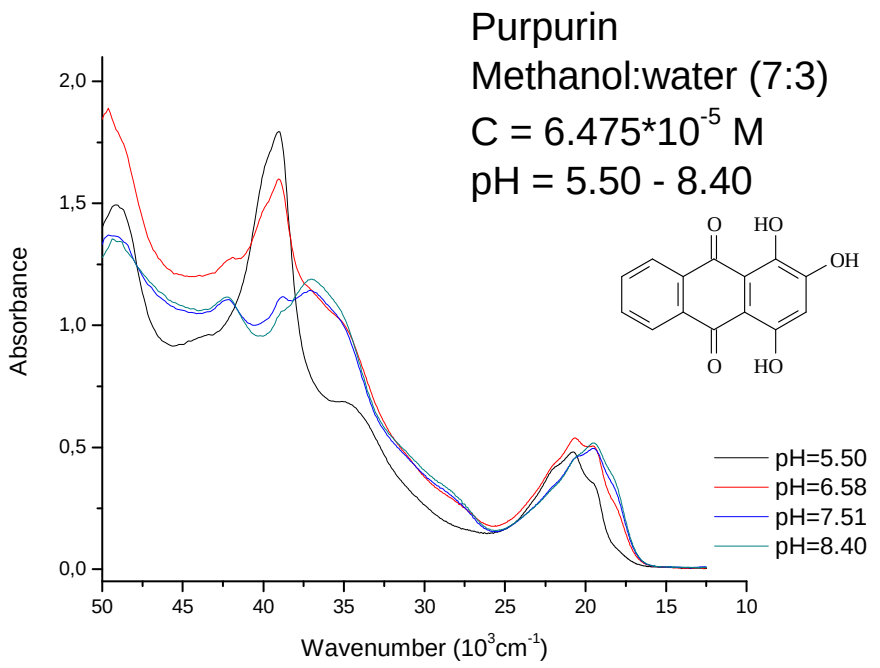
Purpurin
Methanol:water (7:3)
C = 6.475*10-5 M
pH = 5.50 - 8.40
O
HO
OH
O
HO
Absorbance
2,0
1,5
1,0
0,5
0,0
50
45
40
35
30
25
20
15
10
Wavenumber (10³cm⁻¹)
pH=5.50
pH=6.58
pH=7.51
pH=8.40

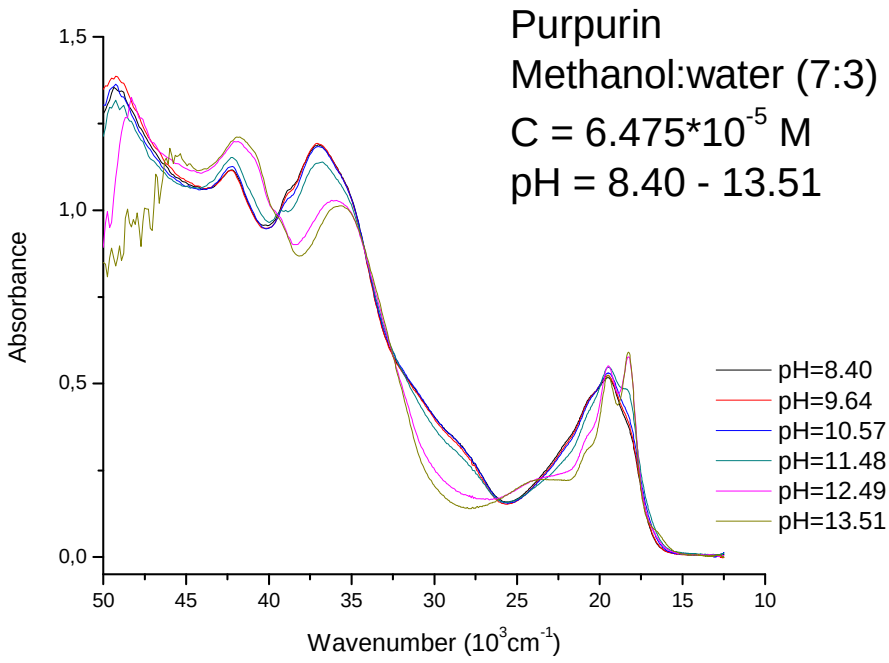
Purpurin
Methanol:water (7:3)
C = 6.475*10-5 M
pH = 8.40 - 13.51
Absorbance
1,5
1,0
0,5
0,0
50
45
40
35
30
25
20
15
10
Wavenumber (10³cm⁻¹)
pH=8.40
pH=9.64
pH=10.57
pH=11.48
pH=12.49
pH=13.51

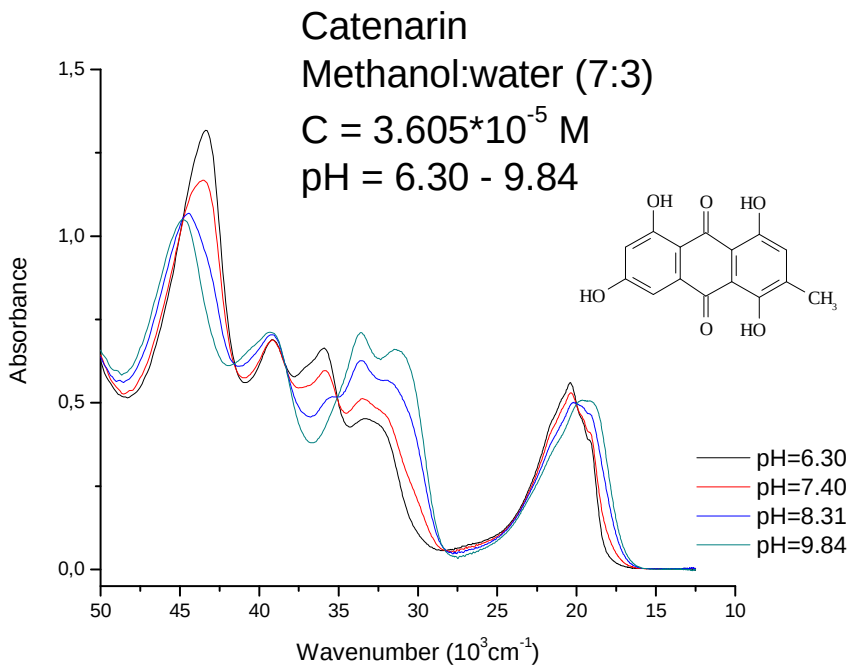
Catenarin
Methanol:water (7:3)
C = 3.605*10-5 M
pH = 6.30 - 9.84
OH
O
HO
HO
CH3
O
HO
Absorbance
1,5
1,0
0,5
0,0
50
45
40
35
30
25
20
15
10
Wavenumber (10^3cm^-1)
pH=6.30
pH=7.40
pH=8.31
pH=9.84

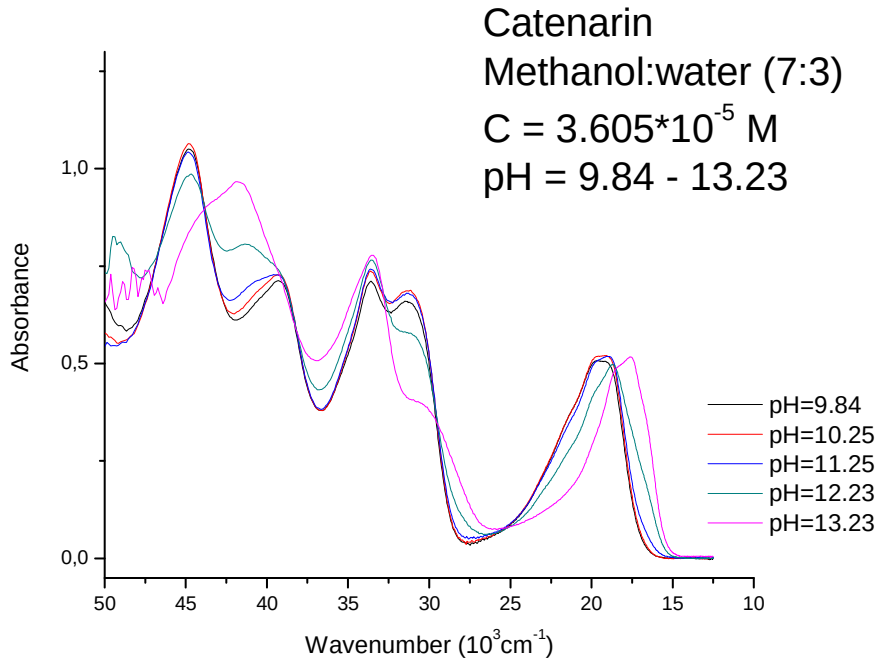
Catenarin
Methanol:water (7:3)
C = 3.605*10-5 M
pH = 9.84 - 13.23
Absorbance
1,0
0,5
0,0
50
45
40
35
30
25
20
15
10
Wavenumber (10^3cm^-1)
pH=9.84
pH=10.25
pH=11.25
pH=12.23
pH=13.23

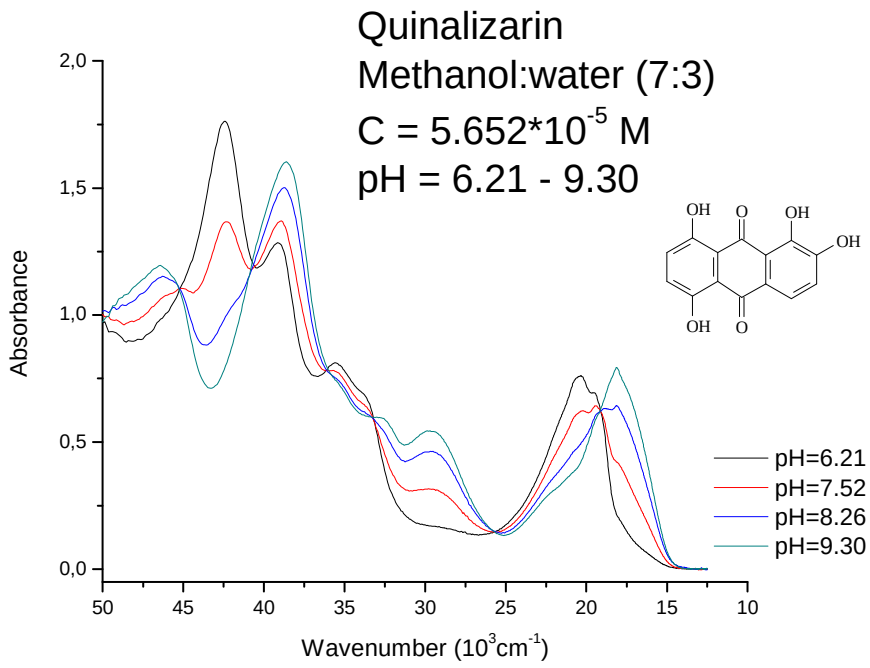
Quinalizarin
Methanol:water (7:3)
C = 5.652*10-5 M
pH = 6.21 - 9.30
OH
O
OH
OH
OH
O
Absorbance
2,0
1,5
1,0
0,5
0,0
50
45
40
35
30
25
20
15
10
Wavenumber (10^3cm^-1)
pH=6.21
pH=7.52
pH=8.26
pH=9.30

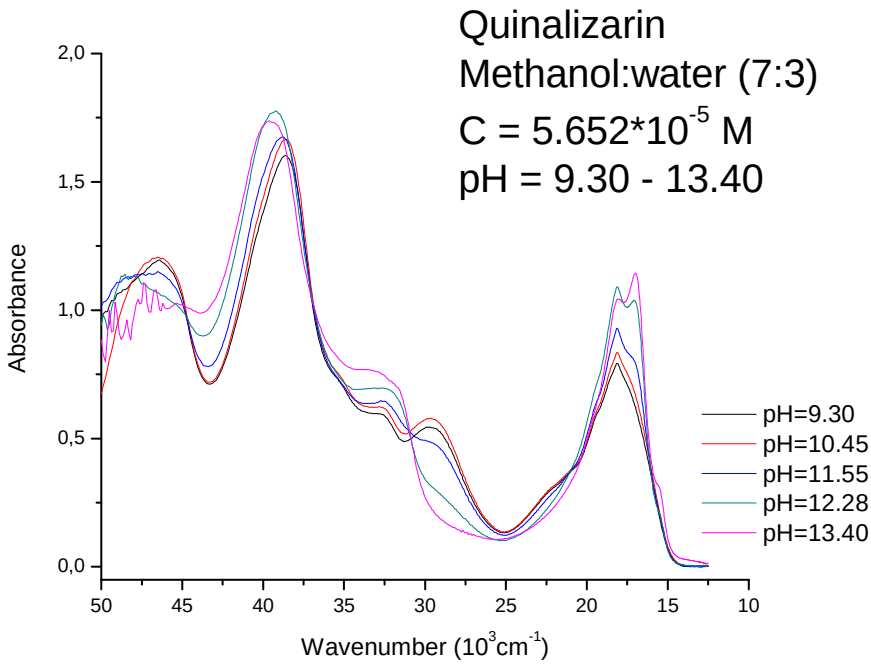
Quinalizarin
Methanol:water (7:3)
C = 5.652*10-5 M
pH = 9.30 - 13.40
Absorbance
2,0
1,5
1,0
0,5
0,0
50
45
40
35
30
25
20
15
10
Wavenumber (10^3cm^-1)
pH=9.30
pH=10.45
pH=11.55
pH=12.28
pH=13.40

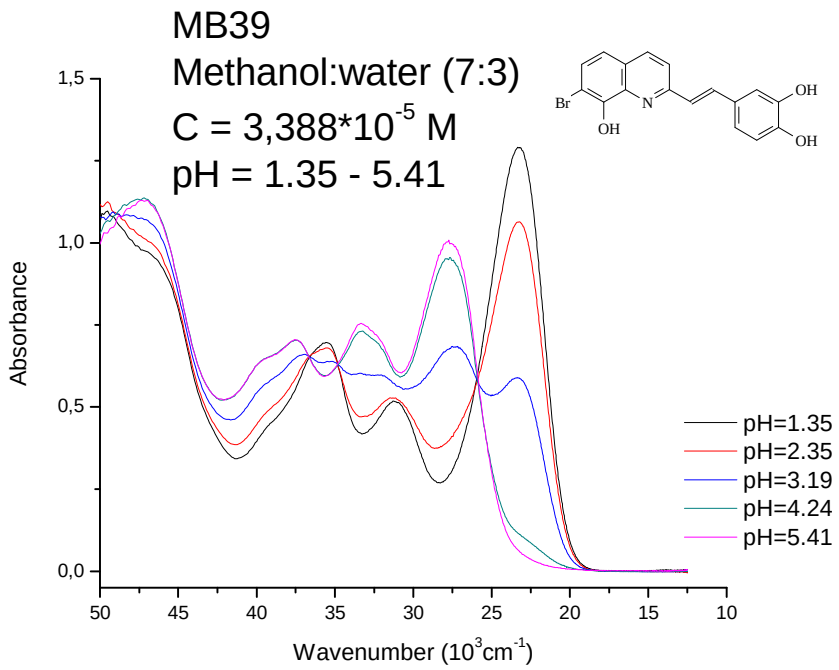
MB39
Methanol:water (7:3)
C = 3,388*10-5 M
pH = 1.35 - 5.41
Br
N
OH
OH
OH
Absorbance
1,5
1,0
0,5
0,0
50
45
40
35
30
25
20
15
10
Wavenumber (10^3cm^-1)
pH=1.35
pH=2.35
pH=3.19
pH=4.24
pH=5.41

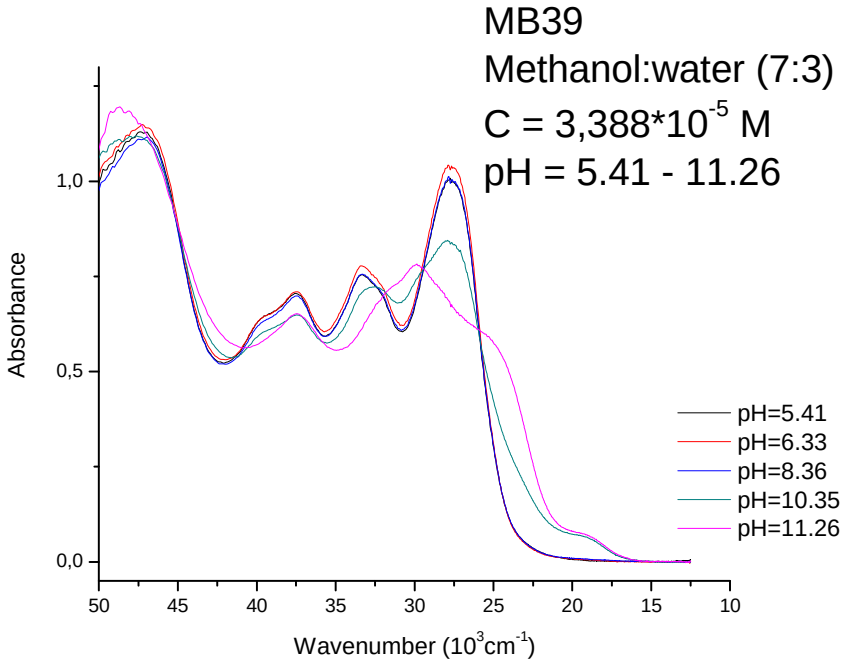
MB39
Methanol:water (7:3)
C = 3,388*10-5 M
pH = 5.41 - 11.26
Absorbance
1,0
0,5
0,0
50
45
40
35
30
25
20
15
10
Wavenumber (10^3cm^-1)
pH=5.41
pH=6.33
pH=8.36
pH=10.35
pH=11.26

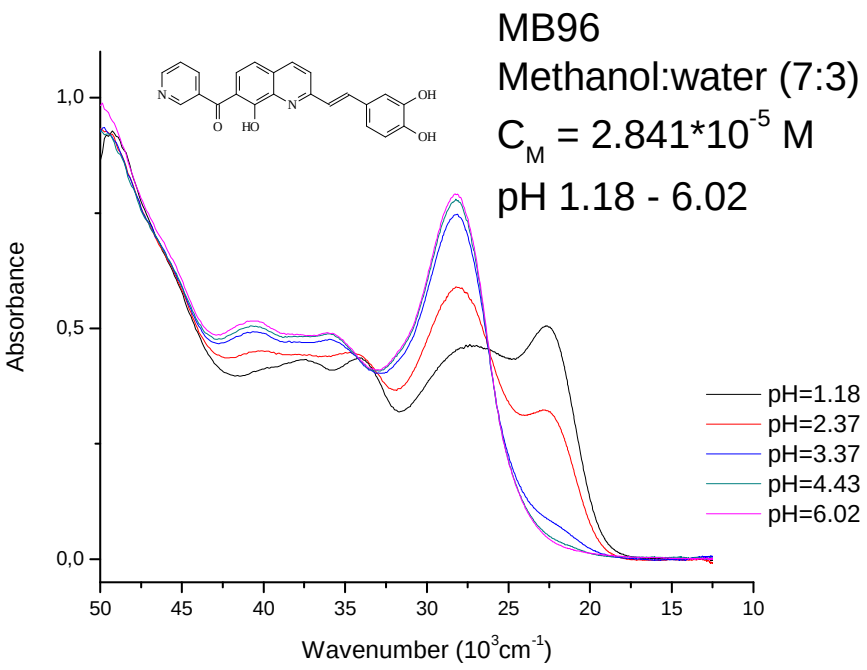
MB96
Methanol:water (7:3)
C_M = 2.841*10^-5 M
pH 1.18 - 6.02
Absorbance
1,0
0,5
0,0
50
45
40
35
30
25
20
15
10
Wavenumber (10^3cm^-1)
pH=1.18
pH=2.37
pH=3.37
pH=4.43
pH=6.02

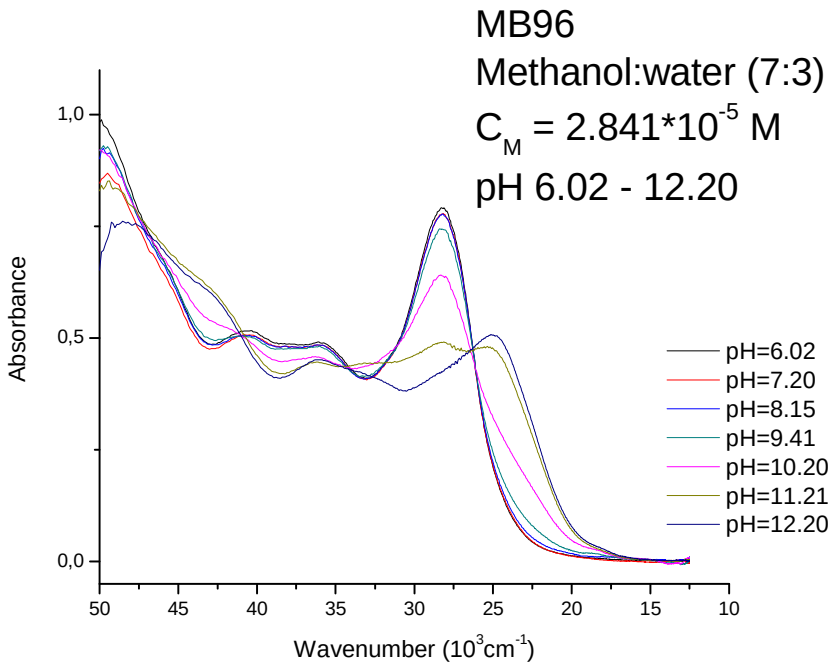
MB96
Methanol:water (7:3)
C_M = 2.841*10^-5 M
pH 6.02 - 12.20
Absorbance
1,0
0,5
0,0
50
45
40
35
30
25
20
15
10
Wavenumber (10^3cm^-1)
pH=6.02
pH=7.20
pH=8.15
pH=9.41
pH=10.20
pH=11.21
pH=12.20

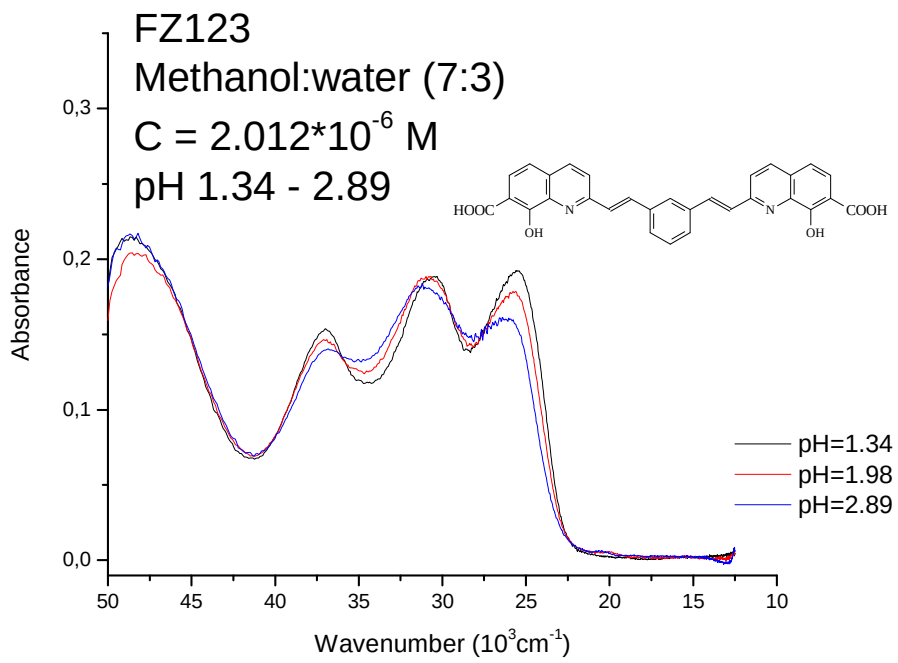
FZ123
Methanol:water (7:3)
C = 2.012*10-6 M
pH 1.34 - 2.89
HOOC
COOH
OH
N
Absorbance
0,0
0,1
0,2
0,3
50
45
40
35
30
25
20
15
10
Wavenumber (10³cm⁻¹)
pH=1.34
pH=1.98
pH=2.89

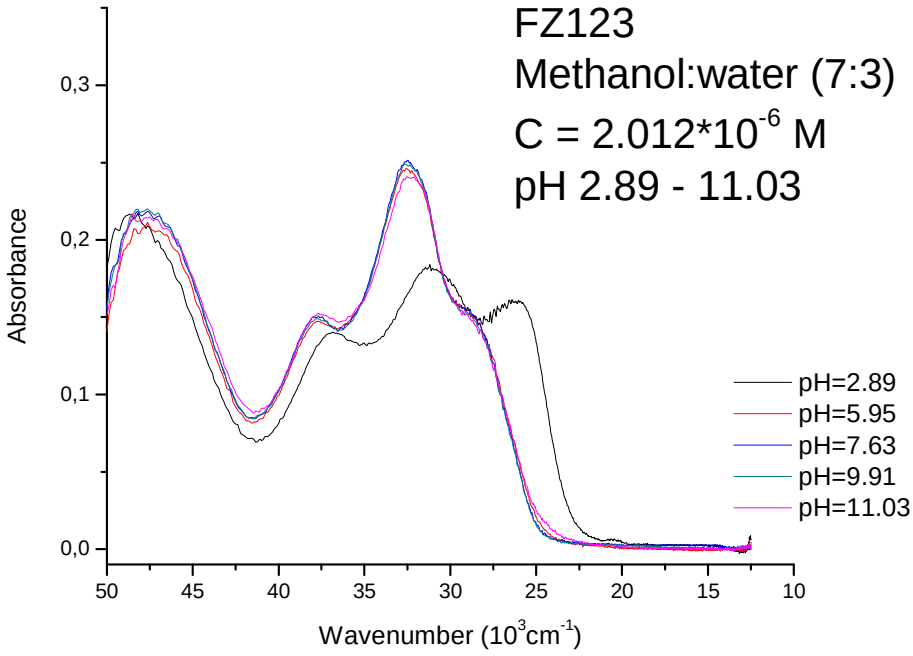
FZ123
Methanol:water (7:3)
C = 2.012*10-6 M
pH 2.89 - 11.03
Absorbance
0,0
0,1
0,2
0,3
50
45
40
35
30
25
20
15
10
Wavenumber (10³cm⁻¹)
pH=2.89
pH=5.95
pH=7.63
pH=9.91
pH=11.03

A1.4.2 LD spectra

We can prepare the PVA samples and measure successfully the LD spectra of alizarin, purpurin and compounds from Prof. Lyazidi. It is quite difficult for the other compounds (catenarin and quinalizarin) to obtain enough LD spectra corresponding to different molecular forms due to limitation of their solubility in the PVA matrix. And the results are shown as follow:

The LD spectra of alizarin and purpurin are measured at room temperature on both the traditional spectrophotometer and at CD1 beamline on the storage ring. This can extend the spectral region up to ca. 6000 cm^{-1} (from 47000 cm^{-1} to 53000 cm^{-1}) because of strong light scattering and baseline absorption of the PVA matrix.

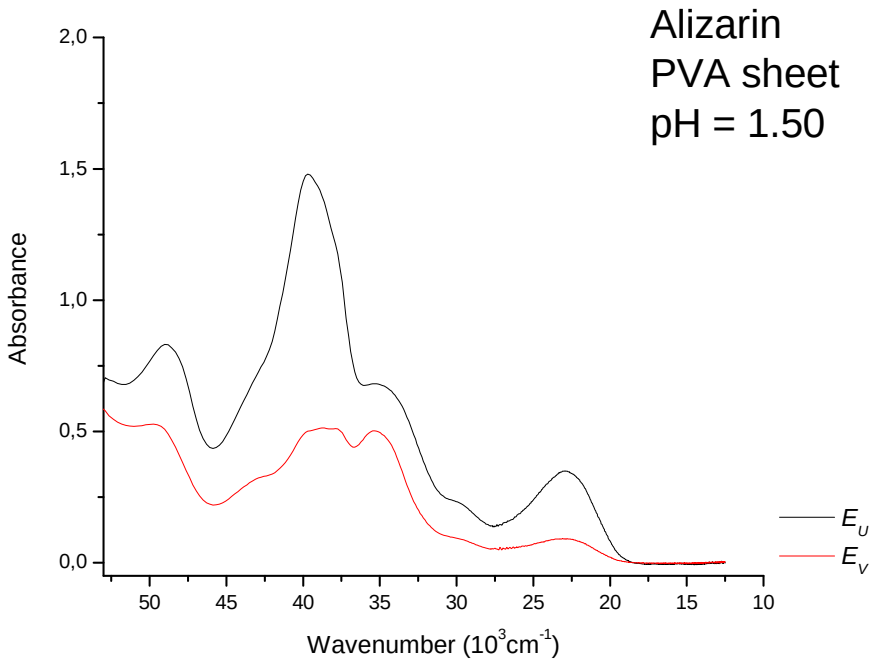

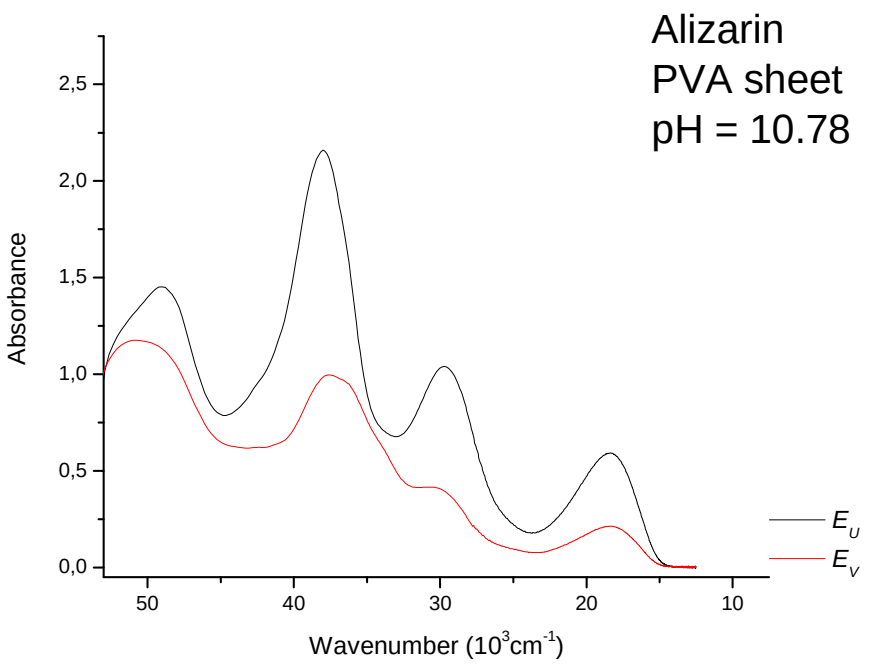
Alizarin
PVA sheet
pH = 10.78
Absorbance
2,5
2,0
1,5
1,0
0,5
0,0
50
40
30
20
10
Wavenumber (10³cm⁻¹)
E_U
E_V

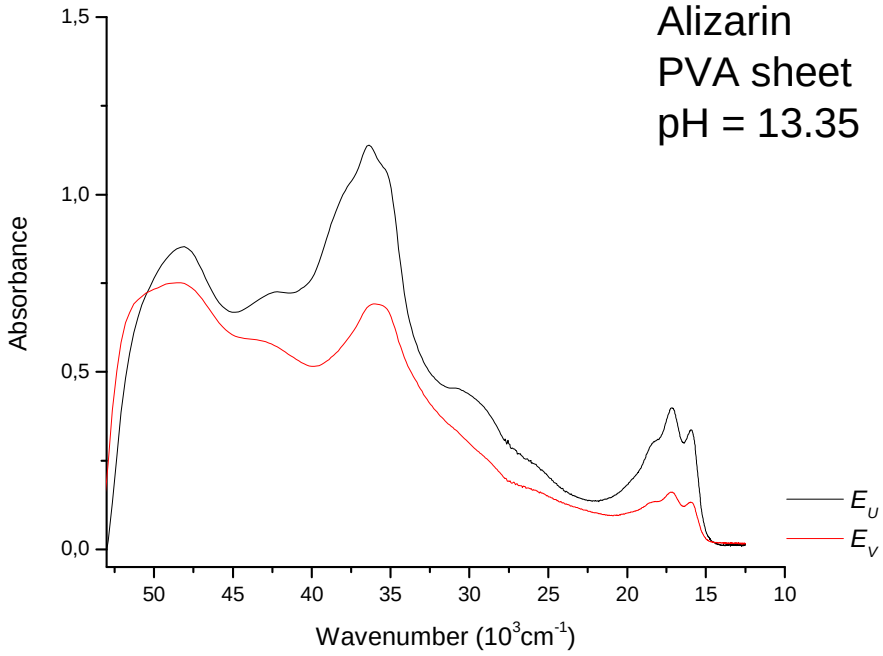
Alizarin
PVA sheet
pH = 13.35
Absorbance
1,5
1,0
0,5
0,0
50
45
40
35
30
25
20
15
10
Wavenumber (10³cm⁻¹)
E_U
E_V

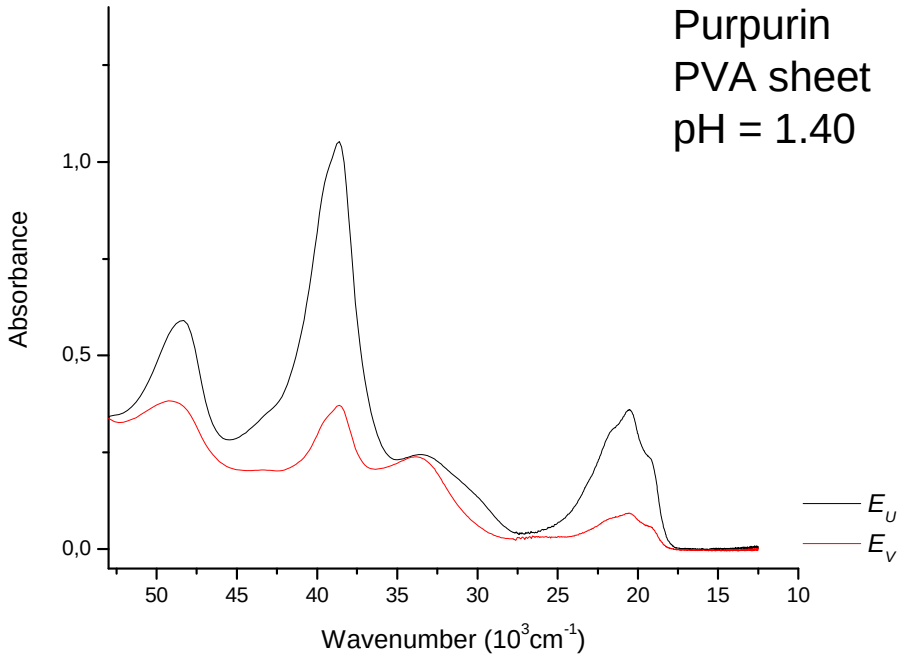
Purpurin
PVA sheet
pH = 1.40
Absorbance
1,0
0,5
0,0
50
45
40
35
30
25
20
15
10
Wavenumber (10^3cm^-1)
E_U
E_V

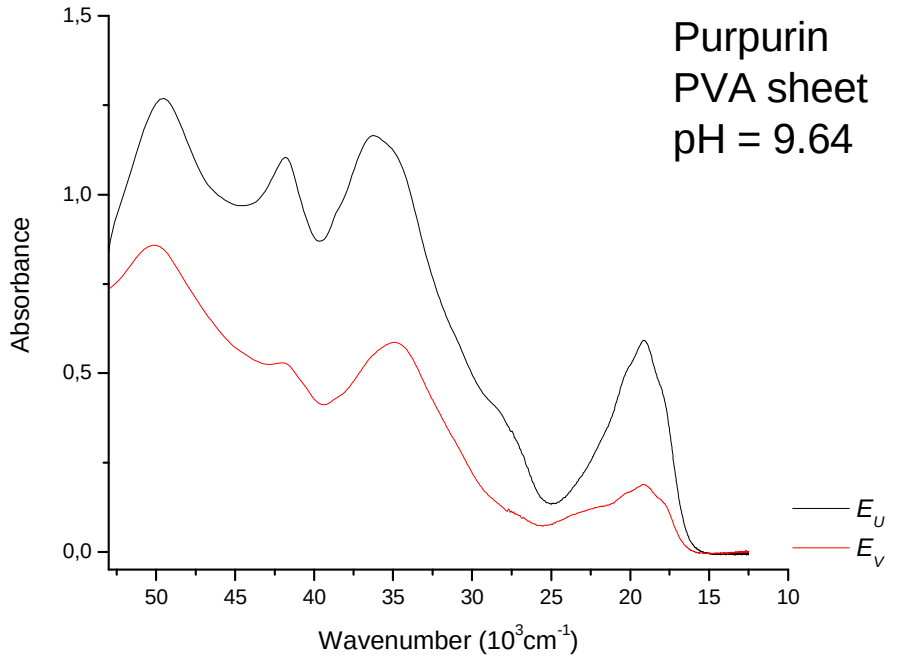
Purpurin
PVA sheet
pH = 9.64
Absorbance
1,5
1,0
0,5
0,0
50
45
40
35
30
25
20
15
10
Wavenumber (10^3cm^-1)
E_U
E_V

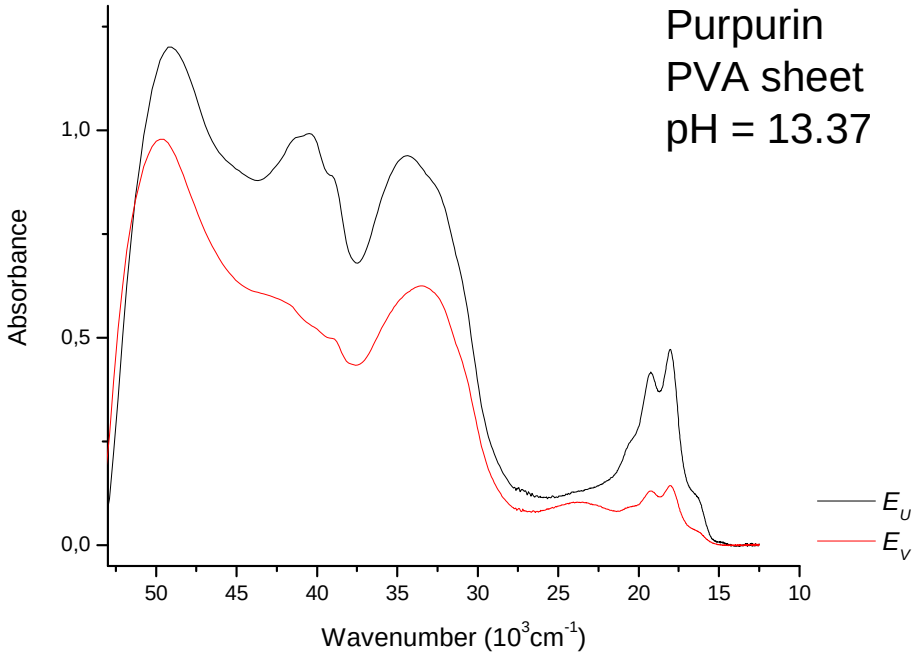

Unfortunately, the LD spectra of compounds from Prof. Lyazidi are only measured at room temperature on a traditional spectrophotometer at our laboratory in the spectral region below 50000 cm^{-1} because these PVA samples are prepared after the schedule of CD1 beamtime at ASTRID in Aarhus.

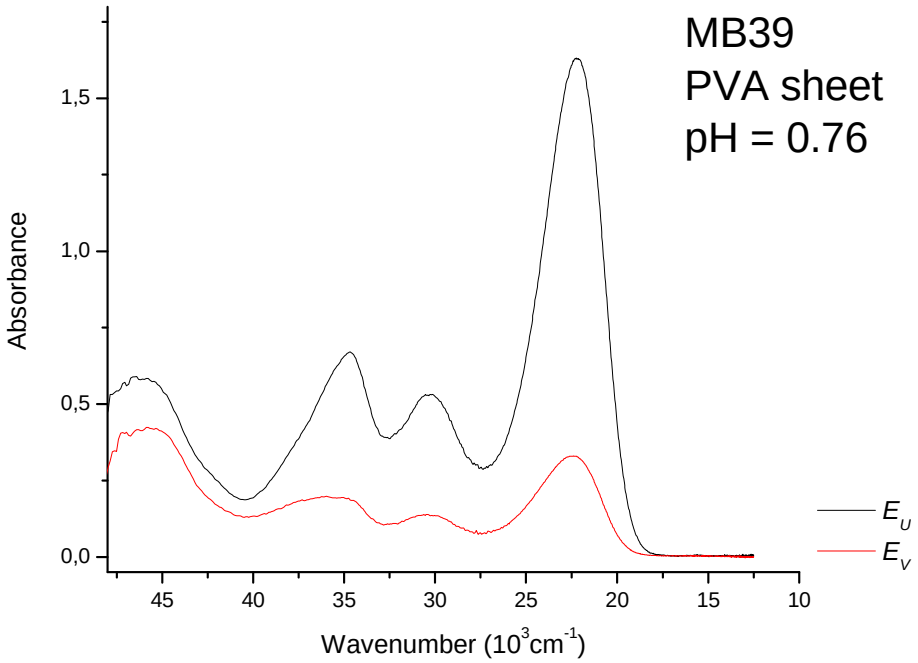

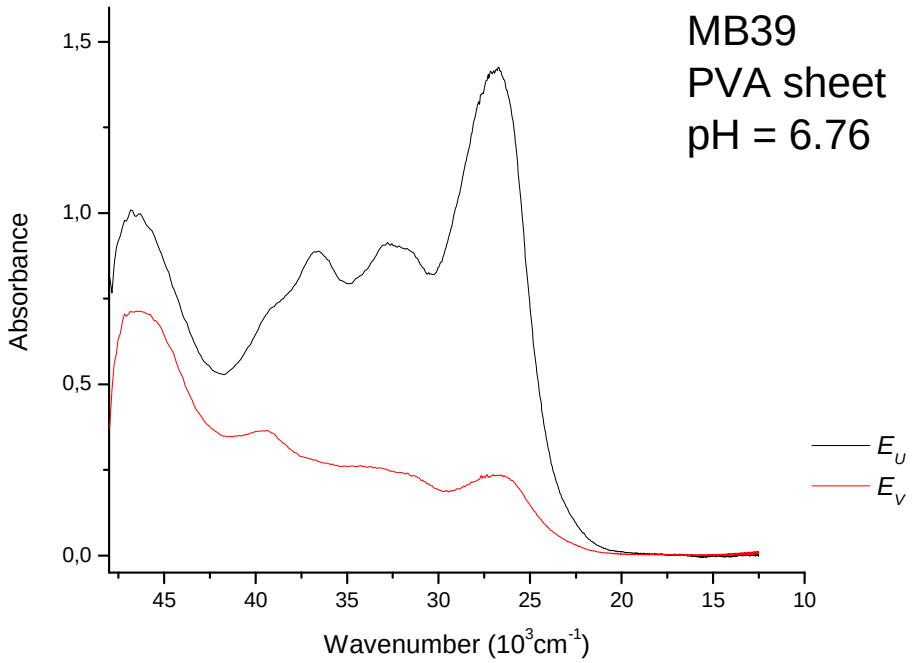
MB39
PVA sheet
pH = 6.76
Absorbance
1,5
1,0
0,5
0,0
45
40
35
30
25
20
15
10
Wavenumber (10^3cm^-1)
E_U
E_V

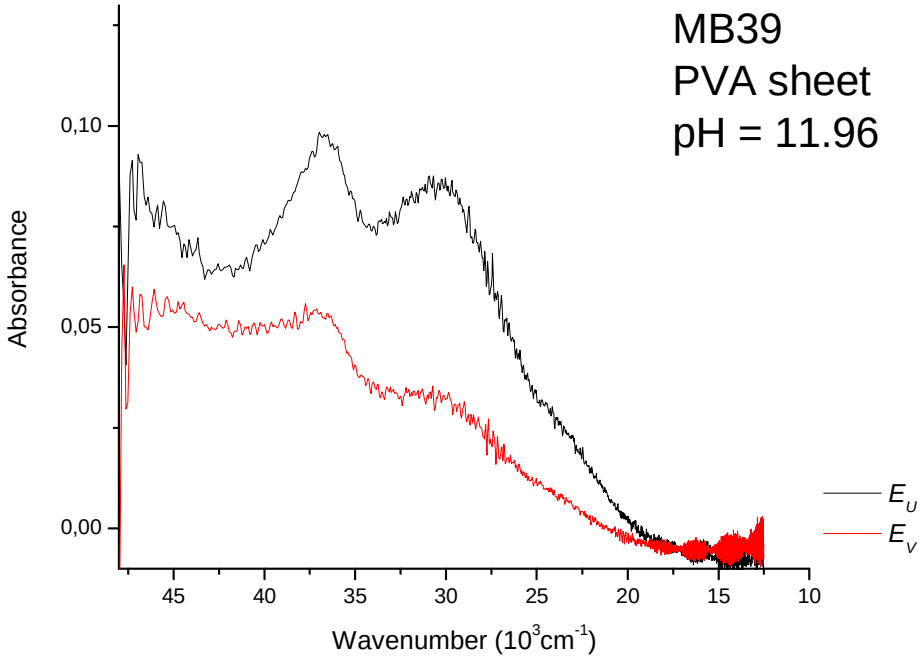
MB39
PVA sheet
pH = 11.96
Absorbance
0,10
0,05
0,00
45
40
35
30
25
20
15
10
Wavenumber (10^3cm^-1)
E_U
E_V

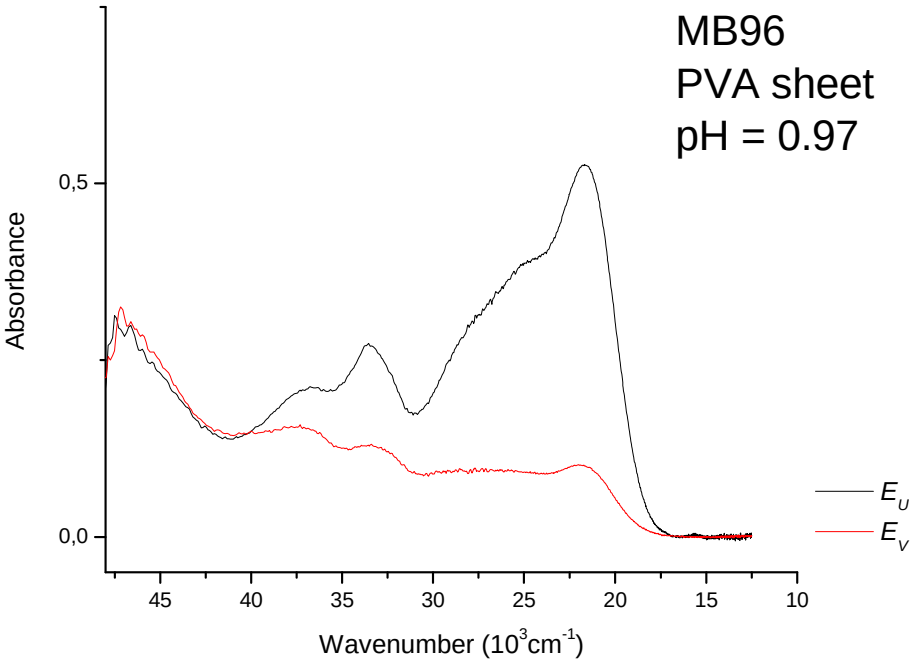
MB96
PVA sheet
pH = 0.97
Absorbance
0,5
0,0
45
40
35
30
25
20
15
10
Wavenumber (10³cm⁻¹)
E_U
E_V

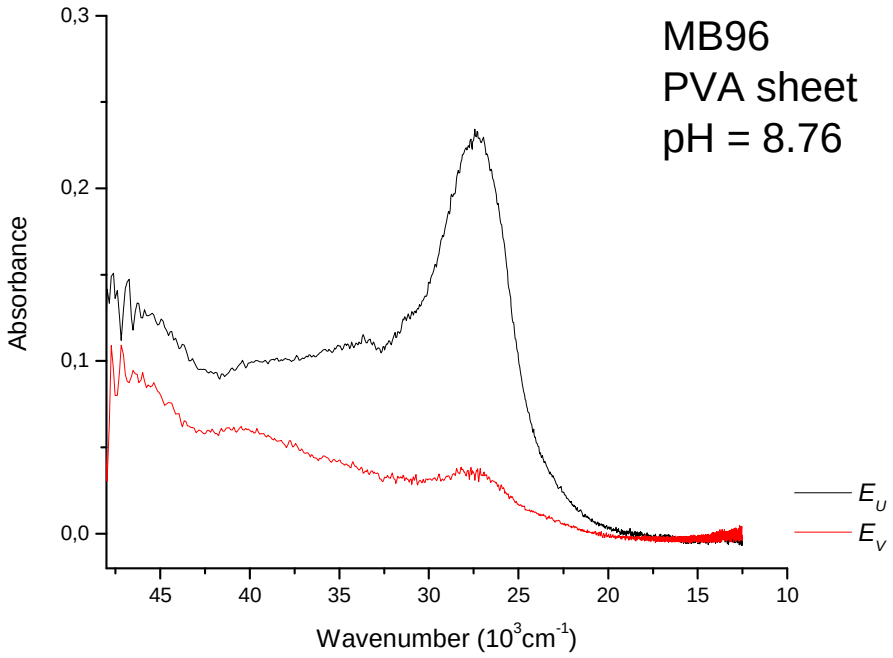
MB96
PVA sheet
pH = 8.76
Absorbance
0,3
0,2
0,1
0,0
45
40
35
30
25
20
15
10
Wavenumber (10³cm⁻¹)
E_U
E_V

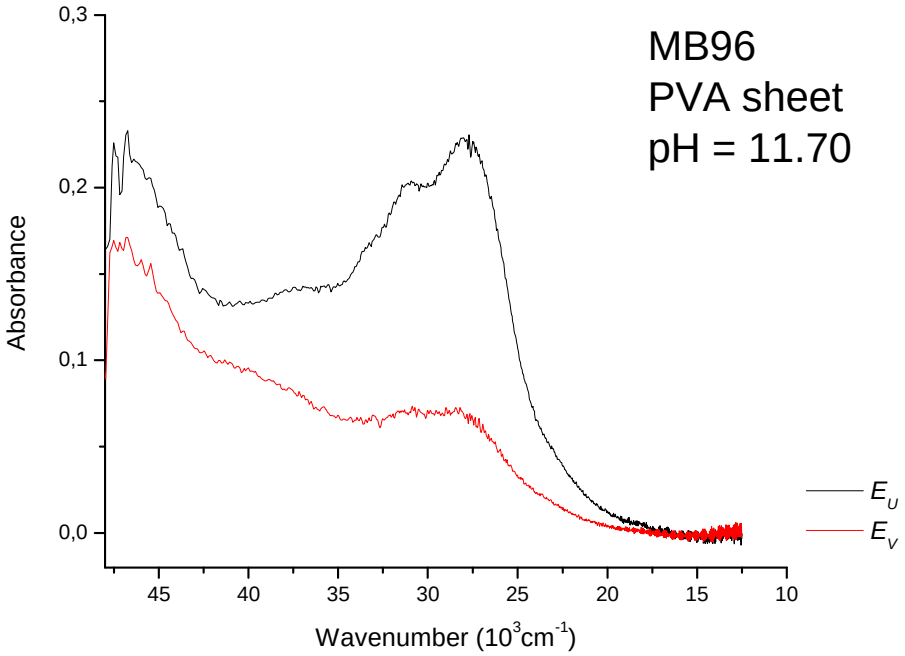
MB96
PVA sheet
pH = 11.70
Absorbance
0,3
0,2
0,1
0,0
45
40
35
30
25
20
15
10
Wavenumber (10^3cm^-1)
E_U
E_V

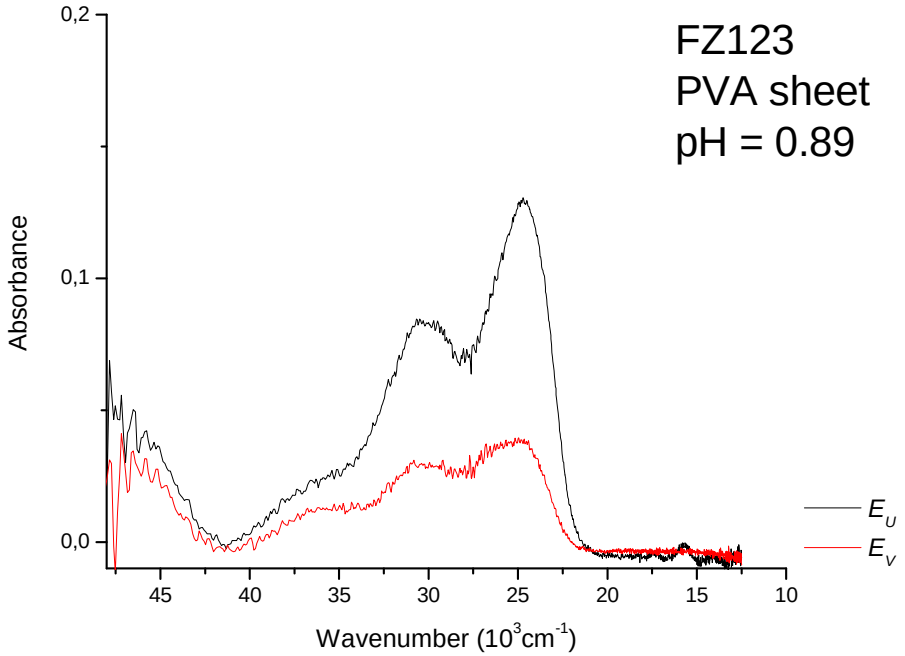
FZ123
PVA sheet
pH = 0.89
Absorbance
0,2
0,1
0,0
45
40
35
30
25
20
15
10
Wavenumber (10^3cm^-1)
E_U
E_V

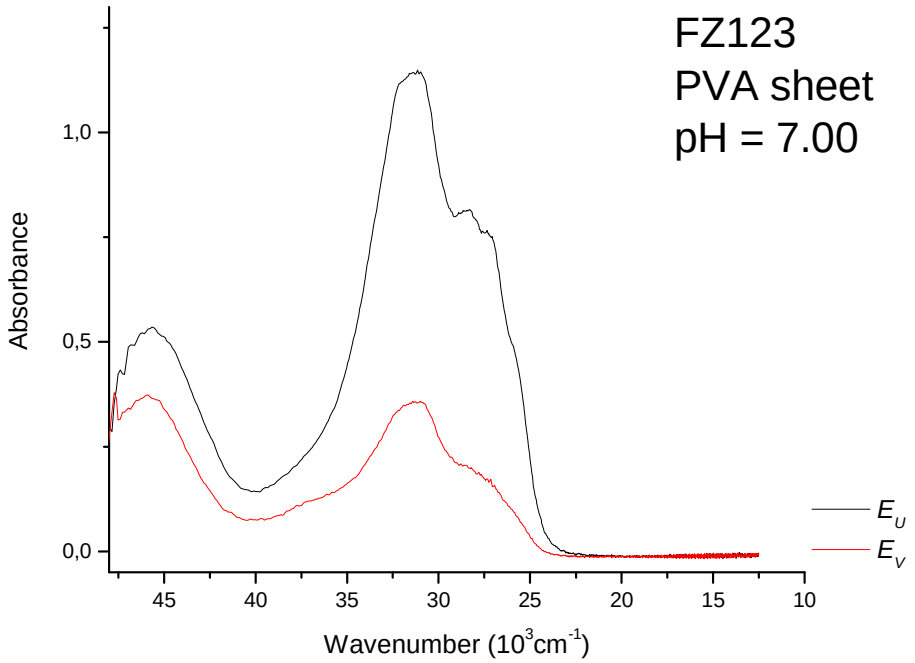
FZ123
PVA sheet
pH = 7.00
Absorbance
1,0
0,5
0,0
45
40
35
30
25
20
15
10
Wavenumber (10^3cm^-1)
E_U
E_V

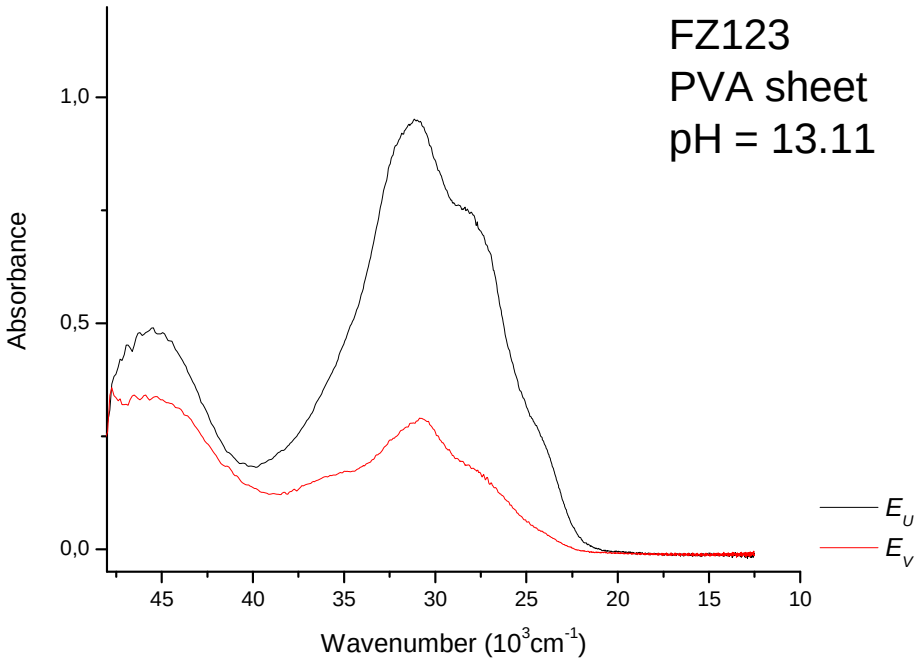
FZ123
PVA sheet
pH = 13.11
Absorbance
1,0
0,5
0,0
45
40
35
30
25
20
15
10
Wavenumber (10^3cm^-1)
E_U
E_V

Appendix 2
Supplementary data for figure 2.5

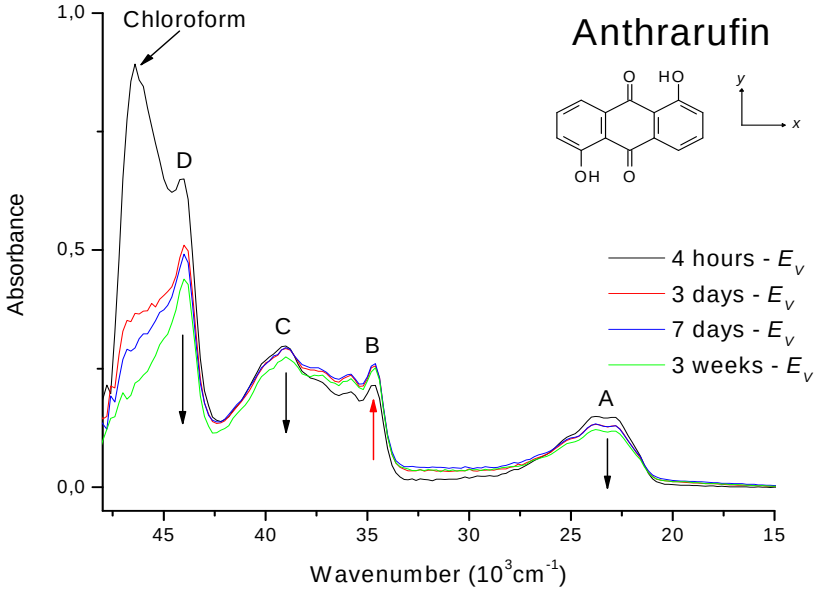

This figure shows the E_V curve of the evaporation of chloroform solvent from thick LDPE in case of Anthrarufin. As can be seen in the figure, chloroform solvent still remains in thick LDPE matrix after 4 hour evaporation. After 3 week evaporation, the intensity of the absorption bands slightly changes: A, C and D decrease while B increases as indicated by arrows. This indicates that the alignment of molecules with the stretching direction becomes better, leading to the increase in intensity of the long polarized transitions and the decrease in intensity of the short polarized transitions. The inset shows the molecular coordinate. The E_U curve is also shown below for comparison.

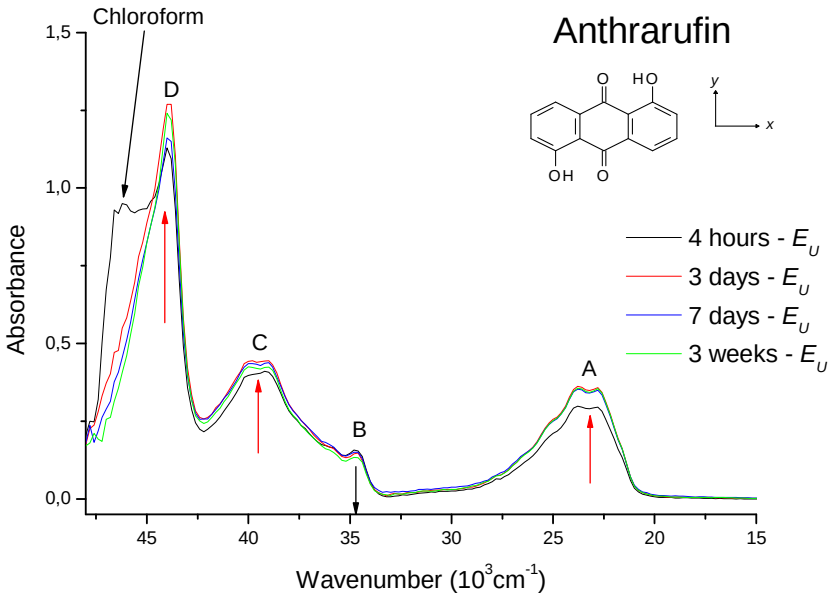

Appendix 3

The LD spectra of all compounds

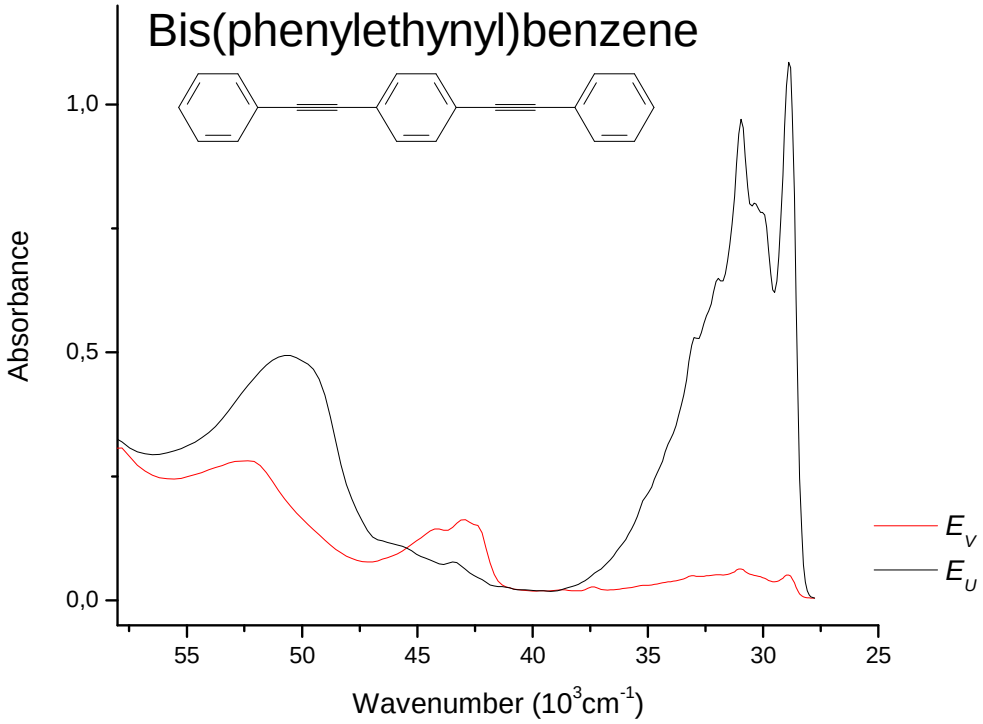

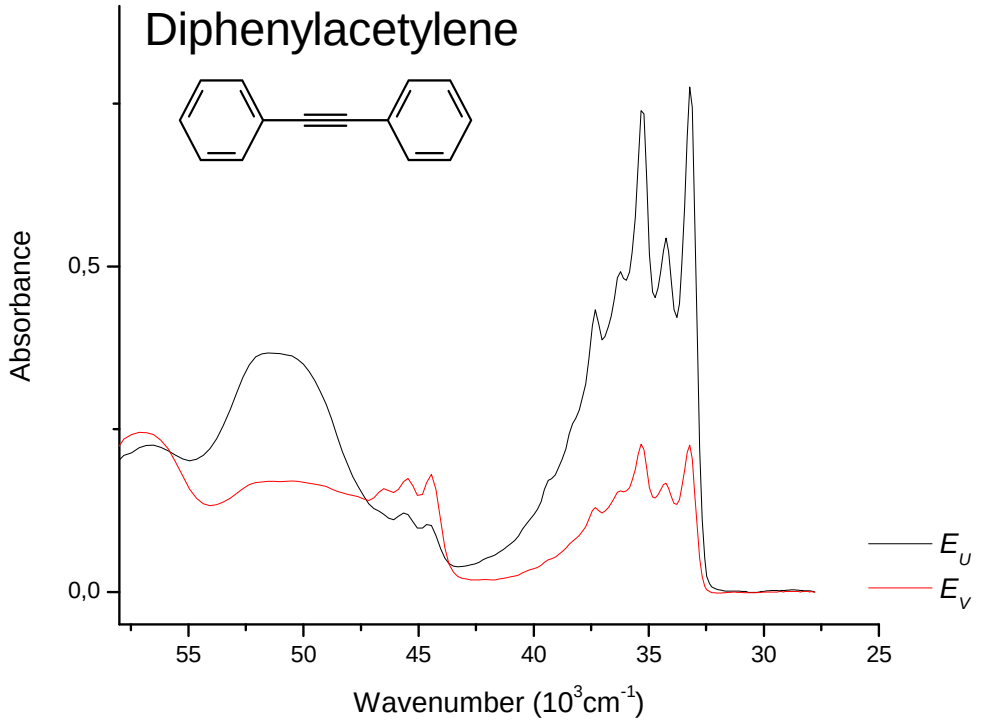
Diphenylacetylene
Absorbance
0,5
0,0
55
50
45
40
35
30
25
Wavenumber (10^3cm^-1)
E_U
E_V

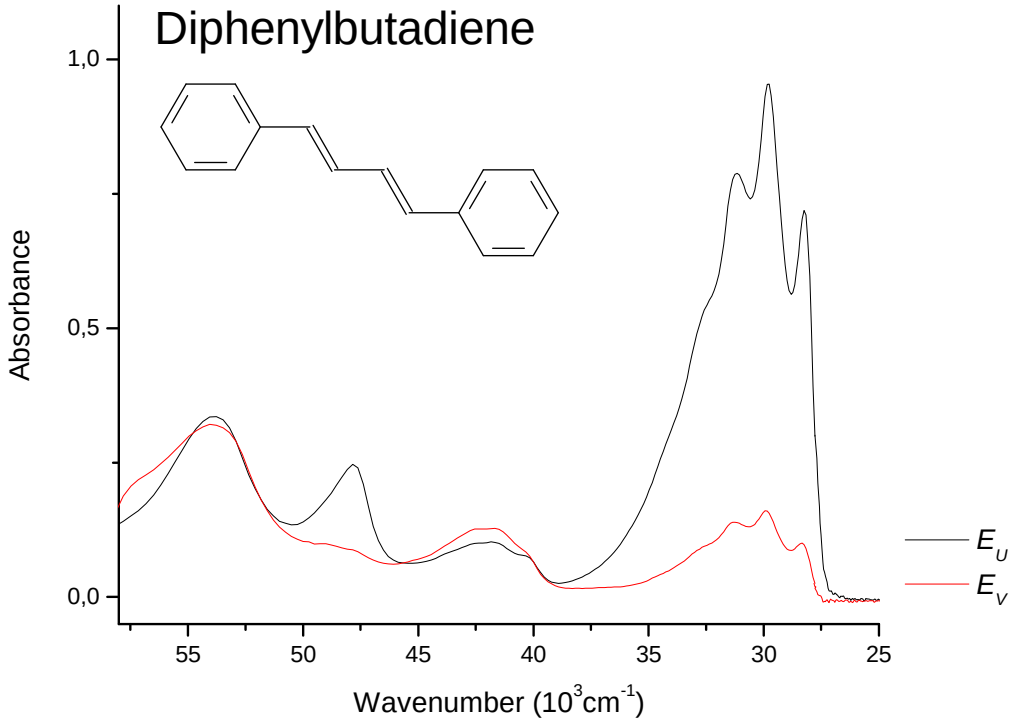
Diphenylbutadiene
Absorbance
1,0
0,5
0,0
55
50
45
40
35
30
25
Wavenumber (10^3cm^-1)
E_U
E_V

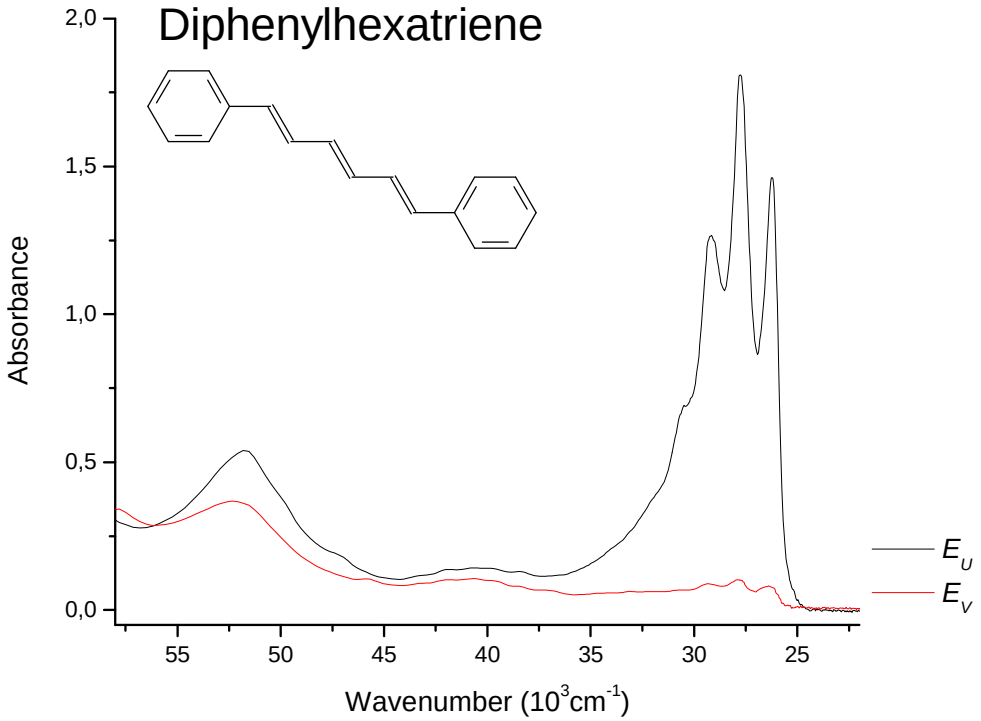
Diphenylhexatriene
Absorbance
2,0
1,5
1,0
0,5
0,0
55
50
45
40
35
30
25
Wavenumber (10^3cm^-1)
E_U
E_V

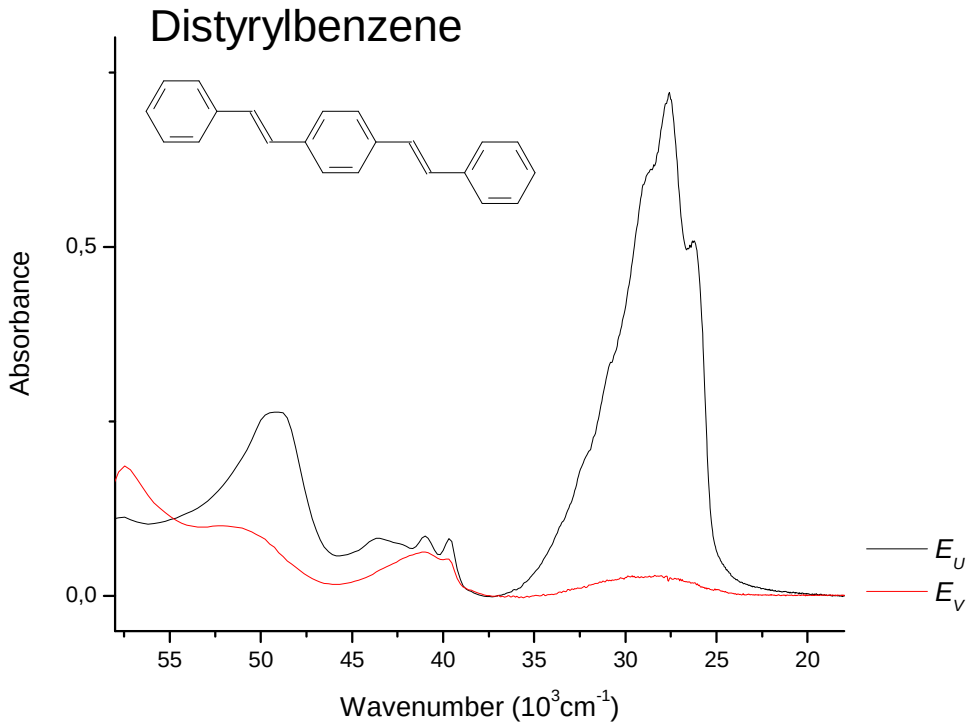
Distyrylbenzene
Absorbance
0,5
0,0
55
50
45
40
35
30
25
20
Wavenumber (10^3cm^-1)
E_U
E_V

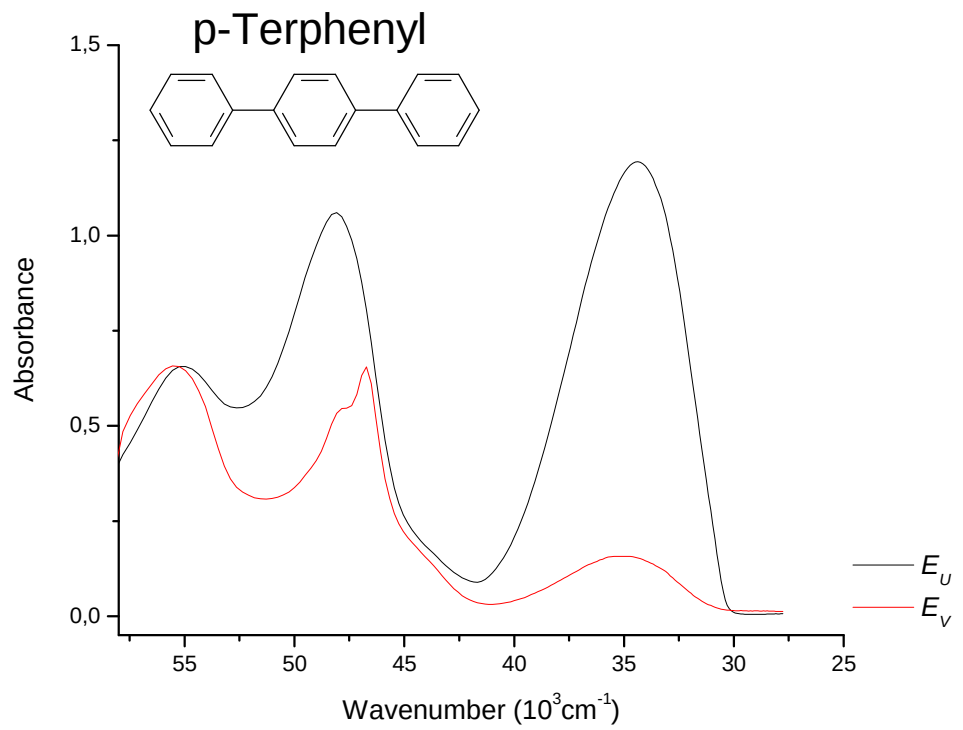
p-Terphenyl
1,5
1,0
0,5
0,0
Absorbance
55
50
45
40
35
30
25
Wavenumber (10^3cm^-1)
E_U
E_V

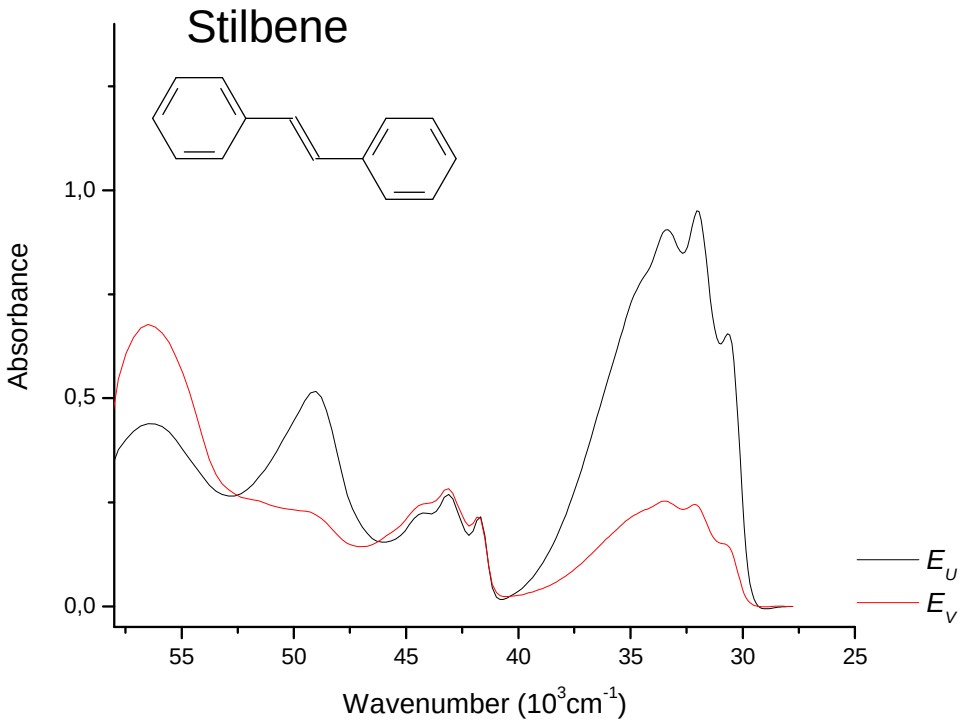
Stilbene
1,0
0,5
0,0
Absorbance
55
50
45
40
35
30
25
Wavenumber (10^3cm^-1)
E_U
E_V

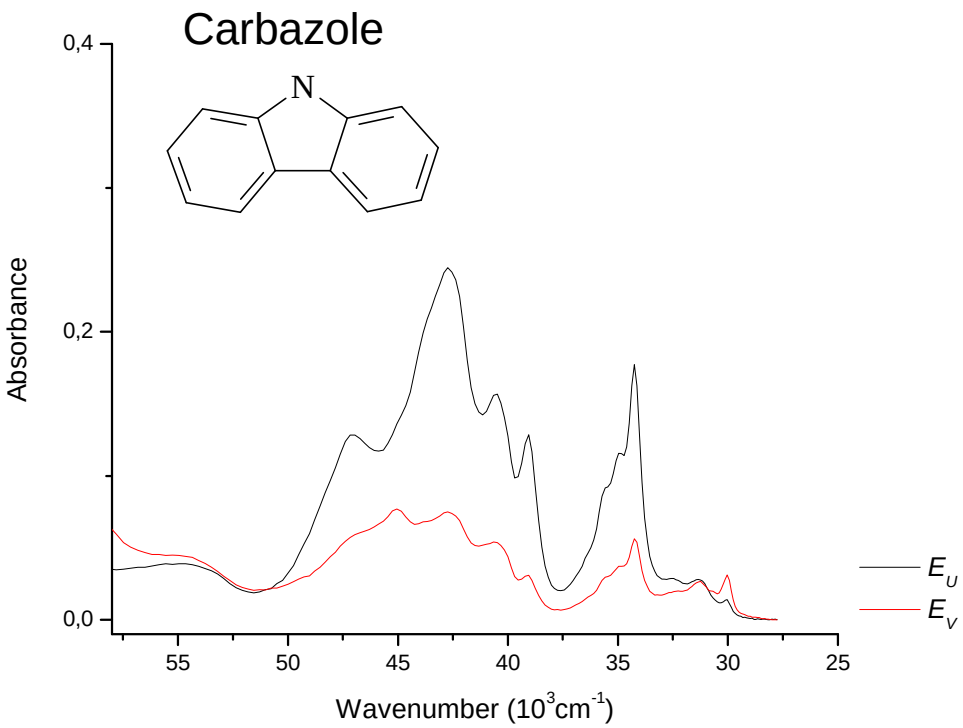
Carbazole
N
0,4
0,2
0,0
Absorbance
55
50
45
40
35
30
25
Wavenumber (10^3cm^-1)
E_U
E_V

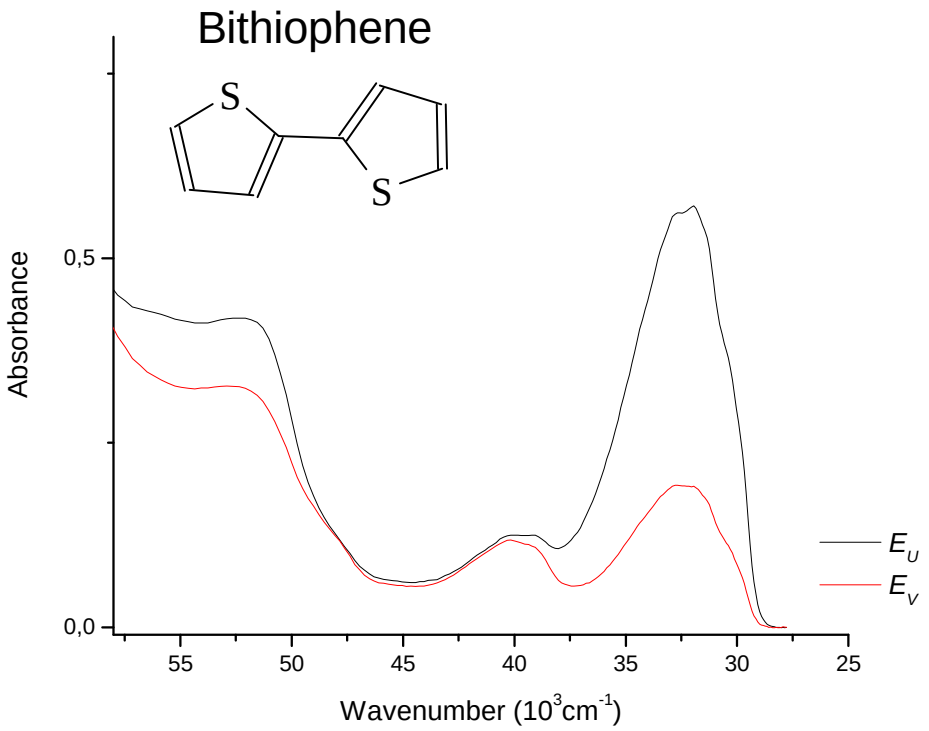
Bithiophene
S
S
0,5
0,0
Absorbance
55
50
45
40
35
30
25
Wavenumber (10^3cm^-1)
E_U
E_V

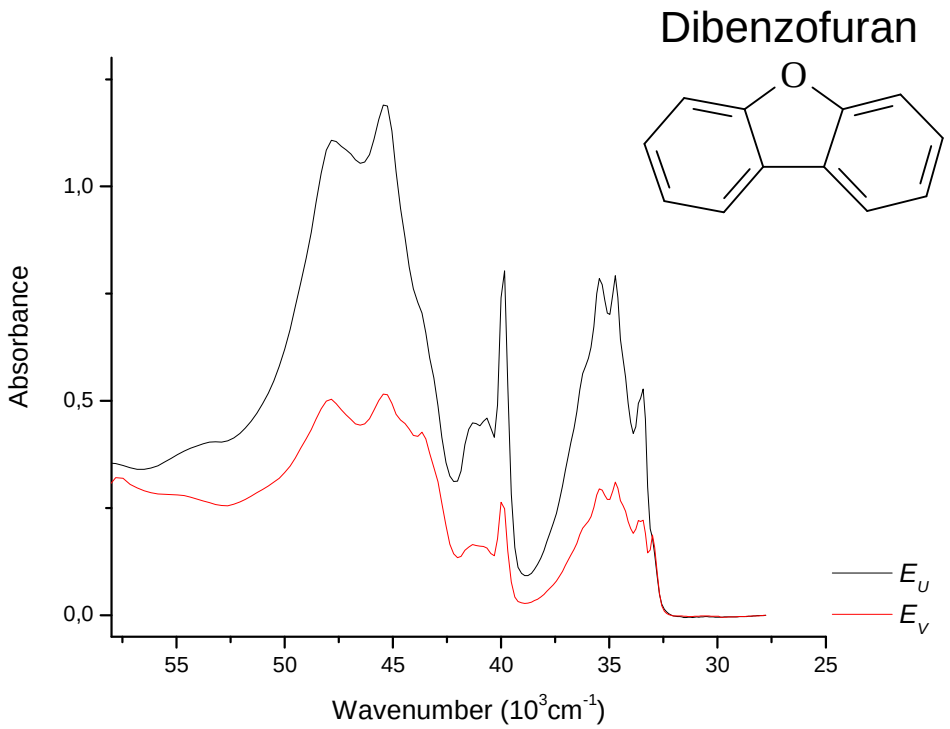
Dibenzofuran
O
Absorbance
1,0
0,5
0,0
55
50
45
40
35
30
25
Wavenumber (10^3cm^-1)
E_U
E_V

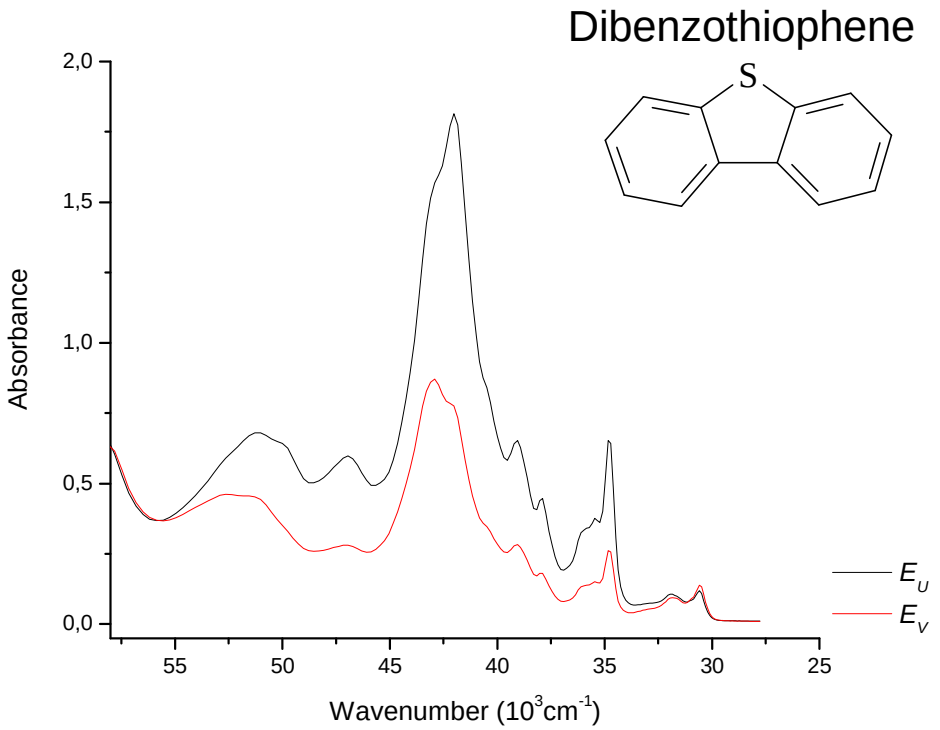
Dibenzothiophene
S
Absorbance
2,0
1,5
1,0
0,5
0,0
55
50
45
40
35
30
25
Wavenumber (10^3cm^-1)
E_U
E_V

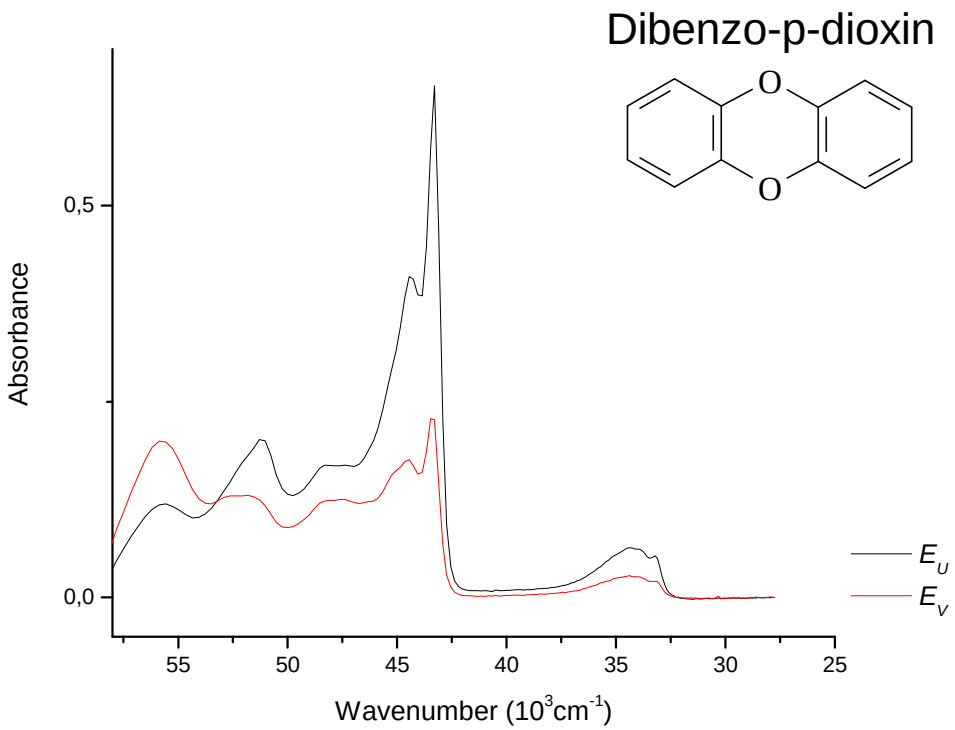
Dibenzo-p-dioxin
O
O
Absorbance
0,5
0,0
55
50
45
40
35
30
25
Wavenumber (10³cm⁻¹)
E_U
E_V

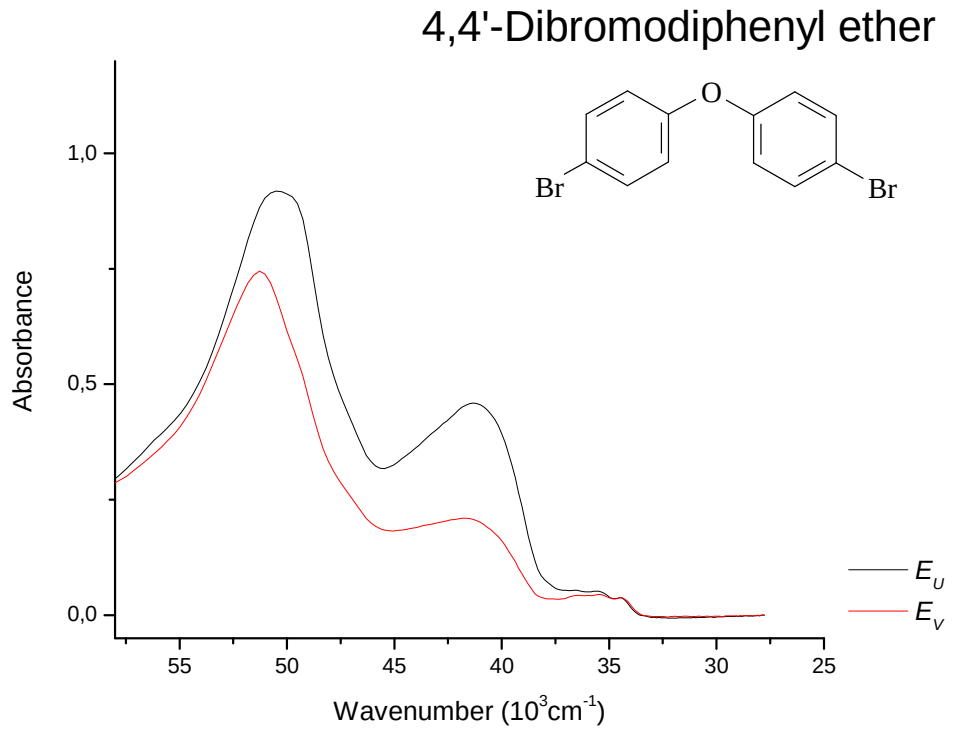
4,4'-Dibromodiphenyl ether
O
Br
Br
Absorbance
1,0
0,5
0,0
55
50
45
40
35
30
25
Wavenumber (10³cm⁻¹)
E_U
E_V

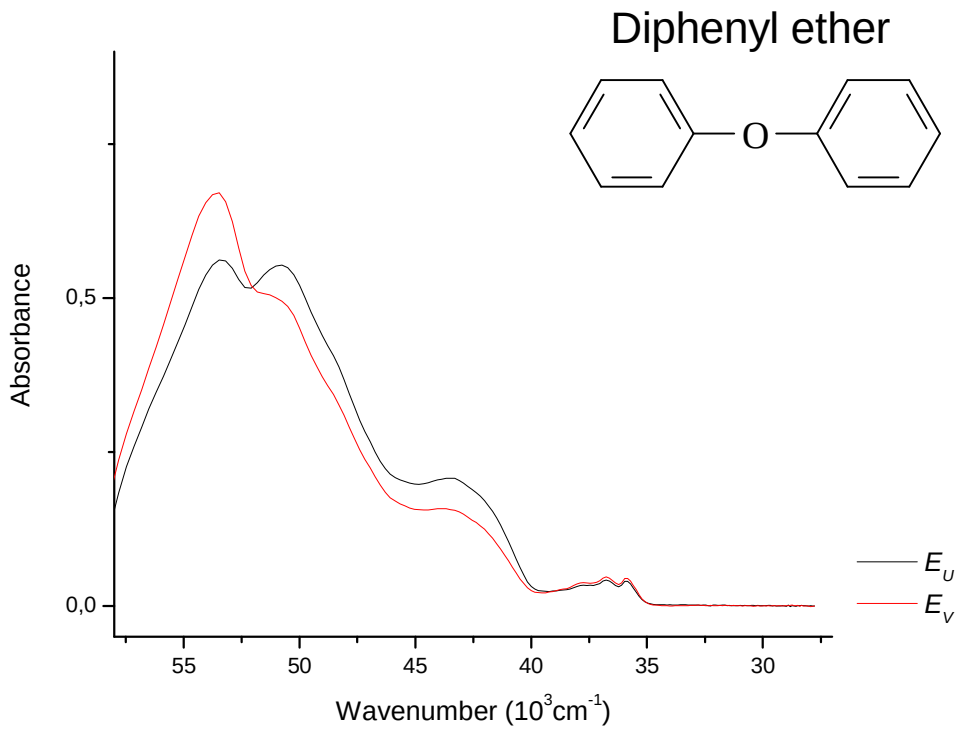
Diphenyl ether
O
Absorbance
0,5
0,0
55
50
45
40
35
30
Wavenumber (10^3cm^-1)
E_U
E_V

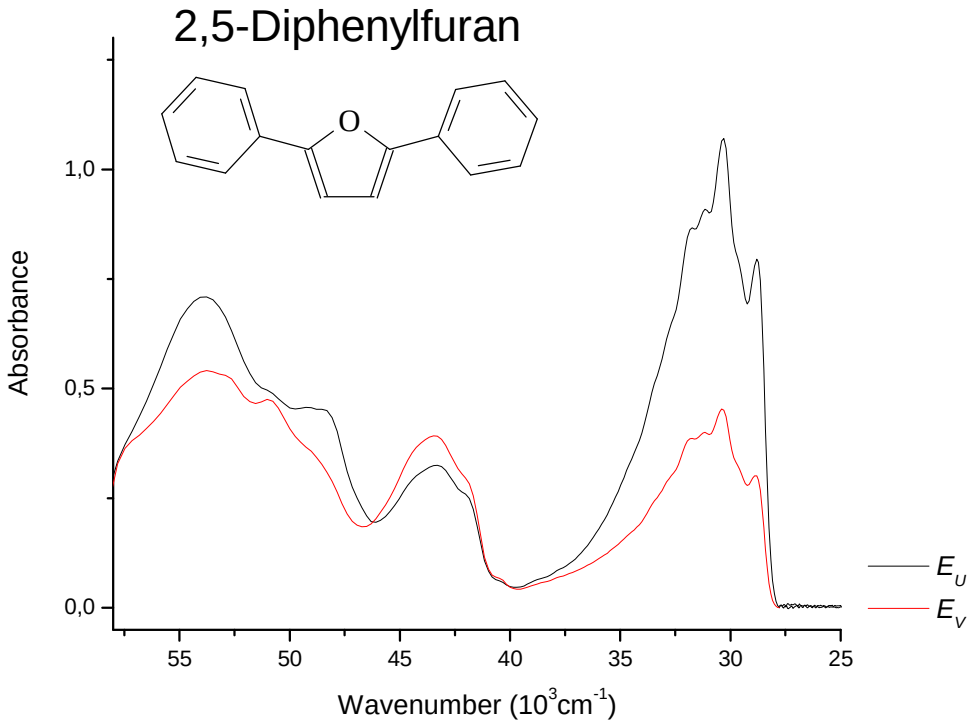
2,5-Diphenylfuran
O
Absorbance
1,0
0,5
0,0
55
50
45
40
35
30
25
Wavenumber (10^3cm^-1)
E_U
E_V

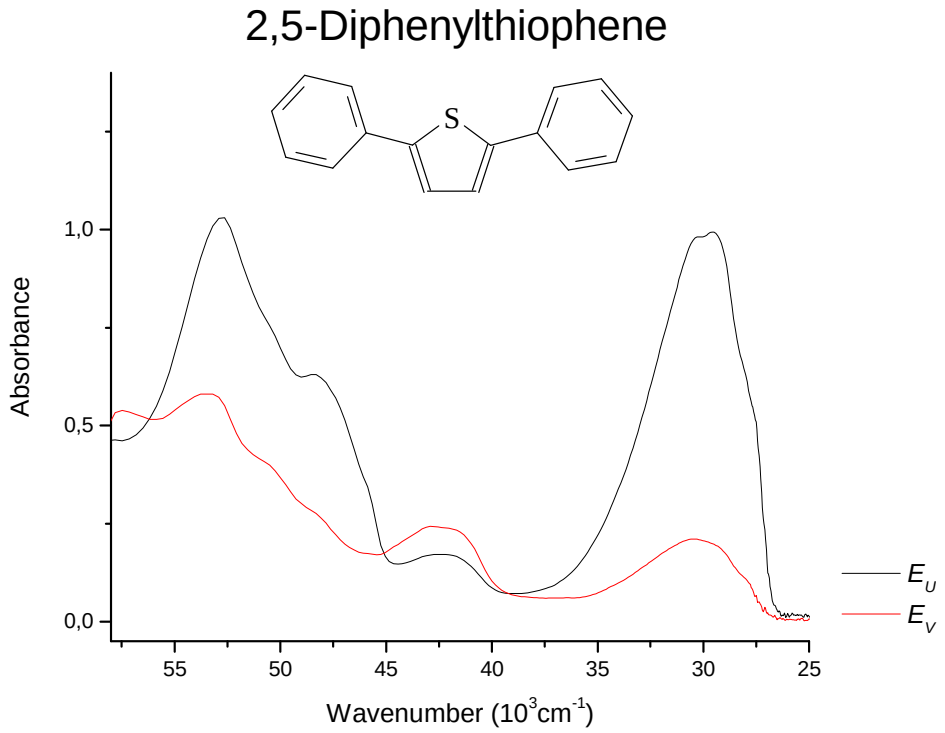
2,5-Diphenylthiophene
S
Absorbance
1,0
0,5
0,0
55
50
45
40
35
30
25
Wavenumber (10^3cm^-1)
E_U
E_V

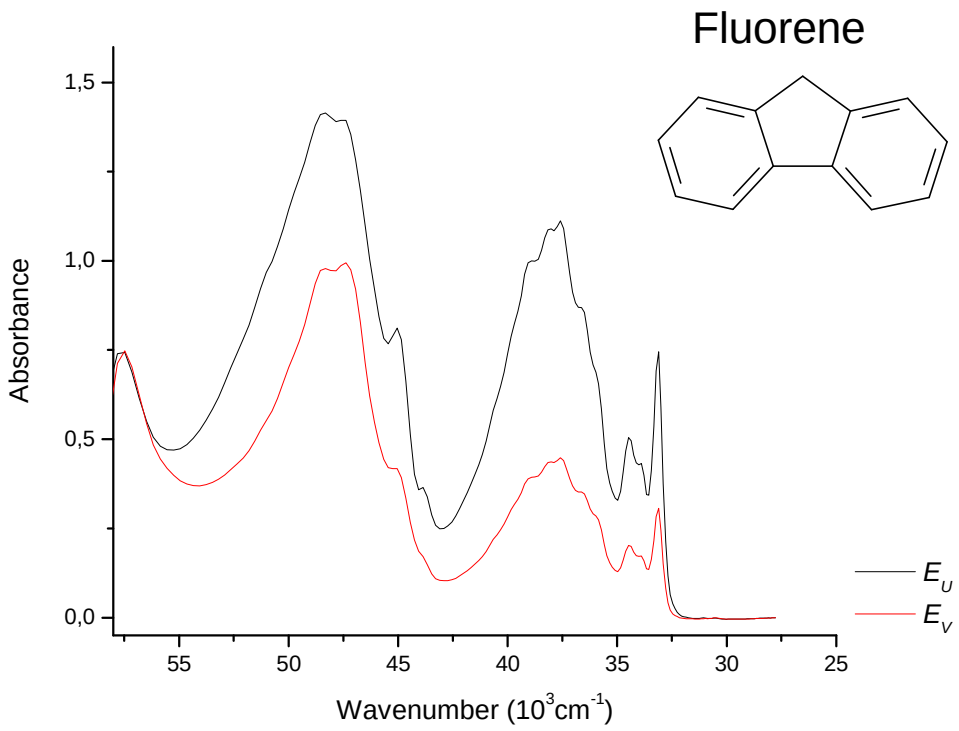
Fluorene
Absorbance
1,5
1,0
0,5
0,0
55
50
45
40
35
30
25
Wavenumber (10^3cm^-1)
E_U
E_V

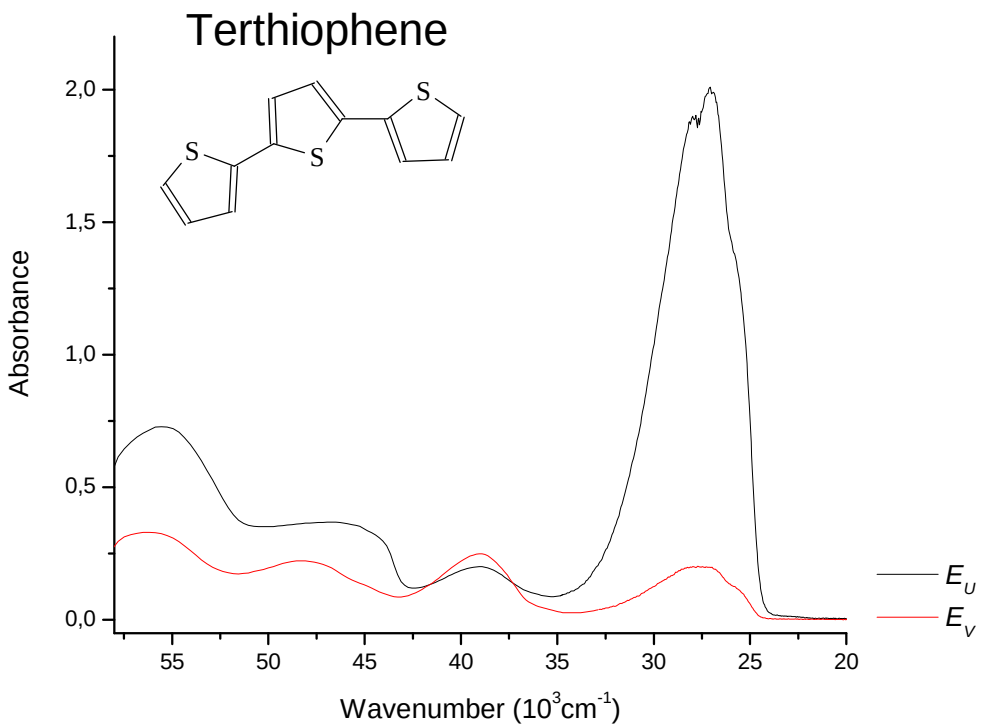
Terthiophene
S
S
S
Absorbance
2,0
1,5
1,0
0,5
0,0
55
50
45
40
35
30
25
20
Wavenumber (10^3cm^-1)
E_U
E_V

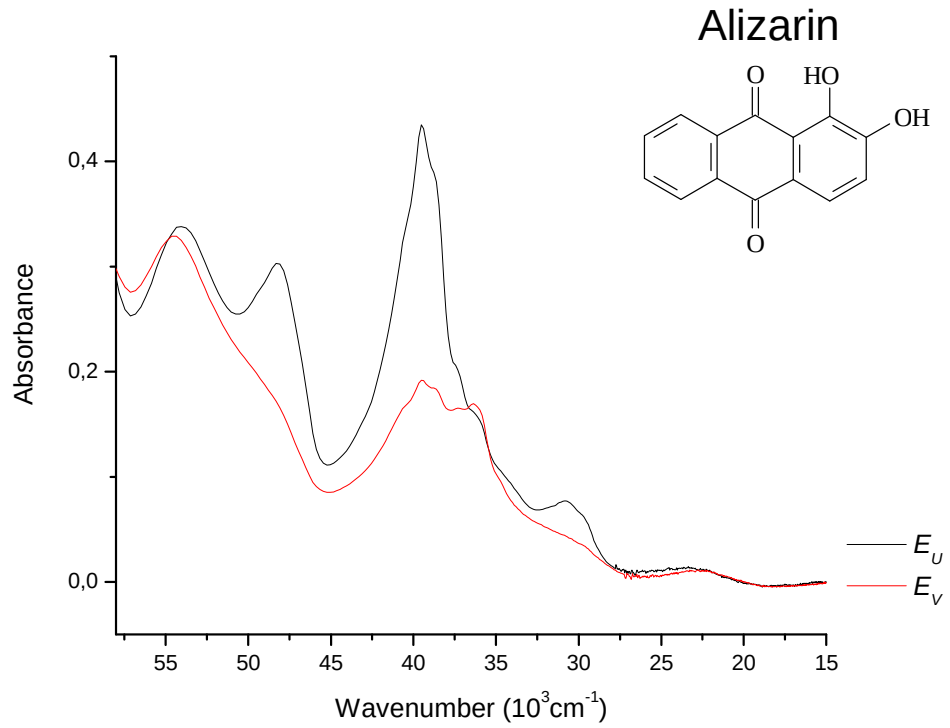
Alizarin
O
HO
OH
O
Absorbance
0,4
0,2
0,0
55
50
45
40
35
30
25
20
15
Wavenumber (10^3cm^-1)
E_U
E_V

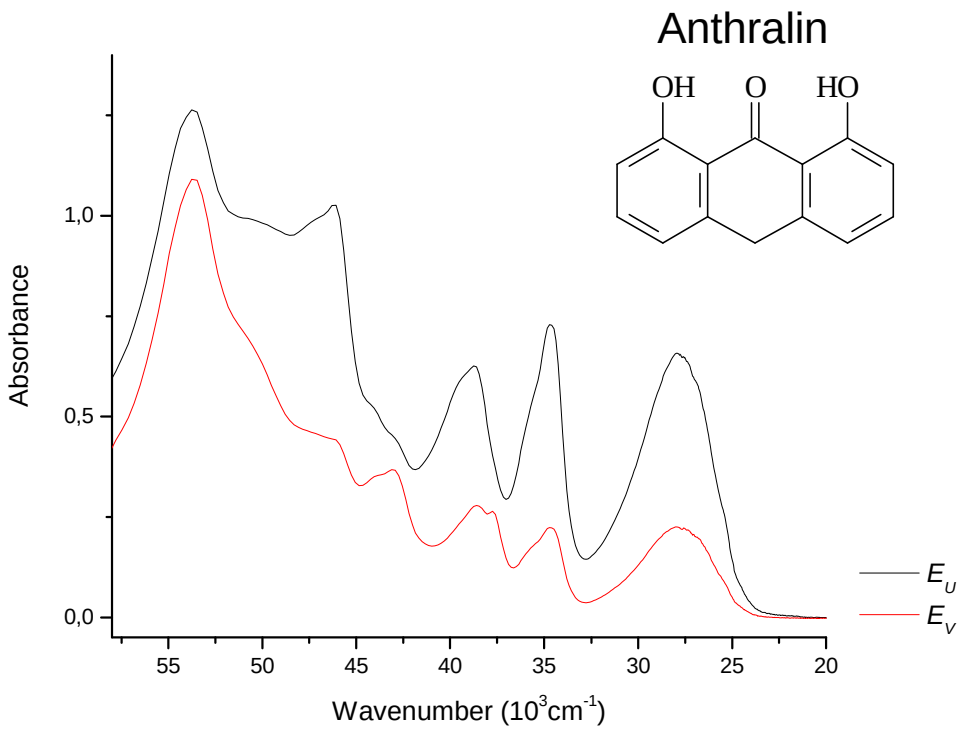
Anthralin
OH
O
HO
Absorbance
1,0
0,5
0,0
55
50
45
40
35
30
25
20
Wavenumber (10^3cm^-1)
E_U
E_V

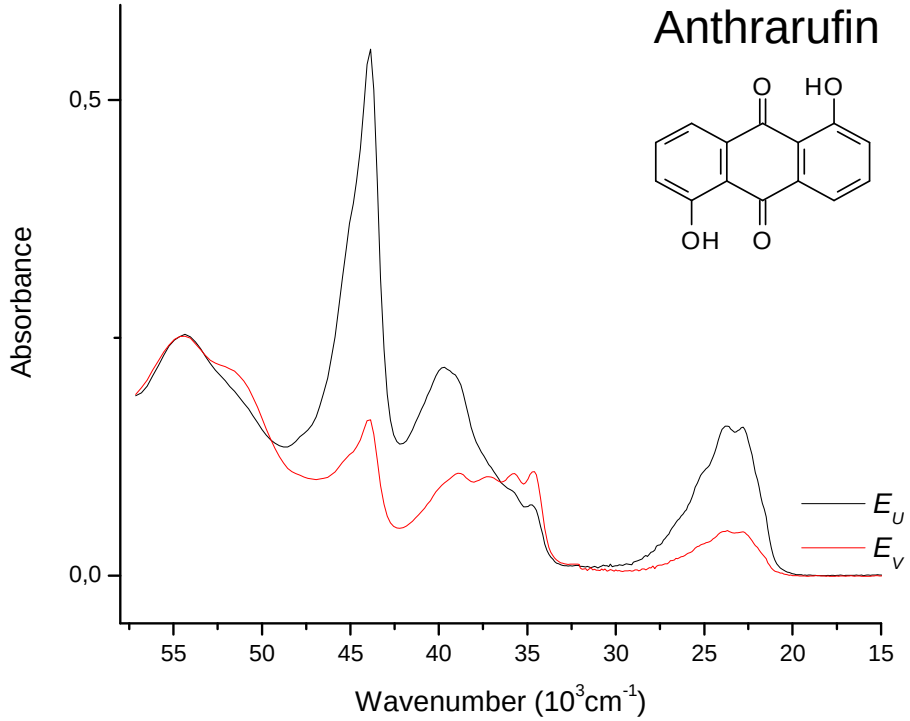
Anthrarufin
O
HO
OH
O
Absorbance
0,5
0,0
55
50
45
40
35
30
25
20
15
Wavenumber (10^3cm^-1)
E_U
E_V

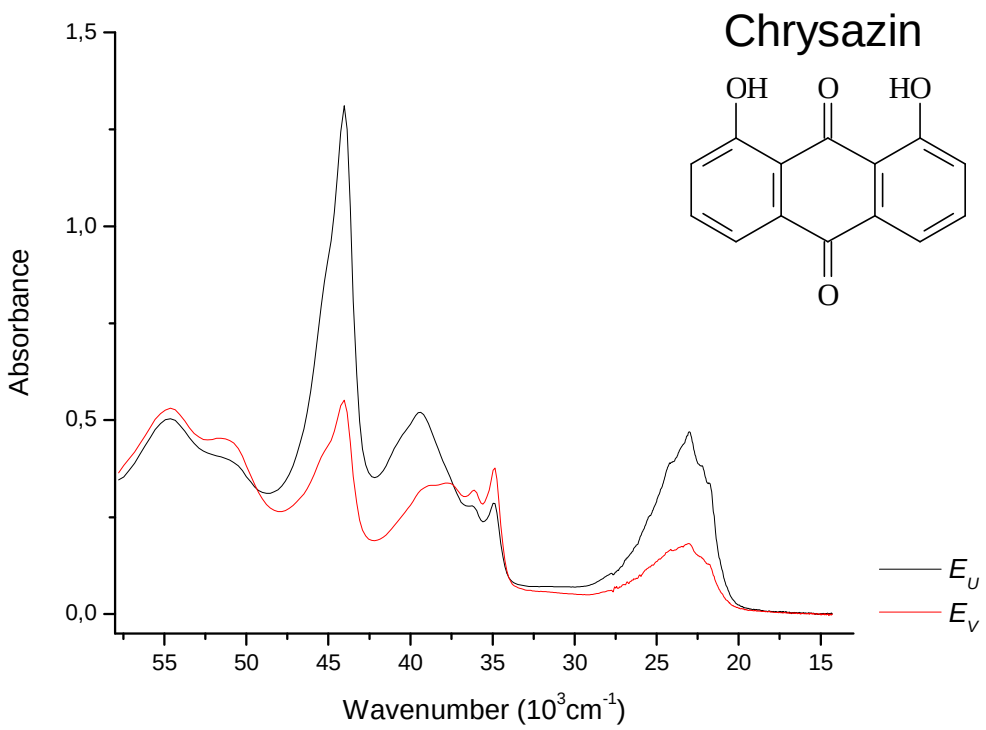
Chrysazin
OH
O
HO
O
1,5
1,0
0,5
0,0
Absorbance
55
50
45
40
35
30
25
20
15
Wavenumber (10³cm⁻¹)
E_U
E_V

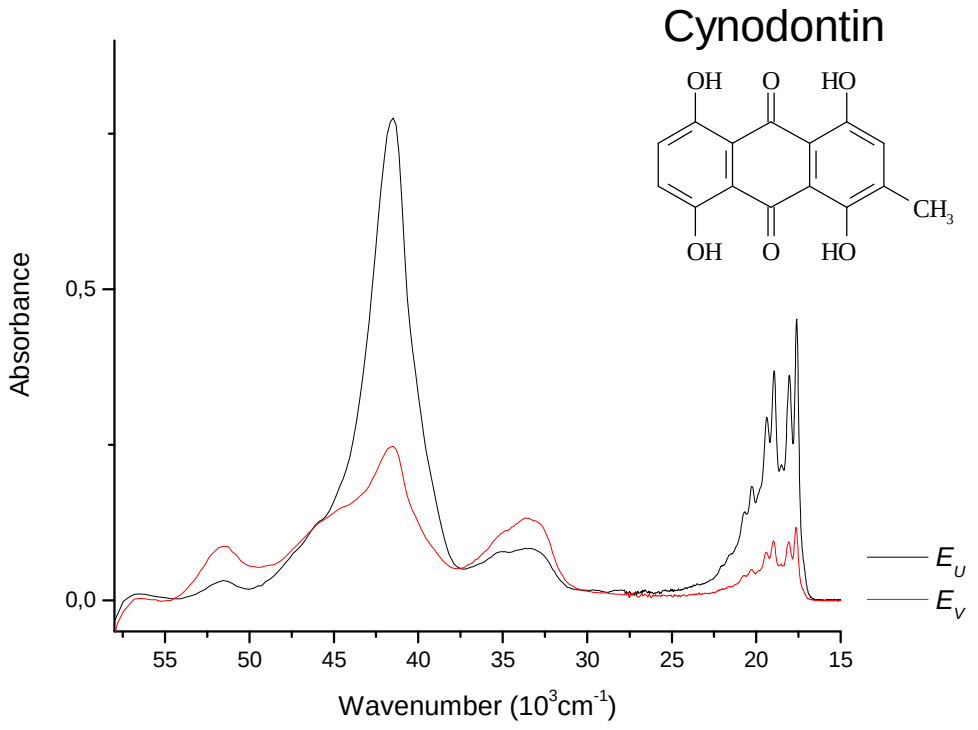
Cynodontin
OH
O
HO
CH3
OH
O
HO
0,5
0,0
Absorbance
55
50
45
40
35
30
25
20
15
Wavenumber (10³cm⁻¹)
E_U
E_V

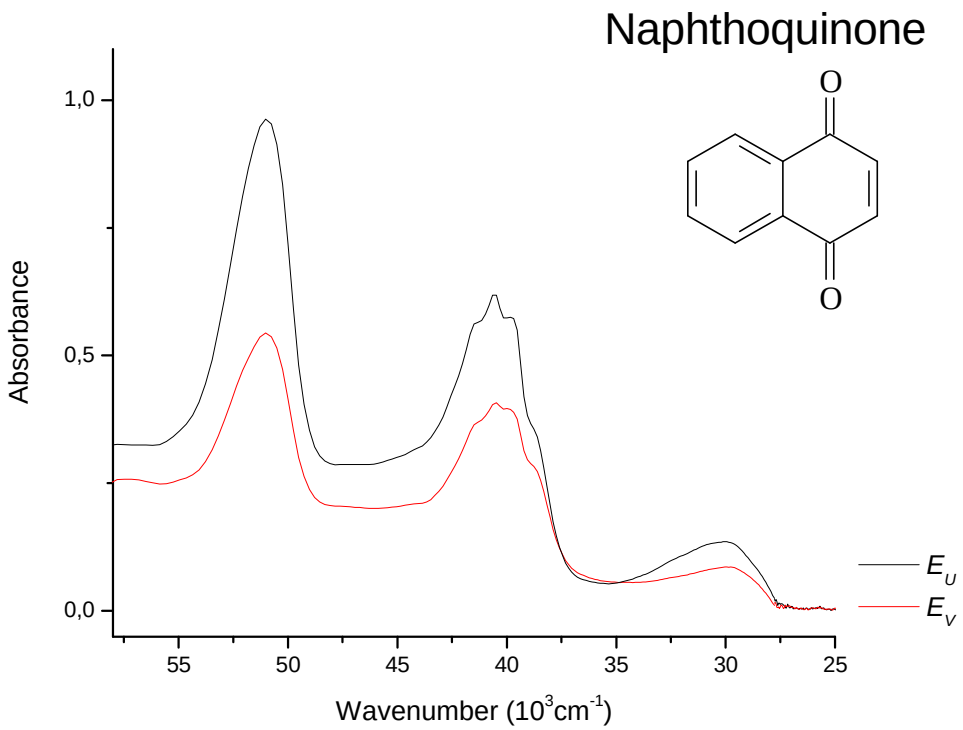
Naphthoquinone
O
O
1,0
0,5
0,0
Absorbance
55
50
45
40
35
30
25
Wavenumber (10^3cm^-1)
E_U
E_V

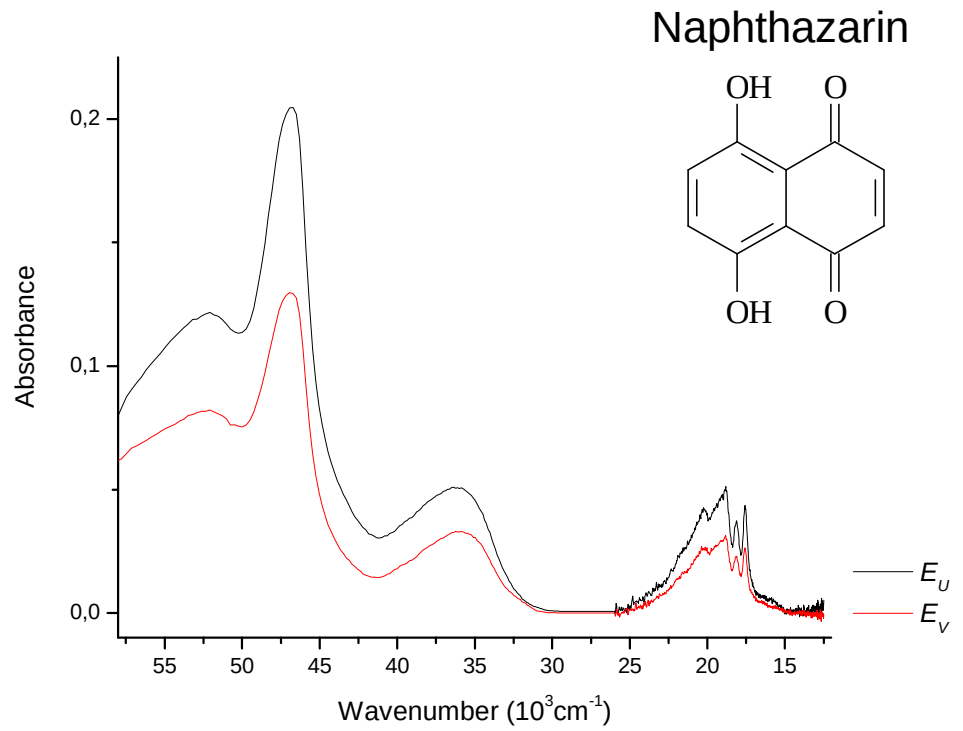
Naphthazarin
OH
O
OH
O
0,2
0,1
0,0
Absorbance
55
50
45
40
35
30
25
20
15
Wavenumber (10^3cm^-1)
E_U
E_V

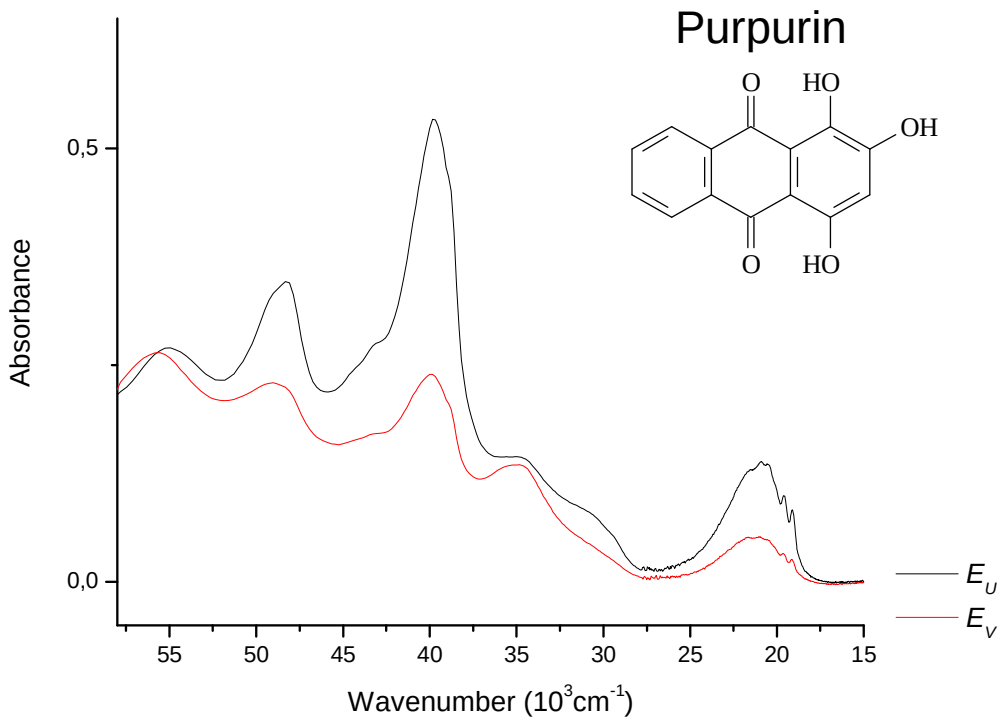
Purpurin
O
HO
OH
O
HO
0,5
0,0
Absorbance
55
50
45
40
35
30
25
20
15
Wavenumber (10^3cm^-1)
E_U
E_V

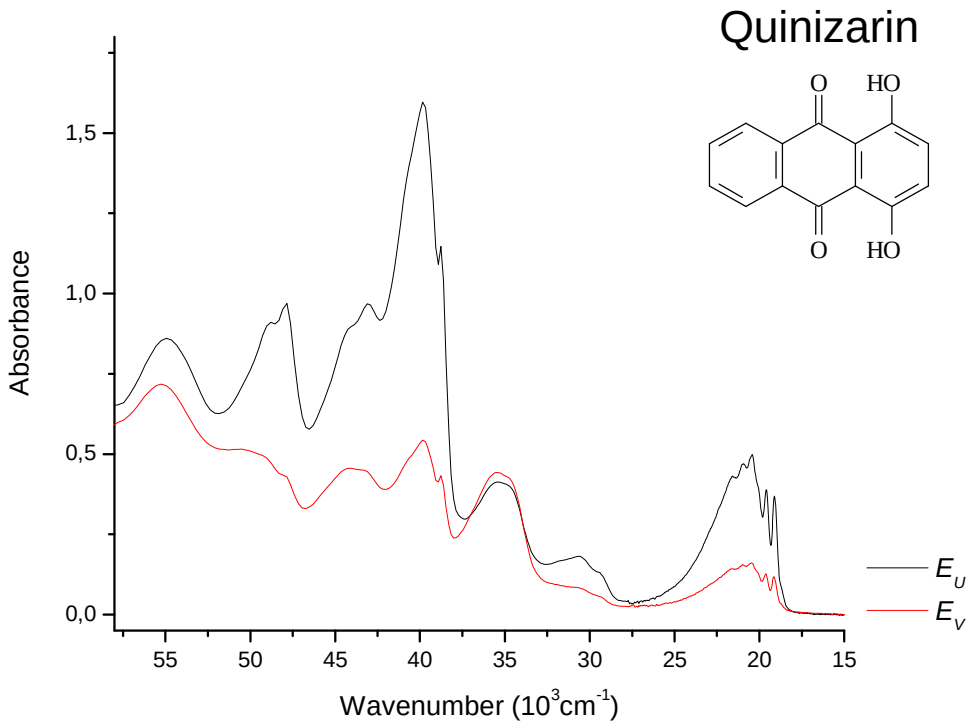
Quinizarin
O
HO
O
HO
1,5
1,0
0,5
0,0
Absorbance
55
50
45
40
35
30
25
20
15
Wavenumber (10^3cm^-1)
E_U
E_V

Appendix 4

Predicted electronic transitions for 1,4-Bis(phenylethynyl)benzene (BPEB)

	LCOAO 11π-11π*			
	Term	$\tilde{\nu}$ [a]	f [b]	Leading Configurations
1	$1\,^1B_{1u}$	28.4	2.62	93%($4b_{2g}$-$5b_{3u}$)
2	$1\,^1B_{2u}$	34.4	$9\cdot10^{-4}$	47%($1b_{1g}$-$5b_{3u}$), 39%($4b_{2g}$-$2a_u$)
3	$1\,^1B_{3g}$	36.4	0	26%($1a_u$-$5b_{3u}$), 21%($2b_{1g}$-$5b_{2g}$), 20%($4b_{2g}$-$3b_{1g}$), 17%($4b_{3u}$-$3a_u$)
4	$2\,^1B_{2u}$	36.4	$2\cdot10^{-3}$	26%($2b_{1g}$-$5b_{3u}$), 21%($1a_u$-$5b_{2g}$), 20%($4b_{2g}$-$3a_u$), 18%($4b_{3u}$-$3b_{1g}$)
5	$2\,^1A_g$	37.5	0	58%($4b_{3u}$-$5b_{3u}$), 38%($4b_{2g}$-$5b_{2g}$)
6	$3\,^1A_g$	40.0	0	54%($4b_{2g}$-$5b_{2g}$), 34%($4b_{3u}$-$5b_{3u}$)
7	$2\,^1B_{1u}$	45.1	0.15	43%($4b_{2g}$-$6b_{3u}$), 29%($4b_{3u}$-$5b_{2g}$), 12%($3b_{2g}$-$5b_{3u}$)
8	$3\,^1B_{2u}$	45.4	0.25	48%($4b_{2g}$-$2a_u$), 45%($1b_{1g}$-$5b_{3u}$)
9	$3\,^1B_{1u}$	45.7	$2\cdot10^{-3}$	60%($3b_{2g}$-$5b_{3u}$), 29%($4b_{2g}$-$6b_{3u}$)
10	$2\,^1B_{3g}$	46.9	0	49%($1a_u$-$5b_{3u}$), 37%($4b_{2g}$-$3b_{1g}$)
11	$4\,^1B_{2u}$	47.0	0.81	48%($2b_{1g}$-$5b_{3u}$), 33%($4b_{2g}$-$3a_u$)
12	$4\,^1A_g$	50.9	0	26%($2b_{1g}$-$3b_{1g}$), 25%($1a_u$-$3a_u$), 16%($4b_{3u}$-$6b_{3u}$), 16%($3b_{2g}$-$5b_{2g}$)
13	$4\,^1B_{1u}$	51.9	0.13	39%($4b_{3u}$-$5b_{2g}$), 13%($4b_{2g}$-$6b_{3u}$), 12%($3b_{2g}$-$5b_{3u}$), 11%($1b_{1g}$-$2a_u$)
14	$3\,^1B_{3g}$	52.3	0	75%($1b_{1g}$-$5b_{2g}$), 18%($4b_{3u}$-$2a_u$)
15	$5\,^1B_{1u}$	52.4	1.32	27%($1b_{1g}$-$2a_u$), 19%($1a_u$-$3b_{1g}$), 19%($2b_{1g}$-$3a_u$), 16%($4b_{3u}$-$5b_{2g}$)
16	$4\,^1B_{3g}$	52.6	0	29%($4b_{2g}$-$3b_{1g}$), 19%($1a_u$-$5b_{3u}$), 18%($2b_{1g}$-$5b_{2g}$), 17%($1a_u$-$6b_{3u}$)
17	$5\,^1B_{2u}$	52.6	0.12	29%($1a_u$-$3b_{1g}$), 19%($2b_{1g}$-$6b_{3u}$), 18%($2b_{1g}$-$5b_{3u}$), 17%($2b_{1g}$-$6b_{3u}$)
18	$5\,^1B_{3g}$	53.1	0	74%($4b_{3u}$-$2a_u$), 19%($1b_{1g}$-$5b_{2g}$)
19	$5\,^1A_g$	54.3	0	41%($3b_{3u}$-$5b_{3u}$), 38%($4b_{2g}$-$6b_{2g}$)
20	$6\,^1B_{1u}$	56.3	0.07	47%($1b_{1g}$-$2a_u$), 19%($2b_{1g}$-$3a_u$), 19%($1a_u$-$3b_{1g}$)
21	$6\,^1A_g$	57.0	0	30%($4b_{3u}$-$6b_{3u}$), 22%($2b_{1g}$-$3b_{1g}$), 22%($1a_u$-$3a_u$), 20%($3b_{2g}$-$5b_{2g}$)
22	$6\,^1B_{3g}$	57.1	0	37%($4b_{3u}$-$3a_u$), 26%($2b_{1g}$-$5b_{2g}$), 16%($3b_{2g}$-$3b_{1g}$)
23	$6\,^1B_{2u}$	57.2	0.92	38%($4b_{3u}$-$3b_{1g}$), 27%($1a_u$-$5b_{2g}$), 16%($3b_{2g}$-$3a_u$)
24	$7\,^1B_{2u}$	58.6	0.01	50%($1b_{1g}$-$6b_{3u}$), 25%($3b_{2g}$-$2a_u$)
25	$7\,^1B_{1u}$	59.6	0.01	43%($2b_{2g}$-$5b_{3u}$), 32%($4b_{2g}$-$7b_{3u}$), 11%($3b_{3u}$-$5b_{2g}$)
26	$7\,^1A_g$	59.6	0	46%($3b_{2g}$-$5b_{2g}$), 18%($4b_{3u}$-$6b_{3u}$), 15%($3b_{3u}$-$5b_{3u}$)
27	$8\,^1A_g$	60.2	0	44%($4b_{2g}$-$6b_{2g}$), 25%($3b_{3u}$-$5b_{3u}$), 17%($4b_{3u}$-$6b_{3u}$)
28	$8\,^1B_{2u}$	62.1	0.42	58%($3b_{2g}$-$2a_u$), 33%($1b_{1g}$-$6b_{3u}$)
29	$8\,^1B_{1u}$	63.2	$1\cdot10^{-4}$	98%($2b_{1g}$-$2a_u$)
30	$9\,^1A_g$	63.2	0	99%($1a_u$-$2a_u$)
31	$7\,^1B_{3g}$	63.2	0	34%($1a_u$-$6b_{3u}$), 28%($2b_{1g}$-$5b_{2g}$), 17%($2b_{1g}$-$6b_{2g}$)

[a] Wavenumber in 10^3 cm^{-1}.
[b] Oscillator strength.

Appendix 5

Orbital diagrams for BPEB

A5.1 Lowest unoccupied molecular orbitals (LUMO)

-0.36 eV	6 $b_{3u}(\pi^*)$	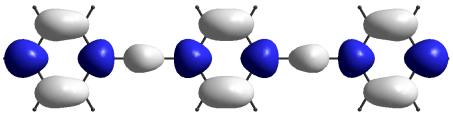
-0.52 eV	3 $a_u(\pi^*)$	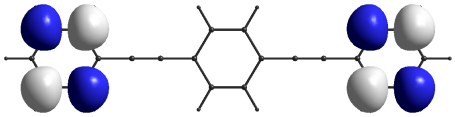
-0.53 eV	3 $b_{1g}(\pi^*)$	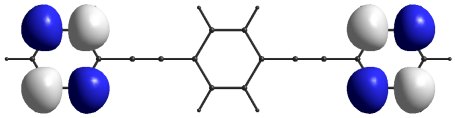
-0.58 eV	2 $a_u(\pi^*)$	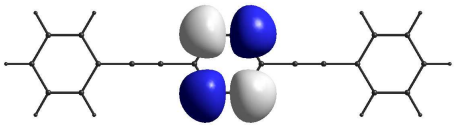
-1.36 eV	5 $b_{2g}(\pi^*)$	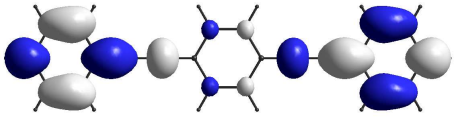
-2.45 eV	5 $b_{3u}(\pi^*)$	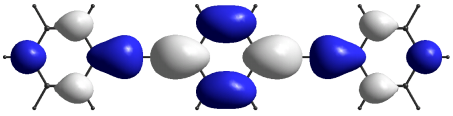

A5.2 Highest occupied molecular orbitals (HOMO)

-8.49 eV	4 $b_{2g}(\pi)$	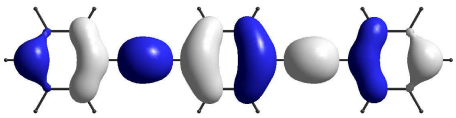
-9.51 eV	4 $b_{3u}(\pi)$	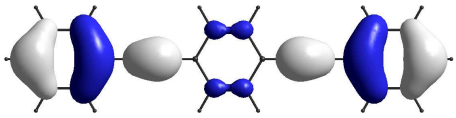
-10.15 eV	2 $b_{1g}(\pi)$	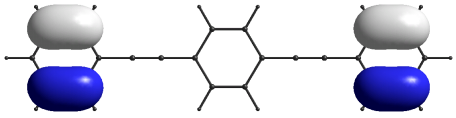
-10.15 eV	1 $a_{u}(\pi)$	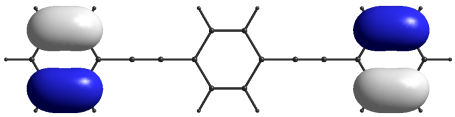
-10.27 eV	1 $b_{1g}(\pi)$	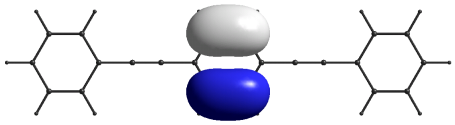
-10.57 eV	3 $b_{2g}(\pi)$	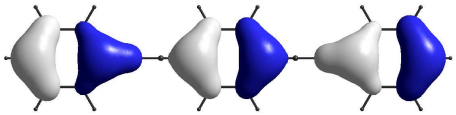

Appendix 6

Predicted electronic transitions for Dibenzofuran

	TD-B3LYP/6-31+G(d,p)			
	Term	$\tilde{\nu}$ [a]	f [b]	Leading Configurations [c]
1	$2\ ^1A_1$	35.8	0.03	80%(2,-1), 16%(1,-2)
2	$1\ ^1B_2$	36.9	0.30	76%(1,-1)
3	$2\ ^1B_2$	42.2	0.03	50%(3,-1), 39%(1,-3)
4	$3\ ^1A_1$	43.7	0.08	22%(2,-3), 57%(1,-2)
5	$3\ ^1B_2$	44.8	0.29	14%(3,-1), 63%(2,-2)
6	$1\ ^1A_2$	46.0	0	98%(1,-4)
7	$1\ ^1B_1$	47.0	$8\cdot10^{-3}$	86%(2,-4), 10%(1,-5)
8	$2\ ^1B_1$	47.4	$7\cdot10^{-3}$	10%(2,-4), 88%(1,-5)
9	$4\ ^1B_2$	47.6	0.44	21%(3,-1), 16%(2,-2), 37%(1,-3)
10	$4\ ^1A_1$	47.7	0.03	27%(4,-1), 50%(2,-3)
11	$2\ ^1A_2$	48.4	0	94%(2,-5)
12	$5\ ^1A_1$	49.4	0.07	21%(4,-1), 51%(1,-6)
13	$3\ ^1A_2$	49.5	0	98%(1,-7)
14	$3\ ^1B_1$	50.4	0.01	94%(2,-7)
15	$5\ ^1B_2$	50.8	0.08	15%(4,-2), 72%(2,-6)
16	$6\ ^1A_1$	50.9	0.02	25%(4,-1), 50%(3,-2), 14%(1,-6)
17	$4\ ^1A_2$	51.2	0	92%(1,-8)
18	$4\ ^1B_1$	52.3	$8\cdot10^{-4}$	84%(2,-8)
19	$5\ ^1B_1$	52.6	$3\cdot10^{-3}$	95%(1,-9)
20	$5\ ^1A_2$	53.2	0	84%(2,-9)
21	$6\ ^1B_2$	53.9	0.44	83%(3,-3)
22	$6\ ^1A_2$	54.5	0	71%(3,-4), 12%(1,-10)
23	$7\ ^1A_2$	54.8	0	12%(3,-4), 79%(1,-10)
24	$7\ ^1A_1$	55.4	$7\cdot10^{-3}$	30%(4,-3), 20%(3,-2), 31%(3,-6)
25	$6\ ^1B_1$	55.6	$4\cdot10^{-3}$	22%(3,-5), 72%(2,-10)
26	$7\ ^1B_1$	56.3	0	70%(3,-5), 18%(2,-10)
27	$8\ ^1B_1$	56.4	$2\cdot10^{-3}$	97%(5,-1)
28	$7\ ^1B_2$	56.9	$5\cdot10^{-4}$	12%(4,-2), 83%(1,-13)
29	$8\ ^1A_2$	57.0	0	94%(1,-12)
30	$9\ ^1B_1$	57.4	$3\cdot10^{-3}$	98%(1,-11)
31	$9\ ^1A_2$	57.9	0	88%(3,-7)
32	$8\ ^1A_1$	58.0	0.08	89%(2,-13)
33	$10\ ^1B_1$	58.0	$2\cdot10^{-3}$	92%(2,-12)
34	$8\ ^1B_2$	58.1	$7\cdot10^{-3}$	54%(4,-2), 11%(2,-14), 12%(1,-13)
35	$10\ ^1A_2$	58.2	0	16%(3,-8), 81%(2,-11)
36	$11\ ^1A_2$	59.1	0	95%(6,-1)
37	$9\ ^1A_1$	59.4	$8\cdot10^{-3}$	10%(4,-1), 16%(4,-3), 12%(3,-2), 13%(3,-6), 11%(1,-6)
38	$12\ ^1A_2$	59.8	0	65%(3,-8), 14%(2,-11)
39	$10\ ^1A_1$	60.3	0.04	87%(1,-14)
40	$11\ ^1B_1$	60.5	$7\cdot10^{-3}$	89%(4,-4)
41	$12\ ^1B_1$	61.0	0.01	88%(3,-9)
42	$13\ ^1B_1$	61.7	$8\cdot10^{-3}$	87%(1,-16)
43	$11\ ^1A_1$	61.7	0.37	20%(7,-1), 26%(4,-3), 32%(3,-6)
44	$9\ ^1B_2$	61.9	$6\cdot10^{-4}$	80%(2,-14)
45	$13\ ^1A_2$	62.0	0	94%(4,-5)
46	$10\ ^1B_2$	62.3	$2\cdot10^{-3}$	92%(1,-15)
47	$14\ ^1A_2$	62.4	0	12%(3,-8), 33%(3,-10), 42%(2,-16)
48	$15\ ^1A_2$	63.2	0	19%(10,-1), 72%(5,-2)
49	$12\ ^1A_1$	63.3	0.01	95%(2,-15)
50	$16\ ^1A_2$	63.6	0	43%(3,-10), 40%(2,-16)

[a] Wavenumber in 10^3 cm^{-1}.
[b] Oscillator strength.
[c] The notation (*i*,-*j*) indicates an excited singlet configuration derived from the ground configuration by promotion of an electron from the i^{th} highest occupied to the j^{th} lowest unoccupied molecular orbital.

Appendix 7

Orbital diagrams for DBF

A7.1 **Lowest unoccupied molecular orbitals (LUMO)**

(-6)	0.49eV	5 a_2 (π^*)	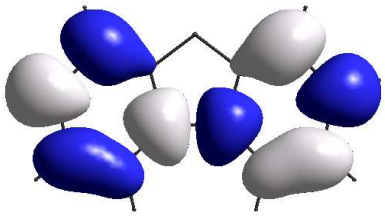
(-3)	-0.12eV	6 b_1 (π^*)	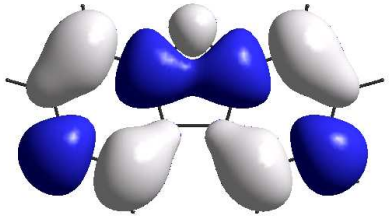
(-2)	-0.36eV	4 a_2 (π^*)	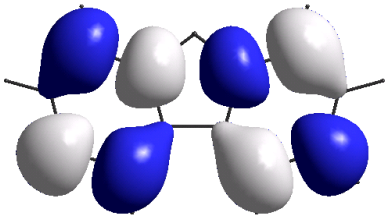
(-1)	-1.33eV	5 b_1 (π^*)	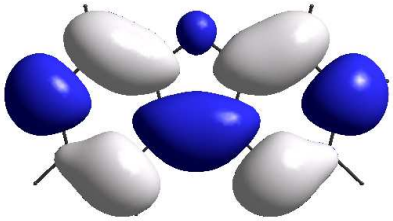

A7.2 Highest occupied molecular orbitals (HOMO)

(1)	-6.31eV	3 a_2 (π)	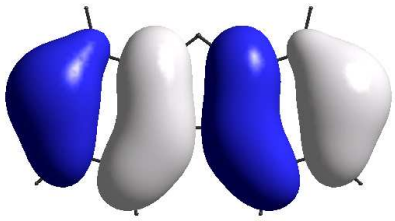
(2)	-6.44eV	4 b_1 (π)	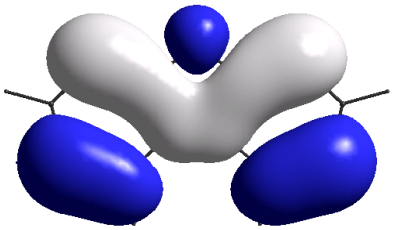
(3)	-7.32eV	2 a_2 (π)	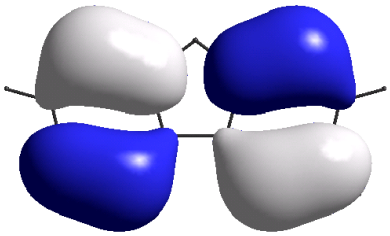
(4)	-8.07eV	3 b_1 (π)	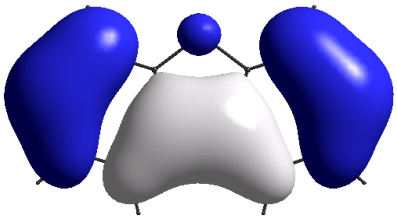

Appendix 8

Predicted electronic transitions for Anthrarufin

	TD-B3LYP/6-31+G(d,p)				
	Term	$\tilde{\nu}$ [a]	f [b]	ϕ [c]	Leading configurations [d]
1	$1\,^1B_u$	23.3	0.23	+6°	85%(1,-1)
2	$1\,^1B_g$	24.8	0	-	94%(3,-1)
3	$2\,^1A_g$	24.8	0	-	83%(2,-1)
4	$1\,^1A_u$	28.1	$1\cdot10^{-4}$	*z*	91%(6,-1)
5	$3\,^1A_g$	28.3	0	-	90%(4,-1)
6	$2\,^1B_u$	35.1	0.15	+93°	81%(5,-1)
7	$4\,^1A_g$	35.6	0	-	88%(1,-2)
8	$3\,^1B_u$	36.7	0.02	+28°	90%(2,-2)
9	$2\,^1A_u$	38.9	$<10^{-4}$	*z*	93%(3,-2)
10	$5\,^1A_g$	40.2	0	-	81%(1,-3), 11%(5,-2)
11	$4\,^1B_u$	40.7	0.05	–3°	63%(2,-3), 31%(4,-2)
12	$2\,^1B_g$	42.2	0	-	92%(6,-2)
13	$5\,^1B_u$	43.8	0.70	0°	54%(4,-2), 28%(2,-3)
14	$6\,^1A_g$	44.7	0	-	67%(7,-1), 18%(5,-2)
15	$3\,^1A_u$	45.1	$3\cdot10^{-4}$	*z*	96%(3,-3)
16	$6\,^1B_u$	46.2	0.10	+38°	61%(8,-1), 25%(1,-4)
17	$3\,^1B_g$	46.6	0	-	95%(9,-1)
18	$7\,^1A_g$	46.9	0	-	61%(5,-2), 18%(7,-1)
19	$7\,^1B_u$	47.8	0.08	–19°	41%(1,-4), 25%(4,-3), 24%(8,-1)
20	$8\,^1A_g$	48.8	0	-	72%(2,-4), 13%(5,-3)
21	$4\,^1A_u$	49.0	$<10^{-4}$	*z*	88%(10,-1)
22	$5\,^1A_u$	49.1	$7\cdot10^{-4}$	*z*	96%(6,-3)
23	$4\,^1B_g$	49.1	0	-	83%(1,-5)
24	$5\,^1B_g$	49.9	0	-	62%(2,-5), 34%(1,-6)
25	$6\,^1B_g$	50.6	0	-	77%(11,-1), 18%(3,-4)
26	$7\,^1B_g$	51.0	0	-	76%(3,-4), 18%(11,-1)
27	$8\,^1B_g$	51.7	0	-	51%(1,-6), 24%(2,-7), 18%(2,-5)
28	$9\,^1A_g$	51.9	0	-	75%(5,-3)
29	$8\,^1B_u$	51.9	0.40	–83°	51%(4,-3), 20%(1,-4)
30	$6\,^1A_u$	51.9	$<10^{-4}$	*z*	66%(1,-7), 31%(2,-6)
31	$7\,^1A_u$	52.8	$<10^{-4}$	*z*	96%(12,-1)
32	$9\,^1B_g$	53.9	0	-	75%(1,-8), 11%(2,-5)
33	$8\,^1A_u$	54.0	$3\cdot10^{-4}$	*z*	62%(2,-6), 26%(1,-7), 10%(1,-5)
34	$10\,^1A_g$	54.4	0	-	68%(4,-4), 14%(2,-9)
35	$10\,^1B_g$	54.6	0	-	68%(2,-7), 11%(1,-8), 10%(1,-6)
36	$9\,^1A_u$	54.9	$3\cdot10^{-3}$	*z*	60%(2,-8), 20%(6,-4), 16%(1,-10)
37	$10\,^1A_u$	55.0	$1\cdot10^{-3}$	*z*	78%(6,-4), 15%(2,-8)
38	$9\,^1B_u$	55.2	0.01	+3°	56%(1,-9), 40%(5,-4)
39	$11\,^1B_g$	56.1	0	-	93%(14,-1)
40	$11\,^1A_g$	56.3	0	-	73%(3,-5), 1 2%(1,-11)
41	$11\,^1A_u$	56.5	$9\cdot10^{-4}$	*z*	87%(15,-1)
42	$12\,^1B_g$	56.6	0	-	91%(4,-5)
43	$10\,^1B_u$	56.7	0.02	–6°	56%(13,-1), 19%(5,-4), 14%(1,-9)
44	$12\,^1A_g$	56.8	0	-	63%(1,-11), 13%(3,-5)
45	$12\,^1A_u$	57.2	0.02	*z*	66%(1,-10), 16%(2,-8)
46	$11\,^1B_u$	57.4	0.13	+12°	40%(7,-2), 21%(13,-1), 20%(5,-4), 13%(1,-9)
47	$13\,^1A_g$	57.7	0	-	53%(2,-9), 21%(8,-2), 13%(1,-11)
48	$14\,^1A_g$	57.8	0	-	75%(1,-12), 11%(8,-2)
49	$13\,^1A_u$	57.9	0.01	*z*	69%(4,-6), 20%(5,-5)
50	$13\,^1B_g$	58.1	0	-	59%(2,-10), 34%(1,-13)

51	$12\,^1B_u$	58.5	0.08	–1°	23%(2,-12), 20%(7,-2), 18%(3,-6)
52	$13\,^1B_u$	58.8	0.05	–49°	49%(3,-6), 14%(2,-12), 14%(2,-11)
53	$15\,^1A_g$	58.9	0	-	43%(8,-2), 18%(1,-12), 17%(16,-1), 11%(2,-9)
54	$14\,^1A_u$	59.1	$3\cdot10^{-4}$	*z*	71%(9,-2), 10%(3,-11)
55	$14\,^1B_g$	59.3	0	-	48%(4,-7), 18%(1,-13), 17%(2,-10)
56	$16\,^1A_g$	59.6	0	-	58%(16,-1)
57	$14\,^1B_u$	59.7	0.12	+68°	34%(6,-5), 22%(3,-8), 10%(2,-11)
58	$15\,^1B_u$	59.7	0.05	–38°	22%(7,-2), 20%(2,-12), 19%(3,-6)
59	$15\,^1A_u$	59.7	$3\cdot10^{-3}$	*z*	88%(1,-14)
60	$15\,^1B_g$	59.8	0	-	41%(1,-13), 34%(4,-7), 13%(2,-10)

[a] Wavenumber in 10^3 cm^{-1}.

[b] Oscillator strength.

[c] In-plane transition moment angle ϕ (*z* designates out-of-plane polarization).

[d] The notation (*i*,-*j*) indicates an excited singlet configuration derived from the ground configuration by promotion of an electron from the i^{th} highest occupied to the j^{th} lowest unoccupied MO.

Appendix 9

Orbital diagrams for Anthrarufin

A9.1 **Lowest unoccupied molecular orbitals (LUMO)**

(-4)	-0.51eV	7 b_g (π^*)	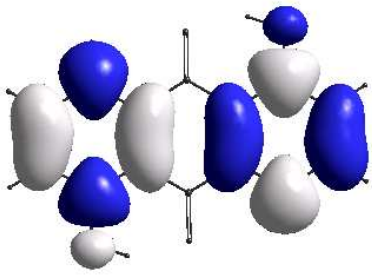
(-3)	-1.22eV	7 a_u (π^*)	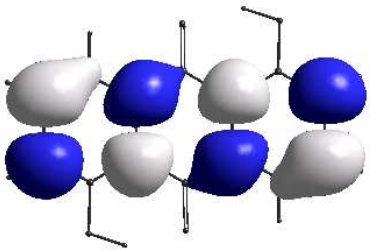
(-2)	-1.95eV	6 a_u (π^*)	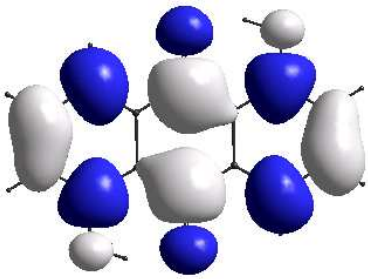
(-1)	-3.52eV	6 b_g (π^*)	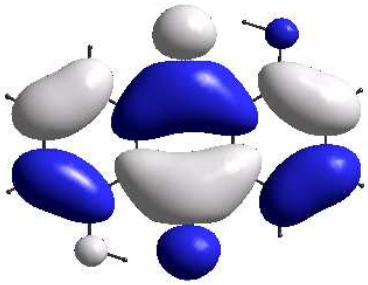

A9.2 Highest occupied molecular orbitals (HOMO)

(1)	-6.84eV	5 a_u (π)	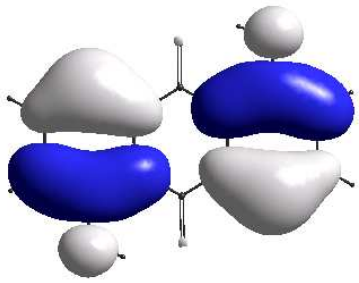
(2)	-7.02eV	5 b_g (π)	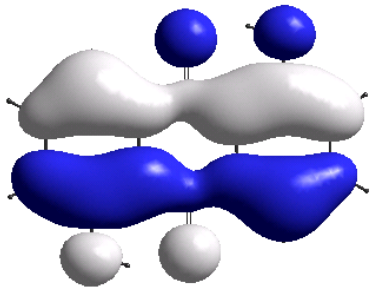
(4)	-7.78eV	4 b_g (π)	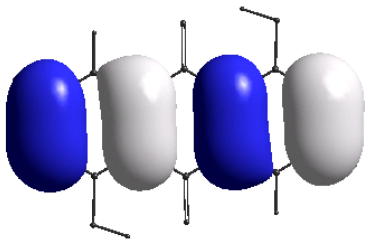
(5)	-8.16eV	4 a_u (π)	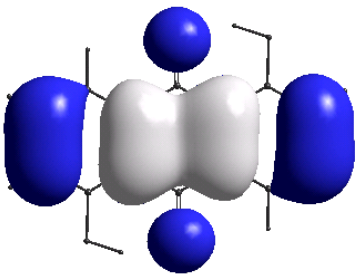

Appendix 10

Character tables

$\mathbf{C_{2v}}$	E	C_2	$\sigma_v(xz)$	$\sigma'_v(yz)$		
A_1	1	1	1	1	z	x^2, y^2, z^2
A_2	1	1	-1	-1	R_z	xy
B_1	1	-1	1	-1	x, R_y	xz
B_2	1	-1	-1	1	y, R_x	yz

$\mathbf{D_{2h}}$	E	$C_2(z)$	$C_2(y)$	$C_2(x)$	i	$\sigma(xy)$	$\sigma(xz)$	$\sigma(yz)$		
A_g	1	1	1	1	1	1	1	1		x^2, y^2, z^2
B_{1g}	1	1	-1	-1	1	1	-1	-1	R_z	xy
B_{2g}	1	-1	1	-1	1	-1	1	-1	R_y	xz
B_{3g}	1	-1	-1	1	1	-1	-1	1	R_x	yz
A_u	1	1	1	1	-1	-1	-1	-1		
B_{1u}	1	1	-1	-1	-1	-1	1	1	z	
B_{2u}	1	-1	1	-1	-1	1	-1	1	y	
B_{3u}	1	-1	-1	1	-1	1	1	-1	x	

$\mathbf{C_{2h}}$	E	C_2	i	σ_h		
A_g	1	1	1	1	R_z	x^2, y^2, z^2, xy
B_g	1	-1	1	-1	R_x, R_y	xz, yz
A_u	1	1	-1	-1	z	
B_u	1	-1	-1	1	x, y	

Appendix 11

Spectrochimica Acta Part A 77 (2010) 279–286

Contents lists available at ScienceDirect

Spectrochimica Acta Part A: Molecular and Biomolecular Spectroscopy

journal homepage: www.elsevier.com/locate/saa

Synchrotron radiation linear dichroism (SRLD) investigation of the electronic transitions of quinizarin, chrysazin, and anthrarufin

Duy Duc Nguyen[a], Nykola C. Jones[b], Søren Vrønning Hoffmann[b], Jens Spanget-Larsen[a,*]

[a] Department of Science, Systems and Models, Roskilde University, Universitetsvej 1, Bldg. 18, DK-4000 Roskilde, Denmark
[b] Institute for Storage Ring Facilities, ISA, Aarhus University, Ny Munkegade 120, Bldg. 1520, DK-8000 Århus, Denmark

ARTICLE INFO

Article history:
Received 23 February 2010
Received in revised form 29 April 2010
Accepted 15 May 2010

Keywords:
Hydroxy-anthraquinones
Electronic transitions
Synchrotron radiation
Linear dichroism (LD)
Polarization directions
Transition moments
Time-dependent density functional theory (TD-DFT)

ABSTRACT

The electronic transitions of the three α,α′-dihydroxy derivatives of anthraquinone, 1,4-dihydroxy-, 1,8-dihydroxy-, and 1,5-dihydroxy-9,10-anthraquinone (quinizarin, chrysazin, and anthrarufin), were investigated by synchrotron radiation linear dichroism (SRLD) spectroscopy on samples aligned in stretched polyethylene. With synchrotron radiation, polarization data could be determined in the UV region up to ca. 58,000 cm^{-1} (7.2 eV), which amounts to an extension by ca. 11,000 cm^{-1} (1.4 eV) relative to the range accessible with a conventional light source. Throughout the investigated region (15,000–58,000 cm^{-1}), essentially similar wavenumbers, intensities, and transition moment directions were determined for chrysazin and anthrarufin, while the spectrum of quinizarin deviated significantly. The results of time-dependent density functional theory (TD-DFT) calculations were in good agreement with the experimental spectra, leading to the assignment of 10 electronic states for quinizarin, and 8 electronic states for chrysazin and anthrarufin. No evidence was found for contributions from different tautomeric or rotameric forms to the observed spectra.

1. Introduction

Hydroxy-anthraquinones are of general interest as dyes and pigments [1] and as model chromophores for biologically active compounds, such as the anthracycline antitumor drugs [2]. In the present investigation we study the electronic transitions of the three α,α′-dihydroxy derivatives 1,4-dihydroxy-9,10-anthraquinone (quinizarin, **Q**), 1,8-dihydroxy-9,10-anthraquinone (chrysazin, danthron, **C**), and 1,5-dihydroxy-9,10-anthraquinone (anthrarufin, **A**) by means of linear dichroism (LD) spectroscopy on samples partially aligned in stretched low-density polyethylene (LDPE), and by quantum chemical calculations.

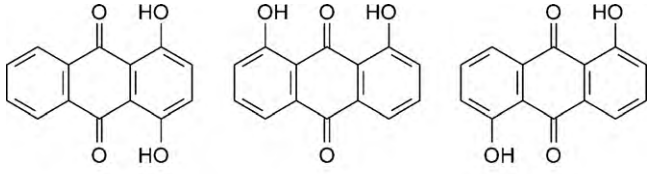

LD spectroscopy yields information on molecular transition moment directions, thereby frequently leading to resolution of otherwise overlapping, differently polarized transitions, and to symmetry assignments of the observed molecular states [3]. We have previously investigated the LD spectra of these [4–6] and related species [7,8] using a traditional UV-VIS spectrophotometer. In the present study, we extend the investigated UV region by the application of synchrotron radiation linear dichroism (SRLD) spectroscopy. The use of synchrotron radiation leads to substantially improved signal to noise ratio in the UV region, compared with conventional technology [9,10]. This is a great advantage when using a solvent medium like LDPE which absorbs and scatters strongly in this region, particularly above 47,000 cm^{-1}. Compared with a traditional source of linearly polarized UV radiation, such as a deuterium lamp equipped with a Glan prism polarizer, synchrotron radiation leads to generally improved precision of the orientation factors derived for the observed transitions (see below) and allows measurements at significantly increased wavenumbers. In the present study, we extend the previously investigated region by ca. 11,000 cm^{-1}, from ca. 47,000 to ca. 58,000 cm^{-1}.

The measured absorption bands for **Q**, **C**, and **A** are assigned to electronic transitions predicted with time-dependent density functional theory (TD-DFT) which is a well-tested theoretical tool in the study of organic chromophores [11–13]. The combined experimental and theoretical results lead to a detailed description of electronic transitions in the 15,000–58,000 cm^{-1} region. Additional information is provided as Supplementary data, referred to in the ensuing text as S1–S16.

* Corresponding author. Tel.: +45 4674 2710; fax: +45 4674 3011.
E-mail address: spanget@ruc.dk (J. Spanget-Larsen).

1386-1425/$ – see front matter © 2010 Elsevier B.V. All rights reserved.
doi:10.1016/j.saa.2010.05.023

2. Experimental

2.1. Sample preparation

Samples of the dihydroxy-anthraquinones **Q**, **C**, and **A** were obtained from commercial sources (BDH Chemical Ltd., White Lund Industrial Estate) or synthesized according to standard procedures [14]. The spectroscopic purity of the compounds was checked by comparison of their UV–VIS absorption spectra with data from the literature. Methanol, ethanol, chloroform (all Merck Uvasol) and pure LDPE 100 μm sheet material (Hinnum Plast, Vordingborg) were used as solvents. Absorption spectra measured in methanol solution are provided as Supplementary data (S1). The dihydroxy-anthraquinones were introduced into the LDPE by submersion of the polymer material into concentrated solutions of the compounds in chloroform at 50 °C for three days. The process was accelerated by repeated sonication. The chloroform solvent was finally evaporated from the samples, residual crystals on the surface were removed with ethanol, and the sample was uniaxially stretched by ca. 500%. Corresponding samples without solutes were produced for use as references.

2.2. LD spectroscopy

Two linearly independent LD absorbance curves were measured at room temperature on the uniaxially stretched samples, one with the electric vector of the sample beam parallel to the stretching direction (U), and one with the electric vector perpendicular to it (V). In both cases the sample beam was perpendicular to the surface of the PE sheet. The resulting baseline-corrected absorbance curves are denoted by $E_U(\tilde{\nu})$ and $E_V(\tilde{\nu})$. UV–VIS LD spectra were recorded in the region 15,000–47,000 cm^{-1} on a Shimadzu MPS-2000 spectrophotometer equipped with Glan prism polarizers as previously described [4–8]. In the UV region, improved results were obtained with synchrotron radiation. The SRLD spectra were recorded at the UV1 [9] and CD1 [10] beamlines on the ASTRID storage ring at the Institute for Storage Ring Facilities (ISA), Aarhus University, Denmark. The radiation exits the beamline through a CaF_2 window into a nitrogen purged purpose built chamber holding the sample. The light was polarized with a MgF_2 Rochon polarizer, passed through the sample and detected with a UV sensitive photomultiplier tube (PMT model 9402B, Electron Tubes, UK). The two beamlines provide a much higher photon flux deep into the UV spectral range as compared to conventional spectrophotometers. This yields an improved signal to noise ratio (the ratio depends on the square root of the number of photons reaching the detector), and we were able to investigate our PE samples up to about 58,000 cm^{-1}. The results are shown in Figs. 1–4 (also provided as S2–S5).

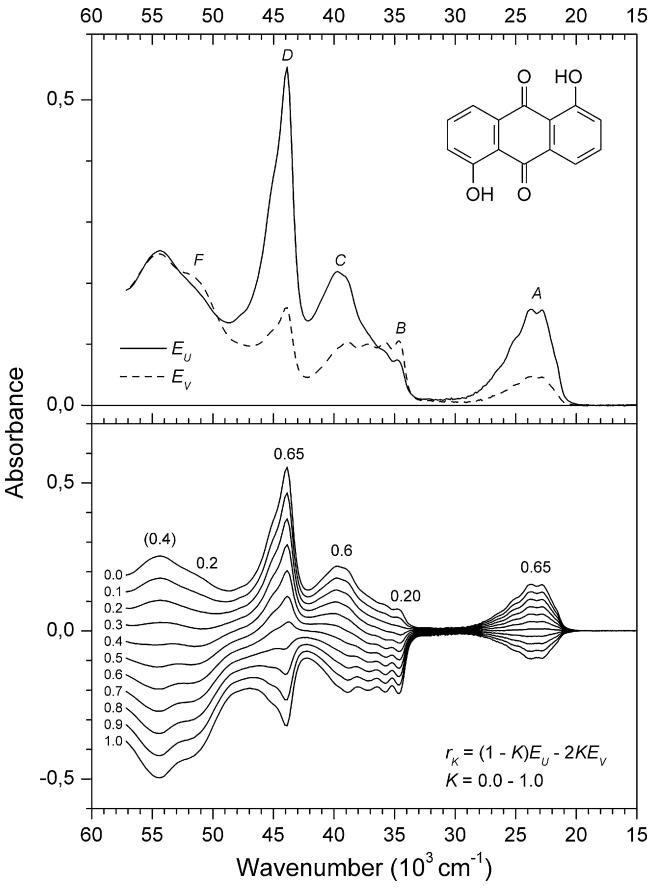

Fig. 1. *Top*: Linear dichroism (LD) of anthrarufin (**A**) aligned in stretched polyethylene. The full and dashed lines indicate the absorbance curves $E_U(\tilde{\nu})$ and $E_V(\tilde{\nu})$ measured with the electric vector of the sample beam parallel and perpendicular to the stretching direction U of the polymer sample. The absorbance was measured with synchrotron radiation, except for the region below 32,000 cm^{-1} where a conventional light source was used. *Bottom*: Family of reduced absorbance curves $r_K(\tilde{\nu})$ with indication of derived orientation factors K (see text; partial absorbance curves $A_1(\tilde{\nu})$ and $A_2(\tilde{\nu})$ with $(K_1, K_2) = (0.65, 0.20)$ are given in Fig. 4).

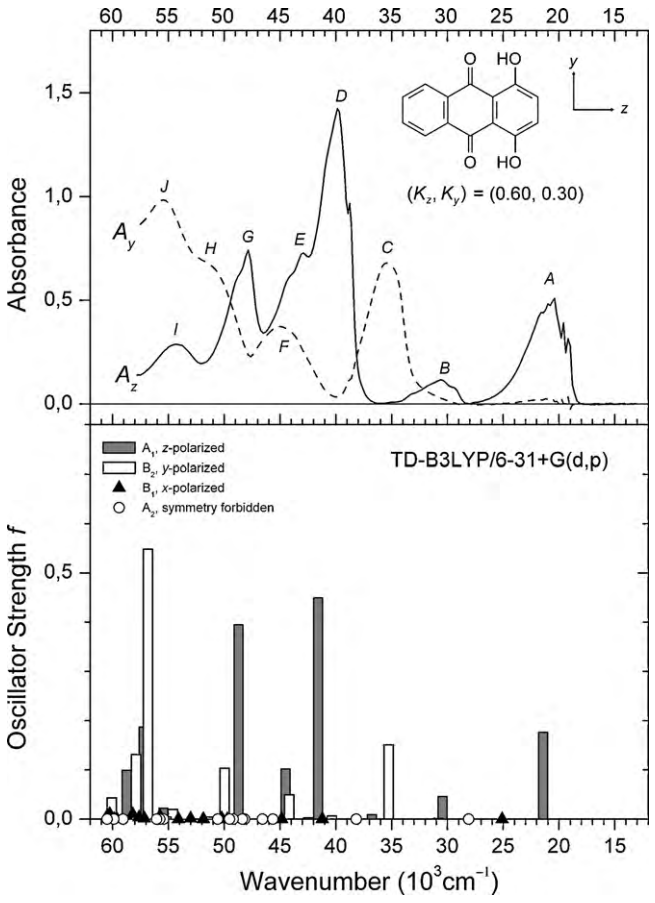

Fig. 2. *Top*: Partial absorbance curves $A_z(\tilde{\nu})$ and $A_y(\tilde{\nu})$ for quinizarin (**Q**) aligned in stretched polyethylene, corresponding to long- and short-axis polarized absorption (full and dashed line). The LD absorbance curves were measured with synchrotron radiation, except for the region below 28,000 cm^{-1} where a conventional light source was used. *Bottom*: Theoretically predicted transitions (Table 1).

3. Calculations

Quantum chemical calculations on **Q**, **C**, and **A** were performed with the GAUSSIAN 03 software package [15] using B3LYP density

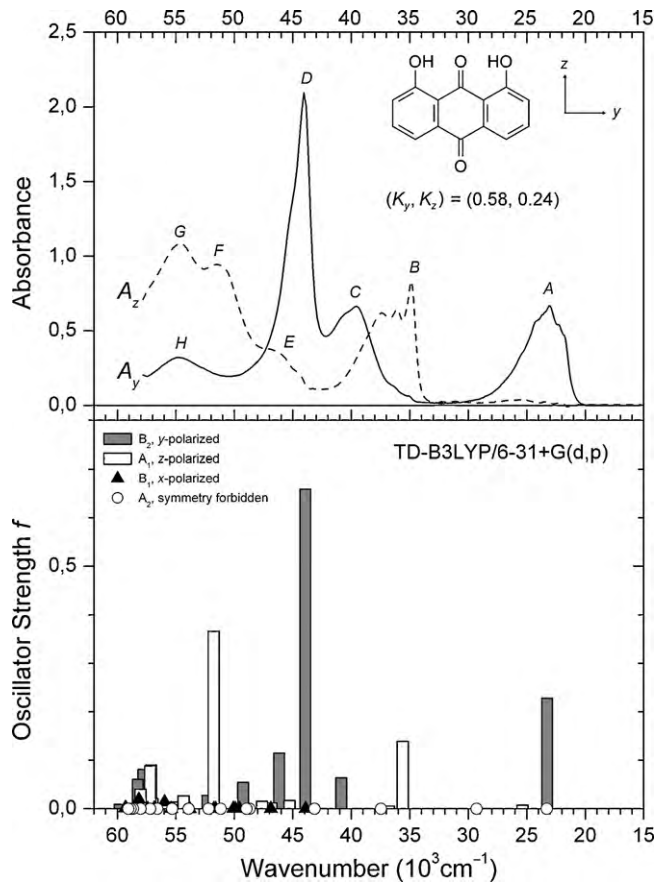

Fig. 3. *Top*: Partial absorbance curves $A_y(\tilde{\nu})$ and $A_z(\tilde{\nu})$ for chrysazin (**C**) aligned in stretched polyethylene, corresponding to long- and short-axis polarized absorption (full and dashed line). The LD absorbance curves were measured with synchrotron radiation, except for the region below 32,000 cm^{-1} where a conventional light source was used. *Bottom*: Theoretically predicted transitions (Table 2).

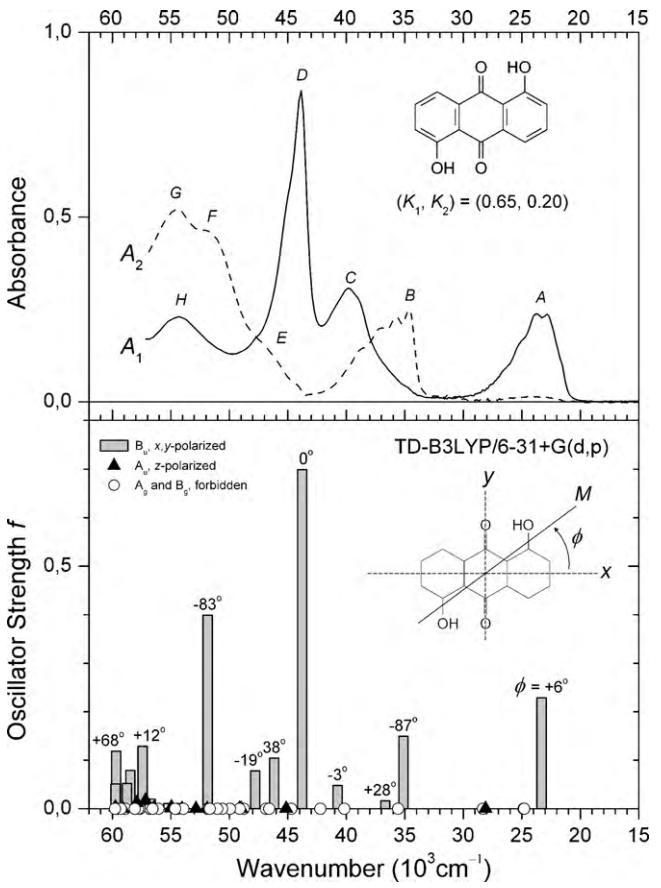

Fig. 4. *Top*: Partial absorbance curves $A_1(\tilde{\nu})$ and $A_2(\tilde{\nu})$ for anthrarufin (**A**) indicating predominantly long- and short-axis polarized absorption (full and dashed line), see text. *Bottom*: Theoretically predicted transitions with indication of computed in-plane transition moment angles ϕ (Table 3).

functional theory [16]. Ground state molecular equilibrium geometries, characterized by strong intramolecular hydrogen bonding, were calculated with the 6-31G(d,p) basis set [15]. The resulting nuclear coordinates are provided in S6–S8. Vertical transitions to the 60 lowest excited singlet electronic states were computed with the TD-B3LYP procedure [17] and the 6-31+G(d,p) basis set [15]. Complete listings of all calculated transitions are given in S9–S11, together with graphs of the four highest occupied π orbitals and the four lowest unoccupied π* orbitals. Selected transitions are contained in Tables 1–3.

To elucidate the possible contribution from other, less stable molecular configurations to the observed spectra, similar calculations were performed for a number of intramolecularly hydrogen-bonded tautomeric forms of **Q**, **C**, and **A**. Results for 9,10-dihydroxy-1,4-anthraquinone and 4,9-dihydroxy-1,10-anthraquinone tautomers of **Q** are provided as S12 and S13. Attempts to locate a minimum corresponding to the 8,9-dihydroxy-1,10-anthraquinone tautomer of **C** failed, and we also failed to locate minima corresponding to 9,10-dihydroxy-1,5-anthraquinone and 5,9-dihydroxy-1,10-anthraquinone tautomers of **A**. In addition, calculations were performed for hydroxy-rotamers of **Q**, **C**, and **A** (S14–S16).

4. Linear dichroism: orientation factors and partial absorbance curves

The directional information that can be extracted from the curves $E_U(\tilde{\nu})$ and $E_V(\tilde{\nu})$ is provided by the orientation factors K_i for the molecular transition moments of the observed transitions [3]:

$$K_i = \left\langle \cos^2(\boldsymbol{M}_i, U) \right\rangle \tag{1}$$

Here $(\boldsymbol{M}_i, U)$ is the angle between the transition moment vector $\boldsymbol{M}_i$ of the ith transition and the uniaxial stretching direction U of the polymer sample. The pointed brackets indicate averaging over all molecules in the light path. A large orientation factor K_i thus indicates efficient alignment of the molecular transition moment vector $\boldsymbol{M}_i$ with the sample axis U, and vice versa. The K_i values were determined by the graphical "trial-and-error" (TEM) procedure [3] which involves formation of linear combinations of $E_U(\tilde{\nu})$ and $E_V(\tilde{\nu})$, for example the family of reduced absorbance curves $r_K(\tilde{\nu})$ [5]:

$$r_K(\tilde{\nu}) = (1 - K)E_U(\tilde{\nu}) - 2KE_V(\tilde{\nu}) \tag{2}$$

A spectral feature due to transition i (a peak or a shoulder) will vanish from the linear combination $r_K(\tilde{\nu})$ for $K = K_i$, and the value of K_i can thus be determined by visual inspection [5]. As an example, the observed absorbance curves $E_U(\tilde{\nu})$ and $E_V(\tilde{\nu})$ and reduced absorbance curves $r_K(\tilde{\nu})$ are shown for **A** in Fig. 1.

In a spectral region where only transitions corresponding to two different K_i values, say K_1 and K_2, contribute to the observed absorption, it is possible to derive the partial absorbance curves $A_1(\tilde{\nu})$ and $A_2(\tilde{\nu})$ [3,5]:

$$\begin{aligned} A_1(\tilde{\nu}) &= (K_1 - K_2)^{-1} r_{K_2}(\tilde{\nu}) \\ A_2(\tilde{\nu}) &= (K_2 - K_1)^{-1} r_{K_1}(\tilde{\nu}) \end{aligned} \tag{3}$$

In case of **Q** and **C** with molecular C_{2v} symmetry, the moment vectors for optically allowed transitions are restricted to three possible

Table 1
Observed and predicted electronic transitions for quinizarin (**Q**).

	MeOH[a]		Stretched PE[b]			TD-B3LYP[c]			
	$\tilde{\nu}$[d]	Log ε	$\tilde{\nu}$[d,e]	A[e]	K[f]	Term	$\tilde{\nu}$[d]	f[g]	Leading configurations[h]
A	20.9	3.9	20.4	0.51	0.60	$2\,^1A_1$	21.4	0.18	77% (1,−1)
						$1\,^1B_1$	25.1	$<10^{-4}$	94% (2,−1)
						$1\,^1A_2$	28.1	0	90% (6,−1)
						$1\,^1B_2$	28.5	7×10^{-4}	88% (3,−1)
B	30.8	3.4	30.6	0.12	0.60	$3\,^1A_1$	30.4	0.05	88% (4,−1)
						$2\,^1B_2$	30.8	3×10^{-3}	85% (1,−2)
C	35.9	4.0	35.5	0.68	0.30	$3\,^1B_2$	35.3	0.15	80% (5,−1)
						$4\,^1A_1$	36.8	9×10^{-3}	90% (1,−3)
						$2\,^1A_2$	38.2	0	93% (2,−2)
						$4\,^1B_2$	40.4	6×10^{-3}	80% (7,−1), 13% (1,−4)
						$2\,^1B_1$	41.2	1×10^{-4}	94% (6,−2)
D	40.2	4.5	39.8	1.42	0.60	$5\,^1A_1$	41.6	0.45	75% (3,−2), 16% (4,−3)
						$5\,^1B_2$	42.5	3×10^{-3}	83% (4,−2)
E	44.6	4.4	42.9	0.73	0.6	$6\,^1A_1$	44.5	0.10	79% (5,−2)
F			45.0	0.37	0.3	$6\,^1B_2$	44.2	0.05	73% (1,−4)
						$3\,^1B_1$	44.9	2×10^{-4}	97% (2,−3)
G			47.8	0.74	0.6	$7\,^1A_1$	48.7	0.39	58% (4,−3), 18% (3,−4)
H[i]			(52)	(0.7)	(0.3)	$7\,^1B_2$	50.0	0.10	65% (3,−3)
						$10\,^1B_2$	54.6	0.02	84% (1,−12)
						$10\,^1A_1$	55.1	0.01	69% (3,−4)
						$11\,^1A_1$	55.5	0.02	54% (13,−1), 36% (5,−4)
I			54.3	0.29	0.6	$12\,^1A_1$	57.2	0.19	48% (5,−4), 34% (13,−1)
J			55.6	0.98	0.3	$13\,^1B_2$	56.8	0.55	33% (1,−11), 26% (4,−4), 13% (7,−3)
						$14\,^1B_2$	57.9	0.13	81% (7,−3)
						$12\,^1B_1$	58.2	0.01	67% (3,−6)
						$13\,^1A_1$	58.8	0.10	51% (5,−5), 28% (2,−8)
						$16\,^1B_2$	60.1	0.04	90% (1,−16)
						$15\,^1B_1$	60.3	0.01	30% (6,−5), 23% (4,−8), 18% (3,−7)

[a] Absorbance peaks measured in methanol solution (see Supplementary data).
[b] Absorbance peaks measured in stretched polyethylene.
[c] In the region above 45,000 cm^{-1}, only transitions with $f \geq 0.01$ are listed (see Supplementary data for full listing of all 60 calculated transitions).
[d] Wavenumber in 10^3 cm^{-1}.
[e] Peak wavenumber and absorbance from the partial absorbance curves in Fig. 2.
[f] Orientation factor, see text.
[g] Oscillator strength.
[h] The notation (i,−j) indicates an excited singlet configuration derived from the ground configuration by promotion of an electron from the ith highest occupied to the jth lowest unoccupied MO.
[i] Shoulder.

directions indicated by the symmetry axes *x*, *y*, and *z*, corresponding to transitions to excited states of B_1, B_2, and A_1 symmetry. We should thus observe only three different orientation factors, K_x, K_y, and K_z. We shall assume that the spectral intensity in the near-UV–VIS regions is dominated by π–π* transitions and thus is polarized in the molecular *y*,*z*-plane. Provided the orientation factors K_y and K_z can be determined from the observed spectra, Eq. (3) can thus be used to construct the partial absorbance curves $A_y(\tilde{\nu})$ and $A_z(\tilde{\nu})$ corresponding to in-plane polarized transitions to states of B_2 and A_1 symmetry. The observed orientation factors are 0.60 and 0.30 for **Q** and 0.58 and 0.24 for **C**, consistent with previously published values [4,5]. In general, organic compounds are aligned in stretched polyethylene according to their molecular shape [3]. With the present designation of symmetry axes (Figs. 2 and 3), we thus have $K_z > K_y$ for **Q** and $K_y > K_z$ for **C**, leading to the assignments $(K_y, K_z) = (0.30, 0.60)$ for **Q** and $(K_y, K_z) = (0.58, 0.24)$ for **C**. The resulting partial absorbance curves $A_y(\tilde{\nu})$ and $A_z(\tilde{\nu})$ for **Q** and **C** are shown in Figs. 2 and 3.

The situation is much less favorable for **A** with C_{2h} molecular symmetry which allows infinite possible moment directions for in-plane polarized transitions. While determination of the orientation factors K_i is reasonably straightforward (Fig. 1), it is much more difficult to derive the moment directions within the molecular framework of **A**. For transitions polarized in the molecular *x*,*y*-plane (Scheme 1, Fig. 4), the task consists in determination of the angles ϕ_i formed by the moments of the observed transitions *i* with a specific, well-defined axis in the plane. Traditionally [3] this axis is chosen as the molecular axis *x* corresponding to the largest value of the average cosine squared, $\langle \cos^2(x, U) \rangle = K_x$. The in-plane axis *y* that is perpendicular to *x* corresponds to the lowest average cosine squared among directions in the plane, $\langle \cos^2(y, U) \rangle = K_y$. For an in-plane polarized transition *i* it can be shown that the following relationship holds [3]:

$$|\phi_i| = \tan^{-1}\sqrt{\frac{K_x - K_i}{K_i - K_y}} \quad (4)$$

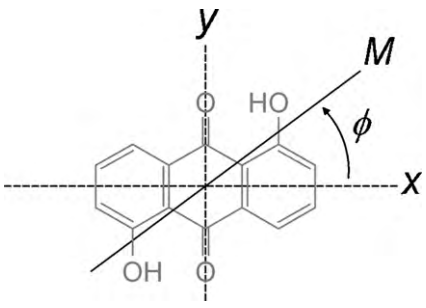

Scheme 1.

Table 2
Observed and predicted electronic transitions for chrysazin (**C**).

	MeOH [a]		Stretched PE [b]			TD-B3LYP[c]			
	$\tilde{\nu}$[d]	Log ε	$\tilde{\nu}$[d,e]	A[e]	K[f]	Term	$\tilde{\nu}$[d]	f[g]	Leading configurations[h]
A	23.4	4.0	23.1	0.67	0.58	$1\,^1B_2$	23.3	0.23	85% (1,−1)
						$1\,^1A_2$	23.3	0	92% (3,−1)
						$2\,^1A_1$	25.4	7×10^{-3}	85% (2,−1)
						$2\,^1B_2$	28.4	$<10^{-4}$	92% (4,−1)
						$2\,^1A_2$	29.3	0	91% (6,−1)
B	35.3	4.1	34.8	0.83	0.24	$3\,^1A_1$	35.6	0.14	82% (5,−1)
						$3\,^1B_2$	35.7	7×10^{-3}	88% (1,−2)
						$4\,^1A_1$	36.8	6×10^{-3}	89% (2,−2)
						$3\,^1A_2$	37.5	0	92% (3,−2)
						$5\,^1A_1$	40.2	$<10^{-4}$	81% (1,−3), 10% (5,−2)
C	39.6	4.3	39.5	0.66	0.58	$4\,^1B_2$	40.9	0.06	58% (2,−3), 37% (4,−2)
						$4\,^1A_2$	43.1	0	93% (6,−2)
						$1\,^1B_1$	43.9	2×10^{-4}	97% (3,−3)
D	44.6	4.7	44.1	2.10	0.58	$5\,^1B_2$	43.9	0.66	47% (4,−2), 33% (2,−3)
						$6\,^1B_2$	46.2	0.11	70% (8,−1), 20% (2,−4)
E[i]			47	0.4	0.2	$6\,^1A_1$	45.3	0.02	68% (7,−1), 15% (5,−2)
						$7\,^1A_1$	46.8	0.01	61% (5,−2)
						$8\,^1A_1$	47.6	0.02	49% (1,−4), 25% (4,−3), 13% (7,−1)
						$7\,^1B_2$	49.3	0.05	61% (2,−4), 17% (5,−3), 14% (8,−1)
F			51.5	0.94	0.2	$9\,^1A_1$	51.8	0.37	50% (4,−3), 19% (1,−4), 10% (2,−8)
G[j]			54.6	1.08	–				
						$8\,^1B_2$	52.3	0.03	73% (5,−3), 10% (2,−4)
						$10\,^1A_1$	54.3	0.03	70% (4,−4)
						$10\,^1B_2$	55.1	0.01	87% (3,−5)
						$10\,^1B_1$	56.0	0.01	51% (1,−10), 40% (2,−9)
						$11\,^1A_1$	57.0	0.02	45% (7,−2), 39% (13,−1)
						$12\,^1A_1$	57.2	0.09	42% (13,−1), 21% (2,−8), 18% (7,−2)
H[j]			54.6	0.32	–	$11\,^1B_2$	57.1	0.09	58% (5,−4), 11% (1,−11), 10% (1,−8)
						$13\,^1B_2$	57.8	0.08	83% (3,−7)
						$14\,^1A_1$	58.0	0.04	37% (2,−8), 16% (7,−2), 13% (2,−12)
						$13\,^1B_1$	58.2	0.02	72% (4,−6), 20% (5,−5)
						$14\,^1B_2$	58.3	0.06	51% (1,−12), 27% (1,−11)

[a] Absorbance peaks measured in methanol solution (see Supplementary data).
[b] Absorbance peaks measured in stretched polyethylene.
[c] In the region above 45,000 cm^{-1}, only transitions with $f \geq 0.01$ are listed (see Supplementary data for full listing of all 60 calculated transitions).
[d] Wavenumber in 10^3 cm^{-1}.
[e] Peak wavenumber and absorbance from the partial absorbance curves in Fig. 3.
[f] Orientation factor, see text.
[g] Oscillator strength.
[h] The notation $(i,-j)$ indicates an excited singlet configuration derived from the ground configuration by promotion of an electron from the ith highest occupied to the jth lowest unoccupied MO.
[i] Shoulder.
[j] Due to coinciding wavenumbers, the individual orientation factors of the peaks *G* and *H* could not be determined by the TEM procedure.

Provided the orientation factors K_x and K_y for the in-plane axes x and y can be derived, the numerical values of the transition moment angles ϕ_i can thus be determined from the observed K_i values. We tentatively define x as the axis parallel to the long-axis of the parent anthraquinone framework, and y as the in-plane axis perpendicular to x, see Scheme 1.

As indicated in Fig. 1, the individual orientation factors K_i observed for **A** fall in two distinct groups with values close to 0.65 and 0.20 (at least in the region below 55,000 cm^{-1}). The features *A*, *C*, and *D* have values close to 0.65, while the values for *B* and *F* are close to 0.20. It is thus possible to construct the pair of partial absorbance curves $A_1(\tilde{\nu})$ and $A_2(\tilde{\nu})$ shown in Fig. 4, corresponding to contributions with $K_1 = 0.65$ and $K_2 = 0.20$ (Eq. (3)). Moreover, we shall assign the values $K_1 = 0.65$ and $K_2 = 0.20$ to the orientation factors of the axes x and y defined in Scheme 1. This implies that $A_1(\tilde{\nu})$ and $A_2(\tilde{\nu})$ indicate absorbance with moment angles $|\phi_i|$ close to 0° and 90° (Eq. (4)), corresponding to predominantly long- and short-axis polarized absorption, respectively. This assignment is consistent with the calculated transition moment directions (see below), and with the long-axis polarization of the color band of **A** (i.e., band *A*) revealed by single crystal spectroscopy [18].

5. Electronic transitions

5.1. Assignment to calculated transitions

Analysis of the observed LD spectra of **Q** and **C** is greatly facilitated by the molecular C_{2v} symmetry of these compounds. Figs. 2 and 3 show the partial absorbance curves $A_y(\tilde{\nu})$ and $A_z(\tilde{\nu})$ for **Q** and **C**, indicating absorbance polarized along the molecular in-plane symmetry axes y and z. The observed spectral features are listed in Tables 1 and 2 together with calculated electronic transitions. The predicted transitions are generally in good agreement with the main features of the observed spectra, particularly in the case of **Q**. The long-axis polarized peaks *A*, *B*, *D*, *E*, *G*, and *I* at 20,400, 30,600, 39,800, 42,900, 47,800, and 54,300 cm^{-1} in the spectrum

Table 3
Observed and predicted electronic transitions for anthrarufin (**A**).

	MeOH [a]		Stretched PE [b]				TD-B3LYP[c]				
	$\tilde{\nu}$[d]	Log ε	$\tilde{\nu}$[d,e]	A[e]	K[f]	$\lvert\phi\rvert$[g]	Term	$\tilde{\nu}$[d]	f[h]	ϕ[g]	Leading configurations [i]
A	23.8	4.0	23.8	0.24	0.65	~0°	$1\,^1B_u$	23.3	0.23	+6°	85% (1,−1)
							$1\,^1B_g$	24.8	0	–	94% (3,−1)
							$2\,^1A_g$	24.8	0	–	83% (2,−1)
							$1\,^1A_u$	28.1	1×10^{-4}	*z*	91% (6,−1)
							$3\,^1A_g$	28.3	0	–	90% (4,−1)
B	35.1	4.1	34.6	0.25	0.20	~90°	$2\,^1B_u$	35.1	0.15	+93°	81% (5,−1)
							$4\,^1A_g$	35.6	0	–	88% (1,−2)
							$3\,^1B_u$	36.7	0.02	+28°	90% (2,−2)
							$2\,^1A_u$	38.9	$<10^{-4}$	*z*	93% (3,−2)
							$5\,^1A_g$	40.2	0	–	81% (1,−3), 11% (5,−2)
C	39.6	4.3	39.8	0.31	0.6	~0°	$4\,^1B_u$	40.7	0.05	−3°	63% (2,−3), 31% (4,−2)
							$2\,^1B_g$	42.2	0	–	92% (6,−2)
D	44.4	4.6	43.9	0.84	0.65	~0°	$5\,^1B_u$	43.8	0.70	0°	54% (4,−2), 28% (2,−3)
							$6\,^1A_g$	44.7	0	–	67% (7,−1), 18% (5,−2)
E[j]			46	0.1	–	–	$6\,^1B_u$	46.2	0.10	+38°	61% (8,−1), 25% (1,−4)
							$7\,^1B_u$	47.8	0.08	−19°	41% (1,−4), 25% (4,−3), 24% (8,−1)
F[j]			52	0.46	0.2	~90°	$8\,^1B_u$	51.9	0.40	−83°	51% (4,−3), 20% (1,−4)
G			54.3	0.52	–	–					
							$9\,^1B_u$	55.2	0.01	+3°	56% (1,−9), 40% (5,−4)
							$10\,^1B_u$	56.7	0.02	−6°	56% (13,−1), 19% (5,−4), 14% (1,−9)
							$11\,^1A_u$	57.2	0.02	*z*	66% (1,−10), 16% (2,−8)
H			54.3	0.23	–	–	$11\,^1B_u$	57.4	0.13	+12°	40% (7,−2), 21% (13,−1), 20% (5,−4), 13% (1,−9)
							$12\,^1A_u$	57.9	0.01	*z*	69% (4,−6), 20% (5,−5)
							$12\,^1B_u$	58.5	0.08	−1°	23% (2,−12), 20% (7,−2), 18% (3,−6)
							$13\,^1B_u$	58.8	0.05	−49°	49% (3,−6), 14% (2,−12), 14% (2,−11)
							$14\,^1B_u$	59.7	0.12	+68°	34% (6,−5), 22% (3,−8), 10% (2,−11)
							$15\,^1B_u$	59.7	0.05	−38°	22% (7,−2), 20% (2,−12), 19% (3,−6)

[a] Absorbance peaks measured in methanol solution (see Supplementary data).
[b] Absorbance peaks measured in stretched polyethylene.
[c] In the region above 45,000 cm^{-1}, only transitions with $f \geq 0.01$ are listed (see Supplementary data for full listing of all 60 calculated transitions).
[d] Wavenumber in 10^3 cm^{-1}.
[e] Peak wavenumber and absorbance from the partial absorbance curves in Fig. 4.
[f] Orientation factor, see text.
[g] In-plane transition moment angle ϕ, see Scheme 1 (*z* designates out-of-plane polarization).
[h] Oscillator strength.
[i] The notation (*i*,−*j*) indicates an excited singlet configuration derived from the ground configuration by promotion of an electron from the *i*th highest occupied to the *j*th lowest unoccupied MO.
[j] Shoulder.

of **Q** are thus easily assigned to the $^1A_1$ states predicted at 21,400, 30,400, 41,600, 44,500, 48,700, and 57,200 cm^{-1}, and the short-axis polarized features *C*, *F*, *H*, and *J* at 35,500, 45,000, 52,000 and 55,600 cm^{-1} can be assigned to the $^1B_2$ states predicted at 35,300, 44,200, 50,000 and 56,800 cm^{-1}.

In the case of **C**, the long-axis polarized peaks *A*, *C*, *D*, and *H* at 23,100, 39,500, 44,100, and 54,600 cm^{-1} can be assigned to the $^1B_2$ states calculated at 23,300, 40,900, 43,900, and 57,100 cm^{-1}. The prominent short-axis polarized band *B* at 34,800 cm^{-1} can safely be assigned to the $^1A_1$ state predicted at 35,600 cm^{-1}, and the shoulder *E* around 47,000 cm^{-1} may correspond to one or more of the optically weak $^1A_1$ states predicted in this region. The absorbance in the region above 50,000 cm^{-1} is characterized by strong short-axis polarized intensity, in qualitative agreement with the calculated spectrum for **C**. Only one strongly allowed $^1A_1$ state is predicted, $9\,^1A_1$ at 51,800 cm^{-1}, but two intense short-axis polarized maxima are observed, namely *F* and *G* at 51,500 and 54,600 cm^{-1}. The observed band profile may be affected by vibronic contributions, which are not accounted for by the theoretical model. Also, more than 45 electronic transitions are predicted for these compounds in the region between 45,000 and 60,000 cm^{-1} (S9–S11) and the observed absorption is most likely due to overlapping contributions from several electronic states, such as $9\,^1A_1$, $10\,^1A_1$, $11\,^1A_1$, and $12\,^1A_1$ in the case of **C**. Finally, the standard TD-DFT procedure is expected to be less accurate in this region [11,17].

The observed spectral features of **A** are listed in Table 3 together with calculated transitions. As discussed above, **A** has C_{2h} molecular symmetry, which means that in-plane transition moment directions are not restricted by symmetry. However, the partial absorbance curves $A_1(\tilde{\nu})$ and $A_2(\tilde{\nu})$ shown in Fig. 4 are strikingly similar to the curves $A_y(\tilde{\nu})$ and $A_z(\tilde{\nu})$ obtained for **C** (Fig. 3). Hence, there seems to be a very close correspondence between wavenumbers, intensities, and polarization directions for the transitions of **A** and **C**. This correspondence is supported by the calculated results (Tables 2 and 3). In spite of different substitution patterns and point group symmetries, the main transitions predicted for **A** and **C** are essentially similar. The bands observed for **A** may thus be assigned in analogy with those of **C**. The peaks *A*, *C*, *D*, and *H* at 23,800, 39,800, 43,900, and 54,300 cm^{-1} in the partial absorbance curve $A_1(\tilde{\nu})$ are easily assigned to the essentially long-axis polarized transitions predicted at 23,300, 40,700, 43,800, and 57,400 cm^{-1}, and the prominent peak *B* at 34,600 cm^{-1} in the partial absorbance curve $A_2(\tilde{\nu})$ can be assigned to the essentially short-axis polarized transition predicted at 35,100 cm^{-1}. The high-energy region is dominated by strong short-axis polarized intensity, in qualitative agreement with the computed spectrum, but assignment of the individual features to the several electronic transitions predicted is not straightforward. Again, this is very similar to the case of **C**.

As discussed above, the spectrum of **Q** deviates from those of **C** and **A**, which in turn are quite similar. According to the results

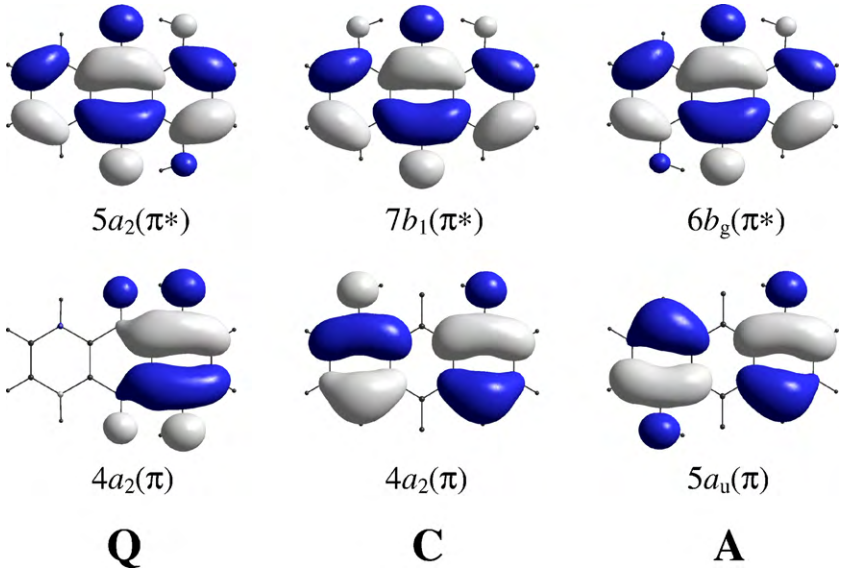

Fig. 5. Diagrams of the highest occupied and lowest unoccupied molecular orbitals (HOMO and LUMO) for quinizarin (**Q**), chrysazin (**C**), and anthrarufin (**A**). In the tables, these orbitals are referred to as (1) and (−1), respectively. More orbital diagrams are provided as Supplementary data.

of the theoretical model, the deviating spectrum of **Q** is due primarily to a marked polarization of the $4a_2(\pi)$ and $3a_2(\pi)$ MOs of this compound, labeled (1) and (4) in Table 1. The $4a_2(\pi)$ HOMO of **Q** is predominantly localized in the benzene ring carrying the two hydroxy substituents, see Fig. 5. This leads to a destabilization of this orbital by 0.45 eV (3600 cm^{-1}) relative to the HOMOs of **C** and **A**, and to a corresponding reduction in energy of the HOMO–LUMO configuration (1,−1), consistent with the observed red shift of the color band (*A*) of **Q**. In contrast to the HOMOs of **C** and **A** (Fig. 5), the HOMO of **Q** has significant amplitude on the carbonyl groups, which means that the HOMO–LUMO transition of **Q** has less hydroxy-to-carbonyl charge transfer character. This may explain why **Q** has lesser tendency to undergo excited state intramolecular proton transfer (ESIPT) than **C** and **A** [19]. The $3a_2(\pi)$ MO of **Q** is polarized in the opposite sense of the $4a_2(\pi)$ HOMO, with localization in the other benzene ring. Amplitude diagrams of this and other orbitals are provided as Supplementary data (S9–S11).

5.2. Possible contributions from tautomers and rotamers

As discussed in the preceding section, the observed spectra are well described by the results of TD-B3LYP calculations for the molecular configurations corresponding to 1,4-dihydroxy-9,10-anthraquinone (**Q**), 1,8-dihydroxy-9,10-anthraquinone (**C**), and 1,5-dihydroxy-9,10-anthraquinone (**A**). However, in a series of publications, Fain et al. have recently argued that the color bands of **Q**, **C**, and **A** and several related compounds must be interpreted in terms of overlapping contributions from a number of tautomeric and rotameric structures (Ref. [20] and literature cited therein). Our present results do not support this interpretation. In the case of **Q**, the tautomeric structures 9,10-dihydroxy-1,4-anthraquinone and 4,9-dihydroxy-1,10-anthraquinone are predicted to give rise to first transitions close to 20,000 cm^{-1} (S12 and S13) which is slightly below the wavenumber 21,400 cm^{-1} predicted for **Q**. They might thus contribute to the complicated profile of the observed color band *A* (Fig. 2). But both tautomers are predicted by our calculations to be about 25 kJ/mol higher in energy than the 1,4-dihydroxy-9,10-anthraquinone structure (i.e., **Q**). According to this result, the 1,4- and 1,10-anthraquinone tautomers should not play any significant role at room temperature. In the case of **C** and **A**, we did not succeed in locating any potential energy minima corresponding to tautomeric structures. We thus failed to locate a minimum corresponding to the 8,9-dihydroxy-1,10-anthraquinone tautomer of **C** (similar to the case of the related compound emodin [8]), and we also failed to locate minima corresponding to 9,10-dihydroxy-1,5-anthraquinone and 5,9-dihydroxy-1,10-anthraquinone tautomers of **A**. The geometry optimizations led to recovery of the stable 9,10-anthraquinone structure, suggesting that these tautomers do not correspond to stable compounds. Rotameric structures involving rotation of one hydroxy group by 180°, thereby breaking an intramolecular hydrogen bond, are predicted by our calculations (S14–S16) to be more than 50 kJ/mol higher in energy than the corresponding hydrogen-bonded structures. It is thus highly unlikely that these conformations should play any significant role at room temperature, particularly not in a non-polar and aprotic solvent like LDPE where stabilization due to intermolecular hydrogen bonding is absent. Moreover, the obvious similarity of the spectra observed in liquid methanol (S1) and in LDPE (Figs. 2–4) suggests that even in the protic solvent, intermolecular hydrogen bonding does not lead to substantial contributions from rotameric structures.

6. Concluding remarks

The present study of quinizarin (**Q**), chrysazin (**C**), and anthrarufin (**A**) provides polarization data for transitions in the spectral region from ca. 15,000 to ca. 58,000 cm^{-1}, thereby extending the previously investigated UV region by about 11,000 cm^{-1}. The observed intensity in the high-wavenumber region is dominated by strong short-axis polarized absorbance peaking around 55,000 cm^{-1}. Throughout the investigated spectral range, the spectral details of **A** and **C** are strikingly similar, while those of **Q** deviate. This situation is well reproduced by the TD-B3LYP results which are in pleasing agreement with the observed spectra. The high density of states in the region above 50,000 cm^{-1} complicates detailed assignments of the observed overlapping band profiles to individual electronic transitions, but the theoretical predictions are consistent with the observed predominance of short-axis polarized intensity. In the region below 50,000 cm^{-1} there is near-perfect agreement between observed and calculated wavenumbers, intensities, and polarization directions. The results of the present analysis do not support the recent assignments of the absorption spectra of **Q**, **C**, and **A** to significant, overlapping contributions from several tautomeric and rotameric forms [20].

Acknowledgements

This work was supported by a grant of beam time on the UV1 and CD1 beamlines at ISA. The stay of Nguyen Duc Duy at Roskilde University was enabled by a PhD scholarship granted by the Vietnamese Ministry of Education and Training. Additional support was provided by an ENRECA grant. We are indepted to Eva M. Karlsen and Fritz Duus for technical and administrative assistance.

Appendix A. Supplementary data

Supplementary data associated with this article can be found, in the online version, at doi:10.1016/j.saa.2010.05.023.

References

[1] H. Zollinger, Color Chemistry: Syntheses, Properties and Applications of Organic Dyes and Pigments, third ed., Verlag Helvetica Chimica Acta AG/Wiley-VCH, Zürich/Weinheim, 2003.
[2] K. Krohn (Ed.), Anthracycline Chemistry and Biology, Top. Curr. Chem. 282 & 283 (2008).
[3] J. Michl, E.W. Thulstrup, Spectroscopy with Polarized Light. Solute Alignment by Photoselection, in Liquid Crystals, Polymers, and Membranes, VCH-Wiley, Deerfield Beach, FL, 1986 (paperback edition 1995).
[4] B.O. Myrvold, J. Spanget-Larsen, E.W. Thulstrup, Chem. Phys. 104 (1986) 305.
[5] F. Madsen, I. Terpager, K. Olskær, J. Spanget-Larsen, Chem. Phys. 165 (1992) 351.
[6] S.H. Jensen, Master's Thesis, Roskilde University, 2003 (in Danish).
[7] K.B. Andersen, E. Chen, A. Hansen, D.C. Hansen, M.B. Hutters, J. Spanget-Larsen, Acta Chem. Scand. 47 (1993) 419;
K.B. Andersen, J. Spanget-Larsen, Spectrochim. Acta A 53 (1997) 2615;
S. Møller, K.B. Andersen, J. Spanget-Larsen, J. Waluk, Chem. Phys. Lett. 291 (1998) 51.
[8] S.C. Nguyen, B.K.V. Hansen, S.V. Hoffmann, J. Spanget-Larsen, Chem. Phys. 352 (2008) 167.
[9] S. Eden, P. Limão-Vieira, S.V. Hoffmann, N.J. Mason, Chem. Phys. 323 (2006) 313.
[10] A.J. Miles, S.V. Hoffmann, Y. Tao, R.W. Janes, B.A. Wallace, Spectroscopy 21 (2007) 245;
A.J. Miles, R.W. Janes, A. Brown, D.T. Clarke, J.C. Sutherland, Y. Tao, B.A. Wallace, S.V. Hoffmann, J. Synchrotron Radiat. 15 (2008) 420.
[11] S. Grimme, in: K.B. Lipkowitz, R. Larter, T.R. Cundari (Eds.), Reviews in Computational Chemistry, vol. 20, Wiley-VCH, Weinheim, 2008, pp. 153–217.
[12] D. Jaquemin, X. Assfeld, J. Preat, E.A. Perpéte, Mol. Phys. 105 (2007) 325;
D. Jaquemin, E.A. Perpéte, I. Ciofini, I.C. Adao, Acc. Chem. Res. 42 (2009) 326.
[13] J. Fabian, Dyes Pigments 84 (2010) 36.
[14] L.A. Bigelow, H.H. Reynolds, Org. Synth., coll. vol. 1 (1958) 476.
[15] M.J. Frisch, G.W. Trucks, H.B. Schlegel, G.E. Scuseria, M.A. Robb, J.R. Cheeseman, J.A. Montgomery Jr., T. Vreven, K.N. Kudin, J.C. Burant, J.M. Millam, S.S. Iyengar, J. Tomasi, V. Barone, B. Mennucci, M. Cossi, G. Scalmani, N. Rega, G.A. Petersson, H. Nakatsuji, M. Hada, M. Ehara, K. Toyota, R. Fukuda, J. Hasegawa, M. Ishida, T. Nakajima, Y. Honda, O. Kitao, H. Nakai, M. Klene, X. Li, J.E. Knox, H.P. Hratchian, J.B. Cross, V. Bakken, C. Adamo, J. Jaramillo, R. Gomperts, R.E. Stratmann, O. Yazyev, A.J. Austin, R. Cammi, C. Pomelli, J.W. Ochterski, P.Y. Ayala, K. Morokuma, G.A. Voth, P. Salvador, J.J. Dannenberg, V.G. Zakrzewski, S. Dapprich, A.D. Daniels, M.C. Strain, O. Farkas, D.K. Malick, A.D. Rabuck, K. Raghavachari, J.B. Foresman, J.V. Ortiz, Q. Cui, A.G. Baboul, S. Clifford, J. Cioslowski, B.B. Stefanov, G. Liu, A. Liashenko, P. Piskorz, I. Komaromi, R.L. Martin, D.J. Fox, T. Keith, M.A. Al-Laham, C.Y. Peng, A. Nanayakkara, M. Challacombe, P.M.W. Gill, B. Johnson, W. Chen, M.W. Wong, C. Gonzalez, J.A. Pople, GAUSSIAN 03, Revision C.02, Gaussian, Inc., Wallingford, CT, 2004.
[16] A.D. Becke, J. Chem. Phys. 97 (1992) 9173, 98 (1993) 5648;
C. Lee, W. Yang, R.G. Parr, Phys. Rev. B 37 (1988) 785.
[17] R. Bauernschmitt, R. Ahlrichs, Chem. Phys. Lett. 256 (1996) 454;
M.E. Casida, C. Jamorski, K.C. Casida, D.R. Salahub, J. Chem. Phys. 108 (1998) 4439;
R.E. Stratmann, G.E. Scuseria, M.J. Frisch, J. Chem. Phys. 109 (1998) 8218;
M. Stener, G. Fronzoni, D. Toffoli, P. Decleva, Chem. Phys. 282 (2002) 337;
J.E. Monat, J.H. Rodriguez, J.K. McCusker, J. Phys. Chem. A 106 (2002) 7399;
M.A.L. Marques, C.A. Ullrich, F. Nogueira, A. Rubio, K. Burke, E.K.U. Gross (Eds.), Time-Dependent Density Functional Theory, Lecture Notes in Physics, vol. 706, Springer, Berlin, Heidelberg, NY, 2006.
[18] N. Namsrai, T. Yoshinari, H. Itoh, S.-I. Nagasaka, Y. Kuriyama, M. Sakamoto, Y. Takahashi, J. Phys. Soc. Jpn. 75 (2006) 044703.
[19] M.P. Marzocchi, A.R. Mantini, M. Casu, G. Smulevich, J. Chem. Phys. 108 (1998) 534.
[20] V.Y. Fain, B.E. Zaitsev, M.A. Ryabov, Russ. J. Org. Chem. 41 (2005) 707.

Accepted for publication in *J. Mol. Spectr.*
Friday, 27 august 2010

Electronic transitions of fluorene, dibenzofuran, carbazole, and dibenzothiophene. From the onset of absorption to the ionization threshold

Duy Duc Nguyen,[a] John Trunk,[b] Lina Nakhimovsky,[c,*] Jens Spanget-Larsen[a,*]

[a] Department of Science, Systems and Models, Roskilde University, DK-4000 Roskilde, Denmark

[b] Biology Department, Brookhaven National Laboratory, Upton, NY 11973, USA

[c] Chemistry Department, Stony Brook University, Stony Brook, NY 11794, USA

ABSTRACT

A comparative study of the electronic transitions of fluorene and its hetero-analogues dibenzofuran, carbazole, and dibenzothiophene was performed in a wide energy range. Gas phase, crystal phase, and linear dichroism electronic transmittance spectra were measured with synchrotron radiation. Electronic transitions to excited singlet states were predicted with time-dependent density functional theory, TD-B3LYP/6-31+G(d,p). Based on the experimental and theoretical results, symmetry assignments of electronic transitions in the vacuum and near-UV region are suggested. The correspondence between excited states in these molecules, similarities, and differences between their electronic spectra are discussed.

Keywords:
Electronic transitions; Synchrotron radiation; Gas phase spectroscopy; Crystal Spectroscopy; Linear dichroism (LD); Polarization directions; Time-dependent density functional theory (TD-DFT)

---

* Corresponding authors.
Lina Nakhimovsky: Tel. 860-321-7485, *E-mail address*: linanakh@yahoo.com
Jens Spanget-Larsen: Tel. +45 4674 2710; *E-mail address*: spanget@ruc.dk

1. Introduction

The electronic properties of fluorene and its hetero-analogues dibenzofuran, carbazole, and dibenzothiophene are of renewed interest for understanding the photo-conductive, photo-refractive, electro-luminescence, and other important properties of macromolecules and polymers, containing these molecules as moieties. Many possibilities for applications of the latter are reported in the literature [1-7]. In addition, molecules with carbazole moieties such as rebeccamicin and its derivatives are being extensively studied as anticancer drugs [8,9]. Dibenzofuran is of interest from the environmental point of view as a parent representative of polychlorinated dibenzofurans of which 2,3,7,8-tetrachloro-dibenzofuran is particularly harmful [10]. The gas phase electronic spectra of fluorene and its hetero-analogues could be of interest in astrophysics, since polycyclic aromatic hydrocarbons, are very common in space and, as a result, they can act as probes of conditions in distant regions [11,12]. Information on higher electronic states of the molecules studied could serve as useful input for calculations of crystal field effects on optical properties of the solid state of the corresponding compounds, as well as for calculations of electronic excited states of polymers and macromolecules with these molecules as moieties.

In this communication, we report the results of a spectroscopic investigation of the electronic transitions of the four title compounds. Gas phase spectra are recorded with synchrotron radiation from the onset of absorption to about 80000 cm^{-1} which is well beyond the ionization limit. The assignment of the observed transitions is supported by the results of synchrotron radiation spectroscopy on thin crystalline flakes and of synchrotron radiation linear dichroism (SRLD) spectroscopy of molecular samples aligned in stretched polyethylene. The assignment is furthermore supported by the results of theoretical calculations by using time-dependent density functional theory (TD-DFT).

2. Experimental

Samples of fluorene (Supelco #48568; Aldrich +98%), dibenzofuran (OEKANAL analytical standard; Aldrich +99%,), carbazole (VETRANAL analytical standard; Ega-Chemie 98-99%), and dibenzothiophene (OEKANAL analytical standard; Aldrich +99%) were obtained from commercial sources as indicated. The spectroscopic purity of the compounds was checked by comparison of their UV-VIS absorption spectra with literature data.

2.1. Gas phase spectra

For measuring gas phase transmittance spectra, powder of the compound studied was placed in a 10 cm path stainless steel cell sealed with CaF_2 windows. The baseline for the vapour spectra was measured at room temperature with the cell under vacuum. No absorption peaks of the compound studied were detected at room temperature. The cell with its content was then heated with heat tape wrapped around the cell. To monitor the temperature of the vapour a thermocouple was attached to the cell. The temperatures sufficient to obtain the vapour spectra in the whole energy range were 125 °C for carbazole, 95 °C for dibenzothiophene, and 80 °C for the other two compounds. The sample chamber was ca. 2 cm longer than the vapour cell, and was filled with argon gas.

2.2. Crystal spectra

Crystals of fluorene, carbazole and dibenzofuran, thin flakes ca. 1.5 mm wide and 0.2-0.5 μ thick, were grown by sublimation in nitrogen atmosphere. The vapour and crystal spectra were recorded at the National Synchrotron Light Source at Brookhaven National Laboratory. Synchrotron radiation is delivered to the sample position using a Modified Wadsworth Monochromator. The photomultiplier tube has a magnesium fluoride window which allows detection of wavelengths down to about 120 nm. The signal from the PMT is converted to voltage using a Transimpedance Amplifier made by Oriel Corporation. A Windows PC running Visual Basic interacts with our Lock-In Amplifier, and samples the high voltage and synchrotron ring signals, which are then plotted as a quantity related to optical density as the monochromator scans through the wavelength region of interest. These data for the sample and the corresponding baseline allow calculation of the optical density of the sample as a function of wavelength.

2.3. Linear dichroism spectroscopy

2.3.1. Sample preparation

Partially aligned molecular samples for LD spectroscopy were produced by using uniaxially stretched low-density polyethylene (LDPE) as an anisotropic solvent [13]. The samples were prepared from 100μm sheet pure LDPE material (Hinnum Plast, DK-4760 Vordingborg). Fluorene, dibenzofuran, and dibenzothiophene were introduced into the LDPE by submersion of the polymer into concentrated solutions of the compounds in chloroform (Merck Uvasol) at 50 °C for 1 day. The chloroform solvent was subsequently evaporated from the polymer. The carbazole sample was produced by sublimation of the compound into

the polymer for 1 day in a sealed container at 50 °C. Residual crystals on the surfaces of the samples were finally removed with ethanol (Merck Uvasol), and the samples were uniaxially stretched by ca. 500%. Corresponding samples without solutes were produced for use as references.

2.3.2. Polarization spectra

Two linearly independent LD absorbance curves were measured at room temperature on the uniaxially stretched polymer samples, one with the electric vector of the sample beam parallel to the stretching direction (*U*), and one with the electric vector perpendicular to it (*V*). In both cases the sample beam was perpendicular to the surface of the PE sheet. The resulting baseline-corrected absorbance curves are denoted by $E_U(\tilde{\nu})$ and $E_V(\tilde{\nu})$. The SRLD spectra were recorded at the UV1 [14] and CD1 [15,16] beamlines on the ASTRID storage ring at the Institute for Storage Ring Facilities (ISA), Aarhus University, Denmark. The radiation exits the beamline through a CaF_2 window into a nitrogen purged purpose built chamber holding the sample. The light was polarized with a MgF_2 Rochon polarizer, passed through the sample and detected with a UV sensitive Photo Multiplier Tube (PMT model 9402B, Electron Tubes, UK). The two beamlines provide a much higher photon flux deep into the UV spectral range as compared to conventional sources [14-16]. This yields an improved signal to noise ratio, and we were able to investigate our PE samples up to about 58000 cm^{-1}. This amounts to an extension by about 11000 cm^{-1} (1.4 eV) relative to the range available with conventional technology, such as a deuterium lamp with prism polarizers [17,18].

The LD spectra were evaluated according to the TEM stepwise reduction procedure [13,19]. The orientation factors (K_y, K_z) [13] determined for the four compounds were for fluorene (0.55, 0.30), dibenzofuran (0.60, 0.30), carbazole (0.63, 0.20), and dibenzothiophene (0.55, 0.25), consistent with previous results [20-23]. The partial absorbance curves [13] corresponding to short- and long-axis polarized transitions to excited states of B_2 and A_1 symmetry, respectively, are shown in Figs. 1 – 4. In the case of dibenzofuran, carbazole, and dibenzothiophene, the A_1 absorbance curve shows a “wiggle” at 250, 285, and 285 nm, respectively, due to incomplete reduction of a strong, sharp peak in the B_2 curve. This is a well-known artifact of the reduction procedure and its physical origin is well understood [13,24].

3. Calculations

Accurate theoretical prediction of electronic transitions is a difficult task. In particular, prediction of transitions in the far-UV region, approaching and above the ionization limit, is extremely demanding in terms of theoretical know-how and computational effort (see, e.g., Ref. [25]). Calculations at a theoretical level suitable for a proper description of transitions in the high-energy region are outside the scope of this investigation. Rather, we have applied standard time-dependent density functional theory (TD-DFT) which is expected to yield useful results for transitions in the near-UV region [26-28]. The calculations were performed with the GAUSSIAN 03 software package [29] by using the B3LYP functional [30,31]. Ground state molecular equilibrium geometries were calculated with the 6-31G(d,p) basis set [29]. The resulting nuclear coordinates are provided as Supplementary data. Vertical transitions to the 150 lowest excited singlet electronic states were computed with the TD-B3LYP procedure [27-29] and the 6-31+G(d,p) basis set [29]. Calculation of radical cation energies with UB3LYP/6-31+G(d,p) lead to prediction of the vertical ionization energies 7.71, 8.14, 7.42, and 7.75 eV for fluorene, dibenzofuran, carbazole, and dibenzothiophene, respectively. This is in fair agreement with the values measured by photoelectron spectroscopy: 7.91, 8.09, 7.60, and 7.93 eV [32].

The calculated electronic transitions are visualized in Figs. 1 – 4. Only transitions with energies below the predicted ionization treshold are shown. In the high-energy region, the high density of states complicates the representation; for the sake of reference, full listings with indication of orbital parentage and other details are provided as Supplementary data.

4. Results and discussion

Following the work by Bree and Zwarich [33], we used the transmittance spectra of thin crystals of fluorene, dibenzofuran and carbazole to assign A_1 electronic transitions in the crystal spectra of the three compounds. As previously discussed [33,36], only A_1 symmetry transitions can be detected in the transmittance spectra of these crystals at normal incidence of light on the *ab* crystal face (containing the short and intermediate crystallographic axes). The correspondence between the electronic transitions of A_1 symmetry in the SRLD spectra, and the respective crystal spectra (measured with electric field vector in the *ab* plane of the crystals) can be seen in Figs. 1 – 3. Comparison of crystal spectra with the SRLD spectra of the same compounds show that assignments of all A_1 transitions in the crystals of these compounds is consistent with the assignments of these transitions by the SRLD polarization spectra (up to about 58000 cm^{-1}), as well as with the results of previous investigations [20-

23,34,35]. We then used this observation to aid in experimental assignments of gas phase A_1 symmetry electronic transitions, especially in the higher energy region which is inaccessible by our SRLD method due to polymer absorption. The B_2 symmetry transitions of all four compounds were assigned from the SRLD spectra.

4.1. Fluorene

The two lowest experimentally detected A_1 transitions in the fluorene crystal spectra (at 280 nm and at around 220 nm) were assigned previously from studies of polarised crystal transmittance and reflectance spectra [33,36]. We have obtained spectra of two polymorphs of the fluorene crystal with the electric field vector of incident light in the ab face of the crystal (Fig. 1, c and d). The lowest A_1 symmetry transition in the crystal spectrum is close in energy for both polymorphs and in agreement with previous results [33,36]. In the spectrum of polymorph I the A_1 transitions can be assigned at 280 nm, 227 nm, 197 nm, 166 nm, and at around 145 nm (Fig. 1, c). The polymorph II is grown from melt between LiF plates under uniaxial pressure in the direction perpendicular to the plates (Figure 1, d). The crystals are sufficiently thin to avoid saturation effects and to determine the maximum of the highest energy A_1 symmetry band (at 130 nm) in the region studied. In this polymorph the two transitions in the region between 190 nm and 240 nm form a single band with a maximum at around 220 nm. Based on results of this work and literature data, the following symmetry assignments of electronic transitions in the fluorene gas phase can be proposed.

A_1 symmetry. As mentioned above, in the crystal spectra there are two A_1 symmetry transitions in the range between 190 and 240 nm. In the *SRLD* spectra in the corresponding energy region there are two closely located bands of this symmetry, therefore we assign these two bands (207 nm and 212 nm) to two separate electronic transitions (Fig. 1, b). Correspondingly, the five A_1 symmetry transitions in the fluorene *gas phase* spectrum can be assigned to bands at 266 nm (37600 cm^{-1}), 202 nm (49500 cm^{-1}), 197 nm (50800 cm^{-1}), 162 nm (61700 cm^{-1}) and ~130 nm (76900 cm^{-1}) (Fig. 1, a). The assignment of the A_1 transition at 162 nm is in agreement with the assignment obtained from polarized fluorescence excitation spectra of fluorene in an argon matrix [37]. The theoretically predicted A_1 symmetry transitions closest to those detected experimentally in the gas phase are - at 257 nm (266 in the gas phase), a group of weak transitions between 215 nm and 192 nm may correspond to the two closely spaced experimental peaks at 202 nm and 197 nm; the one predicted at 170 nm seem to correlate with the experimental band at 162 nm, and the one around 140 nm - with the experimental band at around 125 nm, although the predicted

intensity of the latter is much smaller than the experimentally observed in the corresponding energy region (Fig. 1, top and a).

B_2 symmetry. The B_2 symmetry electronic transitions of fluorene assigned from SRLD spectra are at 302 nm, 267 nm, 223 nm, and ~205 nm in agreement with the assignments suggested by Gleiter and coworkers [20]. The B_2 symmetry shoulders at 278 nm and 273 nm may be a result of vibronic borrowing by the lowest A_1 transition from the second B_2 transition. In the gas phase, B_2 symmetry electronic transitions can be assigned at 296 nm (33800 cm^{-1}), 255 nm (39200 cm^{-1}), 212 nm (47200 cm^{-1}), and ~195 nm (51300 cm^{-1}). According to SRLD spectra there is a weak B_2 transition at around 228 nm. This band is not detectable in the vapor spectrum but it is present in the pentane solution spectrum at 225 nm (spectrum not shown).

In fluorene the theoretically predicted energies of lowest B_2 and A_1 symmetry transitions are at higher energy than the experimentally observed. For all other major transitions there is satisfactory agreement between experimental and theoretical results. According to theoretical predictions there could also be weak B_2 transitions overlapped by the A_1 transitions at 162 nm and 130 nm.

4.2. Dibenzofuran

The transmittance crystal spectrum with electric field vector in the *ab* crystallographic plane closely resembles that in the SRLD spectrum polarized perpendicular to the direction of the polymer stretching (Figure 2, b and c). Theoretical calculation of electronic states in the near-UV region using TD-DFT [21,38] and CASPT2 [38] theory has been reported previously.

A_1 symmetry. Five A_1 symmetry transitions can be assigned in the crystal spectrum of dibenzofuran; they are at 304 nm, 222 nm, ~205 nm, 160 nm and ~ 130 nm. The first three of these transitions correspond to bands at 304 nm, 230 nm and 208 nm in the SRLD spectra. Based on the results of this work and literature data [21,34,35], A_1 symmetry transitions in the gas phase spectra can be assigned at 298 nm (33600 cm^{-1}), 222 nm (45000 cm^{-1}), ~200 nm (50000 cm^{-1}), 157 nm (63700 cm^{-1}), and possibly at 135 nm (74000 cm^{-1}). The theoretically predicted A_1 symmetry transitions, closest to the experimentally detected are at 278 nm, 228 nm, and 203 nm. The transition at 157 nm in the gas phase spectrum correlates with a group of predicted transitions with the strongest at 162 nm. The highest energy experimental band correlates with a group of weak transitions near 135 nm.

B_2 symmetry. The strong B_2 symmetry transitions of dibenzofuran in the SRLD spectra are observed at 288 nm, 251 nm, 220 nm, and 210 nm. The band at around 297 nm can been assigned to a vibronic component of the lowest A_1 transition due to coupling with the lowest B_2 state [21,39-41]. The assignments of three low energy B_2 transitions are similar to previous assignments [21,34,35]. The fourth transition (at 210 nm), to our knowledge, has not been previously assigned. Assuming that the sequence of transitions in the gas phase is the same as in the SRLD spectra, the B_2 transitions in the gas phase are at 282 nm (35400 cm^{-1}), 243 nm (41400 cm^{-1}), 210 nm (47600 cm^{-1}), and ~205 nm (48780 cm^{-1}). The assignment of the latter two features to individual electronic transitions is necessarily tentative. The theoretical calculation predicts B_2 transitions at 271 nm, 237 nm, 223 nm, 210 nm, and 186 nm, but comparison with the observed features is not straightforward. It should be mentioned that the predicted relative intensities of the lowest few B_2 transitions are very sensitive to the choice of calculational procedure [21,35,36,38]. The CASSCF/CASPT2 calculations performed by Ljubic and Sabljic [38] seem to lead to better agreement with the experimental spectrum than the present TD-DFT results.

4.3 Carbazole

Assignments of electronic transitions of carbazole in the near-UV region are similar to those of previous investigations [22,34]. In the vacuum-UV region the symmetry assignments generally correspond to the symmetry assignments in the polarized vacuum ultraviolet fluorescence excitation spectrum of carbazole embedded in an argon matrix [37]. On the basis of previous results [22,34,37] and the crystal and SRLD spectra of this work, the following assignments of bands can be proposed in the gas phase spectrum of carbazole.

A_1 symmetry. Comparison of our gas phase spectrum with the excitation fluorescence spectrum of carbazole in solid argon matrix [37] shows that the strongest broad band between 180 and 150 nm in the former spectrum corresponds to several electronic transitions, A_1 symmetry dominating. Strong transitions of this symmetry were assigned in work [37] at 174 nm (57500 cm^{-1}), and 162 nm (61700 cm^{-1}). Based on this data the following transitions in the gas phase spectrum of carbazole can be assigned as A_1 symmetry - 327 nm (30600 cm^{-1}), 237 nm (42200 cm^{-1}), 218 nm (45900 cm^{-1}) 174 nm (57500 cm^{-1}), and 162 nm (61700 cm^{-1}). These assignments are in agreement with our crystal spectra which show strong presence of transitions of A_1 symmetry in the vacuum UV energy region (Figure 3, c). The theoretical calculations also confirm dominance of A_1 symmetry transitions in the vacuum UV energy region of carbazole (Figure 3, top).

B_2 symmetry. Major transitions of this symmetry in the gas phase spectrum are at 284 nm (35200 cm^{-1}), 243 nm (41200 cm^{-1}), 225 nm (44400 cm^{-1}) and 204 nm (49000 cm^{-1}) and possibly around 178nm (56200. cm^{-1}), which in the argon matrix [36] was assigned at 185 nm.

It is interesting that the fluorescence excitation spectrum of carbazole in the argon matrix has a deep minimum at 166 nm, and no such feature is observed in the transmittance spectrum. This observation might indicate that near 166 nm there is a state which does not relax to the lowest excited state of the carbazole molecule, and thus is not a transition in the molecule of carbazole (possibly it belongs to an ionic species of carbazole).

The theoretically predicted B_2 symmetry transitions, corresponding to the experimentally assigned, are around 260 nm, 233 nm, 242 nm, 212 nm, and 183 nm respectively.

4.4. Dibenzothiophene

The assignments of transition in this molecule in the near-UV region agree with those previously suggested [23,34,35]. The SRLD spectra enabled the resolution of additional features of dibenzothiophene in stretched polymer film - at 213 nm and 200 nm (both B_2), and around 185 nm (A_1). Moreover, the SRLD data indicate the presence of an intense A_1 transition with onset around 180 nm. Based on these results, the following assignments of the main features of the gas phase spectrum can be proposed:

A_1 symmetry: 323 nm (31000 cm^{-1}), ca. 250 nm (40000 cm^{-1}), 224 nm (44600 cm^{-1}), 185 nm (54600 cm^{-1}), and 162 nm (61700 cm^{-1}).

B_2 symmetry: 282 nm (35500 cm^{-1}), 258 nm (38800 cm^{-1}), 229 nm (43700 cm^{-1}), and 200 nm (50000 cm^{-1}). As distinguished from the other molecules studied, one of the experimentally detected B_2 symmetry transitions in the spectrum of dibenzothiophene (229 nm) has a much higher intensity than the three other transitions of this symmetry.

The assignment of transitions of dibenzothiophene below 155 nm is ambiguous, since we cannot base assignments of A_1 symmetry transitions on comparison with experimental crystal spectra. Based on theoretical predictions, the experimental band at around 150 nm (66700 cm^{-1}) can possibly be assigned as B_2 symmetry and the band at around 135 nm (74000 cm^{-1}) as A_1 symmetry. The correlation between the theoretically predicted transitions and the experimentally detected is not quite satisfactory.

5. Concluding remarks

Experimental electronic spectra of fluorene, dibenzofuran, carbazole and dibenzothiophene were measured in gas and crystalline phases, and in stretched polymer sheets. Nine or ten (depending on the compound) major experimentally detected electronic bands were assigned by symmetry in the energy range studied. It is shown that B_2 symmetry transitions dominate in intensity in the near-UV region, while the strongest A_1 symmetry transitions are in the vacuum-UV.

The proposed correspondence between major transitions in the gas phase of the four structural analogues is shown in Figure 5. In several cases, particular in the high-energy region, the correlations are necessarily tentative. The A_1 symmetry transitions tend to shift to lower energies in the sequence fluorene, dibenzofuran, carbazole, and dibenzothiophene. This trend is probably an indication of the effectiveness of conjugation through the bridge containing the heteroatom (and of weak super-conjugation through the methylene bridge in fluorene).

The vertical transitions obtained with standard TD-DFT calculations did not lead to general agreement with the observed spectral features for this series of compounds. Failure to predict transitions in the high-energy region was expected, see Section 3. But even in the near-UV region where TD-DFT results are frequently very useful in the study of organic chromophores [26,28], the present results tend to be problematic. Part of the discrepancy is most likely due to the importance of excited state geometry rearrangements, leading to substantial differences between vertical and adiabatic transitions energies, as recently demonstrated by Ljubic and Sabljic [38]. Moreover, previous analyses [39-41] have demonstrated the importance of vibronic coupling phenomena, indicating partial breakdown of the Born-Oppenheimer approximation. Hence, more advanced theoretical procedures are called for.

Acknowledgements.

Gas phase and crystal spectroscopy were performed at the National Synchrotron Light Source which is supported by the Office of Biological and Enviromental Research and by the Office of Basic Energy of the U.S. Department of Energy, under Contract No. DE-AC02-98CH10886. The work in Denmark was supported by grants of beam time at the Institute for Storage Ring Facilities (ISA) at Aarhus University. The stay of Nguyen Duc Duy at Roskilde University was enabled by a PhD scholarship granted by the Vietnamese Ministry of Education and Training. Additional support was provided by an ENRECA grant. We wish to

thank Phil Johnson, John Sutherland, and Ivan Lubjic for useful discussions, and Søren Vrønning Hoffmann and Nykola C. Jones for technical assistance.

Supplementary data.

Supplementary data associated with this article can be found, in the online version, at …

References

1. S. Gunes, H. Neugebauer, N. S. Sariciftci, Chem. Rev. 107 (2007) 1324.
2. J. V. Grazulevicius, P. Strohriegl, J. Pielichowski, K. Pielichowski, Progress in Polymer Science 28 (2003) 1297.
3. I. I. Perepichka, I. F. Perepichka, M. R. Bryce and L.-O. Pålsson, Chem. Commun. (2005) 3397.
4. J.-F. Morin, M. Leclerc, I. Lévesque, and M. D'Iorio, Proceedings of Materials Research Society, 2001, MRS Spring Meeting, Symposium C.
5. J.-F. Morin, M. Leclerc, D. Adès, A. Siove, Macromolecular Rapid Communications 26 (2005) 761.
6. R. Qiu, L. Song, D. Zhang, Y. Mo, E. Brewer, and X. Huang, International Journal of Photoenergy (2008) Article ID 164702.
7. T. Qi, Y. Liu, W. Qiu, H. Zhang, X. Gao, Y. Liu, K. Lu, C. Du, G. Yu, and D. Zhu, Journal of Materials Chemistry 18 (2008) 1131.
8. J. Merchant, K. Tutsch, A. Dresen, R. Arzoomanian, D. Alberti, C. Feierabend, K. Binger, R. Marnoccha, J. Thomas, J. Cleary, G. Wilding, Clinical Cancer Research 8 (2002) 2193.
9. A. D. Ricart, L. A. Hammond, J. G. Kuhn, C. H. Takimoto, A. Goetz, B. Forouzesh, L. Forero, J. L. Ochoa-Bayona, K. Berg, A. W. Tolcher and E. K. Rowinsky, Clinical cancer research 11 (2005) 8728.
10. US Department of Health and Human Services, Agency for Toxic Substances and Disease Registry, Chlorodibenzofurans (1995).
11. M. Jura, C.J. Bohac, B. Sargent, W.J. Forrest, J. Green, D.M. Watson, G.C. Sloan, F. Markwick-Kemper, C.H. Chen, J. Najita, Astrophysical Journal, 637 (2006) L45.
12. D. Romanini, L. Biennier, F. Salama, A. Kachanov, L.J. Allamandola, F. Stoeckel, Chem. Phys. Letters 303 (1999) 165.
13. J. Michl, E. W. Thulstrup, Spectroscopy with polarized light. Solute alignment by photoselection, in liquid crystals, polymers and membranes, VCH Publishers, Deerfield Beach, FL, 1986 (paperback edition 1995).
14. S. Eden, P. Limão-Vieira, S.V. Hoffmann, N.J. Mason, Chem. Phys. 323 (2006) 313.
15. A.J. Miles, S.V. Hoffmann, Y. Tao, R.W. Janes, B.A. Wallace, Spectroscopy 21 (2007) 245.
16. A.J. Miles, R.W. Janes, A. Brown, D.T. Clarke, J.C. Sutherland, Y. Tao, B.A. Wallace, S.V. Hoffmann, J. Synchrotron Rad. 15 (2008) 420.
17. S.C. Nguyen, B.K.V. Hansen, S.V. Hoffmann, J. Spanget-Larsen, Chem. Phys. 352 (2008) 167.
18. D.D. Nguyen, N.C. Jones, S.V. Hoffmann, J. Spanget-Larsen, Spectrochim. Acta A 77 (2010) 279.
19. F. Madsen, I. Terpager, K. Olskær, J. Spanget-Larsen, Chem. Phys. 165 (1992) 351.
20. J. Spanget-Larsen, R. Gleiter, R. Haider, Helv. Chim. Acta 66 (1983) 1441.

21. J. Spanget-Larsen, D. Liang, E. Chen, E.W. Thulstrup, Asian Chem. Letters 4 (2000) 121.

22. E.W. Thulstrup, A. Brodersen, S.K. Rasmussen, Polycycl. Aromat. Compd. 9 (1996) 273.

23. J. Spanget.Larsen, E.W. Thulstrup, J. Mol. Struct. 661-662 (2003) 603.

24. J. Konwerska-Hrabowska, J. Mol. Struct. 45 (1978) 95.

25. Y. Kawashita, K. Yabana, M. Noda, K. Nobusada, T. Nakatsukasa, J. Mol. Struct. Theochem 914 (2009) 130.

26. M.E. Casida, C. Jamorski, K.C. Casida, D.R. Salahub, J. Chem. Phys. 108 (1998) 4439.

27. S. Grimme, in: K.B. Lipkowitz, R. Larter, T.R. Cundari (Eds.), Reviews in Computational Chemistry, Wiley-VCH, Weinheim, 2008, vol. 20, pp. 153-217.

28. J. Fabian, Dyes & Pigments 84 (2010) 36.

29. M.J. Frisch, G.W. Trucks, H.B. Schlegel, G.E. Scuseria, M.A. Robb, J.R. Cheeseman, J.A. Montgomery, Jr., T. Vreven, K.N. Kudin, J.C. Burant, J.M. Millam, S.S. Iyengar, J. Tomasi, V. Barone, B. Mennucci, M. Cossi, G. Scalmani, N. Rega, G.A. Petersson, H. Nakatsuji, M. Hada, M. Ehara, K. Toyota, R. Fukuda, J. Hasegawa, M. Ishida, T. Nakajima, Y. Honda, O. Kitao, H. Nakai, M. Klene, X. Li, J.E. Knox, H.P. Hratchian, J.B. Cross, V. Bakken, C. Adamo, J. Jaramillo, R. Gomperts, R.E. Stratmann, O. Yazyev, A.J. Austin, R. Cammi, C. Pomelli, J.W. Ochterski, P.Y. Ayala, K. Morokuma, G.A. Voth, P. Salvador, J.J. Dannenberg, V.G. Zakrzewski, S. Dapprich, A.D. Daniels, M.C. Strain, O. Farkas, D.K. Malick, A.D. Rabuck, K. Raghavachari, J.B. Foresman, J.V. Ortiz, Q. Cui, A.G. Baboul, S. Clifford, J. Cioslowski, B.B. Stefanov, G. Liu, A. Liashenko, P. Piskorz, I. Komaromi, R.L. Martin, D.J. Fox, T. Keith, M.A. Al-Laham, C.Y. Peng, A. Nanayakkara, M. Challacombe, P.M.W. Gill, B. Johnson, W. Chen, M.W. Wong, C. Gonzalez, J.A. Pople, GAUSSIAN 03, Revision C.02, Gaussian, Inc., Wallingford CT, 2004.

30. A.D. Becke, J. Chem. Phys. 97 (1992) 9173; 98 (1993) 5648.

31. C. Lee, W. Yang, R.G. Parr, Phys. Rev. B 37 (1988) 785.

32. B. Ruscic, B. Kovac, L. Klasinc, Z. Naturforsch. 33a (1978) 1006.

33. A. Bree, R. Zwarich, J. Chem. Phys. 51 (1969) 903.

34. K.R. Popov, L.V. Smirnov, V.L. Grebneva, L. Nakhimovsky, Opt. Spectrosk. 37 (1974) 1074.

35. N. Igarashi, A. Tajiri, M. Hatano, Bull. Chem. Soc. Jpn. 54 (1981) 1511.

36. M. Tanaka, Bull. Chem. Soc. Jpn. 49 (1976) 3382.

37. M.S. Gudipati, J. Daverkausen, M. Maus, G. Hohlneicher, Chem. Phys. 186 (1994) 289.

38. I. Ljubic, A. Sabljic, J. Phys. Chem. A 111 (2007) 1339.

39. A. Bree, A.R. Lacey, Knight, I.G. Ross, R. Zwarich, Chem. Phys. Lett. 26 (1974) 329.

40. D.J. Funk, R.C. Oldenburg, D.-P. Dayton, J.P. Lacosse, J.A. Draves, T.J. Logan, Applied Spectry. 49 (1995) 105.

41. V.L. Grebneva, K.R. Popov, L.V. Smirnov, R.N. Nurmukhametov, L.A. Nakhimovsky, Opt. Spektrosk. 33 (1972) 55.

42. D.C. Bressler, P.M. Fedorak, M.A. Pickard, Biotechnology Letters 22 (2000) 1119.

Figure captions

Fig. 1. Electronic spectra of fluorene: (top) Theoretical. (bottom) Experimental: a – gas phase spectrum, b -synchrotron radiation linear dichroism spectra, c –polymorph I crystal spectrum, *ab* crystallographic plane, d – polymorph II crystal spectrum, *ab* crystallographic plane.

Fig. 2. Electronic spectra of dibenzofuran: (top) Theoretical. (bottom) Experimental: a – gas phase spectrum, b – synchrotron radiation linear dichroism spectra, c – crystal spectrum, *ab* crystallographic plane.

Fig. 3. Electronic spectra of carbazole: (top) Theoretical. (bottom) Experimental: a – gas phase spectrum, b – synchrotron radiation linear dichroism spectra, c – crystal spectrum, *ab* crystallographic plane.

Fig. 4. Electronic spectra of dibenzothiophene: (top) Theoretical. (bottom) Experimental: a – gas phase spectrum, b –synchrotron radiation linear dichroism spectra.

Fig. 5. Diagram of energy levels for all four compounds (in cm^{-1}); transitions of A_1 symmetry are connected by dashed lines, those of B_2 symmetry by solid lines.

Figure 1

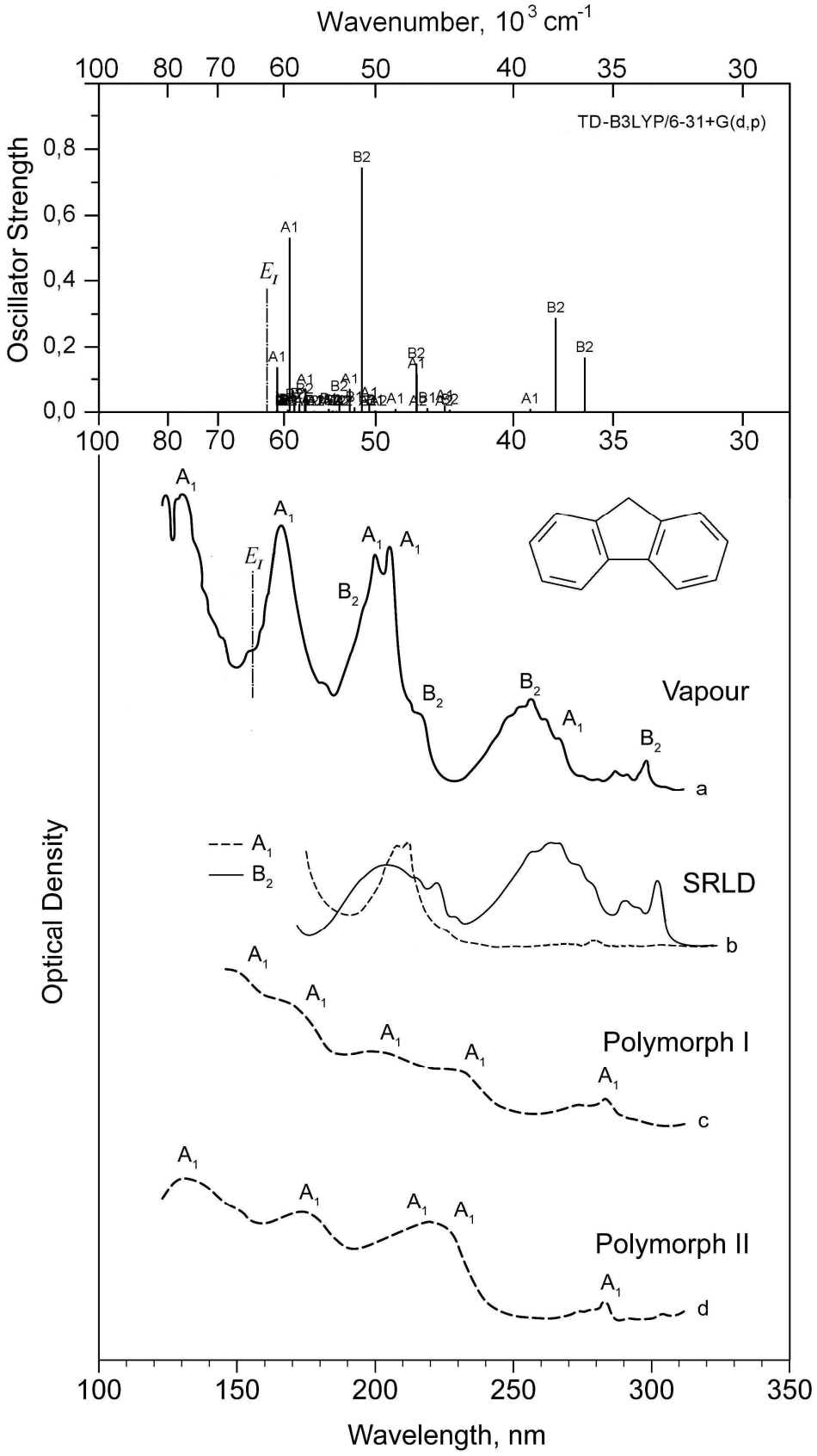
Wavenumber, 10^3 cm^-1
100 80 70 60 50 40 35 30
TD-B3LYP/6-31+G(d,p)
Oscillator Strength
0,0 0,2 0,4 0,6 0,8
B2
A1
E1
Optical Density
Vapour
SRLD
Polymorph I
Polymorph II
a
b
c
d
100 150 200 250 300 350
Wavelength, nm

Figure 2

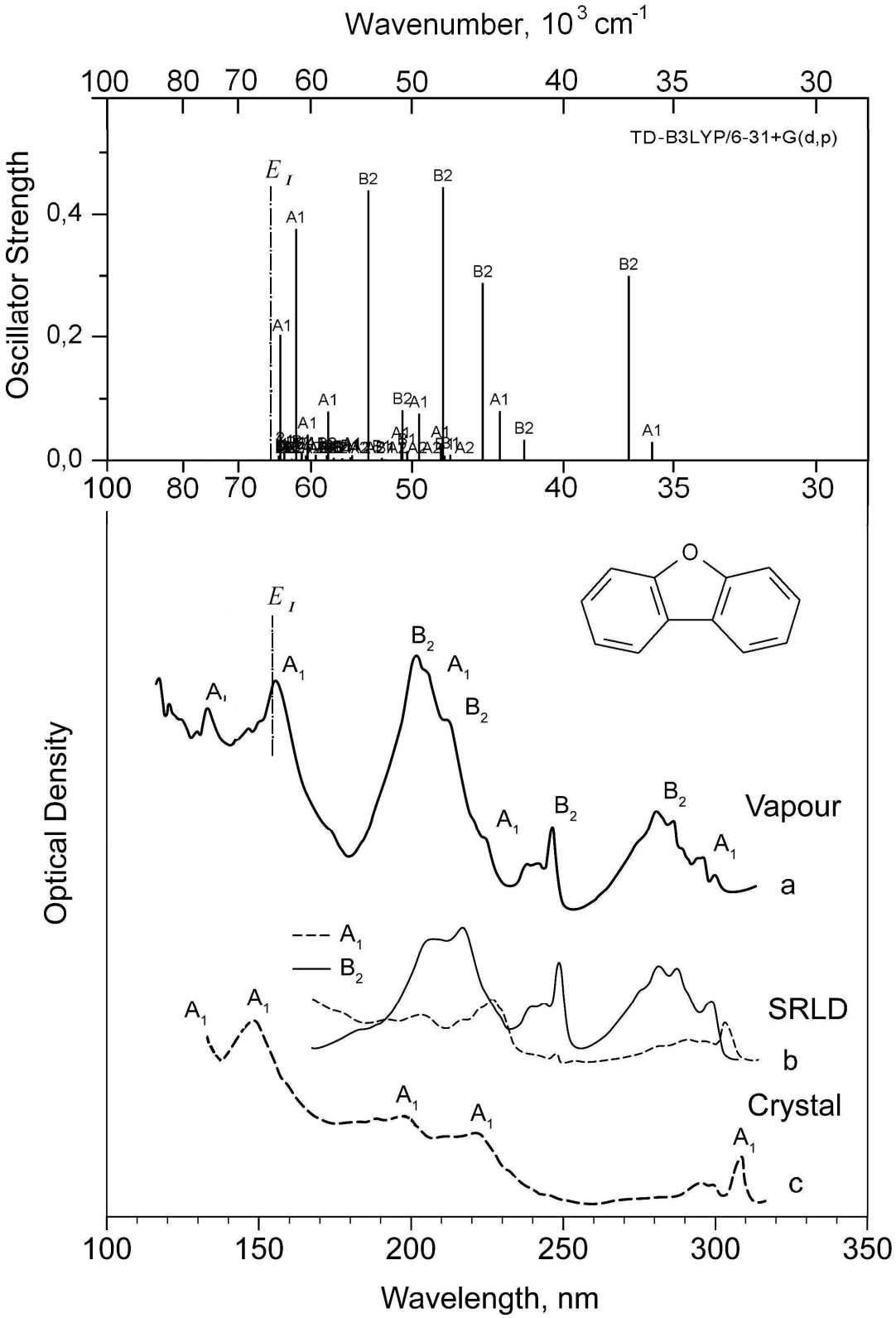
Wavenumber, 10 3 cm-1
100 80 70 60 50 40 35 30
TD-B3LYP/6-31+G(d,p)
Oscillator Strength
0,0
0,2
0,4
E I
B2
A1
Optical Density
Vapour
a
SRLD
b
Crystal
c
100 150 200 250 300 350
Wavelength, nm

Figure 3

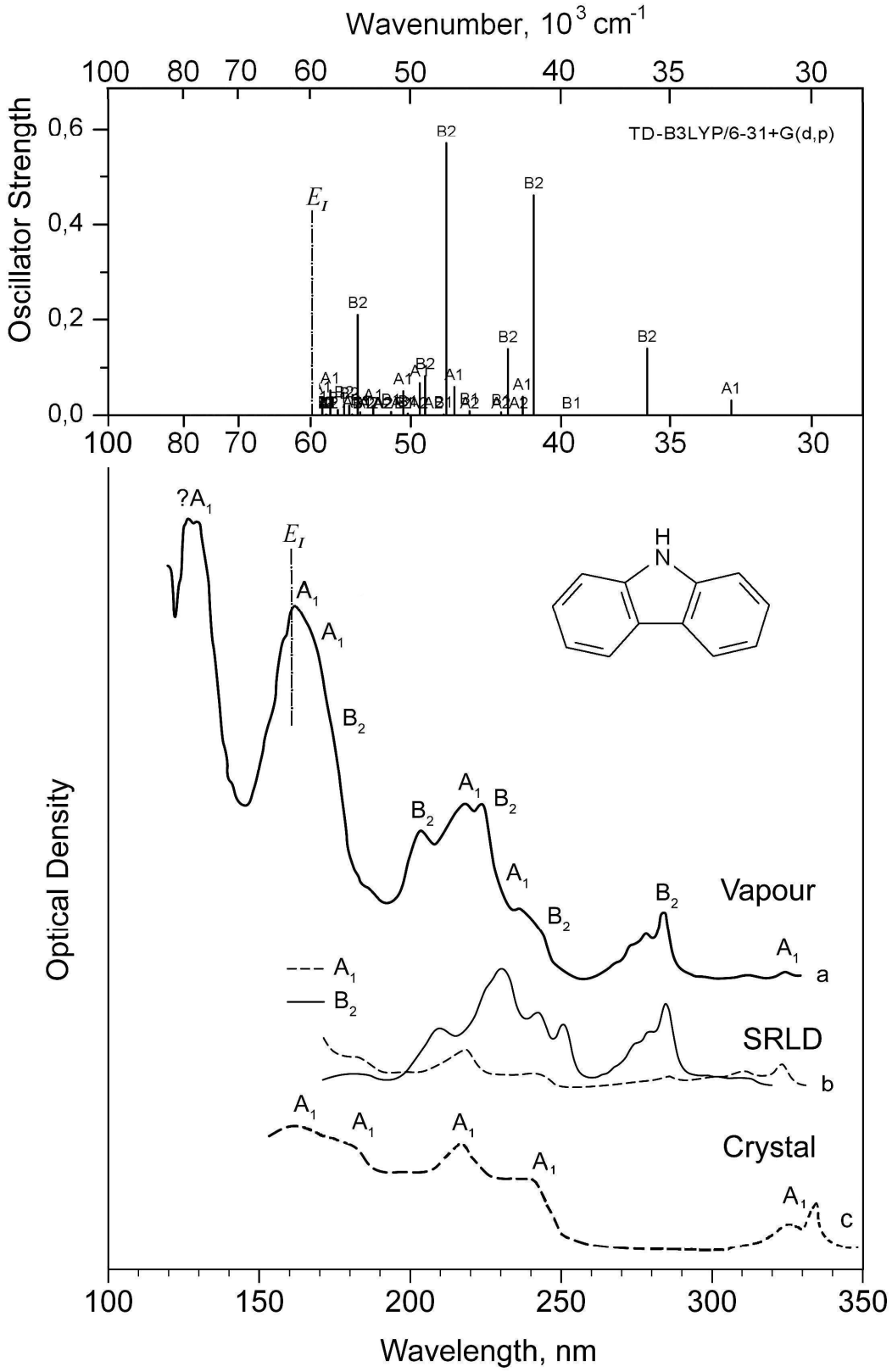
Wavenumber, 10^3 cm^-1
100 80 70 60 50 40 35 30
Oscillator Strength
0,6
0,4
0,2
0,0
TD-B3LYP/6-31+G(d,p)
E_I
B2
A1
B1
?A1
A1
B2
Optical Density
Vapour
a
SRLD
b
Crystal
c
100 150 200 250 300 350
Wavelength, nm

Figure 4

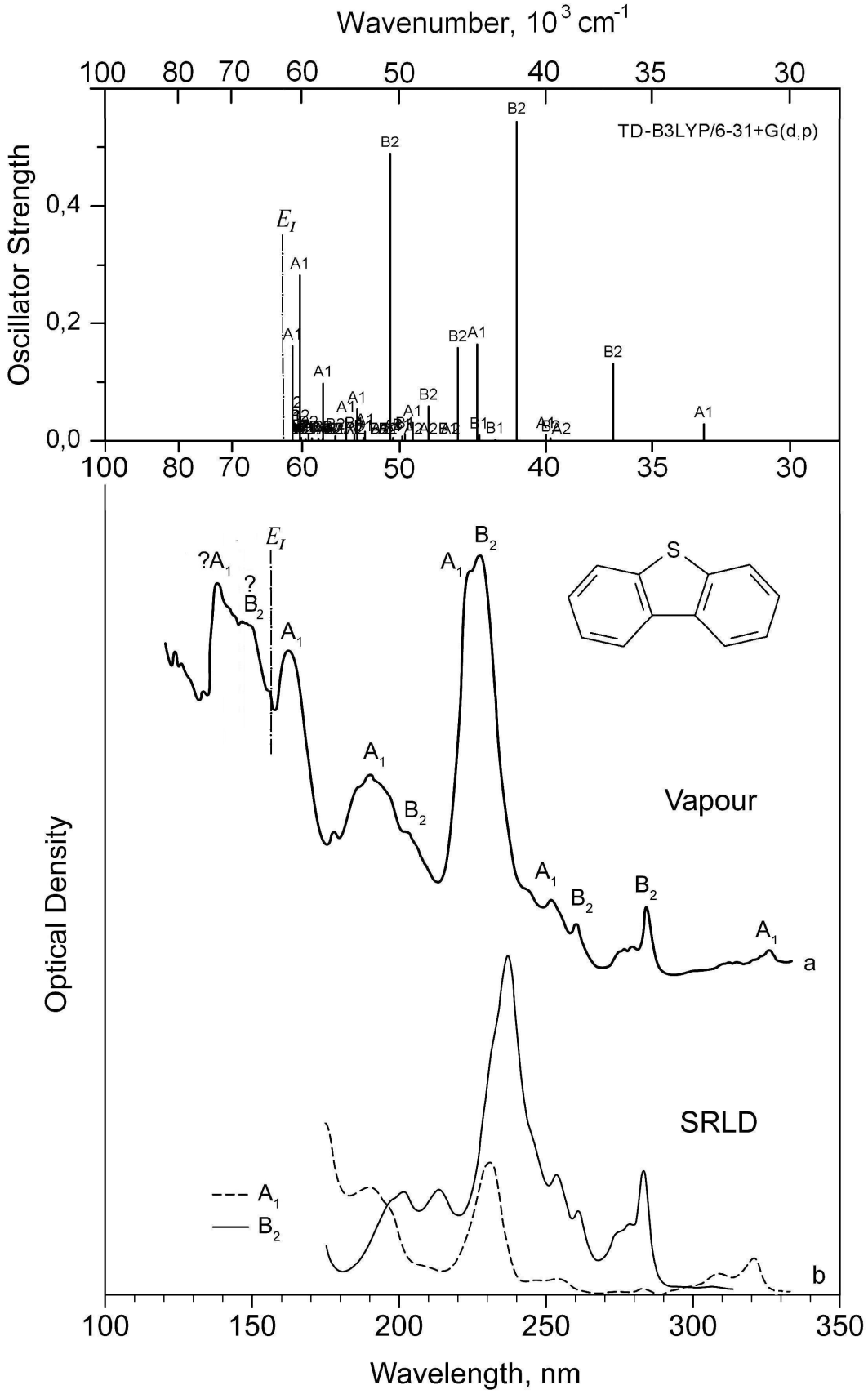
Wavenumber, 10 3 cm-1
100 80 70 60 50 40 35 30
TD-B3LYP/6-31+G(d,p)
Oscillator Strength
0,0
0,2
0,4
E_I
B2
A1
Optical Density
?A1
?
B2
A1
B2
Vapour
a
SRLD
A1
B2
b
100 150 200 250 300 350
Wavelength, nm

Figure 5

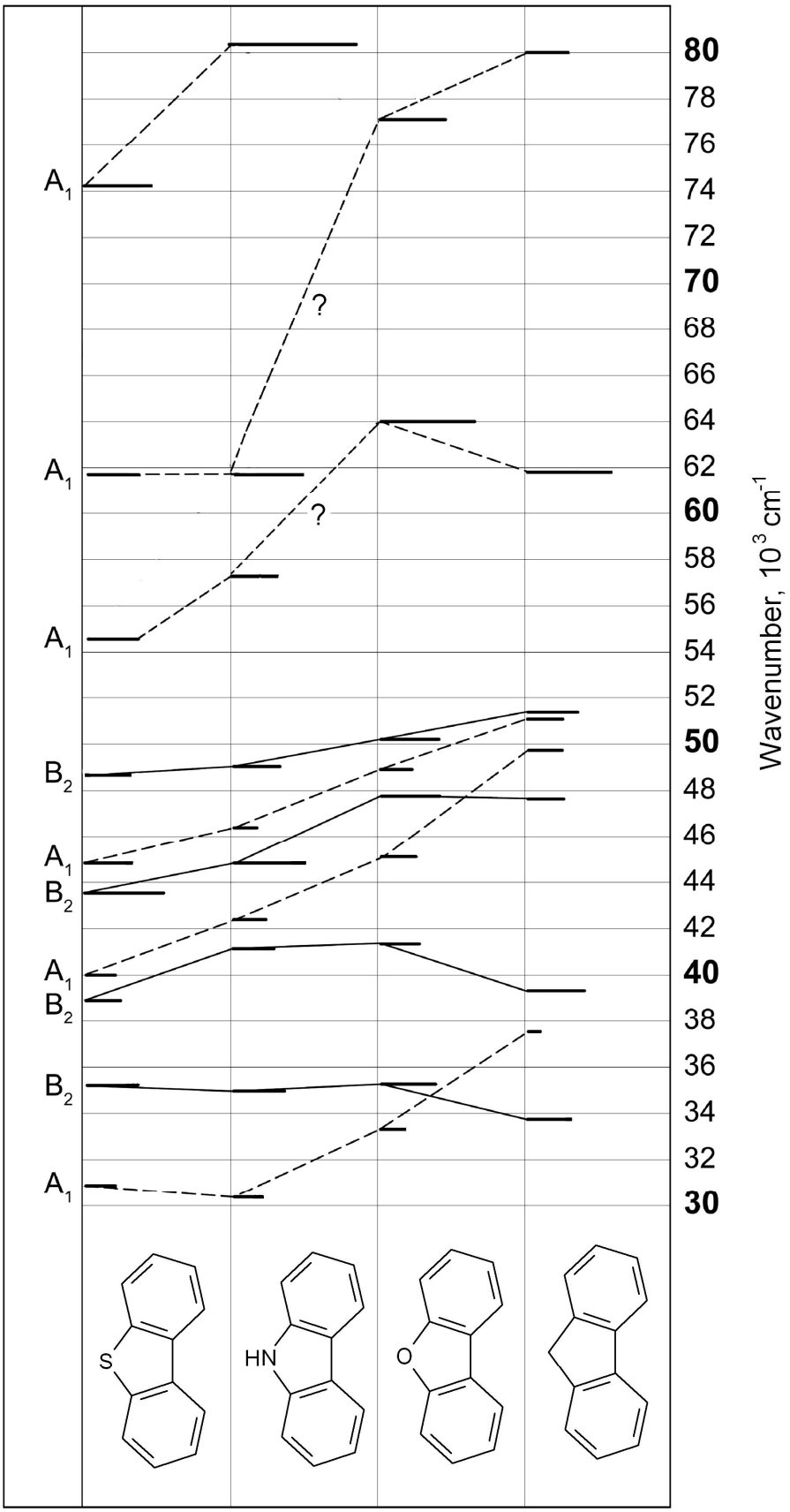
A1
A1
A1
B2
A1
B2
A1
B2
B2
A1
?
?
80
78
76
74
72
70
68
66
64
62
60
58
56
54
52
50
48
46
44
42
40
38
36
34
32
30
Wavenumber, 10^3 cm^-1
S
HN
O